FAULT DIAGNOSIS OF INDUCTION MOTOR USING MULTIPLE TECHNIQUES

Thesis

Submitted by

Arunava Kabiraj Thakur

Doctor of Philosophy (Engineering)

Department of Electrical Engineering

Faculty Council of Engineering & Technology

Jadavpur University

Kolkata, India

2023

INDEX NO. : 44/16/E

1. Title of the thesis: **FAULT DIAGNOSIS OF INDUCTION MOTOR USING MULTIPLE TECHNIQUES**

2. Name, Designation & Institution of Supervisor/s:

Dr. Palash Kumar Kundu
Professor
Department of Electrical Engineering
Jadavpur University, Kolkata-700032, India

Dr. Arabinda Das
Professor
Department of Electrical Engineering
Jadavpur University, Kolkata-700032, India

Dr. Alok Mukherjee
Assistant Professor
Government College of Engineering and Ceramic Technology
Kolkata-700010, India

3. List of Publication:

Journal Publications:

[1] A.K. Thakur, P.K. Kundu, A. Das, "Prediction of unknown fault of induction motor using SVM following Decision Directed Acyclic Graph", Journal of The Institution of Engineers: Series B, 2021, Vol. 102, Issue: 3, pp: 573-583

[2] A. K. Thakur, A. Mukherjee, P. K. Kundu, A. Das, "Classification and authentication of induction motor faults using time and frequency feature dependent probabilistic neural network", Journal of The Institution of Engineers: Series B, 2023, Vol. 104, pp :623–640.

[3] A. K. Thakur, A. Mukherjee, P. K. Kundu, A. Das, "Assessment of different signal processing techniques for classifying induction motor faults using PCA features: A Comparative analysis", Journal of The Institution of Engineers: Series B, 2023, DOI : https://doi.org/10.1007/s40031-023-00948-2.

[4] A. K. Thakur, A. Mukherjee, P. K. Kundu, A. Das, "Appropriate mother wavelet selection with optimal decomposition level for analyzing various faults of induction motor under variation in motor loading", Journal of The Institution of Engineers: Series B (revision submitted).

[5] A. K. Thakur, A. Mukherjee, P. K. Kundu, A. Das, "Performance comparison of different SVM kernels for fault classification of induction motor using time and frequency domain features extracted using PCA", Applied Soft Computing (under review).

[6] A.K. Thakur, A. Das, P.K. Kundu, "Development of Generalized Model of 3-Phase Induction Motor for Performance Study During Different Distorted and Unbalance Voltage*",* International Journal of Computer Sciences and Engineering, 2020, 8(2), pp: 18-25.

Conference Publications

[1] A. K. Thakur, P. K. Kundu, A. Das, "Comparative study of induction motor fault analysis using feature extraction", IEEE Calcutta Conference (CALCON), December 2017, pp: 150-154, doi: 10.1109/CALCON.2017.8280714

[2] A. K. Thakur, P.K. Kundu, "Authentication of unknown fault for a three phase induction motor by stator current spectral analysis", 2016, 2nd International Conference on Control, Instrumentation, Energy & Communication (CIEC), pp: 279-283, doi: 10.1109/CIEC.2016.7513831

Book Chapter

[1] A.K. Thakur, P.K. Kundu, A. Das, "Selection of Optimal Mother Wavelet for Fault Analysis in Induction Motor Using Stator Current Waveform", Advances in Data Science and Computing Technology, 2022, pp: 197-217

4. List of Patents : NIL

5. List of Presentation in National/ International Conferences/Workshop:

[1] A. K. Thakur, P. K. Kundu, A. Das, "Comparative Study of Induction Motor Fault Analysis Using Feature Extraction", 2017 IEEE Calcutta Conference (CALCON), Kolkata, 2-3rd December 2017

[2] A. K. Thakur, P. K. Kundu, "Authentication of unknown fault for a three phase induction motor by stator current spectral analysis*",* 2nd International Conference on Control, Instrumentation, Energy & Communication (CIEC), 20-30th January 2016

[3] A. K. Thakur, P. K. Kundu, A. Das, "Selection of Optimal Mother Wavelet for Fault Analysis in Induction Motor Using Stator Current Waveform", International Conference on Emerging trends in Science and Technology, 2020, 21-22nd August 2020

[4] A. K. Thakur, P. K. Kundu, A. Das, "Prediction of unknown fault of induction motor using SVM following Decision Directed Acyclic Graph", Impact of Changing Energy Mix in the Power Sector, 23rd and 24th November 2019

Statement of Originality

I Arunava Kabiraj Thakur registered on 16th November, 2016 do hereby declare that this thesis entitled "FAULT DIAGNOSIS OF INDUCTION MOTOR USING MULTIPLE TECHNIQUES" contains literature survey and original research work done by the undersigned candidate as part of Doctoral studies.

All information in this thesis have been obtained and presented in accordance with existing academic rules and ethical conduct. I declare that, as required by these rules and conduct, I have fully cited and referred all materials and results that are not original to this work.

I also declare that I have checked this thesis as per the "Policy on AntiPlagiarism, Jadavpur University, 2019", and the level of similarity as checked by iThenticate software is 05 (five)%.

Signature of Candidate: Arunava Kabiraj Thakur
27/02/2023

Date:

Certified by Supervisor(s):
(Signature with date, seal)

1. Palash Kundu
27/2/23
Professor
Electrical Engineering Department
JADAVPUR UNIVERSITY
Kolkata - 700 032

2. Anabinda Das
27/02/2023
Professor
Electrical Engineering Department
JADAVPUR UNIVERSITY
Kolkata - 700 032

3. Alok Mukherjee
27/02/2023
Alok Mukherjee
Assistant Professor
Govt. College of Engg. & Ceramic Technology
Kolkata-700010

CERTIFICATE OF SUPERVISOR

This is to certify that, the thesis entitled "FAULT DIAGNOSIS OF INDUCTION MOTOR USING MULTIPLE TECHNIQUES" submitted by Shri Arunava Kabiraj Thakur, who got his name registered on 16th November 2016 for the award of Ph.D. (Engineering) degree of Jadavpur University is absolutely based upon his own work under the supervision of Dr. Palash Kumar Kundu, Dr. Arabinda Das and Dr. Alok Mukherjee and that neither his thesis nor any part of the thesis has been submitted for any degree / diploma or any other academic award anywhere before.

Palash Kundu
27/2/23

Signature of the Supervisor1

and date with office seal

Professor
Electrical Engineering Department
JADAVPUR UNIVERSITY
Kolkata - 700 032

Arabinda Das
27/02/2023

Signature of the Supervisor2

and date with office seal

Professor
Electrical Engineering Department
JADAVPUR UNIVERSITY
Kolkata - 700 032

Alok Mukherjee
27/02/2023

Signature of the Supervisor3

and date with office seal

Alok Mukherjee
Assistant Professor
Govt. College of Engg. & Ceramic Technology
Kolkata-700010

Acknowledgement

First, I am deeply indebted to my thesis supervisors, Dr. Palash Kumar Kundu, Dr. Arabinda Das and Dr. Alok Mukherjee for their advice and guidance throughout this research work. Without their invaluable guidance, this work would never have been a successful one. This work is a result of their encouragement, support, ideas, and constructive criticism.

I would like to thank Dr. Prithwiraj Purakait, Former Principal, Haldia Institute Technology, Haldia, India, for the support received from him. I am also grateful to Mr. Gautam Das (Assistant Professor, Department of Electrical Engineering, Haldia Institute of Technology) and other technical staffs of Electrical Engineering department of this institute for cooperation to collect data samples of current signals from healthy and different faulty motors under different loading conditions to carry out this research work.

The major inspirations behind my work are my parents Mr. Amitava Kabiraj Thakur, Mrs. Minati Kabiraj Thakur, Mr. Kanti Prasad Bhattacharya, Mrs. Sima Bhattacharya for their continuous encouragement, tireless motivation and taking enormous pains during my tenure of work. Without them, nothing would have been possible. I would especially thanks to my wife Mrs. Srijita Bhattacharya for her continuous encouragement to completion of my Ph.D. To end with, I acknowledge all my well-wishers whom I could not mention and have contributed directly and indirectly towards the completion of my work. I also thank the almighty God for giving me mental patience and physical perseverance for completion of the research work in the present form.

Arunava Kabiraj Thakur
27/02/2023

Jadavpur University, Kolkata, India

Arunava Kabiraj Thakur

Dedicated to
Maa & Baba
And my wife

Who have always supported me in all my endeavours...

Contents

Page No.

List of Figures

List of Tables

List of Abbreviations and Symbols

Abbreviations	*Description*
PCA	Principal component analysis
PC	Principal component
PC1 & PC2	Principal component 1 & Principal component 2
K-NN	K –Nearest Neighbors
FFT	Fast Fourier Transform
BR, BRB	Broken rotor bar fault
FB,FBR	Bearing fault
RM, RML	Rotor Misalignment
RU, RUB	Rotor Unbalance
SW, SWF	Stator winding fault
VU, VUB	Single phase voltage unbalance
HM, HML	Healthy motor
SVM	Support Vector Machine
DDAG	Decision Directed Acyclic Graph
DWT	Discrete Wavelet Transform
CWT	Continuous Wavelet Transform
SNR	Signal to Noise Ratio
PSNR	Peak Signal to Noise Ratio
RMSE	Root Mean Square Error
CC	Correlation Coefficient
L1, L2, L3, L4, L5	1^{st} level, 2^{nd} level, 3^{rd} level, 4^{th} level, 5^{th} level wavelet decomposition respectively.
CS_A	Composite skewness matrix of approximate coefficients
CS_D	Composite skewness matrix of detail coefficients
CK_A	Composite kurtosis matrix of approximate coefficients
CK_D	Composite kurtosis matrix of detail coefficients
CR_A	Composite r.m.s value of approximate coefficients
CR_D	Composite r.m.s value of detail coefficients
CMn_A	Composite median matrix of approximate coefficients

CMn_D	Composite median matrix of detail coefficients
CMdA	Composite mode of approximate coefficients
CMdD	Composite mode of detail coefficients
MRA	Multi Resolution Analysis
NCA	Norm of composite norm matrix
PNN	Probabilistic Neural Network
CNN	Convolution Neural Network
PDF	Probability density function

Symbols	***Description***
γ^2	Squared variance of the Gaussian function
p	Order of polynomial
α	Weighing multiplier
w	Weight vector
b	Bias
σ	Standard deviation
μ	Spread parameter
q	Correlation coefficient
l_1	Lower boundary of the median class
f_m	Frequency of the median class
F (x)	Guassian function
Ψ (t)	Mother wavelet function
$R_{xy}(\tau)$	Cross correlation function
d_j	Distance between two points
r	Coefficient of linear regression
Σ	Summation
p	Order of polynomial
α	Weighing multiplier

Abstract

Induction motors are robust and reliable, yet they are liable to various faults. Unplanned process downtime caused by machine failure can result in exorbitant costs. The economic losses of the process downtime caused by an unexpected outage of the machine exceed the machine maintenance costs considerably. If there are any electrical or mechanical faults in the machine, some abnormalities in the system are discovered, so fault prediction is critical to protect the machine from an unplanned shutdown.

There are limited numbers of skilled specialists for monitoring processes in the plants. Human experts are also unable to identify the exact type of fault due to different types of measurement data. The classification of fault is intended to determine the kind of fault that occurred in the machine and to distinguish the causes of the observed abnormal conditions. Following the determination of the fault condition, the necessary actions will be taken immediately to troubleshoot the problem and reduce economic loss by avoiding an unscheduled machine shutdown. Identification of unknown fault patterns in induction motors is a challenging task in modern industries. Vibration analysis technique and motor current signature analysis technique are two popular techniques for fault identification in the rotating machine, but conventional systems are not adequate to identify unknown faults, and it is very difficult to distinguish the fault types if more than one fault occurs in the machine. Therefore, a sophisticated and intelligent fault classification system needs to be developed to reduce dependency on human beings.

In this research, a robust fault classification system has been developed to identify multiple unknown fault patterns using different fault classifiers. Unknown faults have been classified among the trained known classes of six known faulty induction motors and one healthy induction motor. The unsupervised method of fault classification using current signature analysis does not need any system modelling but does need accurate training.

Experiments were carried out using a data acquisition system to collect data samples (amplitude vs. time) of current signals from various faulty induction motors and one healthy induction motor under various loading conditions. Data samples were also taken from unknown faulty induction motors under various loading conditions.

Intelligent fault classification needs two steps: first, the features are extracted from the input signals, and then the features are fed to the classifier. Dimension reduction of features is essential for reducing computation times and memory storage of an algorithm to make the

classification process simpler. Simultaneously, it is important to retain the most important features from the data and delete the redundant ones. Principal component analysis (PCA)-based feature extraction and dimension reduction techniques have been found to be more efficient than all other dimensionality reduction techniques in terms of classification accuracy. PCA can play an important role for feature extraction and dimension reduction in the current signature analysis method, while in the post processing stage; classifiers can be used for the classification of faults in induction motors. Features are extracted using PCA individually from faulty current signals in the time domain, FFT spectrums of current signals, wavelet coefficients of decomposed current signals, and cross correlated signals to compare the classification accuracies and sensitivities of different signals processing techniques. Various classifiers have been used for fault classification, such as nearest neighborhood, SVM, DDAG, and PNN.

Among various groups of known faults, the technique of the nearest neighbourhood has been used to find the unknown faults. PCA transformations of current signals in the time domain and PCA transformations of current signals' FFT spectra were used separately to make the classifications. The graph shows the two-dimensional characteristics of each phase current signal as well as the signal spectra. The "nearest neighborhood" minimum distance rule is used to classify and authenticate the three unknown faults in both domains. To determine which classification approach is better, the sensitivities of the two have been compared.

Faults have also been classified by applying multiclass SVM, and the DDAG technique has also been applied to overcome the drawbacks of the OAO pairwise SVM classification method, where training data and test data have been kept at the same load. ANNs can handle multi-class problems by producing probabilities for each class, but ANNs can also overfit if training goes on for too long—a problem that SVMs do not have. SVM models are easier to understand. There are different kernels in SVM that provide a different level of flexibility. Classifications have been performed using the features of the time domain and the features of the frequency domain both to select the better one and to select the best SVM kernel for fault classification.

The nonlinear kernels are providing better classification accuracy than the linear kernel, and there is a limitation of the linear kernel for fault classification in the time domain, but the linear kernel is able to classify faults in the frequency domain. The reason for the inability of the linear kernel to classify faults in the time domain has been explained using the linear regression method.

The faults are classified in the time-frequency domain also, and wavelet transforms are normally used for time-frequency domain analysis. For many types of signals, a variable window size is required according to the frequency to increase flexibility. It applies a variable-sized windowing technique. A shorter time interval and a longer time interval are used for the analysis of high-frequency components and low-frequency components of a signal, respectively. Signal analysis using the wavelet transform is very effective for dealing with local aspects of a signal, like breakdown points, trends, and self-similarity. The selection of the most optimal mother wavelet is a challenge when performing a task using wavelets because the same signal produces different results when applied to different mother wavelets due to their different coefficient reconstruction, de-noising, feature extraction, and component separation from the time domain and frequency domain signals, respectively. There are several mother wavelets that are used for fault analysis of induction motors. The optimal mother wavelet has been selected among various mother wavelet families for decomposition of current signals because optimal mother wavelets need to be selected for the current signature-based fault analysis method. The optimal level of decomposition must also be selected because, after a certain level of decomposition, the quality of the de-noised signal may be reduced due to data reduction. The optimal mother wavelet, including the optimal decomposition level, has been selected depending on the results of four parameters. Following the selection of the best mother wavelet, the current signals of all faulty motors were decomposed to classify three unknown faults using multi-resolution analysis. After that, the three unknown faults were classified using the multi-resolution analysis (MRA) technique of wavelets. Statistical features are extracted from the approximate and detail coefficients of decomposed signals at each level, and the Euclidean norm of each feature parameter has also been calculated. The unknown faults have been authenticated by calculating the norm differences.

SVM provides nearly 100% classification accuracy for fault classification in the frequency domain using the RBF kernel, where feature data from trained and test classes are kept under the same loading condition. P. Gangsar and R. Tiwari investigated the importance of fault prediction performance using a load independent classifier because finding test and training data at the same load is not always possible.

The probabilistic neural network (PNN) has been used for fault classification in different domains, where the training of the model has been carried out with faults and the number of fault current signatures recorded at no load condition only, but the testing of the model is carried out with current signatures of unknown faults at three loading conditions. PNN is a type

of neural network that is faster than a multilayer perceptron network and uses Bayes' optimal classification to generate accurate predicted target probability scores. PNN networks are relatively insensitive to outliers. PNN networks generate accurate predicted target probability scores. Faults have been classified by extracting the features through PCA transformation from current signals, FFT spectrums of current signals, and approximate coefficients of decomposed current signals at different levels for comparative study. The wavelet decomposition level has been found to have the highest classification accuracy. The values of the spread parameter have been varied from 0.2 to 0.8 to tune the PNN during training because the classification performance of the PNN varies due to changes in the spread parameter. The appropriate value of each spread parameter was estimated after comparing classification accuracy for each spread parameter.

Different signal processing techniques have been applied to detect faults in induction motors through current signature analysis, but cross correlation is also a signal processing technique that has been applied for fault analysis in induction motors. The cross-correlation technique is the sequence between two input signals that measures the extent of similarity between these two signals, and the idea of a cross-correlation based feature extraction technique is new in pattern recognition problems. Cross correlation has been used in this work to detect faults in the induction motors, and the sensitivities of cross correlated signals with other signals have been compared. Cross correlated signals have been developed to find the degree of correlation between the current signals of healthy motors and the current signals of faulty motors. The cross-correlation technique has been applied earlier for fault classification of transformer winding, monitoring for gearbox fault, and stator winding fault, but this technique has not been applied to detect multiple types of fault patterns in induction machines.

Three unknown types of faults were classified and authenticated using features of signals from different domains, such as time domain signals, cross-correlated signals, FFT spectra, and time-frequency domain (DWT) signals in multiple decomposition levels, using the nearest-neighborhood classification method. The features are extracted from every type of signal using the PCA transformation. Sensitivity depends on the magnitudes of the nearest distances; the higher the distance, the lower the chance of misclassification due to the large data boundary. The sensitivities of every type of signal have been compared, and it has been shown that the sensitivity of fault classification does not depend on the level of wavelet decomposition.

Key words: PCA, FFT, Wavelet transform, cross correlation, MRA, nearest neighborhood, SVM, DDAG, and PNN.

Chapter 1

Introduction

1.1 Introduction

Induction motors are the workhorse of modern industry. Because of the lower cost and increased longevity of the components, fault prediction of induction machines is becoming more important. The detection of a fault in an electric machine and the identification of its type are imperative for preventing the failure of the motor [1, 2].

Faults can be detected after processing the input signals of a rotating machine, and various techniques are successfully applied to predict the rotating machine fault, such as (a) motor current signature analysis (MCSA) [3-5], (b) vibration analysis technique [6-9], (c) temperature monitoring [10], and (d) partial discharge [11]. While current signature analysis is a beneficial and less expensive technique compared to the others because electrical signals are easier to analyze, vibration analysis and motor current signature analysis are both common techniques for defect diagnosis in induction machines. The vibration analysis technique requires more expensive sensors, whereas several electrical sensors are not needed to sense electrical signals. The vibration analysis technique can correctly analyse various types of mechanical related faults, but it has a limitation in detecting electrical related faults. Motor current signature analysis is also a popular fault analysis technique that is used not only to detect electrically related faults but also mechanical faults in induction motors. The method of fault analysis by motor current signature is gaining popularity for the identification of different types of faults at low cost because multiple electrical sensors are not required to sense electrical signals.

The classification of fault is intended to determine the kind of fault that occurred in the machine and to distinguish the causes of the observed abnormal conditions. Following the determination of the fault condition, the necessary actions will be taken immediately to troubleshoot the problem and reduce economic loss by avoiding unscheduled machine shutdown. The conventional methods for different fault analysis in the motor are time-based and spectrum-based signal analysis from current and vibration signals [12]. The signal processing of current signature analysis for fault detection has recently gained much attention because a typical mathematical model is not needed in this technique.

Many studies are available for the diagnostic strategy of signal processing that has been introduced to point out the faults in the machines. To detect anomalies associated with rotating machine operation and bearing problems, the decision tree has been presented (Yang, Park, Kim 2000; Sugumaran, Muralidharan, Ramachandran 2007; Sun, Chen, Li 2007; Lim, Yang, Kim 2000). ANNs (Samanta, Al-Balushi 2003; Nandi and Jack 2002; Al-Balushi, Samanta, Al Araimi 2006), ANFIS (Lei, He, Zi, Hu 2007), FALCON [13], and fuzzy logic (Lindh, Ahola, Spatenka, Rautiainen 2004) have previously

been used to diagnose the state of machines with relatively high accuracy. In most cases, vibration data has been utilised to measure mechanical faults in motors. In addition to these signal processing and analysis techniques in the time domain or frequency domain, the development of an appropriate model for a motor running under faulty conditions provides an alternative way for fault diagnosis. Analytical superfluity is used to detect faults in an induction motor model (Kim, Parlos, Lesecq, and Gentil 2002).

The modelling of an induction motor from a mathematical equation is another way of doing fault diagnosis. When the induction motor is running under different loading conditions, the electrical behaviour of the motor can be observed using a mathematical model. It can identify flaws in the rotor bar and stator winding that are electrical in nature. However, this method requires the development of an accurate mathematical model, which suffers from uncertainties in practical applications. Fault classification using an unsupervised method through current signature analysis (e.g., PCA, SVM, and K-NN) does not need any system modelling but does need accurate training (Casimir, Boutleux, Clerc, and Yahoui 2006). The test data sample can be classified among many trained data samples. It has been seen from the literature review that an artificial intelligence (AI)-based fault classification system helps us identify the types of faults and also the faulty locations because there are fewer experts in the industry for the quick identification of faults very quickly [14].The methods of feature selection provide a way to better understand and improve prediction performance reducing data computation time in machine learning or pattern recognition applications [15]. Feature selection from current signal data of faulty motors is essential to classify the faults because significant features provide an exact description of the condition of the faults, their diagnosis, and their prognosis [16]. A statistical feature extraction technique has been used here to extract relevant features from current signals, reducing the dimensions, and the features are fed into different classifiers. A feature extraction process called principal component analysis (PCA), which is based on statistical learning theory, has been used here for feature extraction and dimension reduction from the current signals [17, 18] of motors with different faulted conditions. PCA has been used because it extracts exact features, reducing irrelevant variables, and is more accurate compared to other dimension reduction techniques [19].

In this work, current signals have been used for different unknown faults of induction motors. Different signal processing techniques in the time domain, frequency domain (FFT), and time-frequency domain have been used to make better fault analysis systems by selecting the optimal mother wavelet and optimal decomposition level. Fault identification through multi-resolution wavelet analysis has also been applied in different loading conditions to identify multiple types of faults. The cross-correlation technique has also been applied to detect various types of faults, and the sensitivities of signals in the time domain, frequency domain, and time-frequency domain have been compared with cross-correlated signals for fault analysis. It has been shown that the sensitivity of

fault analysis can be increased by applying the cross-correlation technique. Fault classification has been performed using multivariate statistical analysis, multiclass SVM, and PNN, with relevant features extracted by PCA from current signals. The classification performances in time domain, frequency domain, and time-frequency domain at different levels have been compared. Multiclass SVM, including the DDAG technique based classifier, has been used to make the classification system more robust for any type of fault classification, and performance analysis of linear and nonlinear kernels is performed to select the best one. The benefits of a probabilistic neural network (PNN) over an artificial neural network (ANN) have been discussed, and PNN is also used to classify unknown faults.

1.2 Objective of the thesis

The main goal of this research work is to conduct a thorough analytical analysis on the use of different machine learning algorithms and different signal processing techniques to identify and categorise the different kinds of induction machine problems. As a result, a thorough review of the literature has been conducted to determine the shortcomings of the currently used fault diagnosis methods. The background motivation of this thesis work stems from research efforts to meet the growing need for the use of AI approaches to fault classification, which can now be done more accurately than with traditional schemes. As a result, this effort has significant socioeconomic effects and increases the need for engineering advancements.

With the following work plans in mind, it has been suggested to create some original fault categorization methods:

- Development of robust fault classification system to detect multiple unknown faults in induction motor.
- To perform unsupervised fault classification to overcome the drawbacks of supervised classification.
- Classification of faults through DDAG to overcome the drawbacks of multiclass SVM and to select best kernel.
- Selection of optimal mother wavelet including the level for different fault analysis through current signals and the classification of unknown faults through MRA of wavelet.
- Comparison of different signal processing techniques to compare the sensitivities of these signal processing techniques for fault analysis.
- Development of robust fault classification system using PNN to overcome the drawbacks of ANN.

The two steps of the common fault diagnosis system are feature extraction and fault recognition. The feature vectors are fed into AI-based classifiers to identify fault patterns. Statistical features extraction technique has been applied to extract features in time domain, frequency domain and

time-frequency domain and to unknown faults in these three domain using same classification model for comparative analysis.

1.3 Fault diagnosis of Induction Motor

The key elements of industry are rotating electrical machines. The unplanned shutdown brought on by a machine failure might be quite expensive. Unplanned machine shutdowns result in increased energy losses and overall economic losses. Maintenance is necessary not only to avoid unplanned shutdowns, but also to extend component life. The aim of this chapter is to introduce the reader to various fault diagnosis techniques that have been reviewed. There are four stages in the condition monitoring system: measurement, data preparation, feature extraction, and classification.

1.3.1 *Purposes of fault diagnosis of induction machines*

Before an unscheduled shutdown, a fault diagnosis is required to predict the need for machine maintenance [20]. The vibrations or current signals are measured at selected time intervals from the machines, and after that the analysis is made either in the laboratory or in the field. Advanced fault diagnosis techniques are required for fault diagnosis and analysis. It provides a warning about incipient failure at a very early stage and the locations where advanced diagnostics are required.

The machine's condition can be predicted online as well. This technique is essential to monitor the motor if any electrical or mechanical fault has occurred in any location of a machine [21, 22]. Observing the nature of the conditions, the expert can decide whether maintenance of the system is required or not to avoid an unscheduled shutdown of the machine and to increase the machine's lifetime. The block diagram of the fault prediction system has been shown in Fig. 1.1. A fault prediction system is essential in the industrial environment for the following reasons:

- **Safety:** monitor machine operation and performance parameters and independently shut down the machine if necessary.
- **Production assurance:** identify developing faults to avoid unscheduled outages and assist operations planning.
- **Predictive maintenance:** Optimize maintenance planning and costs with predictive maintenance.
- **Quality control:** Quality control is the monitoring of the production system to prevent flaws in the product.

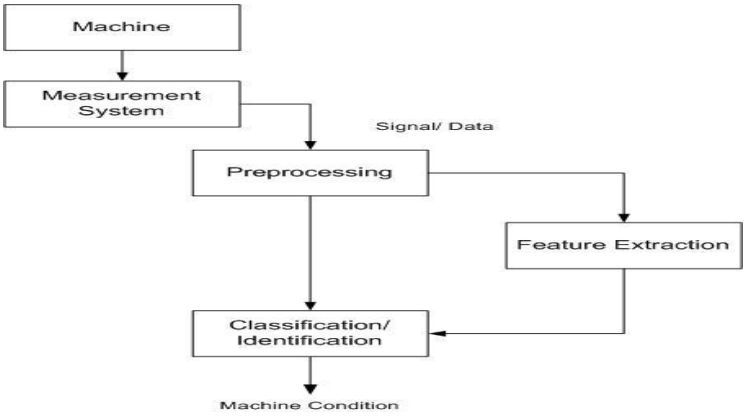

Figure 1.1: *General block diagram of a fault diagnosis system*

1.4 Faults in induction machines

Studies on induction machine failures have identified the most common failure mechanisms. These are categorised according to the components of the machine — stator faults, bearing faults, rotor faults, and other faults [23]. Fig. 1.2 represents the classifications of different types of faults in induction motors.

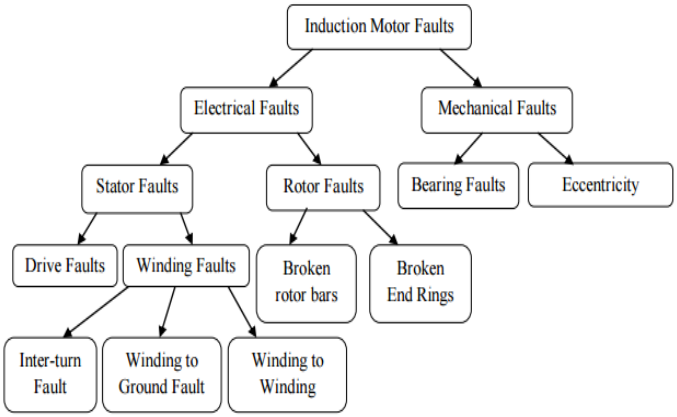

Figure 1.2: *Classification of different type of faults induction motor*

1.4.1 *Causes of faults occur in induction motor*

Unscheduled shutdown of a motor due to faults can result in downtime costs in industries, as well as flaws in products. Faults normally occur in the stator, rotor, bearing, and other parts of a motor. There are a few causes of the faults that occurred in the motor, the causes may be electrically related, mechanically related, or environmental related.

(i) ***Causes of broken rotor bar fault:*** It is referred to as the "broken rotor bar fault" of the motor if one or more bars are partially cracked or broken. A broken rotor bar fault occurs in the induction motor

due to a number of reasons [24]. The causes are (a) manufacturing flaws, (b) thermal stress, (c) frequent motor starts at rated voltage, (d) mechanical stress, and (e) metal fatigue in the rotor bar. The rotor bar may experience additional stress due to the massive end rings of the rotors, which also generate strong centrifugal forces. If any rotor bar is damaged, there will be an uneven distribution of phase currents. This asymmetry of current will cause overheating in the cracked region of the rotor if the motor is operated for an extended period of time, which could result in the bar breaking.

(ii) ***Causes of rotor unbalance:*** If the alignment of the rotor is not in the center, known as air-gap eccentricity, the air-gap between the stator and rotor will not be similar. The air-gap eccentricity is shared by other rotor flaws, like the bowed rotor fault and the rotor mass unbalance fault. Rotor unbalance will cause numerous problems with the motor.

(a) The dynamic eccentricity caused by mass unbalance creates oscillations in the air gap length.
(b) Due to changes in flux density in the air gap, the oscillation in the air gap length alters the induced voltage in the winding.
(c) The frequencies of current produced by induced voltage depend on the frequency of the air gap flux density harmonics [25, 26].

(iii) ***Causes of bearing fault****:* Typically, rotating electrical machines use ball or rolling type bearings. There are some mechanical and electrical problems that create bearing faults. There are several causes of bearing faults, such as improper lubrication, overloading, manufacturing defects, improper mounting, etc. Another cause of bearing related faults is electrical erosion. The high rate of voltage rise and the high switching frequencies create some capacitive discharge currents. The combination of high frequency currents and capacitive discharge currents induces bearing currents and shaft voltages. When the voltage hits a specific level, it discharges via the bearings to earth. When the threshold voltage is reached and a discharge takes place during that period, the obstacle of lubricant film thickness is overcome. Because the voltage is not controlled in motors, it increases once again like a capacitor would, which causes electrical erosion. Any electrical erosion that affects a bearing in an electrical motor can result in early bearing failure and bearing damage. The faulted bearing can be detected by stator current signature analysis [27].

(iv) ***Causes of stator winding fault:*** Insulation breakdown is typically the cause of a stator winding fault [28, 29]. One type of stator winding defect is a coil-to-coil fault (short circuit between two single-phase coils), along with turn-to-turn, phase-to-phase, coil-to-ground, and open circuit failures. These fault types may be caused by mechanical stress, thermal stress, electrical stress, or environmental stress. The degree of these strains will determine if stator defects develop. Stator winding faults create high vibration and supply voltage transients, which reduce the life of the stator winding. If the maintenance is done correctly and the motor is well designed, the stress will be reduced.

1.5 Literature Survey

Various faults are occurring in the electric machines due to overload, frequent motor starts and stops, insufficient lubrication, and inadequate cooling. The reliability of motors needs to be improved due to their significant positions in applications. The statistical occurrences of the most common types of faults are listed in Table 1.1, according to IEEE Standard 493-1997. Induction motors are robust and reliable; yet, they are liable to various faults. These faults are primarily categorised as stator faults, rotor faults, bearing faults, and other faults; the IEEE and EPRI surveys [30, 31] are shown in Fig. 1.3.

Table 1.1: Statistics of motor faults/failure modes

Fault types	**Number of faults**				
	DC motors	**Wound rotor motors**	**Synchronous motors**	**Induction motors**	**All motors**
Stator winding faults	Does not appear	6	16	75	97
Bearing faults	2	10	2	152	166
Rotor faults	3	4	1	8	16
Brushes or Slip rings	2	8	6	Does not appear	16
Shaft faults	Does not appear	2	Does not appear	19	21
Faults in external device	1	1	7	10	19
Other faults	2	1	9	40	52

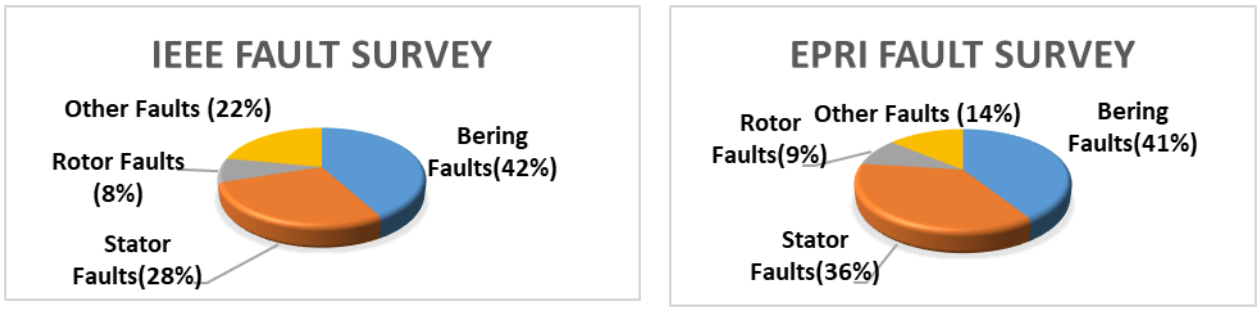

(a) (b)

Figure 1.3: *IEEE and EPRI survey for various types of faults*

1.5.1 *Existing fault diagnosis techniques*

Induction motor defects can be predicted using a variety of monitoring techniques, including vibration analysis, motor current signature analysis, lubricating oil analysis, thermal monitoring, and partial discharge. These techniques are important for the detection of faults, and the applications of these techniques to detect various types of faulty components in a motor have been shown in Table 1.2. Apart from these techniques, artificial intelligence-based techniques have been successfully used to detect electrical and mechanical faults in induction motors.

(a) ***Vibration analysis:*** The vibration analysis technique is the most commonly used in fault diagnosis systems. All rotating machines produce vibration in their running condition. In a healthy state, the vibration range is small, but when a fault occurs due to a change in the dynamic process, the machine produces excessive vibrations. Vibration-based problem identification is the most precise method for assessing the general state of a rotating system. Several sensors mounted on various machine elements are used by this system to store a significant amount of data [32–34]. Depending on the position of the sensor, significant noise variations may arise throughout the measurement process. Mikhail Tsypkin has demonstrated that vibration analysis is an effective and practical method for identifying various types of mechanical and electromagnetic faults in induction motors.

(b) ***Thermal monitoring:*** Thermal monitoring is an indirect method that can be used to detect bearing faults and some stator faults. The temperature rises in the faulty region due to the stator fault (turn to turn), but the incipient fault detection might be too slow before it progresses into a more severe fault. Due to the machine's bearing issue, which can be identified by thermal monitoring, the increased bearing wear raises the temperature and friction in that specific area. The parameters are estimated by measuring the local temperature of the machine. The value of the current in the stator winding will be very high if a stator turn-to-turn fault occurs, which will produce excessive heat. Destruction is possible if the necessary action is not taken in that situation. The thermal model of an electric motor has been introduced by the researchers.

(c) ***Lubricating Oil Analysis:*** For offline defect identification, oil analysis is often conducted via oil sample collection. Online sensors are being used more frequently nonetheless to protect the oil's purity, [35]. Characterization of parts is only done for abnormalities. In the case of significant filter pollution, part characterization, oil contamination, or changes in component characteristics, it can provide a clear indicator of components with excessive wear. Reduction of wear due to metal-to-metal contacts can be achieved using lubricating oil. Several parameters influence the friction and wear of gears. Lubricating oil analysis looks at several oil qualities to find the most cost-effective time between oil changes and signs of fault development. The most important ones are:

- Content of water
- Viscosity
- Contamination of particles
- Additives

(d) ***Motor Current Signature Analysis:*** In order to find mechanical and electrical flaws in rotating machinery, a popular fault detection technique called Motor Current Signature Analysis (MCSA) is performed. MCSA's effort focuses on stator current spectral analysis to detect abnormal conditions caused by various electrical or mechanical faults. The goal of MCSA is to examine harmonics in the stator current since these harmonics are directly related to rotational flux components. Faults in the motor flux distribution, whether electrical or mechanical, result in the creation of new rotational flux components. MCSA assistance was used to identify the following:

- Health of stator winding
- Static and dynamic air gap eccentricity
- Coupling health including belted, geared and direct
- Issues of load
- System load and efficiency
- Health of bearing

Fault analysis through MCSA is less expensive because electrical signals are simpler to measure than other signals, and it does not require multiple expensive sensors.

(e) ***Partial Discharge:*** In liquid or solid dielectrics, conductor-dielectric interfaces, fractures, gaps, inclusions, or bubbles inside liquid dielectrics are the typical places where partial discharge starts [36].

A partial discharge (PD) can occur due to defects in the material, surface contamination, incorrect application, the ageing of the material, or improper installation with material damages. Partial discharge testing is used to indicate the failure of a motor. If left undetected, it can eventually deteriorate the electrical insulation completely, which is one of the causes for forced outages of motors and generators. PD measurement and monitoring are reliable methods that can be used to diagnose the condition of the insulation of a motor, effectively detecting the weak points in the insulation system.

Table 1.2: Techniques to detect various types of faulty components in the motor

Technique	Faults				
	Insulation	Stator winding	Rotor winding	Rotor eccentricity	Bearing
Vibration Analysis	No	No	Yes	Yes	Yes
MCSA	No	Yes	Yes	Yes	Yes
Lubricating oil analysis	No	No	No	No	Yes
Thermal monitoring	Yes	Yes	Yes	No	No
Partial Discharge	Yes	No	No	No	No

1.5.2 *Fault detection using signal processing techniques*

Faults are detected with the help of different signal processing techniques from the last few decades. The signals may be vibration, current, or temperature. The signals are processed in three different domains: time, time-frequency, and frequency.

(a) ***Fault detection using time domain signals:*** Time-domain signal analysis is used to look for irregular changes in machine characteristics over time. These methods are simple to implement and calculate, but they have a low fault sensitivity. Park's transformation is a time-domain method by which current vectors are obtained to form a fault indicative circle [37]. Three current sensors are needed for this procedure, and it is unable to identify the fault's kind. Another well-liked time-domain fault identification technique that examines the symmetry of the motor is sequence component analysis [38, 39]. A model-based fault detection technique is applied in the time domain where fault occurrence is indicated by changes in certain parameters, such as rotor resistance or the unusual output of models [40]. Using a model-based fault detection technique, electrical-related defects can be located. Measured signals, including defect information, are subtracted from the output of the model of healthy motors [41]. The application of a different model for defective induction motors enables a comprehensive study of the machine's input current and voltage [42].

(b) ***Fault detection using signals of frequency domain:*** Additional frequency components are generated in the form of various spectra from vibration or current signals due to various machine faults. The Fast Fourier Transform (FFT) is the most straightforward tool for examining the spectral characteristics of data. Signals that have undergone pre-processing can be used with FFT, such as FFT on extended Park's vectors [43], instantaneous power [44], and air-gap torque [45]. FFT cannot be used for non-stationary signals because it does not provide time information. FFT has some drawbacks, such as spectral leakage, a long measurement period, and low resolution.

(c) ***Fault detection using signals of time-frequency domain:*** Analysis of non-stationary data can be done using cutting-edge time-frequency domain signal processing techniques. These methods are used to perform accurate continuous spectral analysis of a machine's dynamic properties. It offers a constrained moving temporal window that consistently treats non-stationary signals. Wavelet transform (WT), which has better time-frequency characteristics and is more adaptable than other time-frequency analyses, is the most often used time-frequency analysis [46]. WT, also known as wavelet packet decomposition, divides the signal into approximate and detailed frequency levels using low-pass and high pass filters.

1.5.3 *Artificial intelligence based fault classification*

Artificial intelligence (AI) techniques, including deep learning and machine learning, are important data driven methods for fault classification [47]. By analysing the representative system condition, fault classification determines the machine's operational status and the type of breakdown. Artificial intelligence has been used successfully to detect electrical, mechanical, and other faults in induction motors. Automation of the diagnostic process has been made possible by the use of AI tools in the fault analysis of electrical motors and drives. Additionally, it aided in early and accurate detection and the use of human expertise. Previously, statistical learning classifiers such as the Bayesian classifier [48], the K-nearest neighbour algorithm [49], the support vector machine [50], and the artificial neural network [51] were widely used for fault classification in rotating machinery. Recently, deep learning techniques have begun to be applied to fault diagnosis [52]. In the upcoming years, artificial intelligence will broaden the scope of fresh research on the subject. In artificial intelligence, unsupervised learning and supervised learning are the two main methods.

Supervised learning: A supervised learning approach employs labelled data sets to train algorithms for accurate data classification [53]. An algorithm is used to accurately classify test data in classification issues. Linear classifier, MLP, and random forest are the common types of classification algorithms.

Unsupervised learning: Faults can be classified using supervised learning techniques, but pre-processing of the data is no less than a big challenge because it needs to be constantly updated and its computation time is vast. Unsupervised knowledge acquisition solves the problem by classifying the records without the use of labels. It is substantially less complicated to add the labels as soon as the facts have been classified. Finding styles in records that might be impossible to discover through conventional strategies is substantially aided by using them. Unsupervised fault classification requires exact training without exact modelling of machines. Unsupervised fault classification can be performed using multiclass SVM, PNN, and adaptive fuzzy systems.

1.6 Organisation of the thesis

Chapter 1: The Necessity of Fault Prediction for Induction Motors has been described, and conventional fault analysis techniques are also described here. A review of the literature reveals that new techniques must be applied to traditional techniques in order to make fault classification techniques more robust and achieve high classification accuracy. The necessity of AI, has led to the application of machine learning based techniques in the time domain, the frequency domain, and the time-frequency domain to increase the robustness of classification techniques.

Chapter 2: This chapter describes different statistical feature extraction techniques for fault classification. Different signal processing techniques in the time domain, time-frequency domain, and frequency domain have been described, and the advantages of wavelet transformation for fault analysis have been demonstrated. Classification through multivariate statistical analysis has been described. Methods of classification through artificial intelligence and machine learning techniques, viz., SVM, ANN, have been demonstrated in this chapter.

Chapter 3: The unknown faults of induction motor authentication through classification using the nearest-neighborhood classification method have been discussed using data analysis. Three unknown faults are classified phase-wise, and each fault is authenticated if the results of all three phases are the same. The process is applied for the three feature extraction technique. First, features are extracted from current signals by PCA transformation, after which the peak frequency of each phase signal is considered a fault feature and features are extracted from the FFT spectrum by PCA transformation. Three faults are classified and authenticated using three feature extraction techniques to compare the sensitivity of the three feature extraction techniques.

Chapter 4: Faults classification and authentication using multiclass Support Vector Machines (SVM) following Decision Directed Acyclic Graphs (DDAG) have been demonstrated in this chapter. The DDAG technique has been applied to overcome the drawbacks of conventional SVM techniques. Three unknown faults have been classified using five types of kernels to select the best one, including the spread value. This procedure of fault classification has been applied to the time domain feature and the frequency domain feature. The best kernel has been selected after comparing the success rates of fault classification in three loading conditions.

Chapter 5: Fault analysis in the time-frequency domain (Wavelet) has been demonstrated in this chapter. This chapter also describes the limitations of FFT and STFT, as well as the benefits of wavelet transformation. Initially, the best mother wavelet function and level were chosen for the current signal-based fault analysis of an induction motor, and all signals were decomposed for the unknown fault analysis. Multi resolution analysis (MRA) has been demonstrated for induction motor

fault analysis. Three unknown type faults have been authenticated using the MRA norms in three different loading conditions. The changes in values of normative differences are checked.

Chapter 6: The fault classification of ANN has been demonstrated, and the advantages of PNN over ANN have also been demonstrated. Three features are extracted from signals' time domain, time-frequency domain, and domain using PCA transformation, and PCs values from all three domains are fed into PNN to classify three unknown faults in three loading conditions. The performances of three domains for fault classifications have been shown.

Chapter 7: The applications of the cross correlation technique and its advantages for induction motor fault classification have been discussed. Three unknown faults have been classified using the "nearest-neighborhood" classification method by extracting the features from cross-correlated signals in different loading conditions. It has been shown that the sensitivity of cross-correlated signals is greater than that of other time domain, frequency-domain, and time-frequency domain signal analyses.

Chapter 8: The outcomes of different fault classifiers have been discussed, and the robustness of all the classifiers has been compared. The classification accuracy of feature extraction from signals from various domains was compared, and the sensitivities of various feature extraction techniques were also discussed. Lastly, the future scope of the work has been included.

Chapter 2

Different Methods of Fault Classification

2.1 Statistical Analysis

The field of science known as statistics is concerned with the concepts and procedures for gathering, analyzing, and interpreting such data. Like mathematics, it is a scientific approach or tool that is used to manage numerical data in situations where measurement or counting is feasible.

2.1.1 *Skewness*

If a frequency distribution is symmetrical around the mean, or when values of the variable that are equally spaced from the mean have equal frequencies, the distribution is said to be symmetrical. The "extent of asymmetry" in the data is referred to as "skewness." The term "skew" refers to a frequency distribution that is not symmetrical. Skewness literally means "asymmetry" or "lack of symmetry", and "asymmetrical" is what the word "skew" means. As a result, the skewness of a symmetrical distribution is zero. Skewness could also be favourable or unfavourable [54, 55].

2.1.2 *Kurtosis*

The term "kurtosis" describes how "peaky" the frequency curve is. The average, dispersion, and skewness of two distributions may be identical, but one may have a greater concentration of values close to the mode and a stronger peak in the frequency curve than the other. Kurtosis is the term for these properties of the frequency distribution [54, 55]. Kurtosis can only be measured using moments, i.e.,

$$\text{Kurtosis} = \frac{m_4}{\sigma^4} - 3 \qquad (2.1)$$

Here, σ and m_4 denote the standard deviation and fourth central moment, respectively.

2.1.3 *Median*

The median is the middle-most value of a set of observations when the observations are ordered in order of magnitude. The formula can be used to obtain it from a grouped frequency distribution or to perform straightforward interpolation in a cumulative frequency distribution [56]:

$$Median = l_1 + \frac{\left(\frac{N}{2}\right) - F}{f_m} \times c \qquad (2.2)$$

where, l_1 is the median class's lower border, N is its overall frequency, F is its cumulative frequency corresponding to l_1, f_m is its frequency, and c is its width.

The median provides the value of the most central observation, making it in some ways the true indicator of central tendency. Extreme values have no effect on it, and a frequency distribution with open-end classes makes it simple to calculate.

2.1.4 *Mode*

Mode is the value of a given set of observations that happens with the maximum frequency. As a measure of central tendency, it occasionally represents the true characteristics of the frequency distribution. It has the most potent typical or fashionable value. If the frequency distribution is straightforward, the mode can only be determined visually. However, it is challenging to identify the mode precisely in the case of a clustered frequency distribution. In most cases, the following formula is used to calculate it [57]:

$$Mode = l_1 + \frac{d_1}{d_1+d_2} \times e \qquad (2.3)$$

Here, $l_1$is the decrease boundary of the modal magnificence, $d_1$is the frequency distinction between the modal class and the magnificence earlier than it, d_2 is the frequency distinction between the modal elegance and the magnificence after it, and *e* is the not unusual width between the lessons.

The formula is only usable when all classes have the same width. Mode also has some idiosyncrasies. Mode does not exist when all observations happen with equal frequency. Once more, if two or more values occur with the highest frequency, there are several modes.

2.2 Multivariate statistical analysis

The word "multivariate" means to involve multiple dependent variables but have the result in one. This clarifies why multivariate problems are the norm in the actual world. Multivariate analysis **(**MVA) is a statistical procedure that can be applied in different fields for data analysis involving multiple types of observation or measurement. It might also entail resolving issues where many dependent variables are examined alongside other factors at the same time. Type 1 error probabilities can be decreased using multivariate analysis. Multivariate approaches can make it harder to interpret the test results, so sometimes univariate analysis is chosen. Because researchers frequently speculate that a particular outcome of interest is affected or influenced by several factors, this form of analysis is preferred [58].

Different types of multivariate statistical analysis such as principal component analysis (PCA), nearest-neighborhood distance, correlation, and regression have been applied here.

2.2.1 *Nearest distance neighborhood classification method*

The process of classification aims to find a model or function describing and distinguishing data classes or concepts. The aim of classification is to use the derived function to predict the label of data points with unknown class labels. For the classification task, input data is a collection of observations.

Each observation, also known as an example or instance, is denoted by (*x*, *y*), where *x* is the vector of attributes and *y* is the class label or category of the observation. The Euclidean distance is the most common distance metric used in low dimensional data sets [59]. It is also known as the L^2 norm. The Euclidean distance is the usual manner in which distance is measured in the real world, whereas the Manhattan distance tends to be more robust to noisy data. There are several techniques used for classification, such as nearest neighbour classification methods, cluster analysis, and multidimensional scaling methods, which are based on measures of similarity between objects. Instead of measuring similarity, dissimilarity between the objects will also give the same results. For measuring dissimilarity, one of the parameters that can be used is distance. This category of measures is also known as separability, divergence, or discrimination measures. A distance metric is a real-valued function *d*, such that for any point (*x, y),*

$$d_j(x_j, y) = \sqrt{\sum_{i=1}^{m} (x_{j_i} - y_i)^2} \qquad (2.4)$$

where x_j and y are *m*-dimensional vectors that are denoted by $X_j = (x_{j1}, x_{j2}, ...x_{jm})$ and $Y = (y_1, y_2, ...y_m)$ represent the m attribute values of two vectors. The goal is to find similarities between data according to the characteristics found in the data and group similar data objects into clusters. Similarity is typically expressed in terms of a distance function, such as: *d* (*i*, *j*) [60]. Distances are normally used to measure the similarity or dissimilarity between two data objects. According to the nearest neighborhood classification rule, if *x*'s are the data points representing observations for known objects and *y* is the same for unknown object, then *y* will be similar to any x_j's, when $D_j = d_j(x, y) = D_{\min}$

2.2.2 *Principal component analysis*

Principle component analysis (PCA) is a feature selection method that is widely used to obtain dominant information from multi-dimensional data sets [61, 62]. According to mathematics, principal component analysis (PCA) is an orthogonal linear transformation that changes the coordinate (variable) system of the data in such a way that the largest variance by some projection of the data is found to be on the first coordinate (the first principal component), the second largest variance on the second coordinate, and so on. The benefit of PCA is that the data's dimensions are often reduced to two or three [63]. From multi-dimensional datasets, the original data space, *X*, is divided into much fewer dimensions by PCA. The highest variances in the data set are described by a hyperplane in the lower dimension. Measurements are projected onto this hyperplane to produce new coordinates known as scores. It is simple to identify a significant aspect of an unknown variable from a group of variables in this lower dimension and variables. The original data *X* can be represented as a linear combination of a set of *m* orthonormal vectors $\boldsymbol{u}_i$

$$X = \sum_{i=1}^{m} z_i u_i \qquad (2.5)$$

Here, the coefficients z_i can be found in the following equation: $z_i = u_i^T x$. The outcome is a rotation of the coordinate system from the initial data set, *x*, to the new set of coordinates, *z*. Only a portion ($k<m$) of the fundamental vectors is maintained in order to minimize the size of the data set. Each vector *x* is then roughly represented as $\tilde{x} = \sum_{i=1}^{M} z_i u_i + \sum_{i=1}^{d} b_i u_i$. The Principal components are the vectors u_i, which correspond to the eigenvectors of the data set's covariance matrix. The major components and coefficients b_i should be selected so that, on average, the original vector *x* is best approximated. If we choose the vectors u_i that correspond to the biggest eigenvalues of the covariance matrix, the sum of squares of the errors over the entire data set is reduced. The original data set, which is represented in fewer dimensions after PCA transformation (typically 2-3).

Given, $$X = \begin{bmatrix} x_{11}x_{12}.....x_{1m} \\ x_{21}x_{22}.....x_{2m} \\ --------- \\ x_{n1}x_{n2}.....x_{nm} \end{bmatrix} \qquad (2.6)$$

Here, each row in *x* is one measurement, and the number of columns *m* is equal to the length of the measurement sequence. Because the original data set has a high dimension, we use principal component analysis to create a new data set with a reduced dimension. The procedure described above is used to compute the covariance matrix C = cov (X). Its orthonormal basis's ($U = [u_1 u_2 .... u_m]$) eigenvalues λ and eigenvectors u_i are such that, $U^T U = 1$. By using the eigenvalues of the matrix C, this transformation creates a new data matrix with a smaller dimension, where choosing the greatest values λ corresponds to the principal components with the most significance. To ensure successful class separation, the number of PCs to be selected must be adequate. Low-contribution principal components (low values of λ) should be ignored. The first *k* number of PCs is to be considered new features, while the remaining (*m*-*k*) components are to be ignored. By doing so, we are able to create the new data matrix D, which has the dimensions $n \times k$ and new feature variables as z_{ij} indicated by:

$$D = \begin{bmatrix} z_{11}z_{12}.....z_{1k} \\ z_{21}z_{22}.....z_{2k} \\ --------- \\ z_{n1}z_{n2}.....z_{nk} \end{bmatrix} \qquad (2.7)$$

PCA Algorithm:

*Input***:** $[X]_{n \times d}$, original data set.

Output: Transform matrix *R, Reduced dimension data set, z*

i) Standardize the *d*-dimensional dataset using the following:

Mean, $X_m = \frac{1}{n}\sum_{i=1}^{n} X_i$

SD: $= \sqrt{\frac{1}{n-1}\sum_{i=1}^{n-1}(X_i - X_m)^2}$

Standardized data, $X_n = \frac{X_i - X_m}{SD}$ ' for *i=1,2,....d*

ii) Compute the covariance matrix: $COV = \frac{1}{n-1} {X_n}^T \times X_n$

iii) Compute eigenvalues $e_1, e_2, \ldots\ldots e_d$ of *COV* and sort them in descending order.

iv) Compute matrix V which satisfies :

v) $V^{-1} \times COV \times V = D$, where *D* is the diagonal matrix of eigenvalues of COV.

vi) Form eigenvectors (also called Principal components)

vii) Compute reduced dimension data set z :

$z_i = R_i^T \times X$ for i = 1, 2,….., k, where $Z = [z_1, z_2, \ldots\ldots z_k]^T, k < d$, where,

R is the first *k* columns of *V*

2.2.3 *Correlation*

A statistical tool that can be used for induction motor defect analysis is correlation analysis. The term "correlation" is used to describe how strongly two variables are related. If changes in one variable's magnitude frequently correspond with changes in the other variable's magnitude, then two variables are said to be correlated. Positive correlation is a term used to describe two variables when *j* tends to rise as *i* rises. The variables are said to be negatively linked if *j* tends to decline as *i* rises. The variables are referred to as uncorrelated if changes in the values of *i* have no effect on the values of *j*.

The supplied set of *n* pairs of observations on the two variables *i* and *j* is denoted by (i_1 j_1), (i_2 j_2),....(i_n j_n). The correlation coefficient between variables *i* and *j* is then indicated by the symbol q [64].

$$q = \frac{\mathrm{cov}(i, j)}{\sigma_i \sigma_j} \qquad (2.8)$$

Here, cov (*i*, *j*) stands for the covariance of *i* and *j* and σ_i and σ_j are the standard deviations of *i* and *j*, respectively. The Pearson's product-moment formula is used to calculate the linear correlation between variables *i* and *j*. There are numerous more ways to write the formula for q. Equation 2.8 is formed by inserting the explicit expression for cov (*i*, *j*) , σ_i and σ_j and multiplying the numerator and denominator by *n*.

$$q = \frac{\sum (i - \bar{i})(j - \bar{j})}{\sqrt{\sum (i - \bar{i})^2 .2(j - \bar{j})^2}} \qquad (2.9)$$

Now expanding the expression

$$q = \frac{\sum ij - n\bar{i}\bar{j}}{\sqrt{[(\sum i^2 - n\bar{i}^2).(\sum j^2 - n\bar{j}^2)]}} \qquad (2.10)$$

Again the numerator and denominator are multiplied by *n*, and since $n\bar{i} = \sum i$ and $n\bar{j} = \sum j$, it can be written

$$q = \frac{n\sum ij - (\sum i)(\sum j)}{\sqrt{[\{n\sum i^2 - (\sum i)^2.\{n\sum j^2 - (\sum j)^2\}]}} \qquad (2.11)$$

The numerical value of *q* cannot be more than 1 because the correlation coefficient *q* is in between -1 and +1.

2.3 Support Vector Machine

Support vector machine is a statistical learning theory to solve the problem of pattern recognition in classification problems. Classification is performed by finding the separating hyperplane, which separates the functions linearly and nonlinearly. SVM finds a hyperplane for isolation in the feature space to classify unknown feature points in the space.

2.3.1 *Linear Function*

SVM generates an input-output function mapping from the set of labelled training data. These features are extracted from input, and the main goal of SVM algorithms is to use a function to divide the training data set (x_1, y_1), (x_2, y_2), …,(x_n, y_n) into 2 classes (+1,-1) and produce a classifier. In this case, x_i is the feature vector and $y_i \epsilon \{+1, -1\}$ is the class vector. It separates the classes by a hyperplane and is given by

$$(w^T.X) + b = 0 \qquad (2.12)$$

Here, X denotes the feature vector; x_i are called patterns or examples; w is the weight vector, and b is the bias. If and only if,

$(w^T.X) + b>0$ when $y_i = +1$ and $(w^T.X) + b<0$ when $y_i = -1$ (2.13)

the hyperplane $[(w^T.X)+ b]$ separates the data.

In order to be qualified as a better classifier, the distance between the hyperplanes or margin (2/||w||) should be as large as possible [65, 66]. The optimal separating hyperplane maximizes the sum of projected distances over it from the nearest data point in each class. These data points are called support vectors and are shown in Fig. 2.1(a).

2.3.2 *Nonlinear Function*

The linear classifiers cannot be applied for the generation of non-linear decision boundaries. A non-linear classifier is needed for obtaining better accuracy in many applications. The data is mapped from the input space *X* to a feature space *G* to derive a nonlinear classifier out of a linear classifier using the nonlinear function $G : X \rightarrow \phi(X)$. The discriminant function is expressed as:

$$f(X) = W^T \phi(X) + b \qquad (2.14)$$

in the feature space. The representer theorem (Kimeldorf and Wahba, 1971) shows that (for SVMs for non-linear case),

$$W = \sum_{i=1}^{m} \alpha_i \phi(X_i) \tag{2.15}$$

Here, α is a weighing multiplier. Instead of optimizing *W* directly the value of can be optimized. The decision rule is now given by the discriminant function as:

$$f(X) = \sum_{i=1}^{m} \alpha_i \phi(X_i).\phi(X) + b \tag{2.16}$$

The *G* (feature space) may be high dimensional, and the kernel function *k* (*X*, *X'*) can be utilized to make the computation simpler and more efficient. The kernel function, expressed as $k(X, X') = \phi(X)^T \phi(X')$ can be computed efficiently [67]. For linear SVM, the hyperplane separates the feature vectors into two sets of classes, but if the classes are not separable linearly, then the kernel trick is used to separate the classes using a hypersurface by increasing the number of dimensions. Three kernels are commonly used [68, 69]:

(i) The polynomial kernel: $k(X, X') = (X^T X' + 1)^p$, where p is the order of polynomial (2.17)

(ii) The linear kernel: $k(X, X') = (X^T X' + 1)\ \{p=1\}$ (2.18)

(iii) The RBF kernel: $k(X, X') = exp(|X-X'|^2/2\gamma^2)$ (2.19)

Here, the γ^2 is squared variance of the Gaussian function.

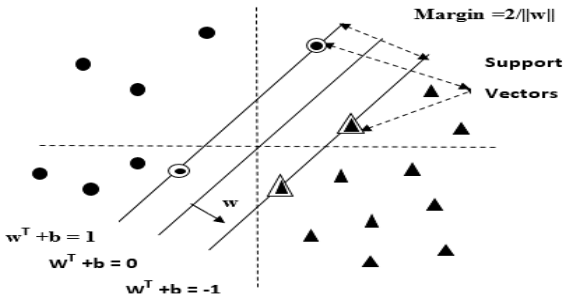

Figure 2.1: (a) *Linear SVM classification*

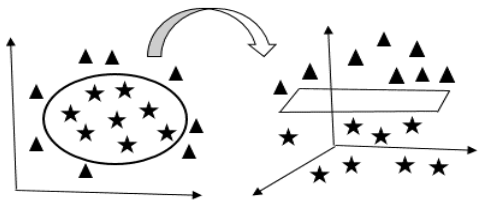

Figure 2.1: (b) *Non Linear SVM classification*

2.4 Artificial Neural Network (ANN)

Based on their connection architecture, neural networks can be divided into two broad groups: feedforward (non-recurrent) and feedback (recurrent). Based on their architectural characteristics, feed-forward networks are further divided into four groups: multilayer perceptrons (MLPs), counter-propagation networks, cerebellar model controllers, and radial basis function networks (RBF Nets). The application of MLPs is the only topic covered in this chapter. RBF Nets and Self-Organizing Feature Maps (SOFMs) are also briefly introduced.

2.4.1 *Multilayer Perceptron*

Neurons are organized into clusters termed “layers” in ANNs. In Fig. 2.2, the name "Multilayer Perceptron" denotes multiple layers of neurons. These layers are the input layer, the output layer, and the hidden layer [70].

Input Layer: It comprises a group of sensory components that take inputs from the outside world.

Output Layer: The output layer is made up of neurons that convey the system's output to the user or outside world.

Hidden Layer: Between the two layers, there are typically a number of hidden layers.

The neuron in the input layer produces output when it receives input, and this output is then used as input by the neurons in the following layer. Up until the output layer is activated and its neurons fire their output to the surrounding environment, the process continues.

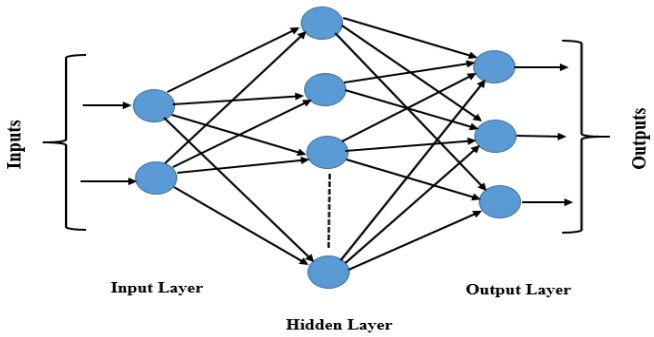

***Figure 2.2**: Multilayer perceptron with a single hidden layer*

Radial Basis Function Network

RBF nets are another form of feed-forward neural networks. Their architecture is very similar to the single hidden layer MLP shown in Fig. 2.2. The transfer functions of the neurons in the hidden and output layers, as well as the weight matrices of these layers, are what differentiate them [71].

The net input to the network's hidden neurons is the vector distance between an RBF net's weight w and its input vector p, multiplied by the bias b. The transfer function of hidden neurons is Gaussian or bell shaped function given by the following expression:

$$F(x) = e^{-sqrt(x)} \tag{2.20}$$

Here, *x* represents the vector distance between the hidden layer neuron's output, *F*(*x*), and its weight vector, w, and input vector, p, multiplied by the bias, b. The output layer neurons operate similarly to the output layer neurons in the MLP, except for the difference that their transfer function is purelin, (of the form y = m*x* + c), that the output layer is linear. Therefore, it is seen that the non-linearity in RBF nets is introduced due to the radial basis transfer function of the hidden layer neurons.

Limitations of ANN: The primary issue with ANNs is the network's mysterious operation. ANN sometimes provides a puzzling solution but doesn't explain why or how it works. The network becomes less reliable as a result.

2.5 Signal Processing techniques

Many researchers have used various methods of signal processing to monitor the health of electrical devices (vibration monitoring, current monitoring, etc.). Signal processing can be broken down into three primary subcategories to detect various faults: spectrum estimating techniques, time-domain approaches, and time-frequency estimation.

2.5.1 *Spectral Analysis*

Techniques for spectral analysis are frequently employed in machine diagnosis. Non-parametric, parametric, and high resolution approaches can all be used for spectrum estimation. Non-parametric techniques are based on optimal band pass analysis and Fourier analysis. The traditional Fourier analysis technique has been applied in this work. The Fourier analysis is described below.

$$x(t) = C_0 + \sum_{n=1}^{n} A_n \sin(n\omega_0 t) + B_n \cos(n\omega_0 t) \tag{2.21}$$

where, *x(t)* can be represented the instantaneous value of current waveform.

C_0= Average value of signal, ω_0 = Angular frequency of fundamental component = $\frac{2\pi}{T}$, *T* = Time period of the wave.

$$A_n = \frac{2}{T}\int_0^T e(t)sin(n\,\omega_0 t)dt \;, B_n = \frac{2}{T}\int_0^T e(t)cos(n\,\omega_0 t)dt \tag{2.22}$$

2.5.2 *Fast Fourier Transform (FFT)*

A signal is classified as discrete-time or counting-time and may be periodic or non-periodic in nature. The discrete signal is formed from a continuous-time signal by sampling. A signal can be represented

in both frequency domain and time domain formats. In the frequency domain, a signal has one or more frequencies. In order to simplify a complicated signal for analysis, frequency domain analysis is required. A signal's Fourier transformation converts it from time-domain to frequency-domain (spectrum) [72,73].

$$F(j\omega) = \int_{-\infty}^{+\infty} f(t)e^{-j\omega t}dt \quad \text{and} \quad f(t) = \frac{1}{2\pi}\int_{-\infty}^{+\infty} F(j\omega)e^{j\omega t}d\omega \qquad (2.23)$$

Discrete –Time Fourier Transform (DTFT):

$$X(e^{j\omega}) = \sum_{n=-\infty}^{+\infty} x[n]e^{-j\omega n} \quad \text{and} \quad x[n] = \frac{1}{2\pi}\int_{2\pi} X(e^{j\omega})e^{j\omega n}d\omega \qquad (2.24)$$

The discrete Fourier Transform (DFT) is able to convert from a time-domain into a frequency domain spectrum using Fourier series for finite length signals.

Assuming discrete signal of finite length sequence $\{x[n]\}_{n=0}^{N-1}$ DFT of the signal is a sequence $X[k]$ for k=0,….., (N-1) as given by :

$$X[k] = \sum_{n=0}^{N-1} x[n]e^{-2\pi jnk/N} \qquad (2.25)$$

The inverse DFT is given by:

$$x[n] = \frac{1}{N}\sum X[k]e^{2\pi jnk/N},\ n = 0.1, \ldots. (N\text{-}1) \qquad (2.26)$$

The Fast Fourier Transform reduces the complexity of the computation steps of the DFT by using an efficient algorithm. The number of multiplicants present has a major impact on the evaluation time for DFT. While DFT requires N^2 multiplication, FFT merely needs N log 2 (N).

Two discrete Fourier transformations of length N/2 are taken into consideration by the FFT method, which is its main benefit. This decomposition can be applied repeatedly until only discrete Fourier transforms of individual points are left if N is a power of 2.

Rewriting $X[k] = \sum_{n=0}^{N-1} x[n]e^{-2\pi jnk/N}$ as $X[k] = \sum_{n=0}^{N-1} x[n]W_N^{nk}$, It is simple to see that as the computation moves forward, the identical values of W_N^{nk} are calculated numerous times. Thus, two N/2-point transforms, one on event input data and the other on odd input data, can be used to produce an N-point DFT.

2.5.3 *Time-frequency analysis (Wavelet)*

FFT can't be used to analyze non-stationary signals. The most popular method for analyzing non-stationary signals is time-frequency analysis, and STFT can be employed in these circumstances. However, STFT has a drawback in that it consistently delivers resolution for all frequencies when

analyzing the entire signal within the same frame. The disadvantage of FFT and STFT is typically solved by using the wavelet transform [74]. The MRA gave rise to the wavelet transform, which computes the wavelet decomposition of the signal from its best scale approximation and is recognized for its ease of use and recursive filtering process. For a variety of reasons, the wavelet transform has recently emerged as one of the most promising mathematical techniques for signal processing. It has gained widespread acceptance in machine fault analysis for signal decomposition into a set of basic functions with variable window size; the basis functions are known as wavelets. It is possible to create the basis by stretching and compressing the "mother" wavelet ψ (t) [75,76].

$$\psi_{t,T}(t)=\frac{1}{\sqrt{S}}\psi\left(\frac{t-T}{S}\right) \qquad (2.27)$$

Here, "S" and "t" are the scaling and shifting parameters, respectively. The wavelet transform is separately computed for different time-domain signal segments at different frequencies. Wavelet coefficients are obtained, at the first level of signal decomposition by applying a mother wavelet. The repetition of this process depends on the scaling and translation of the mother wavelet. The mother is named due to fact that formation is the basis for various processes of transformation. A mother wavelet can be imagined as a windowed function that moves or shifts along the signal of a time-series from the time t = 0 to t =T. In the window, the portion of the signal is multiplied by the mother wavelet, and then it is integrated over all times to get the wavelet coefficients. The wavelet family is typically seen as the one that is most suitable for a given application since it can represent that signal with the fewest number of coefficients feasible. Every application would have one mother wavelet that would be most suited to it. Wavelet theory attempts to decompose spectra into high and low frequency content in an unusual way in order to simplify information extraction processes. Discrete or continuous wavelet transforms are also possible. Although the discrete signal is more effective with less computing time and fewer parameters than the continuous wavelet transform, it also requires more computation time [77]. DWT divides the signal into a collection of wavelet basis functions that are orthogonal to one another.

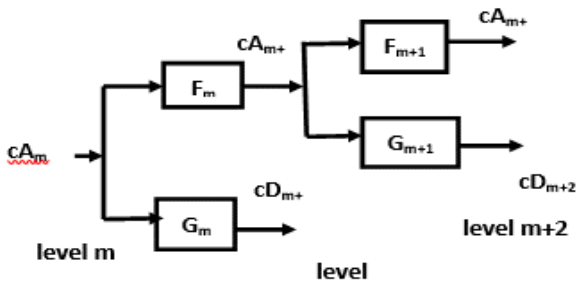

Figure 2.3: *Schematic diagram of the m-th level wavelet decomposition [162]*

The mother wavelet is the original function, and the wavelet functions are scaled, translated, and dilated versions of this original function. There are different mother wavelet functions (Daubechies (db), Symlets (Sym), Coiflets (Coif)) that are used for different fault detection in the machines. The results of DWT-based decomposition are useful data contained in "approximate" and "details" parts, as shown in Fig. 2.3 [78]. The high frequency signal components are referred to as “detail”, while the low frequency signal components are referred to as “approximate”. When computing the "n"-level decomposition, higher detail parts are removed, which reduces the overall frequency of the resulting data. The DWT is implemented in this work to decompose a current signal into scales with resolutions of different time and frequency using a multi-resolution signal decomposition algorithm.

2.5.4 *Cross Correlation of time series signals*

The auto-correlation measures the similarity between a signal and its shifted version. The auto-correlation gauges how similar a signal is to its shifted counterpart. The cross-correlation gauges the similarity between two signal types that are wholly different. Let *x(t)* and *y(t)* denote a pair of real-valued signals. Then the cross- correlation function of this pair of signals is defined as

$$R_{xy}(t) = \int_{-\infty}^{\infty} x(t).y(t-\tau)dt \tag{2.28}$$

where τ is the time lag.

If the two signals *x(t)* and *y(t)* are somewhat similar, then the value of the cross-correlation function $R_{xy}(\tau)$ will be finite over some range of τ. Thus, cross-correlation gives the measure of similarity or coherence, between them [79]. If the signals *x(t)* and *y(t)* have complex values, the cross correlation is defined as follows [80]:

$$R_{xy}(\tau) = \int_{-\infty}^{\infty} x(t).y^{*}(t-\tau)dt \tag{2.29}$$

It is important to note that if the two signals x(t) and y(t) are similar, the value of $R_{xy}(\tau)$ will be finite. If $R_{xy}(\tau)$= 0, then the two signals will not have any similarity between them. The cross-correlation coefficients are the data samples (amplitude vs. time) of a cross-correlated signal.

Chapter 3

Fault Classification using Multivariate Statistical Analysis

Early fault detection in induction machines is essential to reduce downtime costs caused by unscheduled shutdown of the motor. It is also essential to protect the motor and increase the lifetime of the machine component. In this work, a novel mechanism for anticipating and categorising the problem has been developed. Three motors with three distinct loading circumstances and six different known types of faults, including one healthy motor, were used to gather three phase stator currents (amplitude vs. time). Fault classifications have been performed for both the time domain and the frequency domain both.The stator currents have been transformed by the fast Fourier transform (FFT) method. The principal components have been computed on raw data as well as the FFT spectrum. The relative distances have been calculated from scatter plots of different faulty machines and a scatter plot of unknown faulty machines. Comparing the distance matrices, the unknown faults have been authenticated following the minimum distance to the nearest neighbourhood criterion. Comparing two types of scatter plots, one using PCA of raw data and the other using PCA of the FFT spectrum, it has been concluded that the sensitivity of the FFT spectrum PCA yields is better.

3.1 Introduction

Unscheduled shutdowns due to machine failure can cause enormous costs and reduce component life. Early fault detection of induction motors has become very necessary to reduce downtime costs and increase component lifetime. MCSA is a useful technique that is used to localise abnormal conditions in the motor using stator current spectral analysis. With the help of stator current signature analysis, different electrical and mechanical faults (different bearing problems, rotor misalignment, rotor broken bar, and other mechanical faults) can be detected [81–84]. Electrical signals are cheaper, simpler, and easier to measure and store than other types of signals (e.g., vibration, acoustic, etc.), so maintenance costs can be reduced by applying this technique. A pattern recognition technique has been used to detect a broken rotor bar fault in an induction motor using ‘K-Nearest Neighbors’ after extracting the features from current signals [85]. Using "K-Nearest Neighbors" to extract features from current waveforms, three types of faults in induction motors have been classified [86]. The nearest neighbour algorithm has been used with sequence component analysis for online stator fault analysis of rotating machines [87]. The nearest neighbour algorithm has been used to detect faults in current signals in the time domain, but it has not been used to detect faults in the time and frequency domains to compare the sensitivities of the two domains. This chapter discusses a feature extraction technique based on the FFT spectrum and, as a result, principal component analysis (PCA). The purpose of feature selection is to choose pertinent features that enable an accurate description of the defective condition and, as a result, defect classification, diagnosis, and prognosis. Feature extraction

procedures are used to extract the information from each fault condition [88]. These procedures allow for the determination of a machine's health status. It was created to make input features less dimensional for both supervised and unsupervised classification applications, and it can be used to choose features for machine fault classification. In this work, PCA was applied to three phase stator current samples as well as FFT spectrum samples to improve the accuracy of fault classification.

3.2 Experimentation and Data Acquisition

We have carried out the experimentation in the laboratory to capture three phase current signals under six different faulty induction motors and one healthy motor. The rating of each motor is 1 HP, 2 poles, and 60 Hz. Each known faulty motor's data was collected six times under three different loading conditions. A picture of a laboratory has been shown in Fig. 3.1(a), where experiments have been carried out. The data acquisition system has been represented by the block diagram shown in Fig. 3.1(b); where the current signals are captured independently by a three phase power analyzer (Yokogawa WT 500) under three loading conditions. This ensures that variations in loading conditions are accounted for. The maximum inputs of the Yokogawa WT 500 are 40 A_{rms} and 1000 V_{RMS}. Hall effect current sensors are used in this system because they allow the precise measurement of currents, providing accurate phase-shift information. The data samples from the unknown faulty motors are also collected six times at a time interval of 5 to 6 minutes, under three different loading conditions. The WT Viewer software is used on the PC to convert the current waveforms to numerical values, and the 1002 data samples of each phase current are stored in a "CSV" file format. 1002 samples are discovered in 50 milliseconds, or 20,040 samples per second. These induction motors' data are gathered under three different loading scenarios, including:

Loading condition 1: The motor is first operated in the no-load condition, that is, with no mechanical load attached to the motor shaft.

Loading condition 2*:* As there is no electrical load linked to the generator and simply a DC generator (0.75 kW) coupled to the motor, the generator is free to operate at no load.

Load condition 3: Finally, the generator is subjected to a 200 W electrical demand, (while the full load of the generator is 750 W. As a result, 200 W of additional electrical demand is applied to the motor while the generator operates as a mechanical load.

(a)

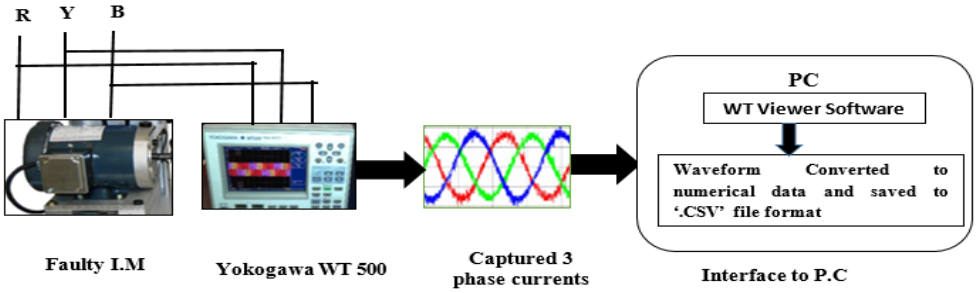

(b)

Figure 3.1: *(a) Experimental setup [18] and (b) block diagram of data acquisition from experimental setup.*

3.3 Methods

Harmonics are detected in the phase currents of the stator if an induction machine defect (mechanical or electrical) occurs. FFT is usually used to find out the spectra of stator currents (three-phase). The primary goal of this research is to identify an unidentified defect utilising raw sensor current data samples and FFT spectrum samples. The PCA transformation over stator current data and the stator current FFT spectrum are used to extract the characteristic features of known fault types. It was determined which type of analysis is more sensitive by comparing the relative distances among PCA scores of fault features in both cases. The methods are explained below.

3.3.1*Principal Component Analysis (PCA)*

An unsupervised multivariate statistical method known as principal component analysis alters the initial data received from an experiment in order to extract features and decrease dimensions. It is a linear dimensionality reduction technique that successfully reduces data dimensions without significantly reducing information [89]. PCA can also be used to compress data without sacrificing its usefulness. A subspace modelling technique known as PCA transforms the original data along a few chosen principal component directions that are orthogonal to one another and along which the data variability is greatest. The details about PCA with mathematical expression have been discussed in Chapter 2.

The features are extracted by PCA from the captured current signals of each induction motor in the time domain, after that, the FFT spectra of the current signals are computed, and again, the features are extracted from the spectra using PCA. The dimensions are reduced to two for each phase of each type of motor in both domains.

3.3.2 *Fast Fourier Transform (FFT)*

The Fourier transform can be used to convert a time-domain signal to a frequency-domain signal. For the purpose of easier analysis, a complex signal must be divided into simpler components using frequency domain analysis. This technique has been described in brief in Chapter 2. The FFT spectrum of each phase current signal of each induction motor has been computed by the FFT algorithm, and after that, features are extracted from the spectrum of each phase current signal by PCA transformation. Two principal components of the spectrum of each phase contain relevant feature information for each type of motor.

3.3.3 *Nearest distance neighbourhood*

A classification tool that is widely used to classify unknown data among multiple trained and known classes is nearest neighbour. The details about this technique have been described in Chapter 2. Euclidean distances are computed from an unknown class to each known class, and the unknown class is identified depending on the minimum value of the distance. Three unknown faults have been classified using the "nearest neighbor" neighbourhood classification method. Each fault will be authenticated if the detected classes for all three phases are the same.

3.4 Result and Discussion

The data samples of three-phase currents (amplitude vs. time) are collected from six known types of faulty induction motors (broken rotor bars (BR), rotor misalignment (RM), faulty bearings (FB), rotor unbalance (RU), single-phase voltage unbalance (VU), stator winding fault (SF)) and one healthy motor (HM) under three loading conditions as discussed in Section 3.2. Current data samples from three induction motors with three unknown faults are also randomly collected under three different loading conditions. In this work, PCA was applied for feature extraction from three phase stator currents as well as the FFT spectrum of currents from each motor to compare fault classification in time and frequency domains both. The classifications are performed in the time domain first, then in the frequency domain. The fault features are extracted from current data samples using PCA transformation, and the two Eigenvectors corresponding to the largest eigenvalues of each phase current of a motor are referred to as principal components (PC1 and PC2), which are significant features of each known and unknown type of fault. Three PC plots of each phase of each motor have been considered as one class, and the Euclidean distance of the PC score for a data set of unknown type with respect to all the PC values of known faults is then computed under three loading conditions

(Table 3.1–3.3). Using the "nearest neighborhood minimum distance classification rule," the unknown fault has been classified phase wise. Each unknown fault has been authenticated if the classification results for all three phases are the same.

The FFT spectra are computed from the stator's current data set (known and unknown types of faults), and data samples are taken (amplitude vs. frequency) from the spectra. In a similar manner, PCs are computed for three phases. The three phase known and unknown PC scores are plotted for both cases (i.e., the stator current data set and the FFT spectrum of the stator current data set) (Fig. 3.3a, b). Then, the Euclidean distance between each PC value for known defects and the unknown type of data set is calculated. The unknown fault has been verified using the nearest neighborhood minimum distance categorization rule. PCA transformation of stator current data for all phases and FFT spectra of stator currents for all phases were used to validate the unknown-type faults. The three unknown faults resemble a broken rotor bar, a stator winding fault, and a faulted bearing because the broken rotor bar, the stator winding fault, and the faulted bearing are the fault types where the minimum relative distances of unknown fault circumstances occur in three phases for all loading conditions.

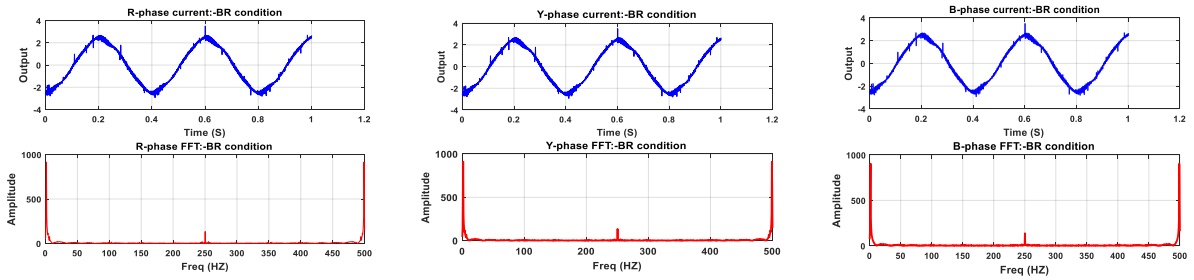

(a) (b) (c)

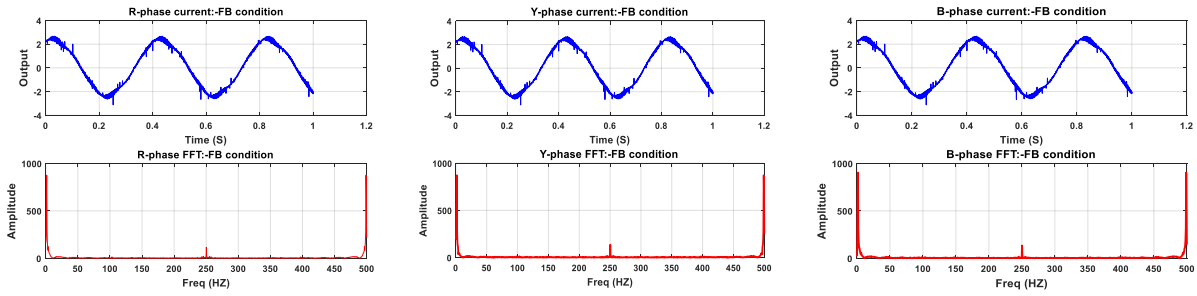

(a) (b) (c)

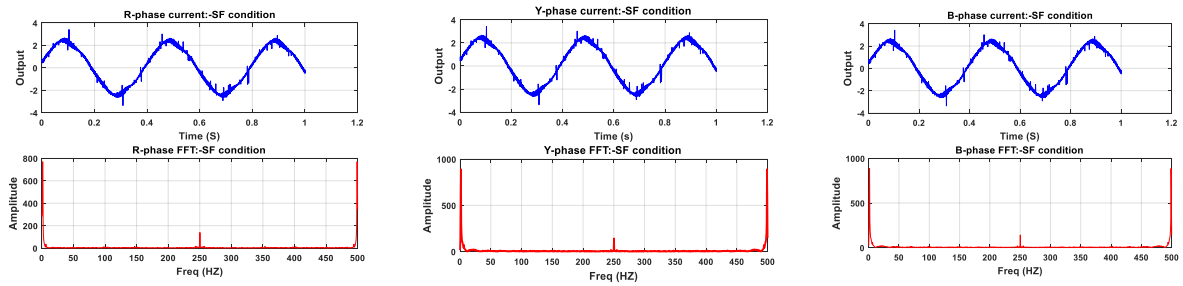

(a) (b) (c)

Figure 3.2*: Current signals in time domain and frequency domain of three faulty induction motors (Broken rotor bar(BR), Faulted bearing(FB), Stator winding fault(SF)) under loading condition 1 for (a) R phase (b) Y phase (c) B phase*

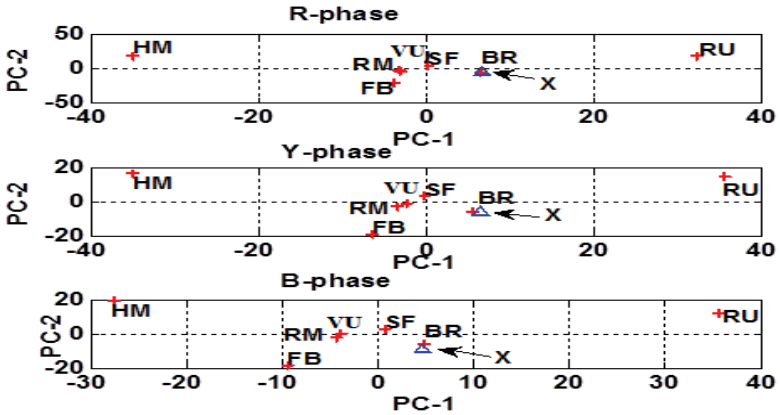

Figure 3.3*: (a) PCA scatter plot of stator current data under loading condition 1, unknown 1=X [18]*

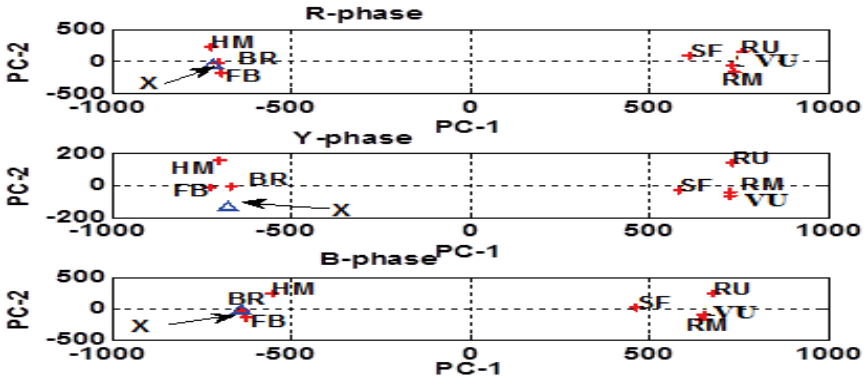

Figure 3.3: *(b) PCA scatter plot of FFT spectrum of stator current data under loading condition 1, unknown 1=X [18]*

**Note: HM (Healthy motor), BR= Bowed rotor, FB= Faulted bearing, RM=Rotor misalignment, RU=Rotor unbalance, VU=Single phase unbalance voltage, SF=Stator winding fault.*

Table 3.1: (a) Relative distances from PCA values of R phase of three unknown type fault to other known type faults under loading condition 1

Unknown Type	Fault Types						
	BR	**FB**	**RM**	**RU**	**SF**	**VU**	**HM**
Unknown 1	**7.22 e-01**	2.32 e+01	1.04 e+01	3.56 e+01	1.17 e+01	1.03 e+01	1.11 e+02
Unknown 2	1.16 e+01	2.93 e+01	9.74 e+00	3.60 e+01	**8.24 e-01**	49.8117	1.27 e+02
Unknown 3	1.85 e+01	**4.59 e+00**	1.61 e+01	5.38 e+01	2.61 e+01	1.86 e+01	1.28 e+02

Table 3.1: (b) Relative distances from PCA values of Y phase of three unknown type fault to other known type faults under loading condition 1

Unknown Type	Fault Types						
	BR	**FB**	**RM**	**RU**	**SF**	**VU**	**HM**
Unknown 1	**1.12e+00**	2.22e+01	9.52e+00	3.82e+01	1.06e+01	8.20e+00	1.18 e+02
Unknown 2	1.17e+01	2.76e+01	8.17e+00	3.92e+01	**6.88e-01**	5.01e+00	1.28 e+02
Unknown 3	1.82e+01	**5.10e+00**	1.52e+01	5.54e+01	2.35e+01	1.82e+01	1.34 e+02

Table 3.1: (c) Relative distances from PCA values of B phase of three unknown type fault to other known type faults under loading condition 1

Unknown Type	Fault Types						
	BR	**FB**	**RM**	**RU**	**SF**	**VU**	**HM**
Unknown 1	**1.82e+00**	2.61e+01	9.92e+00	4.16e+01	1.76e+01	9.30e+00	1.48 e+02
Unknown 2	1.36e+01	2.97e+01	9.28e+00	4.12e+01	**7.18e-01**	7.03e+00	1.32 e+02
Unknown 3	2.41e+01	**5.01e+00**	1.63e+01	6.23e+01	2.89e+01	2.03e+01	1.68 e+02

Table 3.2: (a) Relative distances from PCA values of R phase of three unknown type fault to other known type faults under loading condition 2

Unknown Type	Fault Types						
	BR	**FB**	**RM**	**RU**	**SF**	**VU**	**HM**
Unknown 1	**1.5995**	22.8884	3.9768	94.5027	103.1037	68.1374	113.6055
Unknown 2	100.7058	92.9978	101.0687	25.0383	**1.2066**	61.3489	128.2452
Unknown 3	20.5799	**1.4531**	24.806	81.9012	95.0497	49.8117	129.1329

Table 3.2: (b) Relative distances from PCA values of Y phase of three unknown type fault to other known type faults under loading condition 2

Unknown Type	Fault Types						
	BR	**FB**	**RM**	**RU**	**SF**	**VU**	**HM**
Unknown 1	**1.2146**	20.6001	5.9223	93.8975	103.7712	68.1018	118.3885
Unknown 2	104.0263	95.707	105.0827	25.404	**1.0802**	62.3524	128.5818
Unknown 3	22.8048	**1.3976**	27.4239	81.307	95.9015	49.7853	134.1191

Table 3.2: (c) Relative distances from PCA values of B phase of three unknown type fault to other known type faults under loading condition 2

Unknown Type	Fault Types						
	BR	**FB**	**RM**	**RU**	**SF**	**VU**	**HM**
Unknown 1	**1.3727**	22.2749	4.5784	92.2276	101.5424	67.2517	106.9484
Unknown 2	104.2143	95.9654	104.8171	26.6206	**2.0132**	64.749	121.6411
Unknown 3	21.6528	**1.1784**	26.5209	79.1638	93.0589	48.1048	122.915

Table 3.3: (a) Relative distances from PCA values of R phase of three unknown type fault to other known type faults under loading condition 3

Unknown Type	Fault Types						
	BR	**FB**	**RM**	**RU**	**SF**	**VU**	**HM**
Unknown 1	**1.4127**	132.254	46.4182	19.303	124.7827	134.3813	50.2508
Unknown 2	122.1216	63.6129	136.2424	133.0553	**1.4758**	52.6507	166.808
Unknown 3	130.0075	**1.038**	121.1312	131.8791	63.453	13.7633	159.7195

Table 3.3: (b) Relative distances from PCA values of Y phase of three unknown type fault to other known type faults under loading condition 3

Unknown Type	Fault Types						
	BR	**FB**	**RM**	**RU**	**SF**	**VU**	**HM**
Unknown 1	**0.9615**	138.5961	42.5756	11.631	131.0308	138.0494	44.5876
Unknown 2	132.676	54.7301	143.044	135.9958	**1.2245**	42.8111	165.8662
Unknown 3	141.0888	**2.1089**	133.7722	139.4481	57.3165	14.1496	160.9616

Table 3.3: (c) Relative distances from PCA values of B phase of three unknown type fault to other known type faults under loading condition 3

Unknown Type	Fault Types						
	BR	**FB**	**RM**	**RU**	**SF**	**VU**	**HM**
Unknown 1	**2.2566**	142.2153	46.9363	22.2264	123.1654	141.9167	57.9345
Unknown 2	124.3279	63.4372	132.7063	127.2282	**2.2092**	49.847	166.8238
Unknown 3	141.9026	**1.407**	129.4168	135.6758	60.2704	14.158	166.1579

Table 3.4: (a) Relative distances from PCA values(FFT spectrum of current) of R phase of three unknown type fault to other known type faults under loading condition 1

Unknown Type	Fault Types						
	BR	**FB**	**RM**	**RU**	**SF**	**VU**	**HM**
Unknown 1	**1.02e+01**	1.91e+02	1.45e+03	1.47e+03	1.32e+03	1.43e+03	2.23 e+02
Unknown 2	1.33e+03	1.34e+03	2.97e+02	1.70e+02	**9.37e+00**	2.08e+02	1.77 e+03
Unknown 3	1.57e+02	**2.22e+01**	1.43e+03	1.49e+03	1.33e+03	1.44e+03	1.69 e+02

Table 3.4: (b) Relative distances from PCA values(FFT spectrum of current) of Y phase of three unknown type fault to other known type faults under loading condition 1

Unknown Type	Fault Types						
	BR	**FB**	**RM**	**RU**	**SF**	**VU**	**HM**
Unknown 1	**2.09e+01**	8.08e+01	1.39e+03	1.42e+03	1.25 e+03	1.40e+03	9.21e+01
Unknown 2	1.25e+03	1.32e+03	1.49e+02	2.87e+02	**2.03 e+01**	1.63e+02	1.43e+03
Unknown 3	5.62e+01	**2.59e+01**	1.45e+03	1.48e+03	1.31 e+03	1.46e+03	2.76e+01

Table 3.4: (c) Relative distances from PCA values(FFT spectrum of current) of B phase of three unknown type fault to other known type faults under loading condition 1

Unknown Type	Fault Types						
	BR	**FB**	**RM**	**RU**	**SF**	**VU**	**HM**
Unknown 1	**7.77e+00**	1.39e+02	1.30e+03	1.35e+03	1.11 e+03	1.30e+03	1.57e+02
Unknown 2	1.10e+03	1.11e+03	3.04e+02	3.20e+02	**7.47 e+00**	2.46e+02	1.23e+03
Unknown 3	1.10e+02	**1.76e+01**	1.28e+03	1.38e+03	1.13 e+03	1.29e+03	1.41e+02

Table 3.5: (a) Relative distances from PCA values(FFT spectrum of current) of R phase of three unknown type fault to other known type faults under loading condition 2

Unknown Type	Fault Types						
	BR	**FB**	**RM**	**RU**	**SF**	**VU**	**HM**
Unknown 1	**15.594384**	137.3293	60.03621	102.8263	190.1004	204.5873	1429.081
Unknown 2	198.273	95.49092	158.0512	132.9904	**14.48992**	68.00124	1517.934
Unknown 3	145.8354	**13.73308**	93.04992	53.52567	79.06988	56.99151	1433.986

Table 3.5: (b) Relative distances from PCA values(FFT spectrum of current) of Y phase of three unknown type fault to other known type faults under loading condition 2

Unknown Type	Fault Types						
	BR	**FB**	**RM**	**RU**	**SF**	**VU**	**HM**
Unknown 1	**13.846215**	419.4571	433.3394	418.9174	402.7677	494.9936	614.5629
Unknown 2	499.2253	191.71147	108.4283	122.79723	**16.649359**	131.2715	817.9604
Unknown 3	515.313	**14.95786**	99.18573	59.98965	181.10605	117.5465	822.1678

Table 3.5: (c) Relative distances from PCA values(FFT spectrum of current) of B phase of three unknown type fault to other known type faults under loading condition 2

Unknown Type	Fault Types						
	BR	**FB**	**RM**	**RU**	**SF**	**VU**	**HM**
Unknown 1	**16.40869**	50.2007	101.354	66.83551	87.23706	64.54736	1041.903
Unknown 2	69.21398	113.7942	43.01786	83.20518	**14.8953**	45.40862	992.6587
Unknown 3	71.21319	**18.06855**	145.5587	103.9796	143.035	64.18779	1101.064

Table 3.6: (a) Relative distances from PCA values(FFT spectrum of current) of R phase of three unknown type fault to other known type faults under loading condition 3

Unknown Type	Fault Types						
	BR	**FB**	**RM**	**RU**	**SF**	**VU**	**HM**
Unknown 1	**12.94382**	49.72954	101.721	67.09038	87.75611	64.73262	1042.368
Unknown 2	69.06098	113.5819	42.74768	37.73544	**13.74379**	44.92019	993.1027
Unknown 3	72.1	**16.97086**	146.5902	104.9144	144.117	65.194	1102.046

Table 3.6: (b) Relative distances from PCA values(FFT spectrum of current) of Y phase of three unknown type fault to other known type faults under loading condition 3

Unknown Type	Fault Types						
	BR	**FB**	**RM**	**RU**	**SF**	**VU**	**HM**
Unknown 1	14.81389	137.5778	60.345	103.1495	190.1215	204.7745	1429.621
Unknown 2	198.7243	95.26474	158.2755	132.8926	15.50021	67.02383	1517.244
Unknown 3	146.1343	13.26528	93.26595	53.53943	79.80715	57.09818	1433.153

Table 3.6: (c) Relative distances from PCA values(FFT spectrum of current) of B phase of three unknown type fault to other known type faults under loading condition 3

Unknown Type	Fault Types						
	BR	**FB**	**RM**	**RU**	**SF**	**VU**	**HM**
Unknown 1	12.59438	137.3293	60.03621	102.8263	190.1004	204.5873	1429.081
Unknown 2	197.9189	94.92545	157.5977	132.4495	14.54769	67.46773	1517.324
Unknown 3	146.5485	15.52943	93.72269	54.0832	79.27418	56.52175	1433.617

**Note: Loading condition 1: No Mechanical load, Loading condition 2: With D.C. generator as a mechanical load, Loading condition 3: 200 Watt electrical load connected to the generator (while full load of the generator is 750 W)*

According to the results tabulated in Tables 3.1-3.3 and 3.4-3.6, the relative distance metrics between the PCA score of an unknown type and the other known types are much less than that of the PCA score of the stator current spectrum. Applying this technique, unknown faults have been discovered in all cases where the minimal relative distances of unknown fault conditions exist with respect to known type faults. The relative distances of the PCA spectrum are greater than the relative distances of the raw data PCA value of stator currents, as shown in Tables 3-5 and 6-8.Thus, it may be concluded that feature extraction by PCA transformation of spectra is much more efficient and sensitive than that by PCA transformation of simple original data.

Chapter 4

Fault Classification using SVM and DDAG

This work attempts to develop a robust support vector machine (SVM)-based fault classification scheme for induction motors. Five different kernels, viz., linear, quadratic, polynomial, radial basis, and sigmoidal, are inspected using both the time and frequency domain signals of the three fault currents, and their classification performances are compared. Significant features were extracted in subspace using principal component analysis (PCA) in both the domains for six faulty induction motors, three unknown faulty motors, and one healthy motor. This multiclass classification problem was reformulated as a combined binary classification problem using the decision-directed acrylic graph (DDAG) algorithm to classify faults. To incorporate robustness into the classifier, each fault is authenticated by taking into account all three phases of current for three different loadings. Results revealed that the radial basis function based classifier evolved out to be the most effective among the SVM kernels, considering both time and frequency domain features, with classifier accuracy reaching almost 100% with FFT spectrums; hence, it was found to be optimal compared to the rest. Further, linear regression has been applied over the linear kernel function to authenticate faults.

4.1 Introduction

Identification and classification of faults in induction motors are important for the smooth operation of the system and the longevity of the motor. Besides, identification of the fault is important for elimination of the faulted portion and replacement of the same for fast restoration of the system and reliability of operation. Due to the richness and variability of signals, direct classification of different fault patterns is impossible. Pattern recognition is an unsupervised classification method that uses an algorithm to automatically recognise familiar patterns in unknown data quickly and accurately [90–92]. An artificial intelligence based fault diagnosis system for rotating machines is gaining popularity due to its robustness and adaptive capability [93]. Several AI techniques have been proposed for fault classification of rotating machines over the past few years, such as expert systems [94], fuzzy logic [95], the hybrid FMM-CART model [96], artificial neural networks (ANNs) [97–99], and adaptive neuro-fuzzy inference systems [100, 101]. However, these methods have some limitations in their applications in real scenarios due to their local optimal solution, over-fitting, and low convergence rate [102]. When used to analyse the small training sample, these approaches likewise have low generalization. In the real world, the experts deal with several classes of faults for the fault classification of rotating machines. Multi-class problems can also be handled by ANN, but the system has some defects due to its complicated network, unstable network structure, and long training time [103]. SVMs do not have this type of problem, which is easier to understand, and the different kernels

of SVM provide a different level of flexibility. SVM has been developed for two class classification problems, but it can be applied to multiclass problems [104]. SVM surpasses ANN in classification and has better generalization performance, allowing it to generate decisions that are trustworthy for small samples of data [105]. The multiclass problem can be solved using two important algorithms in the SVM principle: "One Against One" (OAO) and "One Against All" (OAA).The OAO strategy is more suitable, more modular to speed up the decision making process by combining with other classifiers [106]. The OAO SVM is ineffective at classifying data because the number of SVMs grows super-linearly with the number of classes, and its evaluation time is lengthy if there are more than two classes. The drawbacks of OAO SVM can be solved by a decision-directed acyclic graph (DDAG), which removes the uncertainty of unknown data classification in pair wise classification because the data is classified depending on the maximum voting count of membership classes and maintains accuracy while reducing training and evaluation time [107]. The two steps of the common fault diagnosis system are feature extraction and fault recognition [108]. The feature vectors are the input for the AI-based classifiers that identify faults. PCA (Principal Component Analysis) has been used to extract relevant fault features from current signals, which provides a way to improve prediction performance, better understand data in pattern recognition applications while reducing computation time [109, 110]. PCA has been applied before to extract features from vibration signals of rotating machines in the time domain, and SVM has been used for fault classification [111–113]. A bearing fault diagnosis system has been presented based on bi-spectral features from vibration signals using SVM and PCA [114]. According to the literature, SVM-PCA is used to detect faults in a specific component of a rotating machine by extracting features from vibration signals in either the time domain or the frequency domain using a single type of kernel. It has been discovered that a robust classification system for various types of fault patterns (electrical or mechanical) has not been developed, instead of one that uses various types of kernels in the space of time domain features of current signals and frequency domain features of current signals both. Electrical and mechanical faults can be identified using current signature analysis at low cost because it does not require multiple sensors [115–117]. The present manuscript aims to not only develop a robust classification system using SVM and DDAG for any type of fault identification in the time and frequency domains but also analyse the classification performances of different types of kernels. The classifications are performed with multiple kernels rather than one because kernel selection is critical in SVM and directly influences classification performance due to sample separability [118]. P. Gangsar and R. Tiwari investigated the necessity that fault prediction performance using SVM be load independent because finding test data and training data at the same load is not always possible [119], but fault classification has been performed in this work keeping the training data and test data at the same load.

In this work, the current signals of known, unknown faulty motors are collected at three different loads. For training the SVM-based classifiers, fault current signatures corresponding to broken rotor

bar, rotor misalignment, faulty bearing, rotor unbalance, single phase voltage unbalance, stator winding fault, and one healthy motor under different loading conditions were used. The frequency spectra of motor fault current change under time-varying speed conditions [120], so the frequency spectra of time-domain fault current signals are obtained using FFT. PCA was used to extract relevant features from three-phase current signals and separately extract from FFT spectra. These features are used to train the SVM using seven classes to perform the classification process. The fault classification algorithm is run for each phase, for each unknown class of fault, and for each loading condition. Linear, quadratic, polynomial, radial basis, and sigmoidal kernels are used individually to classify each unknown test sample phase-wise, and each kernel develops multiple classifiers for one phase using one vs. one SVM algorithm under one loading condition. The DDAG technique is used to make a graph structure, considering one classifier as a node, to classify the unknown data sample phase wise, accurately reducing evaluation time. The fault is authenticated if the classification results of the three phases are equal. Every nonlinear kernel (quadratic, polynomial, radial basis, and sigmoidal kernels) is able to authenticate three unknown faults in time domain based fault classification, but a linear kernel is unable to authenticate the unknown sample because the maximum number of membership classes have not been found in any particular class for all phases. The linear kernel, as well as the other nonlinear kernels, can authenticate each unknown fault in the frequency domain, and the classification accuracy of both linear and nonlinear kernels is higher in the frequency domain than in the time domain. The linearity of data samples of time domain features and the linearity of data samples of frequency domain features are calculated separately using the linear regression technique to understand the reason for the limitation of the linear kernel for fault classification in the time domain. Overall classification accuracies of both domains for three unknown fault classifications are compared under three loading conditions to select the best kernel among five for induction motor fault classification.

4.2 Dimension reduction and feature extraction by PCA

The work presented in this chapter uses principal component analysis (PCA) to extract features from the faulty signals. The mathematical expression of PCA has been described in Chapter 2, and the PCA algorithm has also been explained to describe how PCA is able to reduce the dimensions of extracted features. PCA is a statistical method that transforms the original data with high dimensions obtained from experiments to extract features and reduce dimensions. PCA has the inherent capability of reducing the dimension of a data set, preserving the most vital directions of variances in decreasing order of importance; thereby extracting the most important features from a multivariate data set. Besides, PCA requires less computational cost; and is therefore used widely in multivariate statistical analysis.

4.3 Feature extraction for classification in time domain and frequency domain

The description about the conversion of signal to frequency spectrum has been described in Chapter 2. Fault classifications have been performed using the features of current signals in the time and frequency domains separately. The current signals are collected in amplitude vs. time mode, after which PCA has been applied for feature extraction and dimension reduction for fault analysis in the time domain. PCA have also been applied to extract features from FFT spectrums of current signals. The two principal components (PC1 and PC2) comprise the precise fault characteristics of the current signal and the FFT spectrum of each defective motor phase. Utilizing several SVM kernels, each unknown data sample from each phase has been categorized.

4.4 Multiclass Classification by Pairwise SVM

SVM has been developed for a two class classification problem, but additionally, it permits categorising data points into two types using binary information. The same method is applied to multiclass classification after dividing the problem into numerous binary classification problems [121, 122].The feature space data obtained through PCA pre-processing is then trained by a pair-wise support vector machine (SVM) using the multiclass-OVO method. SVM is based on machine learning theory and provides a new method of classification with a small training sample [123].The multiclass SVM technique is very important to predict unknown faults among various types of faults.

For multiclass classification having '*k*' classes (*k*>2), the underlying principle is the classification into multiple binary classification problems, called a one-vs.-one (OVO) approach, A binary classifier per each pair of classes, which separates one class and other (*k*-1) classes respectively. However, in the SVM-OVO method, $\frac{k(k-1)}{2}$ number of hyperplanes separates each pair of classes [124]. The PCA scores of the unknown data are then classified using $\frac{k(k-1)}{2}$ times SVM nodes, which return either class 1 or class 2 as the output. The class results are then analysed using a confusion matrix. The results are further authenticated by evaluation method of Decision Directed Acrylic Graph (DDAG). Here, we have already explained the linear and nonlinear SVM classifiers required for the work presented in Chapter 2.The OVO SVM approach constructs possible all binary classifiers from n no of classes that are trained by pair of classes out of n classes, such that total $\frac{k(k-1)}{2}$ hyperplanes will result to separate each pair of classes. A graphical example has been shown in Fig. 4.1 to classify the unknown data sample 'X' among the four classes. There are 4(4-1)/2 = 6 classifiers which separate each pair of classes [125].

The element j is excluded from the list if $\mathbf{F_{ij}}$>0 after pair-wise (i.e., i and j class and $i \neq j$). SVM classification, and this procedure is repeated until the last one is left to classify X. The unknown data sample is classified into the class that corresponds to the element number. Thus It can be said that X

does not belong to class 4 if $\mathbf{F_{14}} > 0$, and hence, it may belong to the other three classes. $\mathbf{F_{12}} < 0$ does not belong to class 1. Thus, the remaining classes are class 2 and class 3. Again, it does not belong to class 3 as $\mathbf{F_{23}} > 0$; hence, it could be inferred that the unknown data sample belongs to class 2.

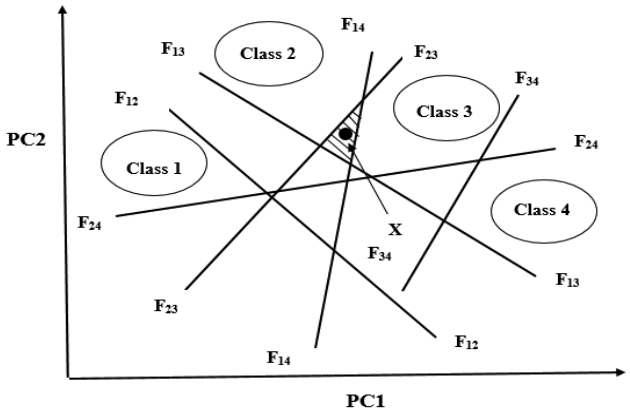

***Figure 4.1**: Pair-wise classification of unknown data point among multiple class*

4.5 Decision Directed Acyclic Graph (DDAG)

A decision-directed acyclic graph (DDAG) has been introduced to overcome the disadvantages of the OVO SVM algorithm. It is similar to pair-wise SVM classification [126]. The node in the structure of the graph, represents activity by a binary classifier out of the total number of binary classifiers: $\frac{k(k-1)}{2}$. Using the OAO method, $\frac{k(k-1)}{2}$ pairwise data sets are trained with SVM. For each pairwise training, the data set corresponding to one of the classes or groups is given class label 1, and the data set for the rest of the groups is given class label 2.

Following membership evaluation, the PCA score of the unknown faulty signal is tested against each SVM node in DDAG for detecting the class, as shown in Fig. 4.2. Each classifier provides one vote for its preferred class, and the final output is selected using the majority vote. One class will be selected as a final output when the DDAG is traversed from its root to its leaf at the bottom. The final output detect $k(k-1)$ number of decision classes for k class classification problem, which is the highest output value of the classifiers [127-129].

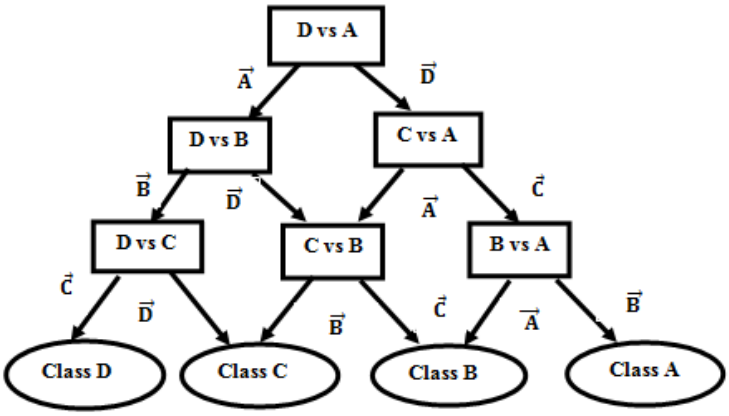

Figure 4.2: *Illustration of an approach for finding the best out of four classes using DDAG*

DDAG Algorithm:

There are two steps in DDAG algorithm:

A) Creation of triangular DDAG graph with computed confusion matrix.

B) Evaluation of membership counts of unknown PCA score with respect to each class.

A) Creation of triangular DDAG graph:

Input: Read total no. of classes, N

PCA score of known faulty signals, S (i , j), for i = 1,2,3,…., N; j = 1, 2

Read PCA score of unknown faulty signal, S_U [1, 2]

Output: DDAG graph, Confusion matrix, C (i , j), for i = 1,2, ….N ,; j = 1,2,…, N

---

i) For i = N to 2

ii) For k = 1 to N-1

iii) For binary SVM node, SVM (i-k)B, form the training data set :

Class -1: X1 = [S (3*,N,1) S (3*N,2; S (3*N-1,1) S (3*N-1,2); S (3*N-2,1) S (3*N-2,2)] ; T1 = [1; 1; 1]

Class-2: L = 1 + (k-1)*3

X2 = [S (L, 1) S (L, 2) ; S (L+1, 1) S (L+1, 2) ; S (L+2,1) S (L+2,2)];

T2 = [2; 2; 2]

iv) Set the kernel function to ‘linear’ or ‘polynomial’ or ‘quadratic’ or ‘radial basis ‘or ‘Sigmoid’.

v) Train SVM (i-k) node with given inputs, outputs and kernel function.

vi) Classify the unknown PCA score, S_U with trained SVM (i - k).

vii) Store the result of classification as 1 (true) or 2 (false) to C (i , k).

viii) End for

ix) End for

x) END

B) Evaluation of DDAG graph by membership count.

Input: Read total no of classes, N

Output: The membership counts of classification result of unknown w.r.t. known class classes, Count (1), Count(2)……Count(N)

---

i) Set i =N;

ii) Count – i = 0

iii) For j = 1 to i-1

iv) If (C(I , j) = = 1)

v) Count - i = Count – i +1

vi) End if

vii) End for

viii) For i = N-1 to 2

ix) Count-i = 0

x) For j = 1 to 2

xi) If (C (i , j)= =1)

xii) Count – i = Count – i +1

xiii) End if

xiv) End for

xv) If (C (i +1,j+1)==1)

xvi) Count – i =Count – i +1

xvii) End if

xviii) End for

xix) Count-1=0

xx) For i =4 to 2

xxi) If (C (i ,1)= =1)

xxii) Count - 1= Count - 1+1

xxiii) End if

xxiv) End for

.

4.6 Linear Regression

In this work, we have used linear regression to estimate *y* as per the following expression:

$$y - \bar{y} = b_{yx}(x - \bar{x}) \quad (4.1)$$

which is called the regression equation of the variable *y* on the variable *x*; and $b_{yx} = \frac{cov(x,y)}{\sigma_x^2} = r\frac{\sigma_y}{\sigma_x}$;

where, $cov(x, y)$ is the covariance between *x* and *y*. Similarly, the regression equation of *x* on *y* is

$$x - \bar{x} = b_{xy}(y - \bar{y}) \quad (4.2)$$

where, $b_{xy} = \frac{cov(x,y)}{\sigma_y^2} = r\frac{\sigma_x}{\sigma_y}$. Thus, substituting the values of b_{yx} and b_{xy}, the regression equations 4.1 and the equation 4.2 may also be re-written as

$$\frac{y-\bar{y}}{\sigma_y} = r\left(\frac{x-\bar{x}}{\sigma_x}\right) \text{ and } \frac{x-\bar{x}}{\sigma_x} = r\left(\frac{y-\bar{y}}{\sigma_y}\right) \quad (4.3)$$

Thus, both regression equations are satisfied when $x = \bar{x}$ and $y = \bar{y}$; implying geometrically that both the regression lines intersect at, the point ($\bar{x}$, $\bar{y}$). Typically, the two regression lines diverge but because they must always cross at ($\bar{x}$, $\bar{y}$), the line will be parallel when their slopes are equal, i.e., $b_{yx} = {}^{1}/_{b_{xy}}$ or, $b_{yx}.b_{xy} = 1$; i.e, $r^2 = 1$; or, $r = \pm 1$. Usually, the two regression equations differ from one another. However, when $r = 1$, they become identical, and in this situation, the variables have a perfect linear connection. Regression equations simplify to $y = \bar{y}$ and $x = \bar{x}$, when $r = 0$, making it impossible to estimate either *y* or *x* using linear regression equations.

4.7 Experimentation

The experiment has been done on the same set up as illustrated in Chapter 3. The three phase currents are collected from six separate induction motors in a motor fault simulator laboratory running under six different fault conditions, viz., broken rotor bars (BRB), rotor misalignment (RML), faulty bearings (FBR), rotor unbalance (RUB), single phase voltage unbalance (VUB), stator winding fault (SWF), and one healthy motor (HML). The data were collected three times, once from all the faulty induction motors and once from three induction motors with an unknown class of fault.

The experiment has been carried out with three separate loading conditions for the motors, in order to incorporate robustness into the design of the algorithm. The suggested approach has been developed and validated for the motor's three different loading conditions.

4.8 Methodology of algorithm development

In this work, six different fault current waveforms, as mentioned earlier, are collected from the induction motors as known fault classes, and those from the unknown class of faults are recorded randomly under three different loading conditions. Using FFT, which creates the fault current spectra from these time domain signals, the fault current signals in the time domain are further transformed

into the frequency domain. Then, using PCA, the fault features are derived from the time-domain current signals and the frequency-domain fault spectrum signatures. The two most vital eigenvectors, corresponding to the largest eigenvalues of each phase, denoted as the first and second principal components (PC1 and PC2) only, are considered in this work, as these are considered the most significant features of any signal. Three PC plots of each phase of each motor have been considered as one class, and each unknown type of fault has been classified phase wise using SVM. This paper investigates five different SVM kernels, including the linear kernel and four nonlinear kernels, namely quadratic, polynomial, radial basis, and sigmoid. This multiclass classification problem was reformulated as a combined binary classification problem using the decision directed acrylic graph (DDAG) algorithm to classify faults. The proposed model is further tested using three different loads on the motor in order to develop a robust classifier model. Each unknown fault has been authenticated if the classification results for all three phases are the same. The classification results are compared for different linear and nonlinear kernels to obtain the optimum kernel function in the present work.

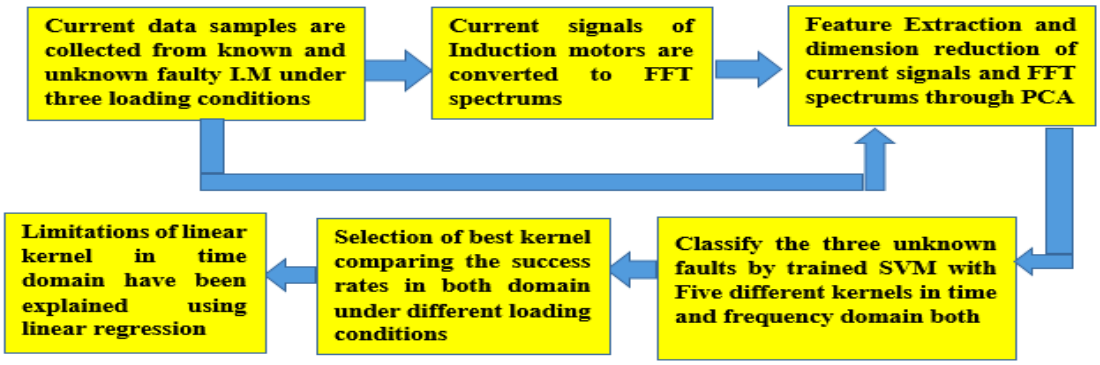

***Figure 4.3**: Work flow diagram of this work*

4.9 Result and Analysis

Three PC scores for each phase of seven different classes of motors, including six separately faulted motors, are labelled with their class numbers as: A-BRB, B-FBR, C-RML, D-RUB, E-SWF, F-VUL, and G-HMR, respectively. The PCA scores obtained on the analysis of the three-phase fault current signals are considered with respect to pairwise faults (e.g., taking BRB and FBR together), and these are trained with SVM. The presented SVM model separates the PCs corresponding to the two fault classes by a hyperplane (kernel trick). The PC score pair, i.e., PC1 and PC2, of one unknown fault is then tested with an SVM classifier. In a similar manner, the PCA score of the same unknown fault is tested with all seven pair-wise considered SVM classifiers in the 21 classification process (i.e., 7(7-1)/2 = 21). The 21 classifiers for seven classes in each phase are constructed by the OVO SVM algorithm. The 21 classifiers for R-phase have been shown in Figure 4.4 using the RBF kernel, when features have been extracted from time domain current signals under one loading condition. In the given subplots of each classifier, R1, R2, and R3 represent the PC values of the R-phase of one known

class of fault under three different loading conditions, considered as a single class of fault, and X is the PC plot of the same R phase of an unknown class of fault. 21 classifiers for the Y and B phases have also been developed similarly.

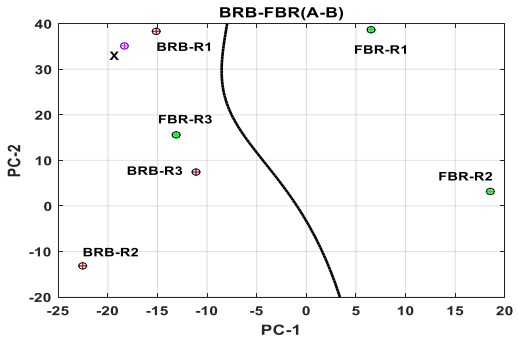

(a)

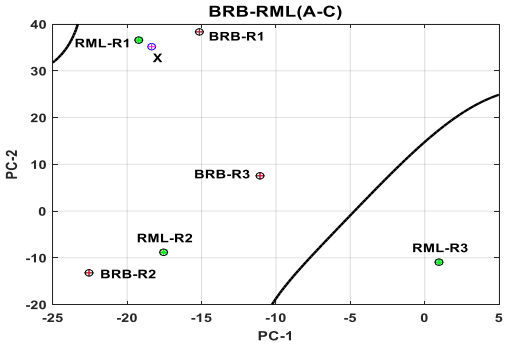

(b)

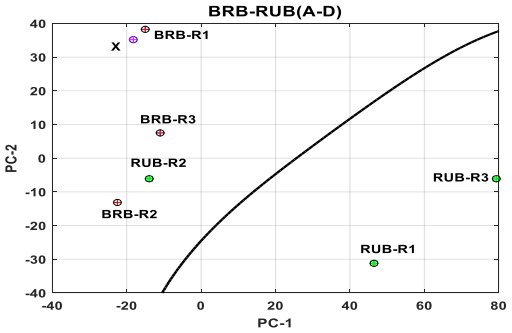

(c)

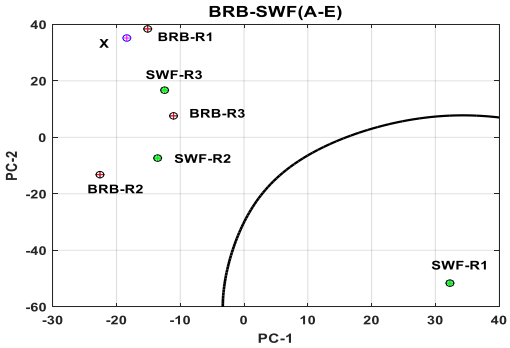

(d)

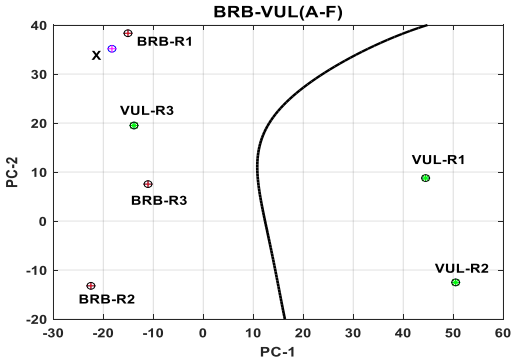

(e)

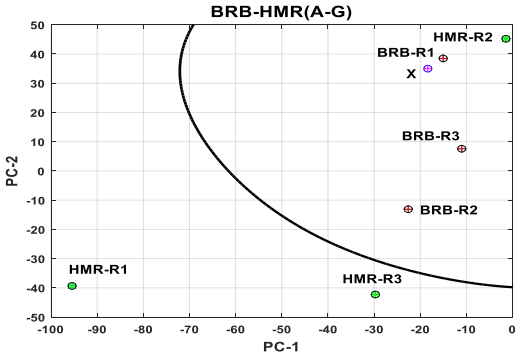

(f)

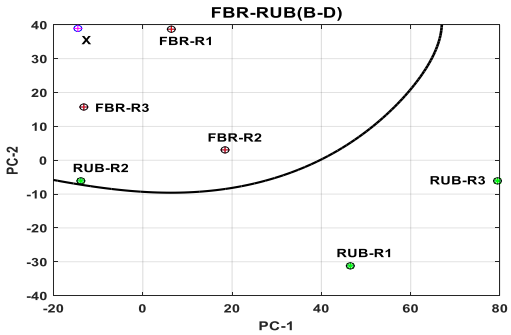
FBR-RUB(B-D)
X
FBR-R1
FBR-R3
FBR-R2
RUB-R2
RUB-R3
RUB-R1
PC-1
PC-2

(g)

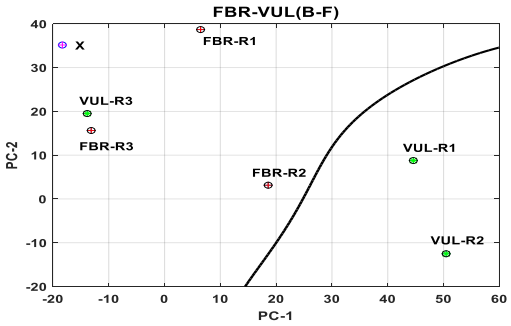
FBR-VUL(B-F)
X
FBR-R1
VUL-R3
FBR-R3
VUL-R1
FBR-R2
VUL-R2
PC-1
PC-2

(h)

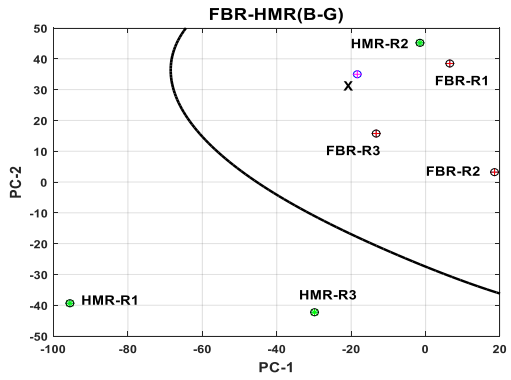
FBR-HMR(B-G)
HMR-R2
FBR-R1
X
FBR-R3
FBR-R2
HMR-R1
HMR-R3
PC-1
PC-2

(i)

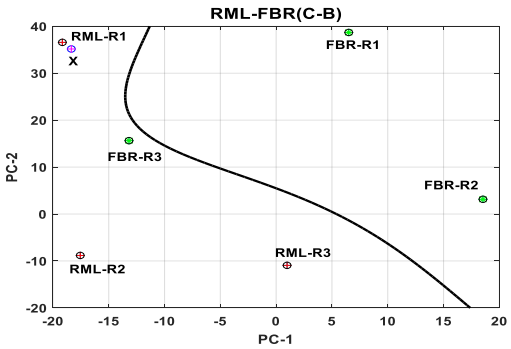
RML-FBR(C-B)
RML-R1
FBR-R1
X
FBR-R3
FBR-R2
RML-R3
RML-R2
PC-1
PC-2

(j)

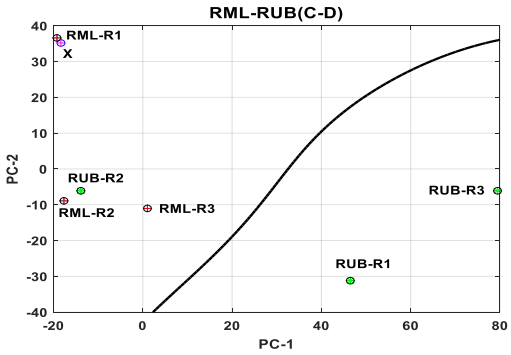
RML-RUB(C-D)
RML-R1
X
RUB-R2
RUB-R3
RML-R2
RML-R3
RUB-R1
PC-1
PC-2

(k)

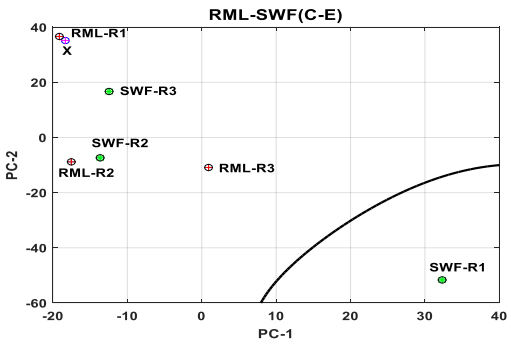
RML-SWF(C-E)
RML-R1
X
SWF-R3
SWF-R2
RML-R2
RML-R3
SWF-R1
PC-1
PC-2

(l)

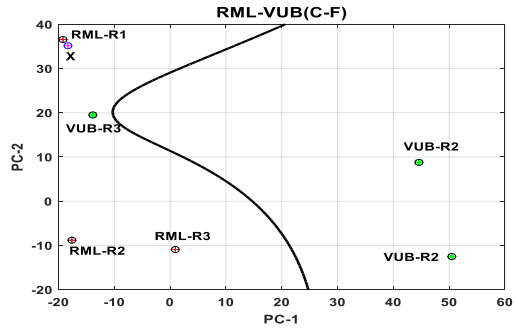
RML-VUB(C-F)
RML-R1
VUB-R3
VUB-R2
RML-R3
RML-R2
VUB-R2
PC-1
PC-2

(m)

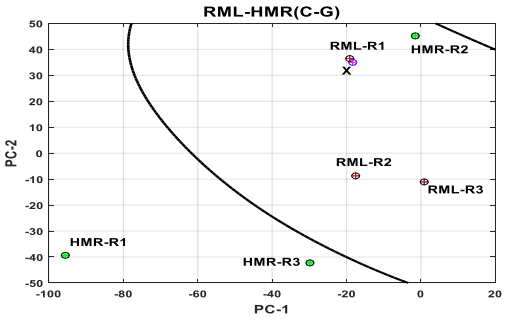
RML-HMR(C-G)
RML-R1
HMR-R2
RML-R2
RML-R3
HMR-R1
HMR-R3
PC-1
PC-2

(n)

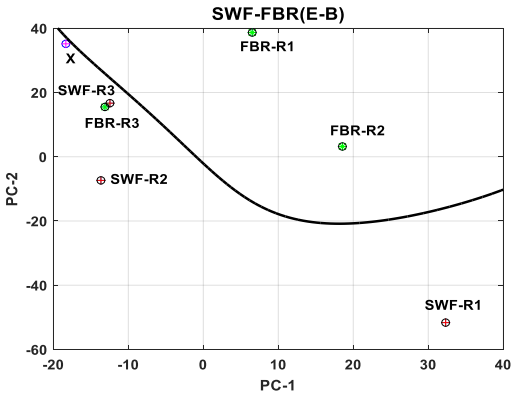
SWF-FBR(E-B)
FBR-R1
SWF-R3
FBR-R3
FBR-R2
SWF-R2
SWF-R1
PC-1
PC-2

(o)

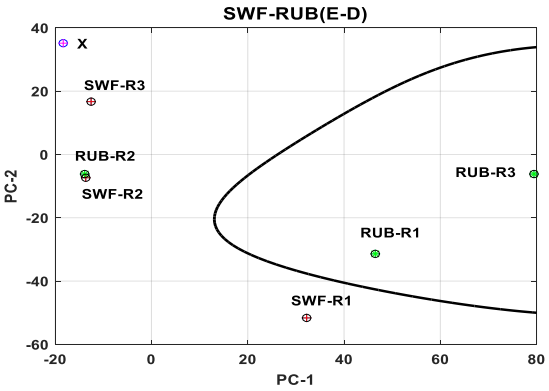
SWF-RUB(E-D)
SWF-R3
RUB-R2
SWF-R2
RUB-R3
RUB-R1
SWF-R1
PC-1
PC-2

(p)

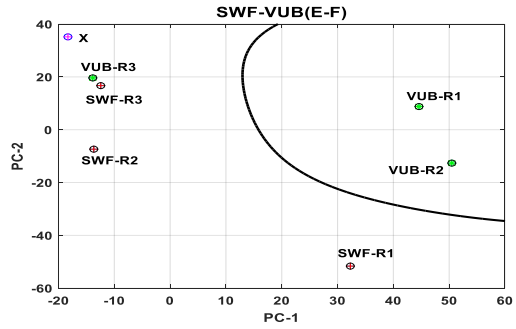
SWF-VUB(E-F)
VUB-R3
SWF-R3
VUB-R1
SWF-R2
VUB-R2
SWF-R1
PC-1
PC-2

(s)

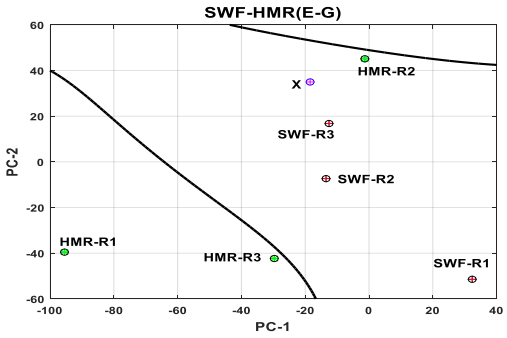
SWF-HMR(E-G)
HMR-R2
SWF-R3
SWF-R2
HMR-R1
HMR-R3
SWF-R1
PC-1
PC-2

(t)

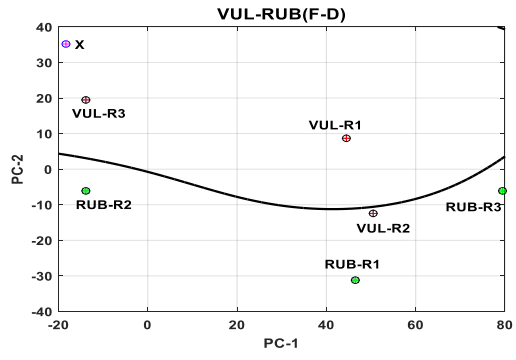
VUL-RUB(F-D)
VUL-R3
VUL-R1
RUB-R2
RUB-R3
VUL-R2
RUB-R1
PC-1
PC-2

(u)

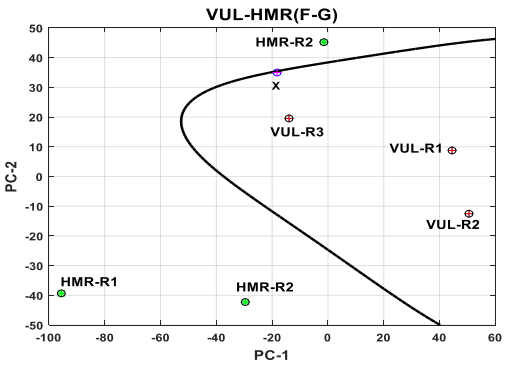
VUL-HMR(F-G)
HMR-R2
VUL-R3
VUL-R1
VUL-R2
HMR-R1
HMR-R2
PC-1
PC-2

(v)

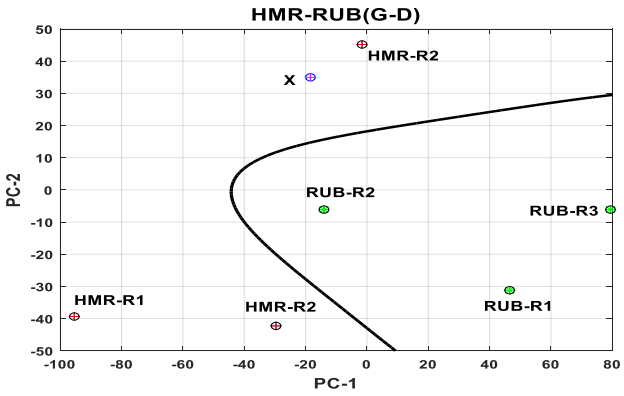

(w)

Figure 4.4: *Output plots of 21 binary classifiers of R-phase using RBF kernel in no mechanical load condition where unknown current data sample is the test sample; where, BRB: Broken rotor bar, FBR: Faulted bearing, RML: Misalignment rotor, RUB: Rotor unbalance, VUL: Single phase voltage unbalance, SWF: Stator winding fault, HMR: Healthy motor and 'X': unknown sample*

A Decision-Directed Acyclic Graph (DDAG) is applied to reduce the evaluation time of pair wise classification using 21 classifiers in each phase, considering each classifier as a node. The evaluation paths of DDAG for R phase, Y phase, and B phase using the RBF kernel have been shown in Fig. 4.5 (a), Fig. 4.5 (b), and Fig. 4.5 (c), respectively; and the unknown sample has been classified for each phase depending on the maximum count of membership classes, which is (7-1) = 6. This classification process has been performed using other four types of kernels, viz., polynomial (3^{rd} order), sigmoid, quadratic, and linear kernels, and the membership classes of three phases for the classification of unknown fault 1 under no load condition (load type 1) have been shown in Table 4.1(a), Table 4.1(b), and Table 4.1(c), respectively, using R, Y, and B phase current signals. The entire procedure has been applied again for the classification of unknown faults 2 and 3 as well. The membership classes for classification of unknown faults 2 and 3 using five kernels under no load condition have also been computed in a similar manner, and the membership classes for classification of unknown faults 2 and 3 using five kernels in no load condition have been shown in Tables 4.2 (a, b, c) and 4.3 (a, b, c), respectively.

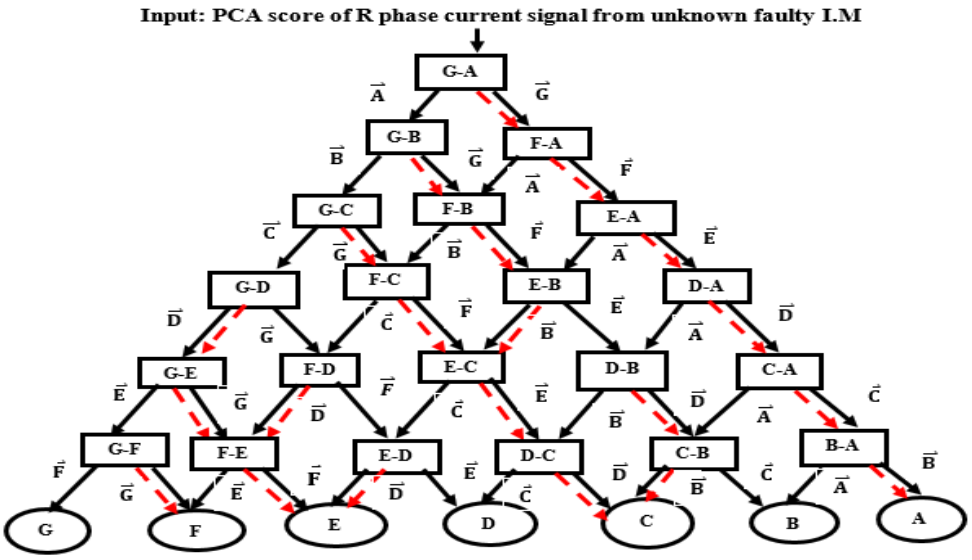

Figure 4. 5: *(a) Directed acyclic graph for detecting unknown fault 1 using RBF kernel under loading 1 condition using R phase current signals*

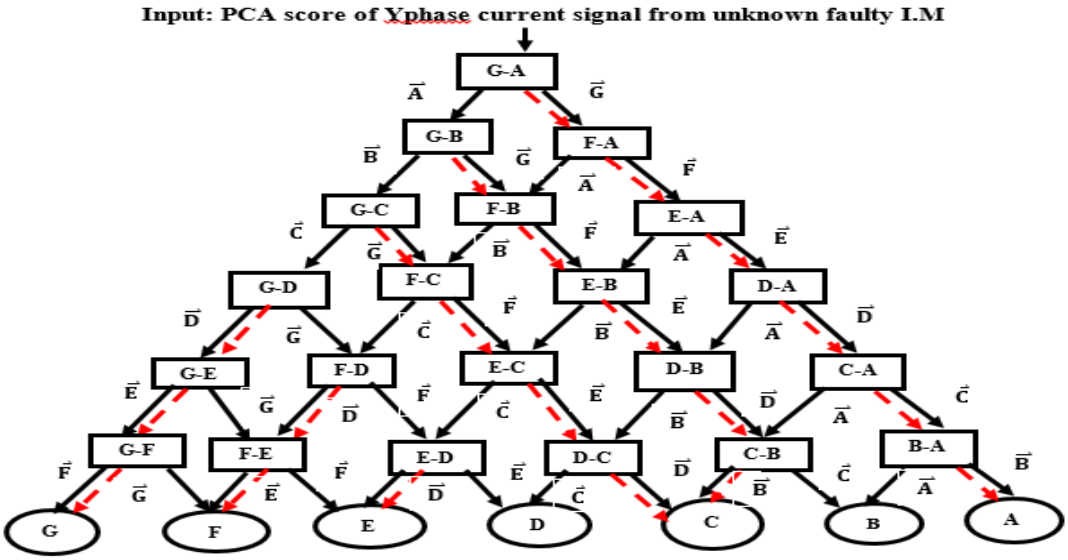

Figure 4. 5: *(b) Directed acyclic graph for detecting unknown fault 1 using RBF kernel under loading 1condition using Y phase current signal*

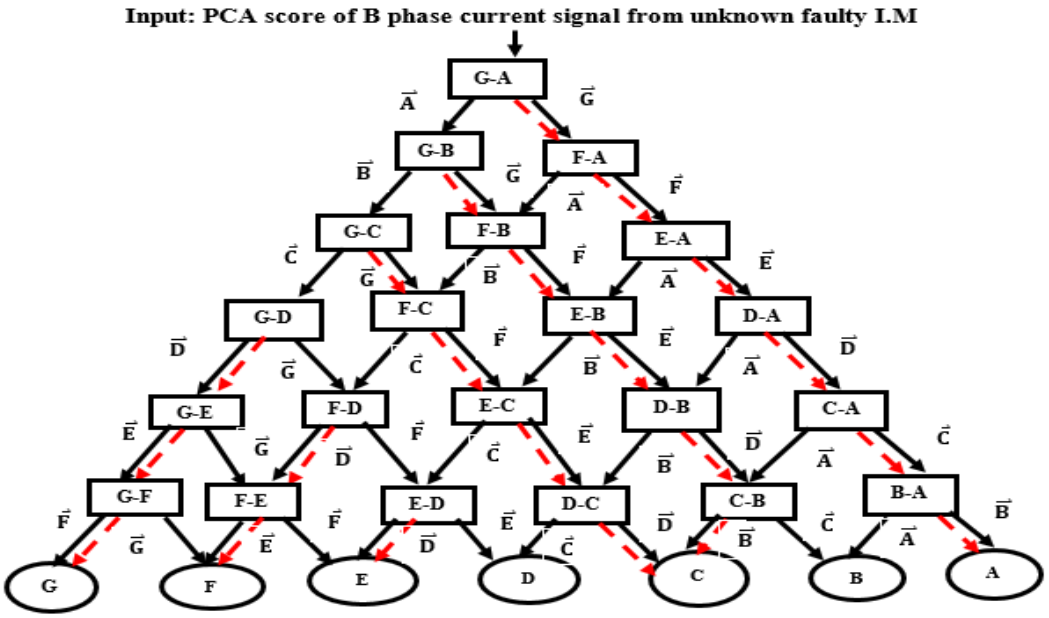

Figure 4. 5: *(c) Directed acyclic graph for detecting unknown fault 1 using RBF kernel under loading 1 condition using B phase current signals*

Table 4.1: (a) Membership classes for classification of unknown fault 1 using R phase current signals in time domain under loading condition 1

Membership class	Polynomial Kernel	RBF Kernel	Sigmoid Kernel	Quadratic Kernel	Linear Kernel
Class G(HMR)	2: (G-D),(G-F)	1: (G-D)	1: (G-D)	2: (G-D),(G-E)	2: (G-D),(G-F)
Class F(VUL)	3: (F-B), (F-D),(F-E)	2: (F-D), (F-G)	3: (F-D),(F-E),(F-G)	3: (F-B), (F-D),(F-G)	2: (F-D),(F-E)
Class E(SWF)	2: (E-D),(E-G)	4 : (E-B), (E-D),(E-F),(E-G)	2: (E-D),(E-G)	3: (E-B),(E-D),(E-G)	2: (E-D),(E-G)
Class D(RUB)	0	0	0	0	0
Class C(RML)	5:(C-B),(C-D),(C-E),(C-F), (C-G)	5:(C-B),(C-D),(C-E),(C-F), (C-G)	5: (C-B),(C-D),(C-E),(C-F),(C-G)	5: (C-B),(C-D),(C-E),(C-F), (C-G)	5: (C-B), (C-D),(C-E),(C-F),(C-G)
Class B(FBR)	3 : (B-D), (B-F), (B-G)	3 : (B-D), (B-F), (B-G)	4: (B-D),(B-E),(B-F),(B-G)	2 : (B-D), (B-G)	4: (B-D),(B-E),(B-F),(B-G)
Class A(BRB)	**6: (A-B),(A-C),(A-D),(A-E),(A-F), (A-G)**	**6: (A-B),(A-C),(A-D),(A-E),(A-F), (A-G)**	**6: (A-B),(A-C),(A-D),(A-E),(A-F), (A-G)**	**6: (A-B),(A-C),(A-D),(A-E),(A-F), (A-G)**	**6: (A-B),(A-C),(A-D),(A-E),(A-F), (A-G)**

Table 4.1: (b) Membership classes for classification of unknown fault 1 using Y phase current signals in time domain under loading condition 1

Membership class	Polynomial Kernel	RBF Kernel	Sigmoid Kernel	Quadratic Kernel	Linear Kernel
Class G(HMR)	4: (G-B),(G-C),(G-E),(G-F)	3: (G-D), (G-E), (G-F)	1: (G-D)	3: (G-D),(G-E),(G-F)	1: (G-D)
Class F(VUL)	3: (F-B),(F-C),(F-E)	2: (F-D), (F-E)	3: (F-D),(F-E),(F-G)	1: (F-D)	3: (F-D),(F-E),(F-G)

Membership class	Polynomial Kernel	RBF Kernel	Sigmoid Kernel	Quadratic Kernel	Linear Kernel
Class E(SWF)	2: (E-B),(E-C)	1: (E-D)	2: (E-D),(E-G)	2: (E-D),(E-F)	2: (E-D),(E-G)
Class D(RUB)	5: (D-B),(D-C),(D-E),(D-F),(D-G)	0	0	0	0
Class C(RML)	0	5:(C-B),(C-D),(C-E),(C-F), (C-G)	4: (C-D),(C-E),(C-F),(C-G)	5: (C-B),(C-D),(C-E),(C-F), (C-G)	5: (C-A),(C-D),(C-E),(C-F),(C-G)
Class B(FBR)	1: (B-C)	4: (B-D), (B-E), (B-F), (B-G)	5: (B-C), (B-D),(B-E),(B-F),(B-G)	4: (B-D),(B-E),(B-F),(B-G)	6: (B-A),(B-C),(B-D),(B-E),(B-F),(B-G)
Class A(BRB)	**6: (A-B),(A-C),(A-D),(A-E),(A-F), (A-G)**	**6: (A-B),(A-C),(A-D),(A-E),(A-F), (A-G)**	**6: (A-B),(A-C),(A-D),(A-E),(A-F), (A-G)**	**6: (A-B),(A-C),(A-D),(A-E),(A-F), (A-G)**	**4: (A-D),(A-E),(A-F),(A-G)**

Table 4.1: (c) Membership classes for classification of unknown fault 1 using B phase current signals in time domain under loading condition 1

Membership class	Polynomial Kernel	RBF Kernel	Sigmoid Kernel	Quadratic Kernel	Linear Kernel
Class G(HMR)	0	0	0	0	0
Class F(VUL)	2: (F-C),(F-G)	3: (F-D),(6_5), (6_7)	3: (F-D),(F-E),(F-G)	2: (F-D),(F-G)	4: (F-C),(F-D),(F-E),(F-G)
Class E(SWF)	3: (E-C),(E-F),(E-G)	2: (E-D), (E-F)	2: (E-D),(E-G)	3: (E-D),(E-F),(E-G)	2: (E-D),(E-G)
Class D(RUB)	4: (D-C),(D-E),(D-F),(D-G)	1: (D-G)	1: (D-G)	1: (D-F)	1: (D-G)
Class C(RML)	1: (C-G)	5: (C-B),(C-D),(C-E),(C-F), (C-G)	4: (C-D),(C-E),(C-F),(C-G)	5: (C-B),(C-D),(C-E),(C-F), (C-G)	3: (C-D),(C-E),(C-F)
Class B(FBR)	5: (B-C),(B-D), (B-E),(B-F), (B-G)	4: (B-D), (B-E),(B-F), (B-G)	5: (B-C), (B-D),(B-E),(B-F),(B-G)	4: (B-D),(B-E),(B-F),(B-G)	6: (B-A),(B-C),(B-D),(B-E),(B-F),(B-G)
Class A(BRB)	**6: (A-B),(A-C),(A-D),(A-E),(A-F), (A-G)**	**6: (A-B),(A-C),(A-D),(A-E),(A-F), (A-G)**	**6: (A-B),(A-C),(A-D),(A-E),(A-F), (A-G)**	**6: (A-B),(A-C),(A-D),(A-E),(A-F), (A-G)**	**5: (A-C),(A-D),(A-E),(A-F),(A-G)**

Table 4.2: (a) Membership classes for classification of unknown fault 2 using R phase current signals in time domain under loading condition 1

Membership class	Polynomial Kernel	RBF Kernel	Sigmoid Kernel	Quadratic Kernel	Linear Kernel
Class G(HMR)	2: (G-A),(G-B)	3: (G-A),(G-B), (G-F)	0	4: (G-A),(G-B),(G-D),(G-F)	0
Class F(VUL)	3: (F-A),(F-B), (F-G)	1 : (F-C)	2: (F-B),(F-G)	0	3: (F-A),(F-B),(F-G)
Class	**6 : (E-A),(E-**	**6 : (E-A),(E-B),(E-**	**6 : (E-A),(E-B),(E-C),**	**6 : (E-A),(E-**	5: (E-A),(E-

Membership class	Polynomial Kernel	RBF Kernel	Sigmoid Kernel	Quadratic Kernel	Linear Kernel
E(SWF)	**B),(E-C), (E-D), (E-F), (E-G)**	**C), (E-D), (E-F), (E-G)**	**(E-D), (E-F), (E-G)**	**B),(E-C), (E-D), (E-F), (E-G)**	B),(E-C),(E-F),(E-G)
Class D(RUB)	5: (D-A), (D-B), (D-C),(D-F), (D-G)	5: (D-A), (D-B), (D-C),(D-F), (D-G)	5: (D-A),(D-B),(D-C),(D-F),(D-G)	4: (D-A),(D-B),(D-C),(D-G)	**6:(D-A),(D-B),(D-C),(D-E),(D-F),(D-G)**
Class C(RML)	4 : (C-A), (C-B),(C-F), (C-7)	2 : (C-B), (C-F)	4: (C-A),(C-B),(C-F),(C-G)	4 : (C-A), (C-B),(C-F), (C-G)	3: (C-A),(C-F),(C-G)
Class B(FBR)	1: (B-A)	2: (B-A), (B-F)	2: (B-A),(B-G)	1: (B-F)	3: (B-A),(B-C),(B-G)
Class A(BRB)	0	2: (A-C),(A-F)	2: (A-F),(A-G)	2: (A-B),(A-F)	1: (A-G)

Table 4.2: (b) Membership classes for classification of unknown fault 2 using Y phase current signals in time domain under loading condition 1

Membership class	Polynomial Kernel	RBF Kernel	Sigmoid Kernel	Quadratic Kernel	Linear Kernel
Class G(HMR)	4: (G-A), (G-B), (G-C), (G-D),(G-F)	4: (G-A), (G-B), (G-C),(G-F)	2: (G-B),(G-F)	5: (G-A),(G-B),(G-C),(G-D),(G-F)	2: (G-B),(G-F)
Class F(VUL)	1: (F-B)	2 :(F-B),(F-C)	1: (F-B)	1: (F-B)	3: (F-A),(F-B),(F-C)
Class E(SWF)	**6 : (E-A),(E-B),(E-C), (E-D), (E-F), (E-G)**	**6 : (E-A),(E-B),(E-C), (E-D), (E-F), (E-G)**	**6 : (E-A),(E-B),(E-C), (E-D), (E-F), (E-G)**	**6 : (E-A),(E-B),(E-C), (E-D), (E-F), (E-G)**	**6:(E-A),(E-B),(E-C),(E-D),(-F),(E-G)**
Class D(RUB)	5: (D-A), (D-B), (D-C),(D-F)	5: (D-A), (D-B), (D-C),(D-F), (D-G)	5: (D-A),(D-B),(D-C),(D-F),(D-G)	4: (4_1), (4_2), (4_3),(4_6)	5: (D-A),(D-B),(D-C),(D-F),(D-G)
Class C(RML)	3: (C-A), (C-B),(C-F)	1: (C-B)	4: (C-A),(C-B),(C-F),(C-G)	3 : (C-A), (C-B),(C-F)	2: (C-B),(C-G)
Class B(FBR)	0	0	0	0	0
Class A(BRB)	2: (A-B), (A-G)	3: (A-B), (A-C), (A-F)	3: (A-B),(A-F),(A-G)	2: (A-B),(A-F)	3: (A-B),(A-C),(A-G)

Table 4.2: (c) Membership classes for classification of unknown fault 2 using B phase current signals in time domain under loading condition 1

Membership class	Polynomial Kernel	RBF Kernel	Sigmoid Kernel	Quadratic Kernel	Linear Kernel
Class G(HMR)	5: (G-A),(G-B),(G-C),(G-D),(G-F)	5: (G-A), (G-B), (G-C), (G-D), (G-F)	5: (G-A),(G-B),(G-C),(G-D),(G-F)	5: (G-A),(G-B),(G-C),(G-D),(G-F)	6: (G-A),(G-B),(G-C),(G-D),(G-E),(G-F)
Class F(VUL)	0	0	0	1: (F-D)	2: (F-A),(F-B)
Class	**6 : (E-A),(E-**	**6 : (E-A),(E-B),(E-**	**6 : (E-A),(E-B),(E-C),**	**6 : (E-A),(E-**	**5: (E-A),(E-**

Membership class	Polynomial Kernel	RBF Kernel	Sigmoid Kernel	Quadratic Kernel	Linear Kernel
E(SWF)	**B),(E-C), (E-D), (E-F), (E-G)**	**C), (E-D), (E-F), (E-G)**	**(E-D), (E-F), (E-G)**	**B),(E-C), (E-D), (E-F), (E-G)**	**B),(E-C),(E-D),(E-F)**
Class D(RUB)	4: (D-A),(D-B),(D-C),(D-F)	4: (D-A), (D-B), (D-C),(D-F)	4: (D-A), (D-B), (D-C),(D-F)	3: (D-A), (D-B), (D-C)	4: (D-A),(D-B),(D-C),(D-F)
Class C(RML)	3: (C-A), (C-B),(C-F)	2: (C-B), (C-F)	3 : (C-A), (C-B),(C-F)	3 : (C-A), (C-B),(C-F)	3: (C-A),(C-B),(C-F)
Class B(FBR)	2: (B-A), (B-F)	2: (B-A),(B-F)	1: (B-F)	1: (B-F)	0
Class A(BRB)	1: (A-F)	2: (A-C),(A-F)	2: (A-B),(A-F)	2: (A-B),(A-F)	1: (A-B)

Table 4.3: (a) Membership classes for classification of unknown fault 3 using R phase current signals in time domain under loading condition 1

Membership class	Polynomial Kernel	RBF Kernel	Sigmoid Kernel	Quadratic Kernel	Linear Kernel
Class G(HMR)	5: (G-A),(G-C),(G-D),(G-E),(G-F)	1: (G-D)	1: (G-D)	5: (G-A),(G-C),(G-D),(G-E),(G-F)	1: (G-D)
Class F(VUL)	2: (F-D), (F-E)	2: (F-D), (F-G)	3: (F-D),(F-E),(F-G)	1: (F-D)	3: (F-D),(F-E),(F-G)
Class E(SWF)	1: (E-D),	3: (E-D),(E-F),(E-G)	2: (E-D),(E-F)	2: (E-D),(E-F)	2: (E-D),(E-F)
Class D(RUB)	0	0	0	0	0
Class C(RML)	4: (C-A),(C-D),(C-E),(C-F)	4: (C-D), (C-E),(C-F),(C-G)	5: (C-A),(C-D), (C-E),(C-F),(C-G)	3:(C-D), (C-E),(C-F)	5: (C-A),(C-D),(C-E),(C-F),(C-G)
Class B(FBR)	**6 : (B-A), (B-C), (B-D), (B-E), (B-F),(B-G)**	**6 : (B-A), (B-C), (B-D), (B-E), (B-F),(B-G)**	**6 : (B-A), (B-C), (B-D), (B-E), (B-F),(B-G)**	**6 : (B-A), (B-C), (B-D), (B-E), (B-F),(B-G)**	**6 : (B-A), (B-C), (B-D), (B-E), (B-F),(B-G)**
Class A(BRB)	3: (A-D), (A-E),(A-F)	5: (A-C), (A-D), (A-E),(A-F),(A-G)	4: (A-D), (A-E),(A-F),(A-G)	4: (A-C),(A-D), (A-E),(A-F)	4: (A-D),(A-E),(A-F),(A-G)

Table 4.3: (b) Membership classes for classification of unknown fault 3 using Y phase current signals in time domain under loading condition 1

Membership class	Polynomial Kernel	RBF Kernel	Sigmoid Kernel	Quadratic Kernel	Linear Kernel
Class G(HMR)	5: (G-A),(G-C),(G-D),(G-E),(G-F)	1: (G-D)	1: (G-D)	3: (7_4),(7_5),(7_6)	1: (G-D)
Class F(VUL)	4: (F-A),(F-C), (F-D), (F-E)	4: (F-C), (F-D), (F-E),(F-G)	3: (F-D),(F-E),(F-G)	2: (6_3),(6_4)	3: (F-D),(F-E),(F-G)
Class E(SWF)	3: (E-A),(E-C),(E-D)	3: (E-D),(E-F),(E-G)	3: (E-C),(E-D),(E-G)	4: (5_1),(5_3),(5_4),(5_6)	3: (E-C),(E-D),(E-F)

Membership class	Polynomial Kernel	RBF Kernel	Sigmoid Kernel	Quadratic Kernel	Linear Kernel
Class D(RUB)	0	0	0	0	0
Class C(RML)	1: (C-D)	2: (C-D),(C-F)	3: (C-D),(C-F),(C-G)	2: (3_4),(3_7)	3: (C-D),(C-E),(C-F)
Class B(FBR)	**6 : (B-A), (B-C), (B-D), (B-E), (B-F),(B-G)**	**6 : (B-A), (B-C), (B-D), (B-E), (B-F),(B-G)**	**6 : (B-A), (B-C), (B-D), (B-E), (B-F),(B-G)**	**6 : (B-A), (B-C), (B-D), (B-E), (B-F),(B-G)**	5: (B-C),(B-D),(B-E),(B-F),(B-G)
Class A(BRB)	5: (G-A),(G-C),(G-D),(G-E),(G-F)	5: (A-C), (A-D), (A-E),(A-F),(A-G)	5: (A-C), (A-D), (A-E),(A-F),(A-G)	4: (A-C),(A-D), (A-E),(A-F)	**6: (A-B),(A-C),(A-D),(A-E),(A-F), (A-G)**

Table 4.3: (c) Membership classes for classification of unknown fault 3 using B phase current signals in time domain under loading condition 1

Membership class	Polynomial Kernel	RBF Kernel	Sigmoid Kernel	Quadratic Kernel	Linear Kernel
Class G(HMR)	0	0	1: (G-D)	0	0
Class F(VUL)	2: (F-D),(F-G)	3: (F-D), (F-E),(F-G)	3: (F-D),(F-E),(F-G)	1: (F-D),(F-G)	**6: (F-A), (F-B), (F-C),(F-D),(F-E),(F-G)**
Class E(SWF)	3: (E-D),(E-F),(E-G)	2: (E-D),(E-G)	2: (E-D),(E-G)	3: (E-D),(E-F),(E-G)	2: (E-D),(E-G)
Class D(RUB)	1: (D-G)	1 : (D-G)	0	1: (D-G)	1: (D-G)
Class C(RML)	4: (C-D),(C-E),(C-F),(C-G)	4: (C-D), (C-E),(C-F),(C-G)	5: (C-A), (C-D),(C-E),(C-F),(C-G)	4:(C-D), (C-E),(C-F),(C-G)	3: (C-D),(C-E),(C-F)
Class B(FBR)	**6 : (B-A), (B-C), (B-D), (B-E), (B-F),(B-G)**	**6 : (B-A), (B-C), (B-D), (B-E), (B-F),(B-G)**	**6 : (B-A), (B-C), (B-D), (B-E), (B-F),(B-G)**	**6 : (B-A), (B-C), (B-D), (B-E), (B-F),(B-G)**	4: (B-C),(B-D),(B-E),(B-G)
Class A(BRB)	5: (A-C),(A-D),(A-E),(A-F),(A-G)	5: (A-C), (A-D), (A-E),(A-F),(A-G)	4: (A-D), (A-E),(A-F),(A-G)	4: (A-C),(A-D), (A-E),(A-F),(A-G)	5: (A-B),(A-C),(A-D),(A-E), (A-G)

It is observed from the above three tables that the unknown fault 1 resembles a broken rotor bar type fault (Class A: BRB fault) except with the linear kernel function. The other nonlinear kernels give identical classification results in favour of the BRB fault using the current signals of all three phases.

Similarly, the nonlinear kernels detect maximum membership classes of class E for unknown fault 2 and class B for unknown fault 3, respectively; although the membership classifications are not illustrated here in details. From the table, it can be said that unknown fault 1, unknown fault 2, and unknown fault 3 resemble a broken rotor bar, a stator winding fault, and a bearing fault, respectively. But the linear kernel again fails to detect the same class for all phases. Hence, the four nonlinear kernels, viz., the polynomial kernel, the RBF kernel, the sigmoid kernel, and the quadratic kernel, have been considered further, discarding the linear kernel function. All three unknown faults have been further authenticated using these four nonlinear kernels under two other loading conditions;

where, the results have been unanimous in each of the cases, and match identically with the results obtained with no load classification.

Fault classifications have further been performed in the frequency domain as well, in order to provide more authentication to the results. The frequency spectra are constructed using the current signals of known classes of faults and the unknown fault induction motors under three different conditions. Fast Fourier Transform (FFT) has been used to obtain the frequency domain spectrums. Fault features are extracted from FFT spectrums using PCA and these features are used to classify three unknown faults using OVO SVM through DDAG. The detected membership classes have been shown for unknown fault type 1 in Table 4.4 (a), Table 4.4 (b) and Table 4.4 (c) respectively using R, Y and B phase current signals. The membership classes of three phases for detection of unknown fault 2 and unknown fault 3 has also been shown in Table 4.5 (a. b, c) and Table 4.6 (a, b, c) respectively.

It is observed from the above three tables that the unknown fault 1 resembles a broken rotor bar type fault (Class A: BRB fault) except with the linear kernel function. The other nonlinear kernels give identical classification results in favour of the BRB fault using the current signals of all three phases are constructed using the current signals of known classes of faults and unknown faulty induction motors under three different loading conditions. The frequency domain spectra were obtained using the Fast Fourier Transform (FFT). Fault features are extracted from FFT spectra using PCA, and these features are used to classify three unknown faults using OVO SVM through DDAG. The detected membership classes have been shown for unknown fault type 1 in Tables 4.4(a), 4.4(b), and 4.4(c), respectively, using R, Y, and B phase current signals. The membership classes of three phases for the detection of unknown fault 2 and unknown fault 3 have also been shown in Tables 4.5 (a, b, c.) and 4.6 (a .b, c.), respectively. It is again observed from these tables that the results obtained using the frequency domain features match identically with the results obtained using the time domain features, as described in Tables 4.1 (a, b, c), 4.2 (a, b, c), and 4.3 (a, b, c) respectively using R, Y, and B phase signals. But, most importantly, it is found that the classification results obtained using the frequency domain features listed in Tables 4.4, 4.5, and 4.6, are similar when using the four nonlinear kernels, as well as the linear kernel. Hence, linear kernels are also yielding correct classification using the frequency domain fault features, which was not true using the time domain features.

Table 4.4: (a) Membership classes for classification of unknown fault 1 using R phase current signals in frequency domain under loading condition 1

Membership class	Polynomial Kernel	RBF Kernel	Sigmoid Kernel	Quadratic Kernel	Linear Kernel
Class G(HMR)	0	5: (G-B),(G-C),(G-D),(G-E),(G-F)	0	0	0
Class F(VUL)	5: (F-B),(F-C),(F-D),(F-E),(F-G)	4: (F-B),(F-C),(F-D),(F-E)	5: (F-B),(F-C),(F-D),(F-E),(F-G)	2: (F-C),(F-G)	5: (F-B),(F-C),(F-D),(F-E),(F-G)
Class E(SWF)	2: (E-D),(E-G)	2: (E-B),(E-D)	2: (E-D),(E-G)	3: (E-B),(E-F),(E-G)	3: (E-C),(E-D),(E-G)
Class D(RUB)	2: (D-C),(D-G)	1: (D-B)	2: (D-C),(D-G)	4: (D-B),(D-E),(D-F),(D-G)	1: (D-G)
Class C(RML)	3: (C-B),(C-E),(C-G)	3: (C-B),(C-D),(C-E)	2: (C-E),(C-G)	4: (C-B),(C-D),(C-E),(C-G)	2: (C-D),(C-G)
Class B(FBR)	3: (B-D),(B-E),(B-G)	0	4: (B-C),(B-D),(B-E),(B-G)	2: (B-F),(B-G)	4: (B-C),(B-D),(B-E),(B-G)
Class A(BRB)	**6: (A-B),(A-C),(A-D),(A-E),(A-F), (A-G)**	**6: (A-B),(A-C),(A-D),(A-E),(A-F), (A-G)**	**6: (A-B),(A-C),(A-D),(A-E),(A-F), (A-G)**	**6: (A-B),(A-C),(A-D),(A-E),(A-F), (A-G)**	**6: (A-B),(A-C),(A-D),(A-E),(A-F), (A-G)**

Table 4.4: (b) Membership classes for classification of unknown fault 1 using Y phase current signals in frequency domain under loading condition 1

Membership class	Polynomial Kernel	RBF Kernel	Sigmoid Kernel	Quadratic Kernel	Linear Kernel
Class G(HMR)	0	0	3: (G-D),(G-E),(G-F)	0	2: (G-D),(G-E)
Class F(VUL)	3: (F-D),(F-E),(F-G)	1: (F-G)	2: (F-D),(F-E)	5: (F-B),(F-C),(F-D),(F-E),(F-G)	4: (F-C),(F-D),(F-E),(F-G)
Class E(SWF)	2: (E-D),(E-G)	2: (E-F),(E-G)	1: (E-D)	3: (E-C),(E-D),(E-G)	2: (E-C),(E-D)
Class D(RUB)	2: (D-C),(D-G)	3: (D-E),(D-F),(D-G)	0	2: (D-C),(D-G)	1: (D-C)
Class C(RML)	3: (C-E),(C-F),(C-G)	5: (C-B),(C-D),(C-E),(C-F),(C-G)	4: (C-D),(C-E),(C-F),(C-G)	1: (C-G)	1: (C-G)
Class B(FBR)	5: (B-C),(B-D),(B-E),(B-F),(B-G)	4: (B-D),(B-E),(B-F),(B-G)	5: (B-C),(B-D),(B-E),(B-F),(B-G)	5: (B-C),(B-D),(B-E),(B-F),(B-G)	5: (B-C),(B-D),(B-E),(B-F),(B-G)
Class A(BRB)	**6: (A-B),(A-C),(A-D),(A-E),(A-F), (A-G)**	**6: (A-B),(A-C),(A-D),(A-E),(A-F), (A-G)**	**6: (A-B),(A-C),(A-D),(A-E),(A-F), (A-G)**	**6: (A-B),(A-C),(A-D),(A-E),(A-F), (A-G)**	**6: (A-B),(A-C),(A-D),(A-E),(A-F), (A-G)**

Table 4.4: (c) Membership classes for classification of unknown fault 1 using B phase current signals in frequency domain under loading condition 1

Membership class	Polynomial Kernel	RBF Kernel	Sigmoid Kernel	Quadratic Kernel	Linear Kernel
Class G(HMR)	0	3: (G-B),(G-C),(G-F)	0	4: (G-B),(G-C),(G-E),(G-F)	0
Class F(VUL)	1: (F-G)	2: (F-B),(F-C)	1: (F-G)	1: (F-B)	1: (F-G)
Class E(SWF)	4: (E-B),(E-C),(E-F),(E-G)	4: (E-B),(E-C),(E-F),(E-G)	4: (E-B),(E-C),(E-F),(E-G)	3: (E-B),(E-C),(E-F)	4: (E-B),(E-C),(E-F),(E-G)
Class	4: (D-C),(D-	5: (D-B),(D-C),(D-	5: (D-B),(D-C),(D-	5: (D-B),(D-	5: (D-B),(D-

Membership class	Polynomial Kernel	RBF Kernel	Sigmoid Kernel	Quadratic Kernel	Linear Kernel
D(RUB)	E),(D-F),(D-G)	E),(D-F),(D-G)	E),(D-F),(D-G)	C),(D-E),(D-F),(D-G)	C),(D-E),(D-F),(D-G)
Class C(RML)	2: (C-F),(C-G)	1: (C-B)	3: (3_2),(3_6),(3_7)	2: (C-B),(C-G)	3: (C-B),(C-F),(C-G)
Class B(FBR)	4: (B-C),(B-D),(B-F),(B-G)	0	2: (B-F),(B-G)	0	2: (B-F),(B-G)
Class A(BRB)	**6: (A-B),(A-C),(A-D),(A-E),(A-F), (A-G)**	**6: (A-B),(A-C),(A-D),(A-E),(A-F), (A-G)**	**6: (A-B),(A-C),(A-D),(A-E),(A-F), (A-G)**	**6: (A-B),(A-C),(A-D),(A-E),(A-F), (A-G)**	**6: (A-B),(A-C),(A-D),(A-E),(A-F), (A-G)**

Table 4.5: (a) Membership classes for classification of unknown fault 2 using R phase current signals in frequency domain under loading condition 1

Membership class	Polynomial Kernel	RBF Kernel	Sigmoid Kernel	Quadratic Kernel	Linear Kernel
Class G(HMR)	2: (G-C),(G-F)	3: (G-A),(G-C),(G-F)	2: (G-C),(G-F)	3: (G-A),(G-C),(G-F)	3: (G-A),(G-C),(G-F)
Class F(VUL)	0	1: (F-C)	0	0	0
Class E(SWF)	**6: (E-A),(E-B),(E-C),(E-D),(E-F),(E-G)**	**6: (E-A),(E-B),(E-C),(E-D),(E-F),(E-G)**	**6: (E-A),(E-B),(E-C),(E-D),(E-F),(E-G)**	**6: (E-A),(E-B),(E-C),(E-D),(E-F),(E-G)**	**6: (E-A),(E-B),(E-C),(E-D),(E-F),(E-G)**
Class D(RUB)	4: (D-A),(D-C),(D-F),(D-G)	3: (D-C),(D-F),(D-G)	4: (D-A),(D-C),(D-E),(D-G)	4: (D-A),(D-C),(D-E),(D-G)	4: (D-A),(D-C),(D-E),(D-G)
Class C(RML)	1: (C-F)	0	1: (C-F)	1: (C-F)	1: (C-F)
Class B(FBR)	5: (B-A),(B-C),(B-D),(B-F),(B-G)	5: (B-A),(B-C),(B-D),(B-F),(B-G)	5: (B-A),(B-C),(B-D),(B-F),(B-G)	5: (B-A),(B-C),(B-D),(B-F),(B-G)	5: (B-A),(B-C),(B-D),(B-F),(B-G)
Class A(BRB)	3: (A-C),(A-F),(A-G)	3: (A-C),(A-D),(A-G)	3: (A-C),(A-F),(A-G)	2: (A-C),(A-F)	2: (A-C),(A-F)

Table 4.5: (b) Membership classes for classification of unknown fault 2 using Y phase current signals in frequency domain under loading condition 1

Membership class	Polynomial Kernel	RBF Kernel	Sigmoid Kernel	Quadratic Kernel	Linear Kernel
Class G(HMR)	0	3: (G-A),(G-B),(G-C)	0	3: (G-A),(G-B),(G-C)	0
Class F(VUL)	4: (F-A),(F-B),(F-C),(F-G)	4: (F-A),(F-B),(F-C),(F-G)	4: (F-A),(F-B),(F-C),(F-G)	4: (F-A),(F-B),(F-C),(F-G)	4: (F-A),(F-B),(F-C),(F-G)
Class E(SWF)	**6: (E-A),(E-B),(E-C),(E-D),(E-F),(E-G)**	**6: (E-A),(E-B),(E-C),(E-D),(E-F),(E-G)**	**6: (E-A),(E-B),(E-C),(E-D),(E-F),(E-G)**	**6: (E-A),(E-B),(E-C),(E-D),(E-F),(E-G)**	**6: (E-A),(E-B),(E-C),(E-D),(E-F),(E-G)**
Class D(RUB)	5: (D-A),(D-B),(D-C),(D-F),(D-G)	5: (D-A),(D-B), (D-C),(D-F),(D-G)	5: (D-A),(D-B), (D-C),(D-F),(D-G)	5: (D-A),(D-B),(D-C),(D-F),(D-G)	5: (D-A),(D-B),(D-C),(D-F),(D-G)
Class C(RML)	2: (C-A),(C-G)	0	2: (C-A),(C-G)	1: (C-A)	2: (C-A),(C-G)
Class B(FBR)	3: (B-A),(B-C),(B-G)	1: (B-C)	3: (B-A),(B-C),(B-G)	2: (B-A),(B-C)	3: (B-A),(B-C),(B-G)
Class A(BRB)	1: (A-G)	2 : (A-B),(A-C)	1: (A-G)	0	1: (A-G)

Table 4.5: (c) Membership classes for classification of unknown fault 2 using B phase current signals in frequency domain under loading condition 1

Membership class	Polynomial Kernel	RBF Kernel	Sigmoid Kernel	Quadratic Kernel	Linear Kernel
Class G(HMR)	1: (G-F)	3: (G-B),(G-C),(G-F)	0	2: (G-B),(G-F)	2: (G-B),(G-F)
Class F(VUL)	0	1: (F-B)	1: (F-G)	1: (F-B)	1: (F-B)
Class E(SWF)	6: (E-A),(E-B),(E-C),(E-D),(E-F),(E-G)	6: (E-A),(E-B),(E-C),(E-D),(E-F),(E-G)	6: (E-A),(E-B),(E-C),(E-D),(E-F),(E-G)	6: (E-A),(E-B),(E-C),(E-D),(E-F),(E-G)	6: (E-A),(E-B),(E-C),(E-D),(E-F),(E-G)
Class D(RUB)	3: (D-B),(D-F),(D-G)	4: (D-B),(D-C),(D-F),(D-G)	4: (D-B),(D-C),(D-F),(D-G)	5: (D-A),(D-B),(D-C),(D-F),(D-G)	5: (D-A),(D-B),(D-C),(D-F),(D-G)
Class C(RML)	4: (C-B),(C-D),(C-F),(C-G)	2: (3_2),(3_6)	3: (C-B),(C-F),(C-G)	4: (C-A),(C-B),(C-F),(C-G)	4: (C-A),(C-B),(C-F),(C-G)
Class B(FBR)	2: (2_6),(2_7)	0	2: (B-F),(B-G)	0	0
Class A(BRB)	5: (A-B),(A-C),(A-D),(A-F),(A-G)	5: (A-B),(A-C),(A-D),(A-F),(A-G)	5: (A-B),(A-C),(A-D),(A-F),(A-G)	3: (A-B),(A-F),(A-G)	3: (A-B),(A-E),(A-F)

Table 4.6: (a) Membership classes for classification of unknown fault 3 using R phase current signals in frequency domain under loading condition 1

Membership class	Polynomial Kernel	RBF Kernel	Sigmoid Kernel	Quadratic Kernel	Linear Kernel
Class G(HMR)	3: (G-A),(G-D),(G-F)	4: (G-A),(G-D),(G-E),(G-F)	4: (G-A),(G-D),(G-E),(G-F)	3: (G-A),(G-D),(G-E)	3: (G-A),(G-D),(G-E)
Class F(VUL)	2: (F-A), (F-D)	1: (F-A)	5: (F-A),(F-C),(F-D),(F-E),(F-G)	1: (F-A)	2: (F-A),(F-D)
Class E(SWF)	4: (E-A),(E-D),(E-F),(E-G)	3: (E-A),(E-D),(E-F)	1: (E-A)	4: (E-A),(E-D),(E-F),(E-G)	4: (E-A),(E-D),(E-F),(E-G)
Class D(RUB)	1: (D-A)	2: (D-A),(D-F)	2: (D-A),(D-E)	2: (D-A),(D-F)	1: (4_1)
Class C(RML)	5: (C-A),(C-D),(C-E),(C-F),(C-G)	5: (C-A),(C-D),(C-E),(C-F),(C-G)	3: (C-A),(C-D),(C-E)	5: (C-A),(C-D),(C-E),(C-F),(C-G)	5: (C-A),(C-D),(C-E),(C-F),(C-G)
Class B(FBR)	**6: (E-A),(E-B),(E-C),(E-D),(E-F),(E-G)**	**6: (E-A),(E-B),(E-C),(E-D),(E-F),(E-G)**	**6: (E-A),(E-B),(E-C),(E-D),(E-F),(E-G)**	**6: (E-A),(E-B),(E-C),(E-D),(E-F),(E-G)**	**6: (E-A),(E-B),(E-C),(E-D),(E-F),(E-G)**
Class A(BRB)	0	0	0	0	0

Table 4.6: (b) Membership classes for classification of unknown fault 3 using Y phase current signals in frequency domain under loading condition 1

Membership class	Polynomial Kernel	RBF Kernel	Sigmoid Kernel	Quadratic Kernel	Linear Kernel
Class G(HMR)	0	0	1: (G-D)	0	2: (G-D),(G-E)
Class F(VUL)	4: (F-A),(F-D),(F-E),(F-G)	3: (F_D),(F-E),(F-G)	3: (F_D),(F-E),(F-G)	3: (F_D),(F-E),(F-G)	1: (F-D)
Class	2: (E-D),(E-G)	2: (E-D),(E-G)	1: (E-D)	2: (E-D),(E-G)	1: (E-F)

Membership class	Polynomial Kernel	RBF Kernel	Sigmoid Kernel	Quadratic Kernel	Linear Kernel
E(SWF)					
Class D(RUB)	1: (D-G)	1: (D-G)	0	1: (D-G)	1: (D-E)
Class C(RML)	5: (C-A),(C-D),(C-E),(C-F),(C-G)	5: (C-A),(C-D), (C-E),(C-F),(C-G)	5: (C-A),(C-D), (C-E),(C-F),(C-G)	5: (C-A),(C-D),(C-E),(C-F),(C-G)	5: (C-A),(C-D),(C-E),(C-F),(C-G)
Class B(FBR)	**6: (E-A),(E-B),(E-C),(E-D),(E-F),(E-G)**	**6: (E-A),(E-B),(E-C),(E-D),(E-F),(E-G)**	**6: (E-A),(E-B),(E-C),(E-D),(E-F),(E-G)**	**6: (E-A),(E-B),(E-C),(E-D),(E-F),(E-G)**	**6: (E-A),(E-B),(E-C),(E-D),(E-F),(E-G)**
Class A(BRB)	3: (A-D),(A-E),(A-G)	4: (A-D),(A-E),(A-F),(A-G)	4: (A-D),(A-E),(A-F),(A-G)	4: (A-D),(A-E),(A-F),(A-G)	4: (A-D),(A-E),(A-F),(A-G)

Table 4.6: (c) Membership classes for classification of unknown fault 3 using B phase current signals in frequency domain under loading condition 1

Membership class	Polynomial Kernel	RBF Kernel	Sigmoid Kernel	Quadratic Kernel	Linear Kernel
Class G(HMR)	0	0	3: (G-A),(G-D),(G-E)	0	3: (G-A),(G-D),(G-E)
Class F(VUL)	5: (F-A),(F-C),(F-D),(F-E),(F-G)	5: (F-A),(F-C),(F-D),(F-E),(F-G)	5: (F-A),(F-C),(F-D),(F-E),(F-G)	4: (F-C),(F-D),(F-E),(F-G)	5: (F-A),(F-C),(F-D),(F-E),(F-G)
Class E(SWF)	2: (E-D),(E-G)	3: (E-A),(E-D),(E-G)	2: (E-A),(E-D)	1: (E-G)	2: (E-A),(E-D)
Class D(RUB)	2: (D-A),(D-G)	1: (4_7)	0	2: (4_5),(4_7)	0
Class C(RML)	4: (C-A),(C-D),(C-E),(C-G)	4: (C-A),(C-D),(C-E),(C-G)	4: (C-A),(C-D),(C-E),(C-G)	4: (C-A),(C-D),(C-E),(C-G)	4: (C-A),(C-D),(C-E),(C-G)
Class B(FBR)	**6: (E-A),(E-B),(E-C),(E-D),(E-F),(E-G)**	**6: (E-A),(E-B),(E-C),(E-D),(E-F),(E-G)**	**6: (E-A),(E-B),(E-C),(E-D),(E-F),(E-G)**	**6: (E-A),(E-B),(E-C),(E-D),(E-F),(E-G)**	**6: (E-A),(E-B),(E-C),(E-D),(E-F),(E-G)**
Class A(BRB)	2: (A-E),(A-G)	2: (A-E),(A-G)	1: (A-D)	4: (A-D),(A-E),(A-F),(A-G)	1: (A-D)

4.9.1 *Classification accuracy*

Each unknown class of fault is examined six times for each phase individually, using each type of kernel for all three loading conditions. As a result, the total number of test cases for each unknown fault classification using a single kernel is (6 faults x 3 loadings) = 18. If one kernel is able to correctly classify the test class of fault *N* number of times for all the three phases out of a total of 18 times, then the success rate of classification or the classification accuracy of that particular kernel for one class of fault becomes as follows:

$$Classification\ accuracy = \frac{Total\ number\ of\ correct\ classification}{Total\ number\ of\ test\ cases} \times 100\ \% = \frac{N}{18} \times 100\ \%$$

Using both the time domain and frequency domain characteristics, the classification success rate is computed for each kernel under three distinct loading conditions. The results are shown in tables 4.7 (a) and (b), respectively.

Table 4.7: (a) Accuracy of classification using different kernels under different loading conditions when features are extracted from fault current signals in time domain

Kernel	Quadratic	Polynomial (3rd order)	Sigmoid	Linear	RBF
		Loading condition 1			
Unknown fault 1	72.23	83.34	83.34	33.34	88.88
Unknown fault 2	72.23	83.34	83.34	33.34	88.88
Unknown fault 3	66.66	77.78	83.34	27.78	83.34
		Loading condition 2			
Unknown fault 1	72.23	83.34	83.34	38.89	88.88
Unknown fault 2	72.23	83.34	83.34	33.34	88.88
Unknown fault 3	72.23	83.34	88.88	33.34	88.88
		Loading condition 3			
Unknown fault 1	77.78	88.88	88.88	38.89	88.88
Unknown fault 2	72.23	83.34	88.88	44.45	88.88
Unknown fault 3	72.23	83.34	83.34	33.34	88.88
Overall Accuracy (%)	**72.23**	**83.34**	**85.12**	**35.19**	**88.26**

Table 4.7: (b) Accuracy of classification using different kernels under different loading conditions when features are extracted from fault current signals in frequency domain

Kernel	Quadratic	Polynomial (3rd order)	Sigmoid	Linear	RBF
		Loading condition 1			
Unknown fault 1	83.34	94.44	94.44	77.78	94.44
Unknown fault 2	88.88	88.88	94.44	83.34	100
Unknown fault 3	83.34	94.44	94.44	72.23	100
		Load condition 2			
Unknown fault 1	88.88	94.44	94.44	83.34	100
Unknown fault 2	88.88	94.44	100	77.78	100
Unknown fault 3	83.34	94.44	94.44	72.23	100
		Loading condition 3			
Unknown fault 1	83.34	94.44	94.44	77.78	100
Unknown fault 2	88.88	94.44	94.44	83.34	100
Unknown fault 3	88.88	94.44	94.44	77.78	100
Overall Accuracy (%)	**86.42**	**93.82**	**95.06**	**78.4**	**98.76**

The above results are represented graphically in Figure 4.6 illustrating a comparative analysis of the classification accuracies obtained using different kernel functions subject to three different loadings on the motor.

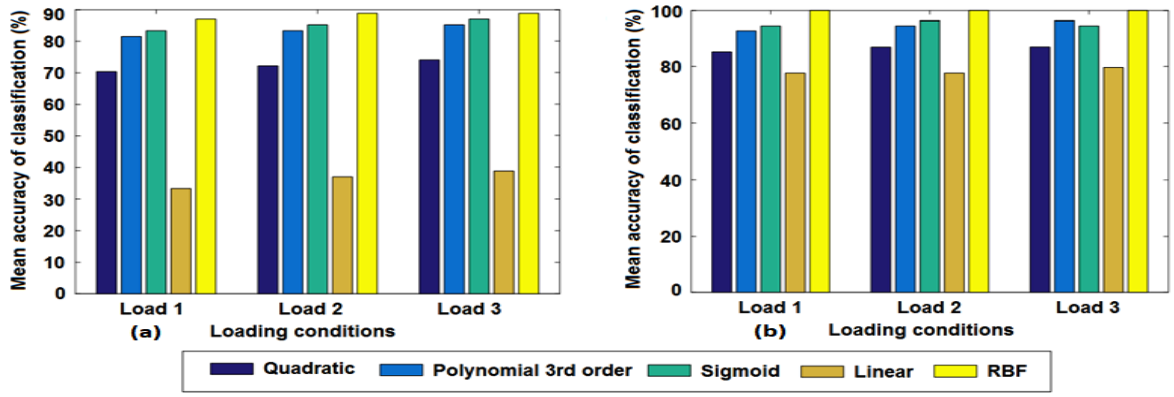

Figure 4.6: *Mean classification accuracies of kernels for three unknown faults under three loading conditions*

The three different loading variations, as described in section4.7 are illustrated as below:

Loading condition 1: No Mechanical load.

Loading condition 2: I.M with D.C. generator as a mechanical load.

Loading condition 3: A 200 Watt electrical load connected to the output of generator (while the full load of the generator is 750 W)

The following observations are made from the above results:

- It is observed that the RBF kernel yields the highest accuracy of classification in the present case, considering all three different loadings. The classification accuracy reaches 100% in all cases, irrespective of the unknown fault type or the load on the motor. Hence, the RBF kernel is selected as the best performing kernel function for this work.
- It is further observed that the mean accuracy of classification, for all the kernel functions, including the linear kernel, has improved significantly using the frequency domain features compared to the time domain features. Thus, extracting PCA features from frequency domain spectrums of various fault currents was discovered to be a superior method when compared to direct analysis of time domain fault current waveforms.
- The performance of a linear kernel in terms of the accuracy of classification of the motor is very poor (in the range of 35%) using direct time domain analysis; and the same has increased to in the range of 78% using frequency domain features; although, this accuracy of classification is still much poorer compared to the highest accuracy achieved using a RBF nonlinear kernel (in the range of 100%).
- Apart from the RBF kernel, other nonlinear kernel functions such as the sigmoid and the polynomial

  Third-order kernel functions also yield appreciable classification accuracy in the range of 95% and 94%, respectively. Hence, these could also be considered for analysis.

4.9.2 *Regression analysis*

We have further analysed the results for the comparison of linearity between the features of the time domain and the features of the frequency domain using linear regression. The linear regression coefficients are estimated using the above results obtained using both domain features.

The coefficient of linear regression (r) has been calculated using expression (4.4) as mentioned in Section 4.6 for each unknown type of fault, keeping two known classes of faults simultaneously. While $r = 1$, they end up identical, and in this situation there is a precise dating between the variables; and while $r = 0$, it can be said that the variables are beyond estimation from the linear regression equations. If the value of r with two major PC values is close to 1, it implies that the plots are linearly separable. The different values of linear regression coefficients for the classes BRB-FBR, with three unknown faults, are illustrated in Tables 4.8 (a) and 4.8 (b) from time and frequency domain analysis under different loading conditions. The graphical representations of the linear regression lines are shown in Figs. 4.7 and 4.8 for time and frequency domains, respectively.

Table 4.8: (a) Linear regression coefficients of BRB-FBR with three unknown faults using time domain feature

Loading conditions	BRB-FBR with unknown type 1			BRB-FBR with unknown type 2			BRB-FBR with unknown type 3		
	R phase	Y phase	B phase	R phase	Y phase	B phase	R phase	Y phase	B phase
Load 1	0.2696	0.2154	0.2968	0.2206	0.1982	0.1435	0.2748	0.3242	0.2923
Load 2	0.2056	0.2912	0.2738	0.1845	0.1284	0.1663	0.3242	0.3653	0.4007
Load 3	0.2457	0.2614	0.2932	0.2011	0.2143	0.1941	0.3008	0.3314	0.3982

Table 4.8: (b) Linear regression coefficients of BRB-FBR with three unknown faults using frequency domain feature

Loading conditions	BRB-FBR with unknown type1			BRB-FBR with unknown type 2			BRB-FBR with unknown type 3		
	R phase	Y phase	B phase	R phase	Y phase	B phase	R phase	Y phase	B phase
Load 1	0.9188	0.9276	0.9074	0.7923	0.8152	0.8013	0.7255	0.7381	0.7892
Load 2	0.8830	0.8961	0.9182	0.8575	0.8882	0.8991	0.7732	0.7425	0.7802
Load 3	0.8932	0.9165	0.9043	0.8241	0.8654	0.8549	0.7523	0.7652	0.7992

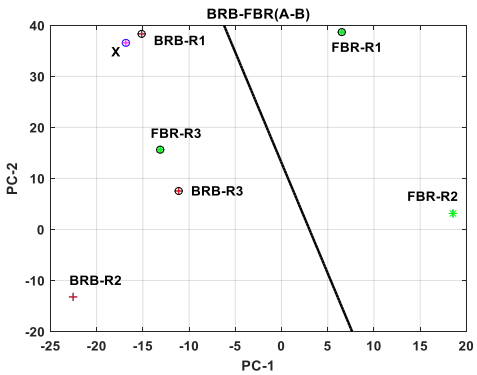

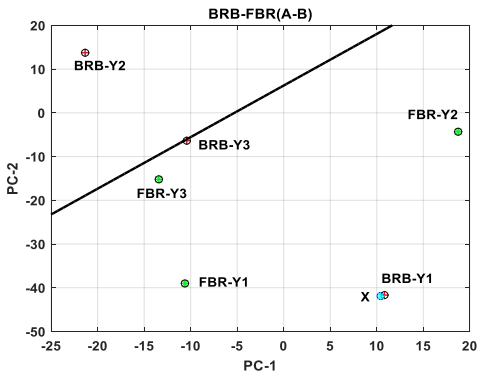

(a) (b)

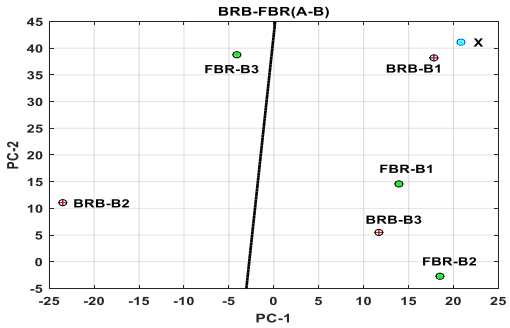

(c)

Figure 4.7: *PC plots of BRB-FBR using time domain features of three phase currents with the unknown 1 by linear kernel (a) R phase (b) Y phase (c) B phase*

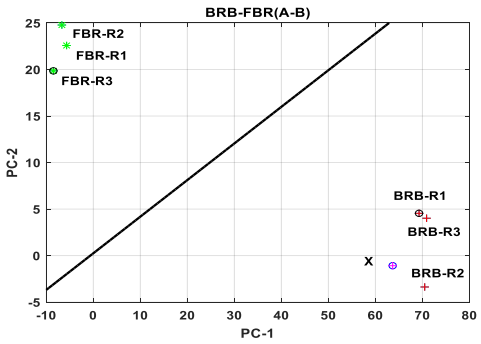

(a)

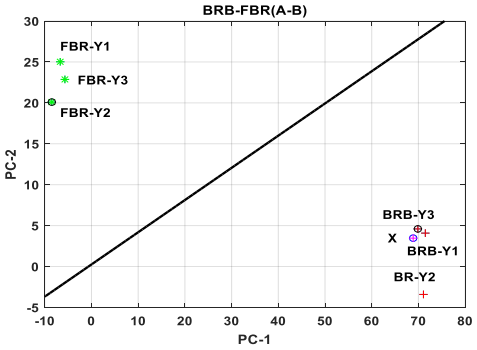

(b)

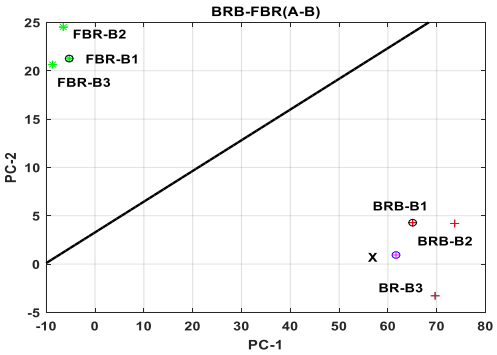

(c)

Figure 4.8: *PC plots of BRB-FBR using frequency domain features of three phase currents with the unknown 1 by linear kernel (a) R phase (b) Y phase (c) B phase*

It is observed from the above figures and tables that the correlation coefficients obtained from the frequency domain features are closer to 1 (with a mean correlation coefficient of 0.84, considering all the three phases and the three different loading conditions); whereas, those obtained from the time

domain features are much less than 1 (with a mean correlation coefficient of 0.26, considering all the three phases and the three different loading conditions). As a result, the slope of the regression line is close to 45 degrees, as seen in all of the sub-figures in Fig. 4.8; however, the slopes of the regression line, as seen in Fig. 4.7 with time domain features, are lying non-uniformly at different angles for different phases, and none of these lines is close to 45 degrees because the correlation coefficients are far from unity.

Chapter 5

Fault Classification using time-frequency domain analysis

Current signature analysis is used successfully for induction motor fault detection. A common mathematical tool for assessing fault signals is the wavelet transform. However, choosing the right mother wavelet is the main challenge with wavelet analysis. Additionally, choosing the best level of decomposition is crucial since as the level of decomposition rises, so do the complexity and computation time. In order to get a result that is noticeably accurate while maintaining a minimal degree of complexity, we have developed a method to select the optimal mother wavelet and decomposition level for fault current signals of three phase induction motors. Here, we analyse the results using mother wavelets from the Daubechies (db), Symlets (Sym), and Coiflets (Coif) groups and decompose fault current signals of three phase induction motors up to five levels. In order to add robustness to the model, we also varied the motor's loading in three distinct steps. We also examined the four main quality metrics—signal to noise ratio (SNR), peak signal to noise ratio (PSNR), correlation coefficient (CC), and root mean square error (RMSE)—and came to the conclusion that Symlet5's mother wavelet decomposed at level 4 was the best option. The current signals of seven motors having different faulty conditions are decomposed in multiple levels using the optimal mother wavelet function for unknown fault classification following multi resolution analysis (MRA) of the wavelet. The unsupervised fault classification has been performed in different loading conditions, and the sensitivity of fault classification has been checked at different levels of decomposition.

5.1 Introduction

Wavelet transform is a powerful technique that has seen widespread application in signal analysis and detection, particularly in signal detection and classification for fault type identification. Additionally, as there are many different types of mother wavelet and it might be challenging to make the best choice, making an optimal mother wavelet selection and selecting the optimal level of decomposition is crucial. Knowing the ideal mother wavelet and level of decomposition beforehand makes it easier to analyse fault waveforms with the least amount of effort, which cuts down on computing time and complexity. To improve fault identification, the discrete wavelet transform (DWT) divides the signal into several wavelet coefficients ('approximation' and 'detail').The accuracy of fault analysis depends on the best mother wavelet choice. Mother wavelets were previously used to detect L-G ground faults while examining various fault resistance levels [133]. M. F. Faizal discussed the significance of choosing mother wavelets that closely match each other to identify voltage sags [134]. Using the minimal description length (MDL) criterion, the optimal mother wavelet has been chosen to compress the power disturbance signal, and the inside permanent motor protection and interior permanent

synchronous motor drive systems have both been subjected to the same criterion [135–138]. The mother wavelet has been used to de-noise the partial discharge signal, with the maximum correlation coefficient value as a criterion (PD) [139, 140]. The optimal mother wavelet for bearing failure identification utilising vibration signals has been chosen using Energy to Shanon Entropy criteria [141, 142]. For one sort of fault detection in rotating machinery and power systems, researchers used one type of criterion to choose the best mother wavelet. They don't use many criteria to choose the best mother wavelet while assessing machine three phase current data for various types of defects. Based on the characteristics of the signal to be processed, selecting the best decomposition level is another crucial task. A signal's level of resolution can be used to identify faults since some sub-bands of the signal may have relevant information. However, the quality of the de-noised signals may be diminished if the wavelet's decomposition level is set too high because the amount of data would be drastically decreased. The selection of an indication is crucial for determining the best level to detect failures. For the purpose of detecting problems in the bearing and gearbox, respectively, researchers chose periodic impulses and GA as indicators from the signals in the time domain using DWT [143, 144]. Gear fault diagnostics has utilised gear meshing frequencies as an evaluation criterion [145].

Twenty mother wavelet functions were considered when choosing the optimal mother wavelet for this study's six types of defective conditions and one healthy condition. For the analysis, samples of stator current data from various defective (electrical and mechanical) induction motors are gathered. Signal to noise ratio (SNR), root mean square error (RMSE), peak signal to noise ratio (PSNR), and correlation coefficient have all been used to pick the mother wavelet. Distorted three-phase stator currents of motors with various fault situations, including the healthy one, are decomposed in several layers using a number of mother wavelet functions (db2-db10, sym3-sym8, and coif1-coif5). The decomposed signals are then reassembled using a reconstruction program. The signal to noise ratios (SNR), peak signal-to-noise ratios (PSNR), root mean square errors (RMSE), and correlation coefficients are calculated from the actual and reconstructed signals for each type of motor current signal at different decomposition levels. The optimal mother wavelet among the twenty mother wavelets given above has been selected based on the highest values of SNR, PSNR, correlation coefficient, and lowest values of RMSE for three phase current signals of all types of motors at all decomposition levels. Applying the same method, the same results were obtained under three different loading circumstances. The optimal level of decomposition has been selected based on the absolute values of the accuracy parameters and the difference in the level of decomposition.

5.2 Limitations of FFT, STFT and advantages of wavelet

The wavelet transform is a common tool in image and signal processing. The Fast Fourier Transform (FFT) converts a signal from the time domain to the frequency domain, changing our perception of the signal from amplitude vs. time to amplitude vs. frequency. FFT is a mathematical tool for converting a signal from the time domain to the frequency domain. Because FFT often translates time

to the frequency of signals and vice versa but does not give simultaneous time and frequency information, it is extremely successful in solving problems involving the location of frequency. The transformation process from time domain to frequency domain of a signal loses time information. It is not efficient for representing discontinuities due to its limited frequency bandwidth and time duration. FFT is not suitable to detect the transient characteristics of a signal: drift, abrupt changes, and trends, which are the most important parts of the signal. It represents a signal with a few coefficients. The short-term Fourier transform (STFT) can be used to evaluate non-stationary signals and improve the performance of the FT, which offers time-frequency informative data. Due to its use of a single window with consistent resolution across all frequencies for the duration of the signal analysis, STFT has this limitation. The time window of STFT is fixed for all the frequencies, by analysing a signal within a set time window, it distinguishes between a signal's temporal and frequency components by analysing a signal within a predetermined time range. The wavelet transform is used for fault analysis accuracy to address the shortcomings of FFT and STFT, and it has gained widespread acceptance in signal processing [146, 147]. It has been shown that wavelet analysis can improve fault diagnosis [148]. For many types of signals, a variable window size is required according to the frequency to increase flexibility. Wavelet analysis is similar in spirit to the Fourier transform, but it has significant advancements for signal processing. It applies a variable-sized windowing technique. For the study of a signal's high- and low-frequency components, respectively, a window of a shorter and longer time interval is used. It is particularly efficient to deal with the local features of a signal, such as trends, breakdown sites, and self-resemblance, through signal analysis utilising the wavelet transform. Additionally, wavelet analysis has the ability to eliminate noise from a signal or compressed signal.

5.3 Signal decomposition using mother wavelets

The wavelet family is typically thought to be the most appropriate for particular applications because it can represent any signal with the fewest number of coefficients possible. Shifting the window in time, signal multiplication, integration, and integration are the steps that make up the computation of the continuous wavelet transform [149]:

$$CWT_{\tau}^{\Psi} = \frac{1}{\sqrt{|S|}} \int f(t)\, \Psi^{*}\left(\frac{t-\tau}{S}\right) dt \qquad (5.1)$$

where, *f(t)* is the input signal, *S* is the scale, τ is the translation, $\Psi(t)$ is the function of transformation called the mother wavelet, given by

$$\Psi_{\tau,S} = \frac{1}{\sqrt{S}}\, \Psi\left(\frac{t-\tau}{S}\right) \qquad (5.2)$$

The parameters of translation $\tau = n.2^{m}$ and scale $s = 2^{m}$ are chosen to sample the CWT on a dyadic grid to get discrete wavelet transform (DWT) coefficients as:

$$\Psi_{m,n}(t) = \frac{1}{\sqrt{2^{m}}}\, \Psi\left(\frac{t-n2^{m}}{2^{m}}\right) \qquad (5.3)$$

Using successive low pass and high pass filters, DWT seeks to extract information from the spectra by splitting them into high- and low frequency components, represented by:

$$x_{high}(k) = \sum_n f(n)\, q(2k - n) \quad (5.4)$$

$$x_{low}(k) = \sum_n f(n)\, r(2k - n) \quad (5.5)$$

where the outputs of the low pass and high pass filters, which have impulse response values of *r* and *q*, respectively, are $x_{high}(k)$ and $x_{low}(k)$ While the "detail" (cD) part of the signal also contains low frequency components, the "approximate" (cA) signal does not [150,151]. Higher detail sections are eliminated when computing the 'm'-level decomposition, which lowers the overall frequency of the resulting data. The mother wavelet is the original function, and the wavelet functions are scaled, translated, and dilated versions of this original function. The signals in the current work were divided into five decomposition levels using mother wavelets from the Daubechies (db), Symlets (Sym), and Coiflets (Coif) families. Below is a description of the mother wavelet families.

5.3.1 *Mother wavelet*

Monique P. Fargues compared the orthogonal and non-orthogonal wavelet for denoising applications for SNR levels, several sample sizes, and thresholding schemes, and he has shown that orthogonal wavelet transforms usually have better denoising performances than the non-orthogonal [152]. The orthogonal decomposition is useful for the non-stationary signal, whose variance depends on the window of the data under consideration. Its decomposition provides information on the variability of wave height with time at different timescales [153]. The orthogonal wavelet transform is able to detect abnormal transients due to early damage to a component, and it uses a fast algorithm that decomposes the current or vibration signal into the minimum number of wavelet series. That's why the orthogonal wavelet transform is very useful for machine fault analysis [154]. For fault analysis, various orthogonal wavelets (Haar, Daubechies, Symlet, and Coiflet) are typically used [155]. The haar (db1) wavelet is not hired here because it cannot be used for distorted continuous signal processing as it isn't continuous and is created via a sequence of rescaled "square-formed" capabilities combined.

5.3.1.1 *Daubechie Wavelet*

The Daubechies wavelet family is gaining popularity due to its compact and orthogonal support abilities, which are used for feature analysis. Daubechies' wavelet family has been used to get details more accurately than others. This wavelet has similarities to QRS complexes and has a low-frequency energy spectrum. The Daubechies wavelet is smoother than the Haar wavelet, which uses overlapping windows. There are four wavelet and scaling coefficients in the Daubechies D4 transform.

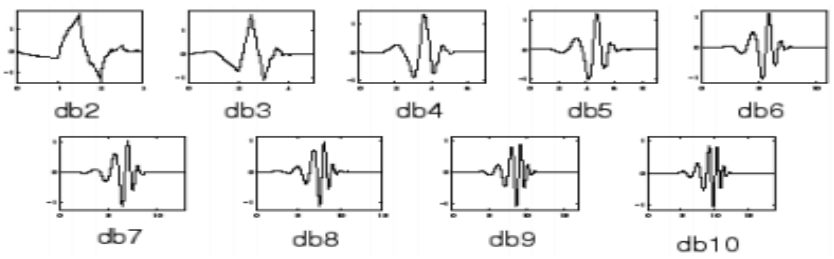

Figure 5.1*: Daubechies wavelet family.*

5.3.1.2 *Symlet wavelet*

Daubechies proposed the Symlet wavelet family as an orthogonal and nearly symmetrical set of wavelets as modifications to the DB family. The properties of the Symlet wavelet family and the Daubechies wavelet family are similar. The Symlet wavelet family's denoising performances are effective. In practice, Symlet wavelets are chosen with an even number of wavelets as Daubechies. The signal performance is better with Symlet wavelet, and the signal to noise ratio of a reconstructed or denoised signal can be improved using Symlet wavelet.

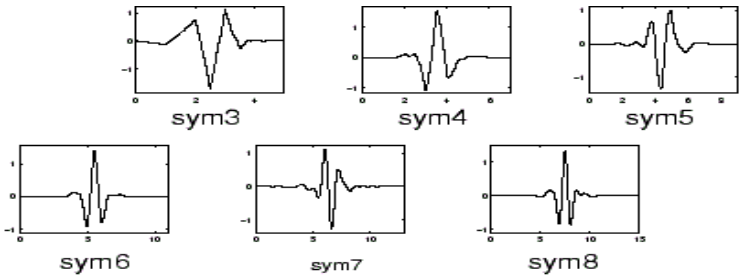

Figure 5.2: *Symlet wavelet family.*

5.3.1.3 *Coiflet wavelet*

The Daubechies wavelet served as the basis for Coiflet's creation. It employs windows that overlap considerably and has an even higher processing overhead. Since it employs six scaling and wavelet function coefficients, an increase in pixel averaging and differencing results in a smoother wavelet and greater versatility in a number of signal processing approaches. Both the scaling function and the wavelet function have 2N moments that are equal to zero. A support of length 6N-1 is shared by the two functions. The filter has the same organisational principles as Haar and Daubechies. The Coiflet wavelet employs the mirror method as well.

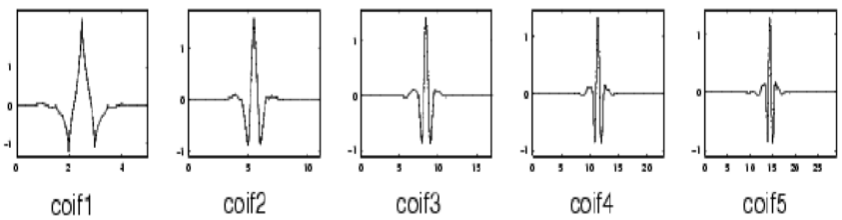

Figure 5.3: *Coiflet wavelet family*

5.4 Experimentation

The experimentation has been performed on the same set up as illustrated in Chapter 3. The three phase current signals are collected from six induction motors with six known types of fault conditions: broken rotor bars (BR), faulted bearings (FB), misaligned rotors (RM), rotor unbalance (RU), stator winding fault (SF), single phase voltage unbalance (VU), and healthy motors (HM) under three loading conditions. The loading conditions have been explained in Chapter 3 (section 3.2).

5.5 Determination of optimal mother wavelet

Even though DWT performs satisfactorily, choosing the best mother wavelet to perform a task involving wavelets can be difficult because the same signal yields different results when applied to various mother wavelets due to its various feature extraction, de-noising, component separation, and reconstruction of coefficients from the frequency domain and time domain signals. As a result, the performance of the induction motor's fault analysis can be affected by the choice of the mother wavelet function.

5.5.1 *Current signal reconstruction based on wavelet decomposition*

The decomposition analysis is described in DWT, and the other half of the story is how the actual signal can be restored to its original state using the signal's deconstructed components without losing any information. This name of the process is called "synthesis of reconstruction." The mathematical manipulation of the process of reconstruction is called the inverse discrete wavelet transform (IDWT). The process of wavelet reconstruction consists of filtering and up-sampling. Up-sampling (or interpolation) is done by padding zero between every two coefficients. The filters' design for decomposition and reconstruction is based on a well-known technique called "quadrature mirror filters." The reconstructed approximations and details are the actual constituents of the original signal. In fact, it is found when the approximate coefficient vector cA1 and detail coefficient cD1 are combined because the coefficient vectors are produced with the help of down-sampling. Before combining the approximations and details, reconstruction is necessary. The process can be extended to the multi-level component analysis; all of the components of the reconstructed signal are found to have similar relationships. That is, the original signal can be reassembled in several ways.

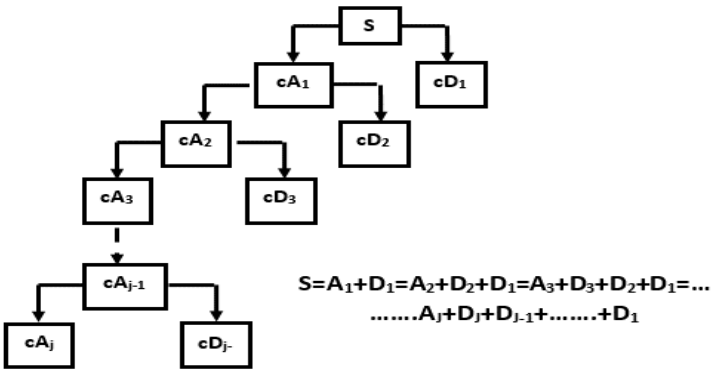

Figure 5.4 *Signal reconstruction after decomposition*

5.5.2 *Accuracy parameters to select the optimal mother wavelet and optimal decomposition level*

The inverse discrete wavelet transform (IDWT), which reconstructs the signal without losing any information, assembles the deconstructed components of the signal. The discrete wavelet transform (DWT) breaks down the signal into detailed and approximate coefficients. In the current study, we compared the original and recreated signals and used four accuracy metrics to measure how closely the signals were rebuilt. These are shown below:

Root Mean Square Error (RMSE): The current sample of the original and reconstructed signal has been used for analysis, and the square root of the mean square error has been computed. The mean squared error (MSE) measures the average of the squares of deviations or errors, i.e., the difference between the original and reconstructed signal. The RMSD or RMSE is found by taking the square root of MSE [156]. RMSE is estimated as follows:

Mean square error = $\frac{1}{M}\sum_{n=1}^{M}[x(p)-\tilde{x}(p)]^2$ (5.6)

Root mean square error (RMSE) = $\sqrt{\frac{1}{M}\sum_{n=1}^{M}[x(p)-\tilde{x}(p)]^2}$ (5.7)

where, M is the length of the signal, and *x(p)* is the *p*-th sample data of the current signature for the provided type of fault and $\tilde{x}(p)$ is the *p*-th sample data of reconstructed signal.

If the RMSE value is lower, a mother wavelet's de-noising performance will be improved. Under three different loading situations, RMSE has been determined for each level of decomposition and for each of the 20 numbers of mother wavelets indicated above.

Signal to Noise Ratio (SNR): SNR, or signal-to-noise ratio, is a measurement of how strong the preferred signal is in comparison to background noise. SNR directly impacts the performance of the denoising of a mother wavelet function. The smaller the MSE, the greater the SNR, and the better the denoising effect. To raise the SNR, noise reduction is necessary. The signal strength is stronger in comparison to the noise levels when the SNR value is higher.

The following expectations are made for this accuracy measure, which is used to assess the de-noising effectiveness of any particular mother wavelet [157, 158]:

$$SNR = 10log_{10}\left(\frac{\sum_{n=1}^{M}x(p)^2}{\sum_{n=1}^{M}[x(p)-\hat{x}(p)]^2}\right) \quad (5.8)$$

For each of the five levels of decomposition, the SNR between the denoised signal and the noise produced by each defective motor is computed.

Peak Signal to Noise Ratio (PSNR): The peak magnitude of a signal and the mean square error between the original signal and the reconstructed signal produced after decomposition are used to quantify it as another way to measure standard distortion, as follows [159]:

$$PSNR = 10log_{10}\left(\frac{MAX^2}{MSE}\right) \quad (5.9)$$

Here, MAX is the maximum possible value of the signal, and MSE is the mean square error of the reconstructed signal. The quality of the reconstructed signal will be better with a lower value of MSE and a higher value of PSNR.

Statistical correlation: A statistical tool that determines the strength of a link between variables is correlation analysis. The correlation coefficient (q) between two variables j and i for an n-pair of two-dimensional observations, represented as (i_1 j_1), (i_2 j_2), (i_3 j_3), (i_n j_n) etc., is defined as [160]:

$$\text{Correlation coefficient } (q) = \frac{\sum_{k=1}^{n}\left(v_k - \frac{1}{n}\sum_{j=1}^{n} v_j\right)\left(i_k - \frac{1}{n}\sum_{j=1}^{n} i_j\right)}{\sqrt{\sum_{k=1}^{n}(v_k - \frac{1}{n}\sum_{j=1}^{n} v_j)^2}\sqrt{\sum_{k=1}^{n}(i_k - \frac{1}{n}\sum_{j=1}^{n} i_j)^2}} \quad (5.10)$$

The signals of current and vibration from the rotating machine carry a lot of information about different fault conditions. Statistical parameters for different fault conditions can be found by statistical analysis of the acquired current signals. The parameters, called statistical features, carry information about time domain signals about the different fault conditions. The features are also used to detect faults, and some of the features can be used individually to distinguish between healthy and faulty components. Major information about the fault situation is carried by the current signals. Therefore, in order to identify the best mother wavelet, we computed the correlation coefficients between the original signal and the wavelet decomposed signal [161]. The block diagram that represents the steps of correlation coefficients from different mother wavelet families has been shown in Fig. 5.5.

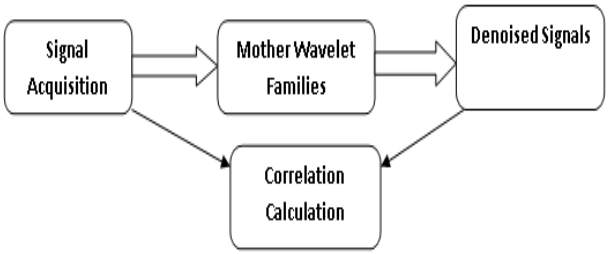

Figure 5.5: *The correlation block diagram between the noisy and de-noised signals using mother wavelet families [162]*

5.5.3 *Flow of Work*

The suggested work is designed to investigate two distinct topics: choosing the best mother wavelet and choosing the best level of decomposition for categorizing the fault pattern of a three-phase induction motor. The work's primary objective is to choose the best mother wavelet from a set of twenty options, including db2 to db10, Symlet3 to Symlet8, and Coif1 to Coif5. The second challenge

is determining the optimal level of waveform decomposition for the fault current in order to categorise the motor failure. Six different faults have been applied to a specific three phase induction motor in order to suit both purposes. The data from the motor's normal operation is also taken into account. As previously established, these defects include BR, FB, RM, RU, SF, and VU. These errors have been tested under three distinct loading scenarios, including no load, generator load, and motor load using a 200 W generator. Four accuracy parameters, such as SNR, RMSE, PSNR, and CC, have been used in the subsequent study of the three phase line fault currents. The outcomes are clearly demonstrated in the following two segments.

- In this study, we have described a method for selecting the optimum mother wavelet for six different classes of induction motor problems using three phase line current signals. The work for choosing the ideal level of wavelet decomposition of the signal has been further extended. The work presented here is intended to investigate two specific topics: identification of the best mother wavelet and identification of the best level of decomposition, in order to categorise the fault pattern of a three phase induction motor.
- The six various faults have been executed in order to fulfill both of the objectives, and the data in a healthy state is also taken into account. As previously established, these faults include BR, RM, FB, SF, RU, and VU. Data samples of current signals are collected from six dysfunctional and one healthy motors, as shown in the experiments section.
- Finding the optimal mother wavelet among 20 options, such as db2 to db10, Coif1 to Coif5, and Sym3 to Sym8, is the first duty of the work. The best way to describe this is that it's like a game of hide-and-seek for the intrepid traveler. The decomposed signal of each level of each type of motor has been reconstructed using approximation coefficients. Since the Haar (db1) wavelet family is made up of a series of rescaled "square-shaped" functions joined together and is not continuous, it cannot be used for the analysis of distorted continuous signals. The optimal mother wavelet for this application was chosen out of 20 mother wavelets from the daubechie family (db2-db10), the symlet family (sym3-sym8), and the coiflet family (coif1-coif5).
- Four criteria for accuracy form the basis of the selection procedure. When the three-phase currents are analysed using the twenty different mother wavelets mentioned above, the four different parameters, including the signal-to-noise ratio (SNR), peak signal-to-noise ratio (PSNR), correlation coefficient (CC), and root mean square error (RMSE), are seen to vary for the six different faults and the motor's healthy condition.
- An approach for choosing the optimal mother wavelet was previously put forward in [162]. However, the authors only considered two factors—RMSE and correlation coefficient—after examining the line current signals of faulty motors. In addition, the motor was evaluated under a single loading scenario, and the approach stated in [162] only used one degree of decomposition. As a result, the current work aims to thoroughly analyse and develop a

reliable method for selecting the optimal mother wavelet. As a result, we have added two more useful components to the current study: altering the motor's workload and varying the degree of wavelet decomposition.

- We were able to obtain the data by adjusting the load on the motor in three steps: no load, generator load, and motor with generator running with an additional electrical load of 200 W. For twenty distinct mother wavelet numbers, we also divided the current signals into five stages of decomposition for six different faults and one healthy motor. Four accuracy parameters, such as SNR, PSNR, RMSE, and CC, have been used in the subsequent study of the three phase line fault currents.
- The entire method of analysis has been illustrated in graphical form, as shown in Fig. 5.6.

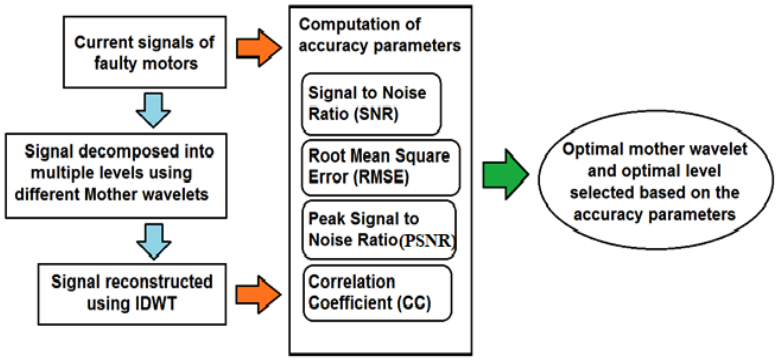

Figure 5.6: *Work flow diagram of this work*

5.5.4 *Result to determine the optimum mother wavelet*

In the first section of the investigation, the variations of the four different parameters, including the signal-to-noise ratio (SNR), peak signal-to-noise ratio (PSNR), correlation coefficient (CC), and root mean square error (RMSE) values, are observed for the six different faults and the motor's healthy condition. These characteristics were derived by employing twenty different mother wavelets with five levels of decomposition to analyse the three-phase currents. The reconstructed signals after the first level of decomposition of three phase currents have been shown in Figs. 5.7, 5.8, and 5.9 for broken rotor bars, stator winding faults, and faulted bearings, respectively. It is also possible to modify the load on the motor in three independent stages, starting with no-load and moving on to loading the motor with the generator's dead mechanical weight and then 200 W of electrical load.

In order to compare the fluctuations of all other elements, such as loading, mother wavelet, level of decomposition, and phase, with the variations of the four accuracy parameters, the broken rotor fault (BR), one of the most common failures encountered in induction motors, is taken into consideration. After that, changes to these parameters are displayed sequentially alongside changes to other variables. With five levels of wavelet decomposition and twenty mother wavelets, Fig. 5.10 shows an example instance that demonstrates how the SNR parameter changes for the BR fault solely under these three loadings.

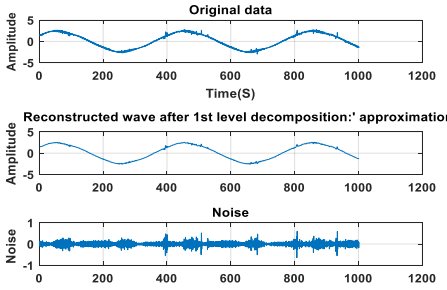

(a)

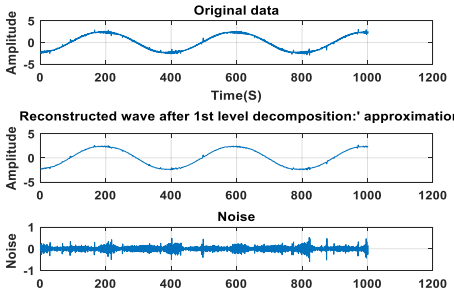

(b)

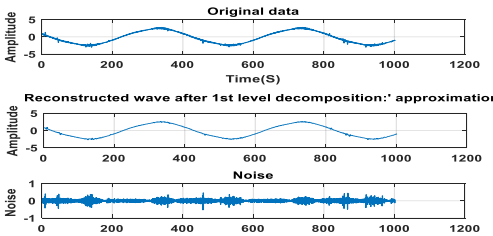

(c)

Figure 5.7: *Reconstructed signal after first level decomposition of broken rotor bar fault under loading 1 condition,(a) R phase, (b) Y phase, (c) B phase*

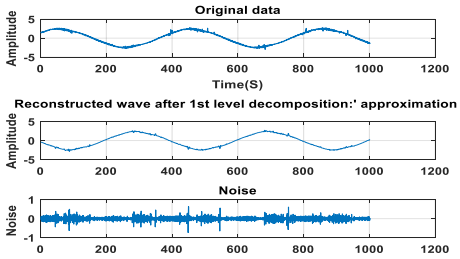

(a)

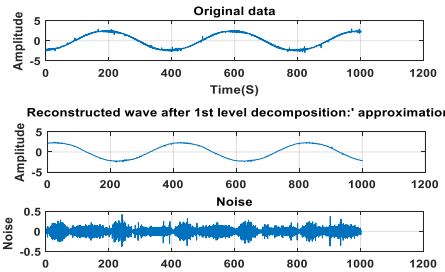

(b)

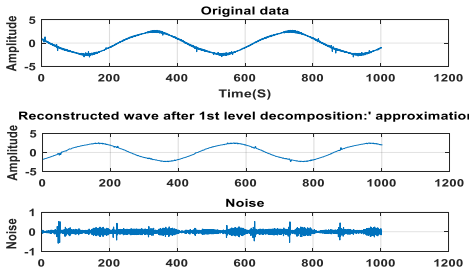

(c)

Figure 5.8: *Reconstructed signal after first level decomposition of stator winding fault under loading 1 condition, (a) R phase, (b) Y phase, (c) B phase*

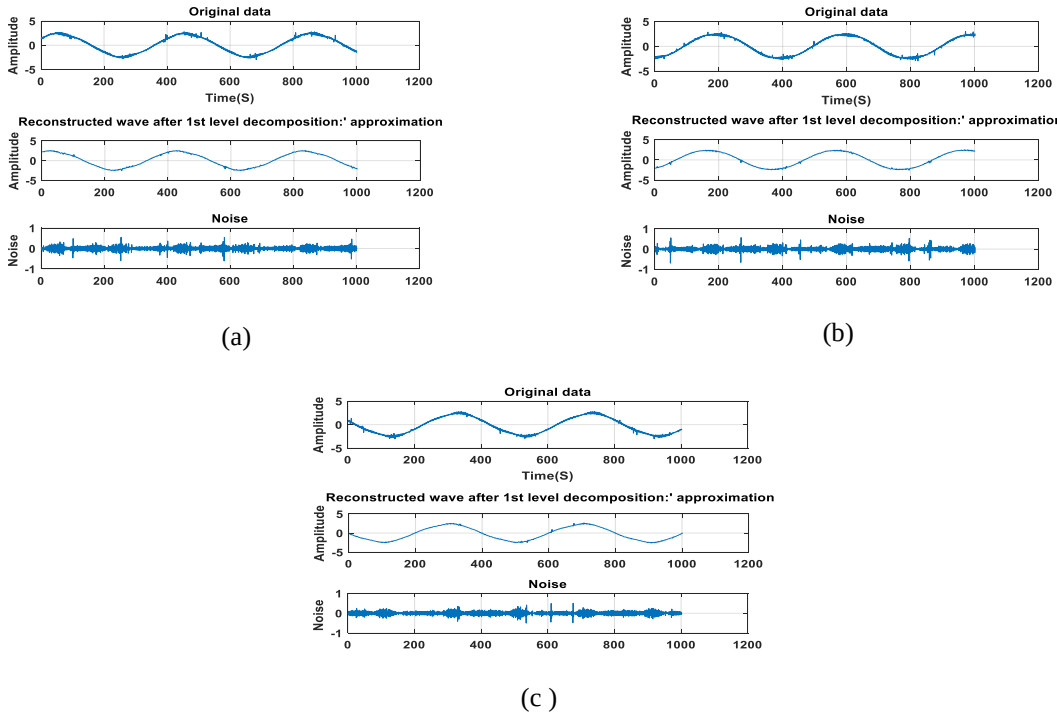

Figure 5.9: *Reconstructed signal after first level decomposition of faulted bearing under loading 1 condition, (a) R phase, (b) Y phase, (c) B phase*

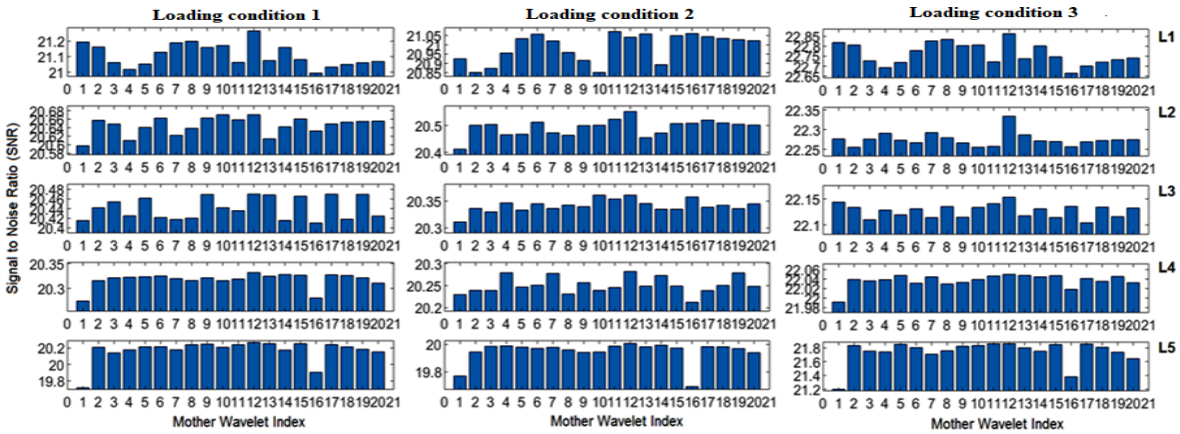

Figure 5.10 *Using R phase line current data, a comparison is made to show how the SNR for a BR fault varies with 20 different mother wavelets (Mother wavelet Index 1 to 9: db2 to db10; 10 to 15: Symlet3 to Symlet8; 16 to 20: Coif1 to Coif5), all five levels of wavelet decompositions (L1, L2, L3, L4, and L5), and three different loading conditions (loading condition 1, loading condition 2, loading condition 3)*

When the results of Fig. 5.10 are compared, it becomes clear that there is a significant difference between the mother wavelets, notably up to level 3 wavelet decomposition (L3) for each of the three loading circumstances. According to careful observation, the Mother Wavelet Index of 12 for the Symlet5 mother wavelet consistently generates the highest SNR among the competitors. Particularly at the lowest levels of decomposition, this is clearly seen. With level-5 wavelet decomposition, the SNR values vary so little that it is practically unnoticeable (L5). Similar to this, Figs. 5.11, 5.12, and 5.13 show the variations in RMSE, PSNR, and CC for BR faults, respectively, together with variations in the other parameters.

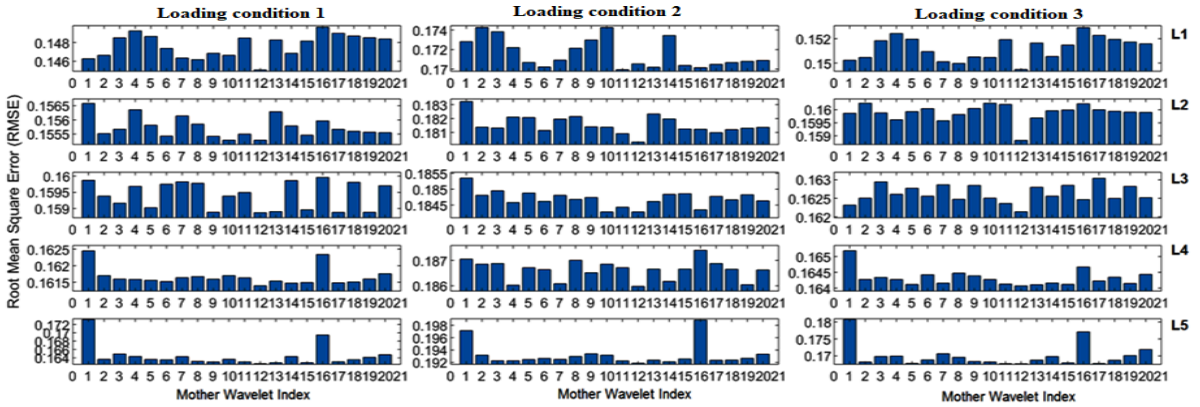

Figure 5.11: *Using R phase line current data, a comparison was made to show how the RMSE for a BR fault varied with 20 different mother wavelets (Mother wavelet Index 1 to 9: db2 to db10; 10 to 15: Symlet3 to Symlet8; 16 to 20: Coif1 to Coif5), all five levels of wavelet decompositions (L1, L2, L3, L4 and L5), and three different loading conditions (loading condition 1, loading condition 2, loading condition 3)*

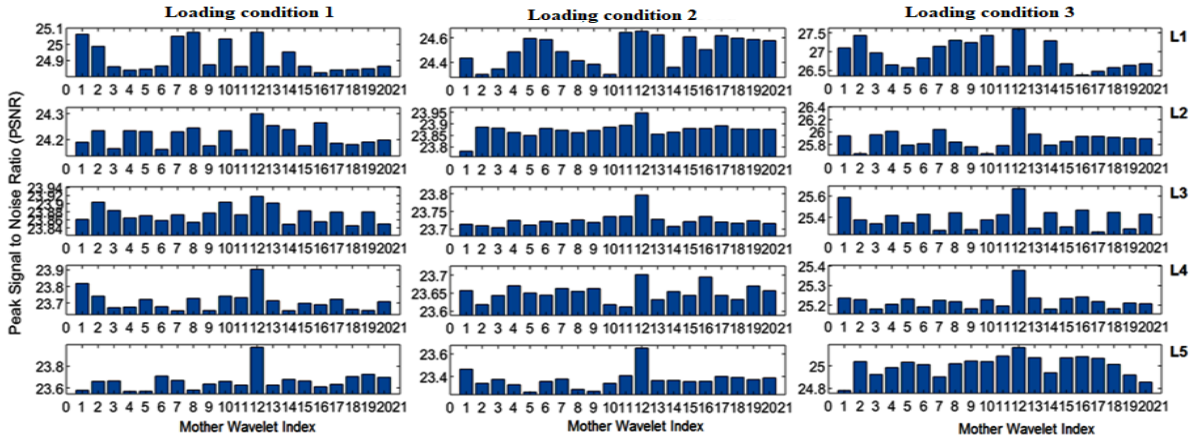

Figure 5.12: *Using R phase line current data, a comparison is made between the PSNR variation for BR fault using 20 different mother wavelets (Mother wavelet Index 1 to 9: db2 to db10; 10 to 15: Symlet3 to Symlet8; 16 to 20: Coif1 to Coif5), all five wavelet decomposition levels (L1, L2, L3, L4 and L5), and three different loading conditions (loading condition 1, loading condition 2 and loading condition 3)*

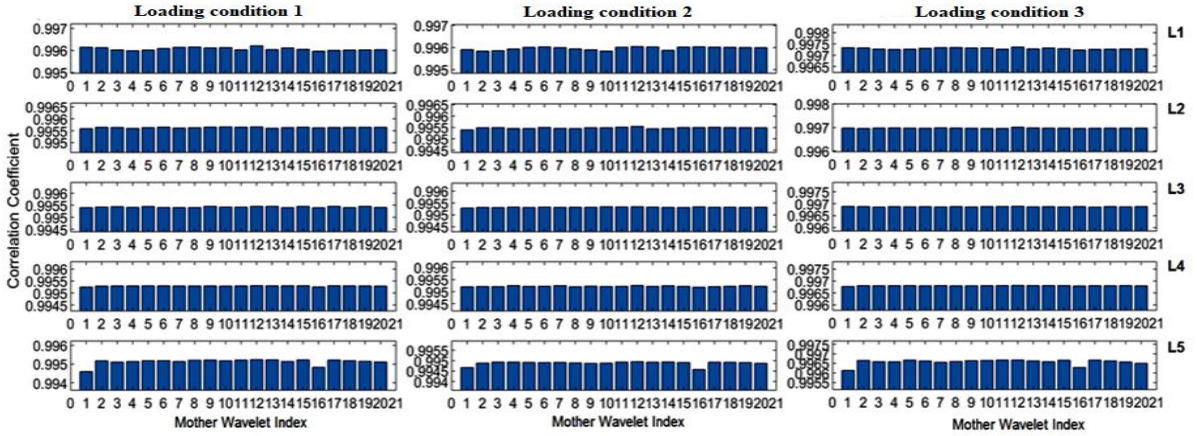

Figure 5.13: *Using R phase line current data, a comparison is made to show how the CC for a BR fault varies with 20 different mother wavelets (Mother wavelet Index 1 to 9: db2 to db10; 10 to 15: Symlet3 to Symlet8; 16 to 20: Coif1 to Coif5), all five levels of wavelet decompositions (L1, L2, L3, L4 and L5), and three different loading conditions (loading condition 1, loading condition 2 and loading condition 3)*

Fig. 5.11 makes it abundantly evident that the Mother Wavelet Index 12 consistently has the lowest RMSE under practically all conditions, independent of variations in loading or the degree of wavelet decomposition of the signal. Up until, say, level 3, this variance is once again predominant. Thereafter, an increasing consistency of the values is seen. No matter the degree of decomposition, the Mother Wavelet Index: 12, which is the Symlet-5 mother wavelet, consistently has the highest PSNR values, as seen in Fig. 4. However, the correlation coefficients, as seen in Fig. 5.13, are the least variable under all three loadings, regardless of the mother wavelet or the degree of decomposition. Further observation reveals that Fig. 5.13's bar diagrams are more uniform and that most of them deviate from one another by very small margins. Because of this, the Symlet5 mother wavelet does not have supremacy over the others, as was the case with the SNR, RMSE, and PSNR parameters, as illustrated in Figs. 5.10, 5.11, and 5.12, respectively. Therefore, it can be concluded that although the correlation coefficient has a narrower margin of variation than the others—SNR, RMSE, and PSNR—it is still an adequate accuracy measure for identifying the optimal level in the suggested task. As a result, we took into account this important statistical characteristic for the analysis that follows.

Various other defects have also undergone sequential analysis. Fig. 5.14 shows the SNR values derived using R-phase line current signals for the variation of all six possible faults under no-load conditions. Once more, it is shown that additional faults also point to Symlet5 as the best mother wavelet because it consistently produces the highest SNR levels across nearly all six faults, depending on the level. The variation in SNR levels is once again noticeable in the lower levels of wavelet decomposition, up to level 3, and then progressively becomes uniform thereafter; thus, the conclusion drawn from Fig. 5.10, which only considers the BR fault, also applies to other faults. This is distinctly observed in Fig. 5.14.

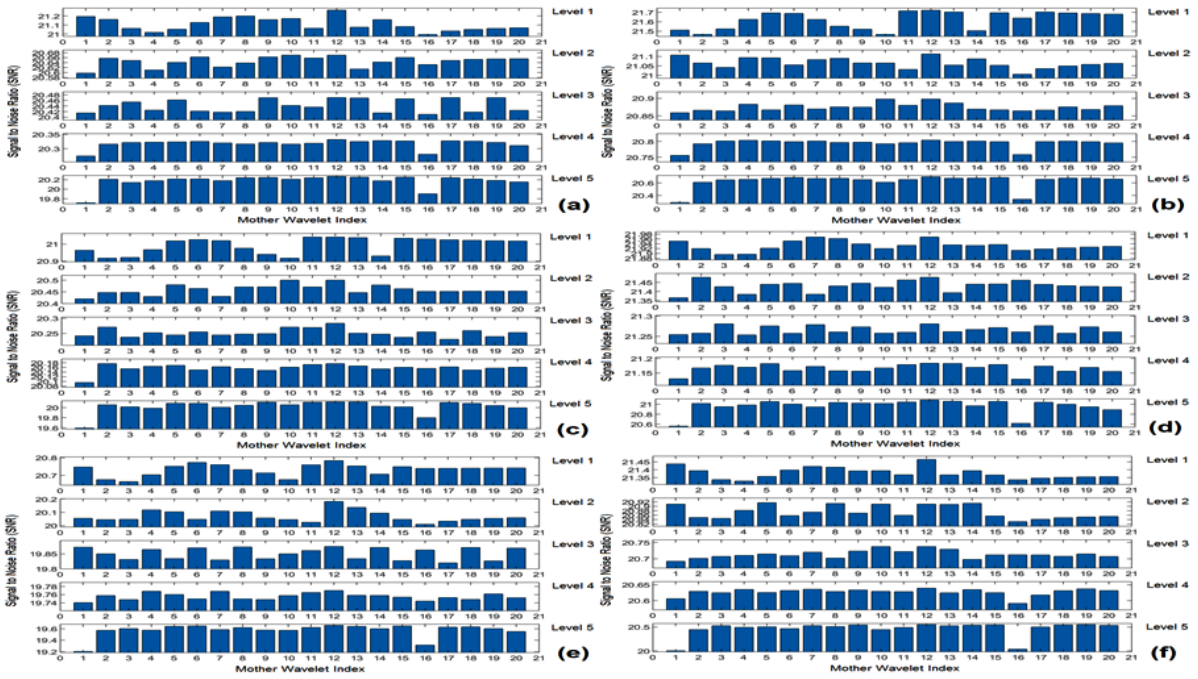

Figure 5.14: *Comparison using 20 different mother wavelets (Mother wavelet Index 1 to 9: db2 to db10; 10 to 15: Symlet3 to Symlet8; 16 to 20: Coif1 to Coif5), all five levels of wavelet decompositions, under loading condition 1, and R phase line current data to show variation of SNR for variation of all six faults (a) BR, (b) FB, (c) RM, (d) RU,(e) SF and (f) VU*

Fig. 5.14 depicts the observations described above using only R phase current data and no load circumstances for the various faults. We further examined each of the faults in a similar way for each of the three loading scenarios and with each of the three phase current signals using twenty different mother wavelets with five levels of decomposition. It has been noted that for each of the fault classes, Symlet5 mother wavelets typically yield the best value for each parameter. The number of optimal cases acquired with Symlet-5 mother wavelet and the number of optimal cases acquired with any other mother wavelet were compared in our data comparative study. With regard to the classes of errors in Table 5.1, we have specifically illustrated the results. It should be noted that we considered 20 mother wavelet numbers and 4 accuracy metrics for each of the 7 types of faults and the healthy state. Each parameter is further examined for 3 different loading circumstances, 5 levels of decomposition, and all three-phase current signals. As a result, each fault class's total number of observations is as follows:

The number of observations for each class of fault = (3 loading conditions) × (current signals of 3 phase) × (5 decomposition levels) × (4 accuracy parameters) = 180

These results are summarized further and described graphically in Fig. 5.15 (a), and the magnified form of Figure 5.15 (a) is shown in Fig. 5.15 (b), which shows a prominent comparison of the optimal results obtained with Symlet5 or any others.

Table 5.1: Results of observations with optimum parameter found with Symlet5 mother wavelet under six different fault conditions, one healthy condition and the overall representation; considering all parameters together (SNR, RMSE, PSNR and CC), all three phases and all five levels of wavelet decomposition

Fault Class	BR		FB		RM		RU		SF		VU		HM	
Mother wavelet	Sym5	Oth	Sym5	Oth	Sym5	Oth	Sym5	Oth	Sym5	Oth	Sym5	Oth	Sym5	Oth
Number of optimum parameters	169	11	173	7	175	5	174	6	169	11	177	3	169	11
Percentage of optimum parameters	93.89	6.11	96.11	3.89	97.22	2.78	96.67	3.33	93.89	6.11	98.33	1.67	93.89	6.11

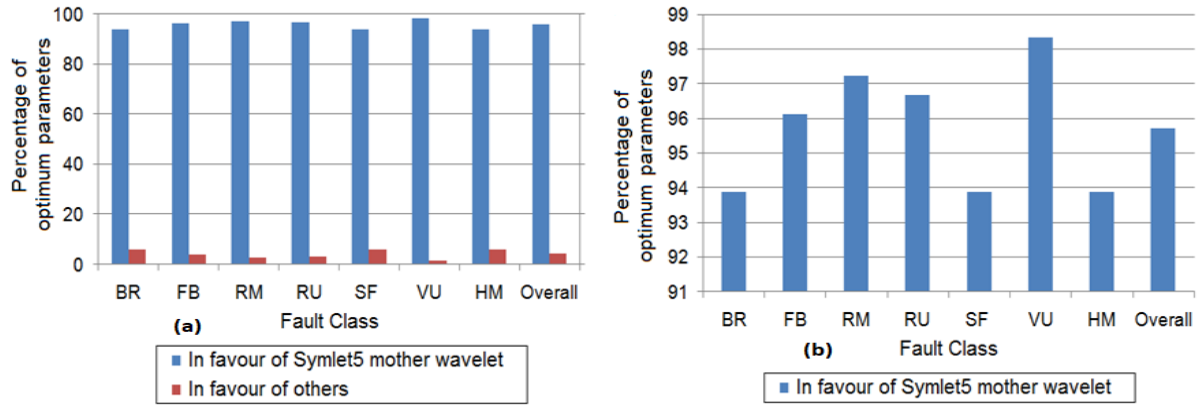

Figure 5.15: *(a) Considering all parameters (SNR, RMSE, PSNR, and CC), all three phases, and all five levels of wavelet decomposition, the comparison shows the percentage of observations under six different fault conditions, one healthy condition, and the overall representation with the optimum parameter found with Symlet5 mother wavelet (b) magnified view of Fig. 5.15 (a)*

Fig. 5.15 (b) shows that in more than 95% of the total observed cases, Symlet5 is used to achieve the best accuracy parameter value when SNR, RMSE, PSNR, and CC are taken into account together. Additionally, Symlet 5 considers all fault types, decomposition levels, phases, and motor loading. From these findings, Symlet5 is deduced to be the ideal mother wavelet with a greater than 95% confidence level. Additionally, it is noted that even for individual faults like BR and FR, the accuracy of the best findings in favour of Symlet5 is close to 94% (as seen in Fig. 5.15(b)), with the maximum accuracy being above 98%. (for a VU fault). As a result, the standard deviation of these final results for individual mistakes, as shown in Fig. 5.15(b), is similarly close to 1.833%, which is noteworthy from all angles.

These overall results from Table 5.1 and Fig. 5.15 are divided into four categories according to the pattern of load, current phase, accuracy parameter, and decomposition level. These categories are independently detailed in tabular representations in tables 5.2, 5.3, 5.4, and 5.5. Fig. 5.16, which shows the accuracy of improved parameters separately for the four different components stated above, was created by again summing these data.

Table 5.2: For seven different fault patterns and three variation in loading conditions, detailed results are shown that demonstrate the number of fault parameters that Symlet5 mother wavelet can handle at their optimum level. These results take into account all of the parameters (SNR, RMSE, PSNR, and CC), all three phases, and all five levels of wavelet decomposition.

Pattern of load	BR		RM		FB		SF		RU		VU		HM	
	Sym5	Oth	Sym5	Oth	Sym5	Oth	Sym5	Oth	Sym5	Oth	Sym5	Oth	Sym5	Oth
Loading 1	52	8	58	2	57	3	52	8	58	2	57	3	59	1
Loading 2	57	3	60	0	59	1	60	0	56	4	60	0	54	6
Loading 3	60	0	57	3	57	3	57	3	60	0	60	0	56	4

Table 5.3 : For seven different fault patterns and variation of all three phases, detailed results are shown that demonstrate the number of fault parameters that Symlet5 mother wavelet can handle at their optimum level. These results take into account all of the parameters (SNR, RMSE, PSNR, and CC), all three phases, and all five levels of wavelet decomposition.

Phase	BR		RM		FB		SF		RU		VU		HM	
	Sym5	Oth	Sym5	Oth	Sym5	Oth	Sym5	Oth	Sym5	Oth	Sym5	Oth	Sym5	Oth
R Phase	58	2	56	4	59	1	57	3	56	4	57	3	56	4
Y Phase	55	5	59	1	55	5	58	2	59	1	60	0	54	6
B Phase	56	4	60	0	59	1	54	6	59	1	60	0	59	1

Table 5.4 : For seven different fault patterns, against the variation of all fault parameters (SNR, RMSE, PSNR, and CC), detailed results showing the number of optimum fault parameter levels found in favour of Symlet5 mother wavelet are shown. These results take into account all three phases, all three loading conditions, and all five levels of wavelet decomposition.

Parameter of Accuracy	BR		RM		FB		SF		RU		VU		HM	
	Sym5	Oth	Sym5	Oth	Sym5	Oth	Sym5	Oth	Sym5	Oth	Sym5	Oth	Sym5	Oth
SNR	42	3	43	0	44	0	42	0	44	0	44	0	43	0
RMSE	41	4	44	0	44	0	41	0	44	0	44	0	43	0
PSNR	44	1	44	0	42	0	44	0	43	0	45	0	41	0
CC	42	3	44	0	43	0	42	0	43	0	44	0	42	0

Table 5.5 : For seven different fault patterns and variation of all five levels of wavelet decompositions, detailed results are shown that demonstrate the number of fault parameters that Symlet5 mother wavelet can handle at their optimum level. These results take into account all of the parameters (SNR, RMSE, PSNR, and CC), all three phases, and all five levels of wavelet decomposition.

Level of decomposition	BR		RM		FB		SF		RU		VU		HM	
	Sym5	Oth	Sym5	Oth	Sym5	Oth	Sym5	Oth	Sym5	Oth	Sym5	Oth	Sym5	Oth
Level 1	32	4	36	0	36	0	36	0	32	4	36	0	35	1
Level 2	34	2	32	4	34	2	36	0	36	0	33	3	32	4
Level 3	36	0	36	0	35	1	36	0	36	0	36	0	34	2
Level 4	36	0	36	0	33	3	30	6	34	2	36	0	34	2
Level 5	31	5	35	1	35	1	31	5	36	0	36	0	34	2

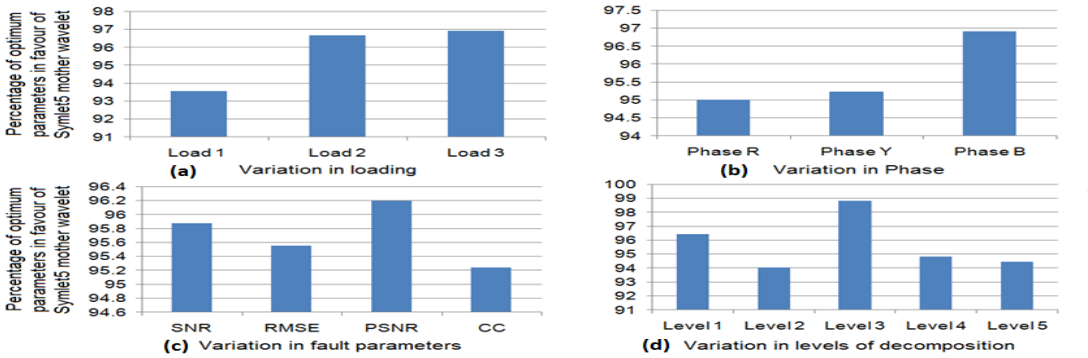

Figure 5.16: *Comparison showing the percentage of observations with the Symlet5 mother wavelet's optimal parameter under changes in (a) motor loading, (b) electrical phase, (c) fault parameters (SNR, RMSE, PSNR, and CC), and (d) wavelet decomposition levels; remaining parameters in each case are taken into account collectively*

The percentage of observations with the ideal parameter discovered using the Symlet5 mother wavelet with modifications in loading, phase, accuracy parameters (SNR, RMSE, PSNR, and CC), and levels of wavelet decomposition, can be seen by carefully observing the subfigures of Fig. 5.16. The key observations are listed as follows:

- Fig. 5.16 (a) shows that the loading condition 3 with a 200 W electrical load applied to the generator has the highest optimised parameter accuracy with Symlet5, followed by the no-load condition and generator load (Loading Condition 2). (Condition of loading 1). These levels are near 97% for loads 3 and 2, but are shown to be close to 93.5% for load 1.
- Fig. 5.16 (b) shows that phase B generates the best accuracy, around 97%, as contrasted to phases R and Y, which have these levels at or near 95%; nevertheless, the margin is running about between 95% and 97%, which is essentially equivalent and has only minimal efficacy. Additionally, it demonstrated that the Symlet5 mother wavelet provided the greatest results for the accuracy parameter, being approximately 95% accurate even in the worst case scenario. It also showed that all three line currents produce results that are nearly equivalent.
- Fig. 5.16 (c), which contrasts the outcomes of the four distinct accuracy parameters, can be used to make a similar argument. It demonstrates that CC has the lowest accuracy, which is also more than 95%, and PSNR has the highest accuracy, exceeding 96%. This difference's margin is very small in all respects. Therefore, Symlet5 is the most precise mother wavelet with more than 95% precision, even in the worst-case scenario, according to all four metrics.
- Fig. 5.16 (d) displays a comparison of the percentage of ideal parameters for five different levels of decomposition. Level 3 appears to produce the greatest proportion of observations that support Symlet5. The lowest accuracy is found at level 2, which is likewise near 94%, whereas this level of accuracy is close to 99%. As a result, it is also demonstrated that Symlet5 is generally invariant with respect to the level of wavelet decomposition with respect to the number of observations.

Thus, taking into account all four study factors, it can be concluded that Symlet5 mother wavelet produces the largest percentage of the optimal parameter. Therefore, it can be said that Symlet5 is the best mother wavelet for the investigation of induction motor faults that has been proposed.

5.6 Determination of optimum level of wavelet decomposition

The selection of the optimal level of decomposition is also an important task because the quality of the de-noised signal may be reduced after a certain level of decomposition due to data reduction [163]. Determining the best amount of decomposition based on the type of data being processed is so crucial.

After identifying Symlet5 as the ideal mother wavelet as described in the analysis above, the next stage of the proposed work's analysis entails determining the ideal level of wavelet decomposition. As a result, we have examined the best observations for each factor. These variables include the three phases, all three fault classes (BR, RM, FB, RU, VU, SF), one healthy condition, four accuracy measures (SNR, PSNR, CC, and RMSE), and all three loading conditions. These four accuracy metrics are plotted against each of the five decomposition levels for each of the seven fault classes for each of the three loading situations, as shown separately in Figs. 5.17, 5.18, 5.19, and 5.20. Given that Symlet5 mother wavelet was already determined to be the best option in the previous section. In order to observe the fluctuations of the four accuracy parameters for all seven faults and one healthy motor under three distinct loading conditions, we increased the decomposition level using Symlet5 mother wavelet exclusively for the fault current signals from level 1 to level 5.

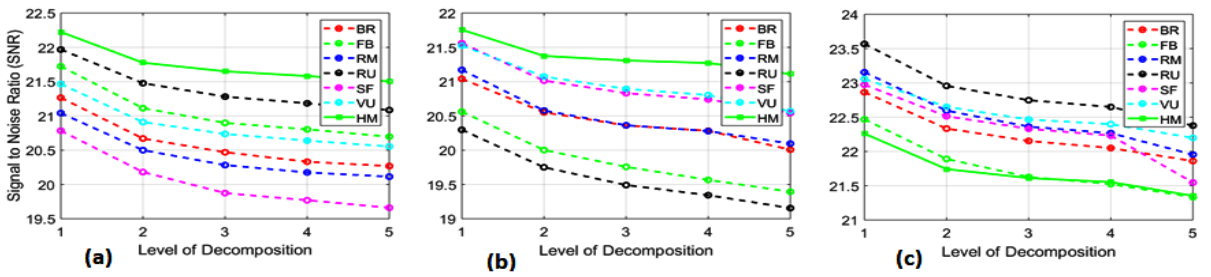

Figure 5.17: *SNR values comparison of seven fault for five levels of decomposition classes using Symlet5 mother wavelet over the line R fault current waveforms in three different loading conditions, (a) loading 1 condition, (b) loading 2 condition, and (c) loading 3 condition*

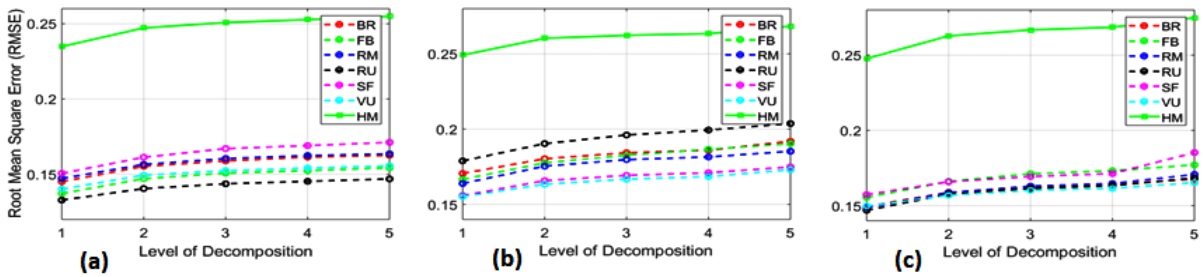

Figure 5.18: *Using the Symlet5 mother wavelet over the R line fault current waveforms under three loading conditions, (a) loading condition 1, (b) loading condition 2 and (c) loading condition 3, the root mean square errors (RMSE) for seven fault classes for five wavelet decomposition levels are compared*

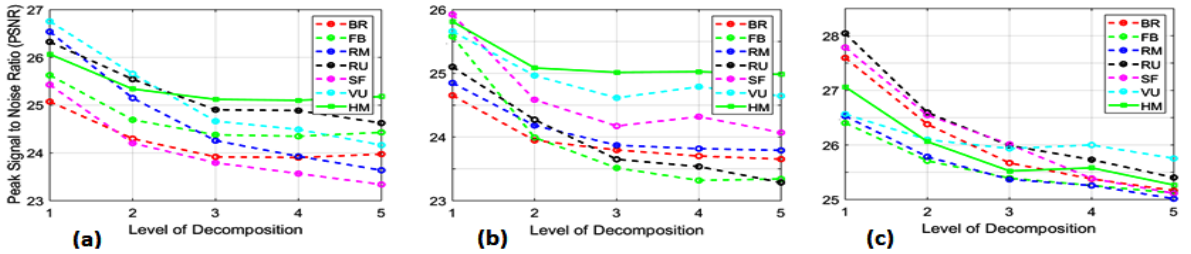

Figure 5.19: *PSNR values for seven classes of faults were compared for five levels of decomposition using Symlet5 mother wavelet over the line R fault current waveforms under three distinct loading conditions: (a) loading condition 1, (b) loading condition 2 (c) loading condition 3*

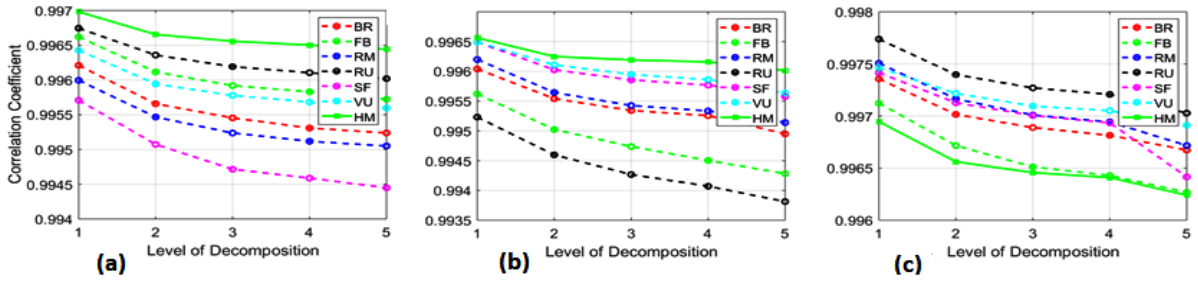

Figure 5.20: *Using the Symlet5 mother wavelet over the line R fault current waveforms under three loading conditions, (a) loading condition 1, (b) loading condition 2and (c) loading condition 3, CC values for seven classes of faults for five wavelet decomposition levels were compared*

From the graphs above, it can be seen that several of the curves have a tendency to saturate around the decomposition level 5. From level 4 forward, some of the curves also start to saturate early; nevertheless, some of these continue to show a slight upward tendency even until level 5. Overall, it can be concluded that level 5 is nearly ideal because it is then that the changes in the accuracy parameters start to saturate and the computing complexity doesn't rise noticeably. When we investigated changes to the same parameters using current signals of Y phase and B phase, we discovered a similar tendency of the curves. As previously indicated, we also changed the motor's load in three phases and looked into those changes. In sub-figures (b) and (c) of each of the figures from Fig. 5.17 to Fig. 5.20, we have plotted these data for each of the four accuracy metrics for both generators with no load and generators with a 200 W load, and once again, we have found similarities. More importantly, we have noticed that, rather than heading towards saturation, the signal degradation is persisting more in the event of higher loadings.

To pinpoint this gradual shift in the parameter values, additional research has been done. This is done by using the Symlet5 mother wavelet to calculate the difference in parameter values derived from the subsequent stages of wavelet decomposition, and then presenting this incremental change in parameter values in two-dimensional graphical plots for the four quality parameters from Fig. 5.21 to Fig. 5.24. The difference in the level of decomposition is shown on the x-axis of each of these plots, i.e.

Difference in the level of decomposition (i) = Level (i+1) – Level (i)

And the y-axis displays the difference in accuracy parameter values for each modification in level of decomposition, i.e.,

The accuracy parameter value for the difference in the decomposition level (i) is equal to the difference ofthe accuracy parameter value for the (i+1)-th level and the accuracy parameter value for the i-th level.

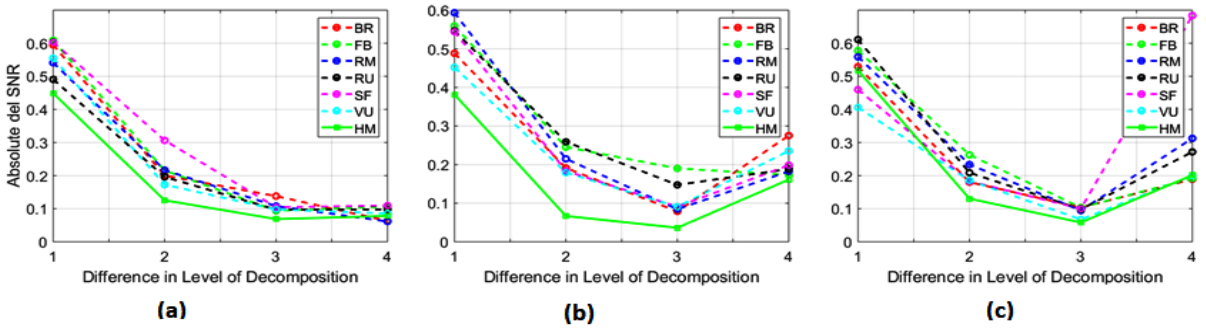

Figure 5.21: *Using the Symlet5 mother wavelet over the line R fault current waveforms under three different loading conditions, (a) loading condition 1, (b) loading condition 2 and (c) loading condition 3, incremental SNR changes for seven fault classes for five levels of decomposition were compared*

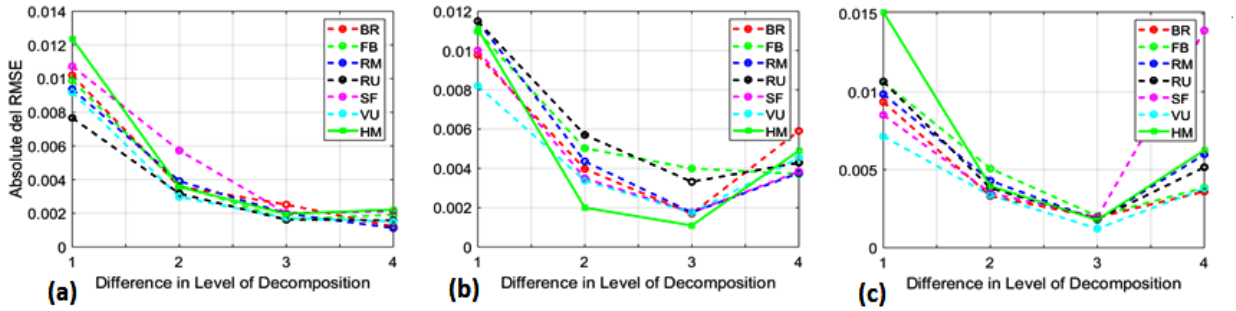

Figure 5.22: *Comparison of incremental changes in RMSE values of seven fault classes for five decomposition levels using Symlet5 mother wavelet over the line R fault current waveforms under three different loading conditions, (a) loading condition 1 (b) loading condition 2 and (c) loading condition 3*

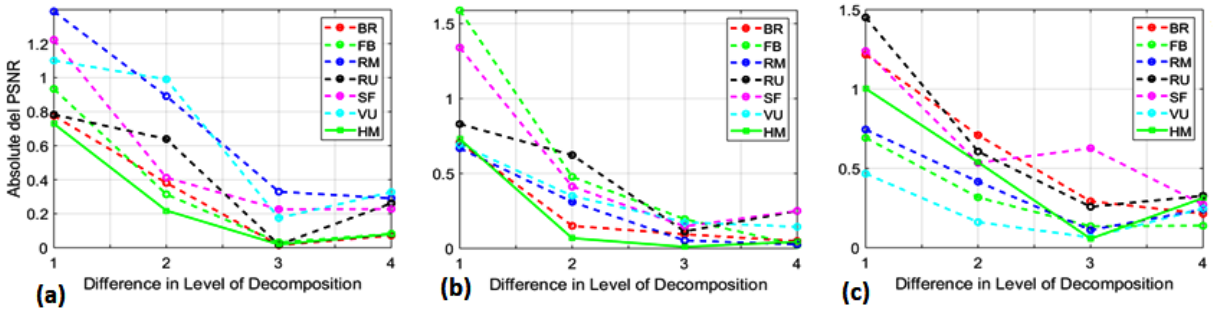

Figure 5.23: *Comparison of incremental PSNR changes of seven fault classes for five decomposition levels using Symlet5 mother wavelet over the fault current waveforms of R phase under three different loading conditions, (a) loading condition 1, (b) loading condition 3, (c) loading condition 3*

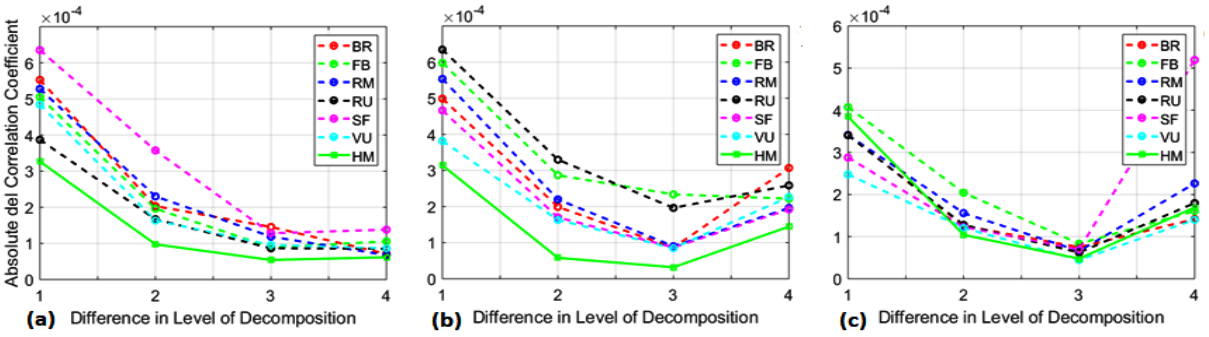

Figure 5.24: *Comparison of incremental CC changes of seven fault classes for five decomposition levels using the Symlet5 mother wavelet over the line R fault current waveforms under three different loading conditions, (a) loading condition 1, (b) loading condition 2, (c) loading condition 3*

These graphs demonstrate that the majority of the curves associated with distinct fault circumstances start to saturate from level 4 onward as these incremental curves, which represent the differential change in values, begin to flatten gradually. For all accuracy metrics and all faults, this tendency towards saturation is particularly evident for faults executed under no load conditions. In fact, we find that the curves practically reach saturation at level 4 and higher. Similar outcomes are discovered when phases Y and B are also explored.

Since the present study aims to identify the optimal degree of wavelet decomposition of the signal, we have made a trade-off between the saturation of the accuracy parameters and the computing complexity of the analysis. As a signal's level of breakdown rises, processing complexity rises quickly. Therefore, to build a straightforward and less complicated model, the level of decomposition should be as low as is practical. We have observed once again that the parameter values are not precisely saturating, even after level 5 of decomposition has been reached, despite the fact that the rate of change in parameter values is decreasing, particularly in the no-load situation. Level 4 is clearly the ideal level under the no-load scenario, owing to the saturation of the accuracy parameters and the fact that the complexity of analysis increases sharply with level of decomposition.

However, the pattern for the other two loading types is just slightly different. The four figures above show that, for a small number of faults and a small number of coefficients, the rate of change in parameter values has decreased gradually up to level 4; that is, for the transition from level 3 to level 4, the difference in parameter values is in a falling mode; however, following that, the gap in parameters unexpectedly climbs somewhat rather than becoming more saturated. In particular, for larger loads and for all the accuracy measures, it suggests that the SNR, PSNR, and CC have decreased with higher descent, and the RMSE has similarly increased starting at this level 4. This abrupt decline is also shown from Fig. 5.17 to Fig. 5.20, which is where it is seen through close inspection. The quality of the reconstructed signal has predictably dropped due to this tendency of abrupt parameter value drops starting at level 4, and this has come at the expense of increased computational complexity. More crucially, comparing sub-figures (b) and (c) of each of Figs. 5.21 to

5.24 will show that from no load to generator load, and eventually more in the case of additional 200 W loading, there has been an increase in this propensity of sharp dips in accuracy parameter values. From this, it may be inferred that as the degree of breakdown increases, accuracy decreases more quickly with an increase in motor workload. Therefore, it may be concluded that level 4 is the best level of decomposition for the present work, especially when considering the motor's various loads.

5.7 Multi Resolution Analysis (MRA)

According to the integer number of the discrete step in scale and translation, indicated by q and r, DWT provides a number of wavelet coefficients. If c_0 and e_0 the segmentation step sizes for the scale and translation respectively, the scale and translation of RMS of these parameters will be $c = c_0^q$ and $e = re_0c_0^q$. From now on, the discrete wavelet coefficients are given by

$$DWT(q,r) = \int_{-\infty}^{\infty} \frac{1}{\sqrt{c=c_0^q}} f(t)g\left(c_0^{-q}t - re_0\right)d(t) \text{--------- (5.6)}$$

where, the discrete wavelet with scale and translation is indicated by the notation $g\left(c_0^{-q}t - re_0\right)$. The high pass and low pass filters of MRA are collectively referred to as the MRA high pass and low pass filters, respectively. This is how the MRA technique is typically described.

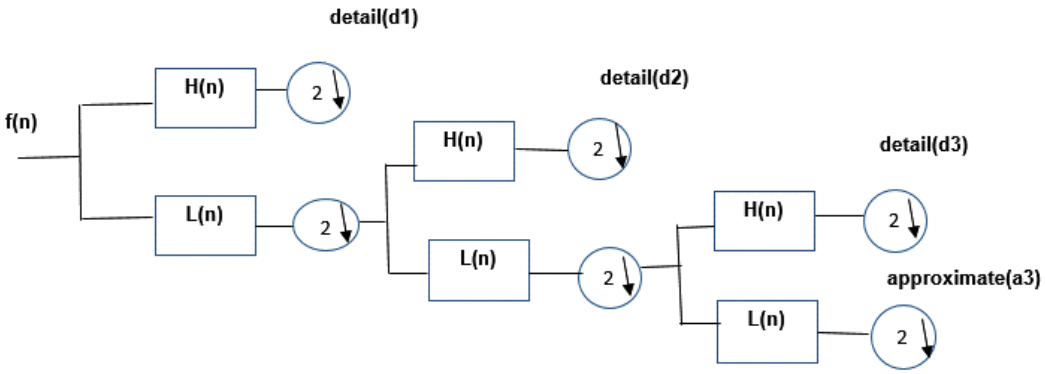

***Figure 5.25** : Idea of multi resolution analysis of wavelet.*

To categorise the three different groups of errors in the time-frequency domain in this work, we used wavelet analysis. The Symlet5 mother wavelet is used to deconstruct the three phase current waveforms of all defective induction motors, including the healthy one, up to the fifth level of decomposition. Fig. 5.25 depicts the wavelet-based signal decomposition methodology. The information provided by d1 is situated in the frequency range between F/4 and F/2 since the sampling frequency of the original signal is F. The signal d2 transmits the signal data between the frequency bands F/8 and F/4. Similar to d2, d3 transmits data in the frequency region between F/16 and F/8. The remaining information of the original signal between 0 and F/16 is retained at the approximation level (a3). As a result, extracting critical information from the original signal into multiple frequency bands

while also matching the information to the relevant time frame is simple.The approximate coefficients of each decomposed current signal are used to extract the features.

The three phase original current signals of each motor are decomposed by the Symlet5 mother wavelet function at different decomposition levels to get information in different frequency bands.

5.8 Fault classification using multi resolution analysis (MRA)

In recent years, the wavelet transform has emerged as one of the most rapidly developing mathematical and signal processing methods due to a number of distinguishing advantages. In order to compute the wavelet decomposition of the signal from its best scale approximation, MRA gave rise to the wavelet transform, which is renowned for its simplicity and recursive filtering process. The discrete wavelet transform's multi-resolution analysis divides a signal into various time-frequency components while also establishing a suitable criterion for identifying the noise within each component. In MRA, the approximate and detail coefficients are monitored for each level by computing different feature parameters with statistical tools. It has been widely used in image processing, but few works have been done in the domain of electrical system fault analysis. Numerous analyses have been done using wavelets for fault diagnosis of electrical systems in the time-frequency domain, but it has been observed that very few analyses have been done for fault diagnosis using MRA based statistical tool monitoring. MRA of DWT is suitable to detect abnormalities in power systems by identifying harmonic frequencies in a small range (1.5625-3.125 Hz to 49.2–902 Hz) [164] and also in the range of 0.05 Hz [165,166].MRA has been used for brush loose contact analysis in AC locomotive systems, extracting features from DWT coefficients (approximate and detailed) of current signals by statistical tools to select the best fit level, and these three tools have also been used for inner turn fault analysis of traction motors [56, 167]. The best fit level selection has been done using MRA of DWT based kurtosis, skewness, RMS, mode, mean, and median values for fault analysis in solar-wind microgrids, and these parameters have been used to optimise level for line to ground fault detection in HVDC systems [57, 168]. It is also used to detect supply unbalance in a 3 phase induction motor and to detect the presence of harmonics in the current spectrum of an arc furnace transformer [169, 170]. Additionally; it has been applied to the static switch in microgrids for fault localization, classification, and detection, employing MRA of DWT and a Taguchi-based artificial neural network (ANN) [171]. Multiresolution decomposition of DWT, including a few statistical tools, has been applied to compute statistical indices of total harmonic distortion of current and voltage signals, and after that, the input feature parameters have been fed to a random forest based classifier to classify faults in microgrids [172]. It has been seen from previous work that MRA has been used to extract relevant features from input signals for one type of fault identification of motors [173], transformers, and microgrids.

The motivation of this work is to identify three different types of faults in induction motors by extracting statistical features using MRA of DWT and a norm based classification system. Three

phase current signals have been collected from six motors with six different types of known faults, including one healthy motor, and current signals from three motors with three unknown types of faults under different loading conditions. Three phase current signals have been decomposed into multiple levels using the DWT algorithm, and Skewness, Kurtosis, RMS value, Median, and Mode have been computed from approximate and detail coefficients. The feature matrices of skewness, kurtosis, RMS value, median, and mode have been constructed from approximate and detailed coefficients of three phase current signals in multiple decomposed levels, but it is essential to reduce the rank of the matrix for the classification problem [174]. The Frobenius norm has been used [175] to convert each multidimensional feature matrix to a scalar value. The composite norm of each MRA feature parameter of each faulty motor has been computed, and the norms of 10 feature parameters of each faulty motor have been found. The total norm of all norms for each faulty motor has been computed, and the norm differences are calculated from one unknown faulty motor to all known faulty motors. The unknown fault has been identified based on the minimum value of the norm difference. The fault classification process has been applied to identify three unknown faults for multi decomposition levels, and the same process has also been applied under different loading conditions. The sensibilities of norms have also been verified with the changing of decomposition levels.

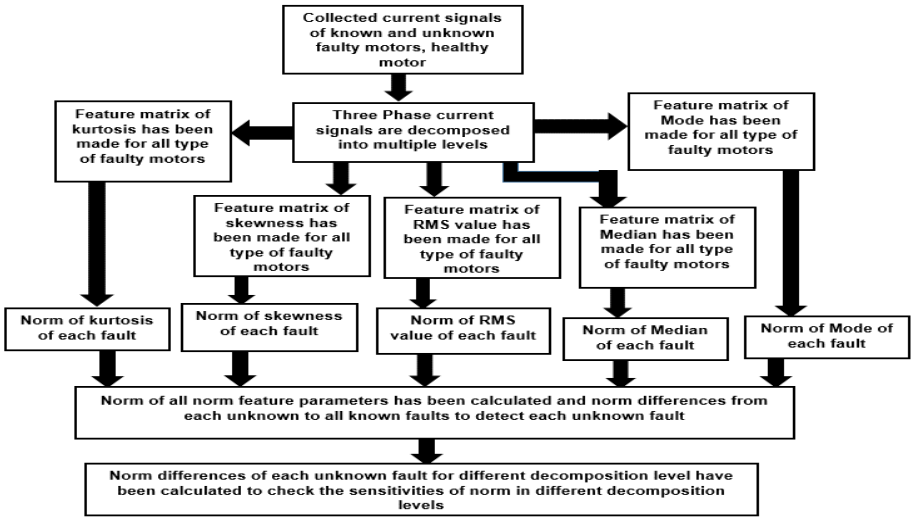

***Figure 5.26**: Work flow diagram of fault classification through MRA of wavelet*

Kurtosis, Skewness, RMS ,Median and Mode values for MRA:

The mathematical expression of Kurtosis, skewness has been discussed in Chapter 2 along with the square root of the arithmetic mean of the square of the function that defines the continuous waveform, which is the r.m.s. value of a set of values.

$$\text{R.M.S} = \sqrt{\frac{1}{T}\int_{t-T}^{t} f(t)} \qquad (5.11)$$

where T is the time period of a signal and $f(t)$ is the current signal. The current signals have been decomposed into multiple levels using high pass and low pass filters. The statistical feature

parameters skewness, kurtosis, and r.m.s. value have been computed from the approximate and detail coefficients of each level of decomposed current signals. There are three phases of each type of motor, and the composite matrices for the three phases of skewness, kurtosis, and r.m.s. value of each type of motor have been made using these feature parameters of 1st level to *i*-th level decomposed signals as follows:

$$S = \begin{bmatrix} S_{A1} S_{A2} S_{A3} \dots \dots \dots S_{Ai} \\ S_{D1} S_{D2} D_{D3} \dots \dots \dots S_{Di} \end{bmatrix} \quad (5.12)$$

$$K = \begin{bmatrix} K_{A1} K_{A2} K_{A3} \dots \dots \dots K_{Ai} \\ K_{D1} K_{D2} K_{D3} \dots \dots \dots K_{Di} \end{bmatrix} \quad (5.13)$$

$$R = \begin{bmatrix} R_{A1} R_{A2} \dots \dots \dots \dots R_{Ai} \\ R_{D1} R_{D2} R_{D3} \dots \dots R_{Di} \end{bmatrix} \quad (5.14)$$

Here, *S* is the matrix of skewness for assessment of approximate and detail coefficients: skewness of approximate coefficients and detailed coefficients of DWT at the *i*-th decomposition level. K is the matrix of kurtosis for the assessment of approximate and detail coefficients, which are kurtosis of the approximate coefficient and detail coefficients of DWT at the *i*-th decomposition level. are the r.m.s. values of the approximate coefficients and detailed coefficients of DWT at the *i*-th decomposition level, and R is the r.m.s. matrix. Consider three phase system

(i) For R phase : $Sr_{A1}, Sr_{D1}, Kr_{A1}, Kr_{D1} Rr_{A1}, Rr_{D1}$ etc.

(ii) For Y phase: : $Sy_{A1}, Sy_{D1}, Ky_{A1}, Ky_{D1} Ry_{A1}, Ry_{D1}$ etc.

(iii) For B phase: $Sb_{A1}, Sb_{D1}, Kb_{A1}, Kb_{D1} Rb_{A1}, Rb_{D1}$ etc.

The composite skewness matrix of approximate coefficients are:

$$CS_A = \begin{bmatrix} Sr_{A1} Sr_{A2} S_{rA3} \dots \dots \dots Sr_{Ai} \\ Sy_{A1} Sy_{A2} \; Sy_{A3} \dots \dots Sy_{Ai} \\ Sb_{A1} Sb_{A2} Sb_{A3} \dots \dots \dots Sb_{Ai} \end{bmatrix} \quad (5.15)$$

The composite skewness matrix of detailed coefficients are:

$$CS_D = \begin{bmatrix} Sr_{D1} Sr_{D2} S_{rD3} \dots \dots \dots Sr_{Di} \\ Sy_{D1} Sy_{D2} \; Sy_{D3} \dots \dots Sy_{Di} \\ Sb_{D1} Sb_{D2} Sb_{D3} \dots \dots \dots Sb_{Di} \end{bmatrix} \quad (5.16)$$

The composite kurtosis matrix of approximate coefficients are:

$$CK_A = \begin{bmatrix} Kr_{A1} Kr_{A2} K_{rA3} \dots \dots \dots Kr_{Ai} \\ Ky_{A2} K_{yA3} \dots \dots \dots \dots \dots Ky_{Ai} \\ Ky_{A2} K_{yA3} \dots \dots \dots \dots \dots Ky_{Ai} \end{bmatrix} \quad (5.17)$$

The composite kurtosis matrix of detailed coefficients are:

$$CK_D = \begin{bmatrix} Kr_{D1}Kr_{D2}Kr_{D3} \dots\dots\dots Kr_{Di} \\ Ky_{D1}Ky_{D2}Ky_{D3} \dots\dots\dots Ky_{Di} \\ Kb_{D1}Kb_{D2}Kb_{D3} \dots\dots\dots Kb_{Di} \end{bmatrix} \quad (5.18)$$

The composite r.m.s value of approximate coefficients are:

$$CR_A = \begin{bmatrix} Rr_{A1}Rr_{A2} \dots\dots\dots\dots Rr_{Ai} \\ Ry_{A1}Ry_{A2} \dots\dots\dots\dots Ry_{Ai} \\ Rb_{A1}Rb_{A2} \dots\dots\dots\dots Rb_{Ai} \end{bmatrix} \quad (5.19)$$

The composite r.m.s value of detailed coefficients are:

$$CR_D = \begin{bmatrix} Rr_{D1}Rr_{D2}Rr_{D3} \dots\dots Rr_{Di} \\ Ry_{D1}Ry_{D2}Ry_{D3} \dots\dots Ry_{Di} \\ Rb_{D1}Rb_{D2}Rb_{D3} \dots\dots Rb_{Di} \end{bmatrix} \quad (5.20)$$

The mathematical expression for Median and Mode have been discussed in Chapter 2.

Median and mode have been computed from the approximate and detail coefficients of decomposed current signals at multiple decomposition levels. Following that, composite median and mode matrices were constructed for each type of motor using the feature parameters of decomposed three-phase current signals from the first to the *i*-th level.

$$Mn = \begin{bmatrix} Mn_{A1}Mn_{A2}Mn_{A3} \dots\dots\dots Mn_{Ai} \\ Mn_{D1}Mn_{D2}Mn_{D3}\dots\dots\dots\dots Mnd_{Di} \end{bmatrix} \quad (5.21)$$

$$Md = \begin{bmatrix} Md_{A1}Md_{A2}Md_{A3} \dots\dots\dots Md_{Ai} \\ Md_{D1}Md_{D2}Md_{D3}\dots\dots\dots\dots Md_{Di} \end{bmatrix} \quad (5.22)$$

As the wavelet decomposition level is 7, so the maximum values of *i* is 7.

Here, M_{nAi}, M_{nDi} are median of approximate coefficient and detailed coefficients of DWT at *i*-th decomposition level.M_{dAi}, M_{dDi} are mode of approximate coefficient and detailed coefficients of DWT at *i*-th decomposition level.

Consider three phase system

(iv) For R phase : $Mnr_{A1}, Mnr_{D1}, Mdr_{A1}, Mdr_{D1}$ etc.
(v) For Y phase: $Mny_{A1}, Mny_{D1}, Mdy_{A1}, Mdy_{D1}$ etc.
(vi) For B phase: $Mnb_{A1}, Mnb_{D1}, Mdb_{A1}, Mdb_{D1}$ etc.

The composite median matrix of approximate coefficients are:

$$CMn_A = \begin{bmatrix} Mnr_{A1}Mnr_{A2}Mnr_{A3} \dots\dots\dots\dots Mnr_{Ai} \\ Mny_{A1}Mny_{A3} \dots\dots\dots\dots\dots\dots Mny_{Ai} \\ Mnb_{A1}Mnbr_{A2}Mnb_{A3} \dots\dots\dots\dots Mnbr_{Ai} \end{bmatrix} \quad (5.23)$$

The composite median of detail coefficients are:

$$CMn_D = \begin{bmatrix} Mnr_{D1}Mnr_{D2}Mnr_{D3} \dots\dots\dots\dots Mnr_{Di} \\ Mny_{D1}Mny_{D3} \dots\dots\dots\dots\dots\dots Mny_{Di} \\ Mnb_{D1}Mnb_{D2}Mnb_{D3} \dots\dots\dots Mnb_{Di} \end{bmatrix} \quad (5.24)$$

The composite mode of approximate coefficients are:

$$CMd_A = \begin{bmatrix} Mdr_{A1}Mdr_{A2}Mdr_{A3} \dots\dots\dots\dots Mdr_{Ai} \\ Mdy_{A1}Mdy_{A2}Mdy_{A3} \dots\dots\dots\dots Mdy_{Ai} \\ Mdb_{A1}Mdby_{A2}Mdby_{A3} \dots\dots\dots\dots Mdb_{Ai} \end{bmatrix} \quad (5.25)$$

The composite mode of detailed coefficients are:

$$CMd_D = \begin{bmatrix} Mdr_{D1}Mdr_{D2}Mdr_{D3} \dots\dots\dots\dots Mdr_{Di} \\ Mdy_{D1}Mdy_{D2}Mdy_{D3} \dots\dots\dots\dots Mdy_{Di} \\ Mdb_{D1}Mdb_{D2}Mdb_{D3} \dots\dots\dots\dots Mdb_{Di} \end{bmatrix} \quad (5.26)$$

For R-phase:

$$MRA_r = \begin{bmatrix} Sr_{A1}Sr_{A2}Sr_{A3} \dots\dots\dots Sr_{Ai} \\ Sr_{D1}Sr_{D2}Sr_{D3} \dots\dots\dots Sr_{Di} \\ Kr_{A1}Kr_{A2}Kr_{A3} \dots\dots\dots Kr_{Ai} \\ Kr_{D1}Kr_{D2}Kr_{D3} \dots\dots\dots Kr_{Di} \\ Rr_{A1}Rr_{A2}Rr_{A3} \dots\dots\dots\dots R_{Ai} \\ Rr_{D1}Rr_{D2}Rr_{D3} \dots\dots Rr_{Di} \\ Mnr_{A1}Mnr_{A2}Mnr_{A3} \dots\dots\dots Mnr_{Ai} \\ Mnr_{D1}Mnr_{D2}Mnr_{D3}\dots\dots\dots\dots Mnrd_{Di} \\ Mdr_{A1}Mdr_{A2}Mdr_{A3} \dots\dots\dots Mdr_{Ai} \\ Mdr_{D1}Mdr_{D2}Mdr_{D3}\dots\dots\dots\dots Mdr_{Di} \end{bmatrix} \quad (5.27)$$

For Y-phase:

$$MRA_y = \begin{bmatrix} Sy_{A1}Sy_{A2}Sy_{A3} \dots\dots\dots Sy_{Ai} \\ Sy_{D1}Sy_{D2}Sy_{D3} \dots\dots\dots Sy_{Di} \\ Ky_{A1}Ky_{A2}Ky_{A3} \dots\dots\dots Ky_{Ai} \\ Ky_{D1}Ky_{D2}Ky_{D3} \dots\dots\dots Ky_{Di} \\ Ry_{A1}Ry_{A2} \dots\dots\dots\dots Ry_{Ai} \\ Ry_{D1}Ry_{D2}Ry_{D3} \dots\dots Ry_{Di} \\ Myn_{A1}Myn_{A2}Myn_{A3} \dots\dots\dots Myn_{Ai} \\ Myn_{D1}Myn_{D2}Myn_{D3}\dots\dots\dots\dots Mynd_{Di} \\ Myd_{A1}Myd_{A2}Myd_{A3} \dots\dots\dots Myd_{Ai} \\ Myd_{D1}Myd_{D2}Myd_{D3}\dots\dots\dots\dots Myd_{Di} \end{bmatrix} \quad (5.28)$$

For B-phase:

$$MRA_b = \begin{bmatrix} Sb_{A1}Sb_{A2}Sb_{A3} \dots\dots\dots Sb_{Ai} \\ Sb_{D1}Sb_{D2}Sb_{D3} \dots\dots\dots Sb_{Di} \\ Kb_{A1}Kb_{A2}Kb_{A3} \dots\dots\dots Kb_{Ai} \\ Kb_{D1}Kb_{D2}Kb_{D3} \dots\dots\dots Kb_{Di} \\ Rb_{A1}Rb_{A2} \dots\dots\dots\dots Rb_{Ai} \\ Rb_{D1}Rb_{D2}Rb_{D3} \dots\dots Rb_{Di} \\ Mbn_{A1}Mbn_{A2}Mbn_{A3} \dots\dots\dots Mbn_{Ai} \\ Mbn_{D1}Mbn_{D2}Mbn_{D3}\dots\dots\dots\dots Mbnd_{Di} \\ Mbd_{A1}Mbd_{A2}Mbd_{A3} \dots\dots\dots Mbd_{Ai} \\ Mbd_{D1}Mbd_{D2}Mbd_{D3}\dots\dots\dots\dots Mbd_{Di} \end{bmatrix} \quad (5.29)$$

Fault classification using Norm:

The Frobenius norm of a matrix $B \in R^{pxn}$is defined as $||B||_F = \sqrt{t_r(B^T B)}$, where t_r is a matrix's trace, or the sum of its diagonal entries. The Frobenius norm is useful for measuring of the root-mean-square(RMS) gain of the matrix, its average response along given mutually orthogonal directions in space. It does not capture the error variance well; it only captures the average effect of noise. If a noise vector has a finite set of directions that are represented by the standard basis such as e1, e2,... en, the average value of the square error norm is:

$$\frac{1}{n}\sum_{i=1}^{n}||B\,e_i||_2^2 = \frac{1}{n}\sum_{i=1}^{n}||b_i||_2^2 \quad (5.30)$$

b_i is the ithcolum of *B*. The above quantity can be written as$\frac{1}{n}||B_F^2||$.

$$||B||_F = \sqrt{\sum_{i=1}^{p}\sum_{j=1}^{n}B_{ij}^2} = \sqrt{t_r(B^T B)} \quad (5.31)$$

Here,$||B||_F$ is the Frobenius norm of *B*. The *p* x *n* matrix *B*'s Frobenius norm, also known as the Euclidean norm, is calculated as the square root of the sum of the absolute squares of the matrix's elements [176].

The composite MRA is given by:

$$MRA = \left[\|MRA_y\|, \|MRA_y\|, \|MRA_b\|\right] \quad (5.32)$$

where $\|MRA_y\|, \|MRA_y\|$ and $\|MRA_b\|$ are the norms of $MRA_r, MRA_y \; and \; MRA_b$ respectively.

The norm of composite MRA is: $M = \|MRA\|$ (5.33)

Multiple decomposition levels are used to decompose the three-phase current signals of six faulty motors named broken rotor bars (BR), rotor misalignment (RM), faulted bearing (FB), stator winding fault (SF), rotor unbalance (RU), single phase voltage unbalance (VU), and one healthy motor.

The feature matrix of kurtosis, median, mode, skewness, and RMS value have been made individually from approximate and detailed coefficients of decomposed three-phase current signals at different levels. The norms can be calculated from the MRA matrix for three phases, which contain 30 features (10 features for each phase) for each type of fault. The norm differences can be calculated from one norm of an unknown fault to other norms of known faults. The unknown fault can be identified depending on the minimum value of the norm difference.

Here, the Frobenius norm has been computed from each feature matrix, and 10 norms for each type of fault have been formed to identify the norm value of each feature matrix of each unknown fault close to each feature norm of each known fault.

Each norm of a feature matrix is a scalar value, but an unknown fault cannot be authenticated from 10 scalar values. The norm differences need to be computed for the norm of each unknown fault compared to the norms of other known faults to authenticate each unknown fault. If the 10 norms are combined to form a composite single matrix, then the norm can be found from the matrix of 10 norms as follows:

The matrix norms for all three phases' above features are computed as follows:

1) $NCS_A = norm(CS_A) = \|CS_A\|$
2) $NCS_D = norm(CS_D) = \|CS_D\|$
3) $NCK_A = norm(CK_A) = \|CK_A\|$
4) $NCK_D = norm(CK_D) = \|CK_D\|$
5) $NR_A = norm(CR_A) = \|CR_A\|$
6) $NR_D = norm(CR_D) = \|CR_D\|$
7) $NCmn_A = norm(CMn_A) = \|CMn_A\|$
8) $NCmn_D = norm(CMn_D) = \|CMn_D\|$
9) $NCmd_A = norm(CMd_A) = \|CMd_A\|$
10) $NCmd_D = norm(CMd_D) = \|CMd_D\|$

$$CA = \begin{bmatrix} \|CS_A\| \\ \|CS_D\| \\ \|CK_A\| \\ \|CK_D\| \\ \|CR_A\| \\ \|CR_D\| \\ \|CMn_A\| \\ \|CMn_D\| \\ \|CMd_A\| \\ \|CMd_D\| \end{bmatrix} \tag{5.34}$$

$$NCA = norm(CA) \tag{5.35}$$

The norms of the composite norm matrix have been computed for known and unknown faults, and the norm differences of two composite norm matrices (*NCA1* and *NCA2*) have been computed to find out the similarity between them as follows:

$$D = NCA1 - NCA2 \quad (5.36)$$

The norm differences from each unknown fault to known faults have been found, and each unknown fault has been authenticated based on the minimum value of the norm difference.

5.8.1 *Results for fault classification using MRA*

The data samples of three phase currents (amplitude vs. time) are collected three times from induction motors with six known types of faults (broken rotor bars (BR), rotor misalignment (RM), faulty bearings (FB), stator winding faults (SW), rotor unbalance (RU), single-phase voltage unbalance (VU), and one healthy motor (HM) in three loading conditions. Additionally, six random current data samples from induction motors with three unidentified problems are obtained under three different loading circumstances. The three loading conditions are described in the experimentation section of the chapter.

The current signals of each faulty motor and one healthy motor are decomposed into 3rd, 4th, 5th, 6th, and 7th levels using the Symlet5 mother wavelet function. Initially, three unknown types of faults were classified using MRA in multiple decomposition levels under one loading condition, and then the same process was used to classify. The feature matrices of skewness, kurtosis, median, mode, and RMS value for each phase of each type of motor have been constructed by extracting features from the approximate and detail coefficients of the 1st-3rd decomposed level, 1st -4th decomposed level, 1st -5th decomposed level, 1st to 6th decomposed level, and 1st -7th decomposed level individually. The composite feature matrices for each feature of each fault type have also been formed at different decomposition levels using statistical feature parameters of approximate and detail coefficients for the three phases of each fault type. Norms have been computed from each feature matrix of each fault type to convert each feature matrix to a scalar value. 10 norms of 10 feature parameters (5 feature parameters for approximate coefficients and 5 feature parameters for detail coefficients) for each type of faulty motor have been found, and a norm matrix for each type of faulty motor has been formed using the 10 feature parameters. The norm feature parameters of each type of motor, including three unknown types of faulty motors (X1, X2, and X3), have been presented in Table 5.6 (a) for decomposition levels from 1st to 5th under one loading condition. The X1, X2, and X3 are the unknown types of faults 1, 2, and 3, respectively. From Table 5.6 (a), it has been seen that every feature of the 10 features of unknown fault 1, unknown fault 2, and unknown fault 3 is similar to the features of broken rotor bar fault, stator winging fault, and faulted bearing, respectively. However, unknown faults cannot be authenticated from the feature parameters of multiple dimensions, so it is essential to convert the features of multiple dimensions to a scalar value because all the data are correlated. Again, the norm of 10 norms has been computed for each type of motor in the norm matrix to convert multidimensional features to single dimensional features. The norm differences of one unknown type of motor to other known types of motors have been calculated, and each unknown type

of fault has been identified based on the minimum value of the norm differences of one unknown type to other known faults. Table 5.6 (b) shows the norm differences between three classes of unknown type faults and other known classes for the first through fifth decomposition levels. From the distance table, it has been seen that unknown type fault 1 (X1), unknown type fault 2 (X2), and unknown type fault 3 (X3) resemble broken rotor bars, stator winding faults, and faulted bearings, respectively. Tables 5.6(a) and 5.6(b) show that the classification results are identical. Tables 5.7 (a, b) and 5.8 (a, b) show the results of applying the fault identification process to other two loading conditions for the first to fifth decomposition levels. The classification results are the same under the other two loading conditions as well. The composite norms of MRA feature parameters for different types of faulty motors with unknown type fault 1 under loading condition 1 have been shown in Fig. 5.27 for 1^{st} to 5^{th} level decomposition.

The classification process was also applied to other decomposition levels, and the minimum values of norm differences were calculated individually for three unknown types of faults in different decomposition levels (1st to 3rd, 1st to 4th, 1st to 5th, 1st to 6th, and 1st to 7th) under three loading conditions to test the sensitivities of norm differences with changing decomposition levels. The results have been reflected in the bar chart (Fig. 5.28).

Table 5.6: (a) Composite norms of feature parameters of known type and three unknown type of faults under loading condition1(1^{st} to 5^{th} level decomposition)

Norm of feature parameters	BR	FB	RM	RU	SF	VU	HM	X1	X2	X3
Norm of CS_A	24.7802	23.9099	24.2131	24.0729	23.1781	23.4051	43.2746	24.78368	23.19097	23.91678
Norm of CS_D	0.5181	0.5253	0.5543	0.5847	0.6066	0.5611	0.8956	0.518205	0.607359	0.525521
Norm of CK_A	5.8276	5.8532	5.7482	5.9169	6.2129	6.2617	5.8738	5.827436	6.213889	5.852943
Norm of CK_D	0.1759	0.4206	0.3375	0.2958	0.5812	0.6766	0.4302	0.175722	0.582727	0.420342
Norm of CR_A	3.9746	4.3079	3.8372	5.1769	4.5900	4.3189	1.8440	3.989913	4.601799	4.299742
Norm of CR_D	41.8165	34.8051	37.7747	38.3139	33.2339	41.8243	21.9103	41.79655	33.26309	34.65729
Norm of CMn_A	3.2322	3.9806	3.5921	2.3433	4.0668	5.3933	10.0019	3.263673	4.189515	4.04281
Norm of CMn_D	34.4752	33.9242	33.6328	34.4436	33.6452	34.7077	62.1901	34.43357	33.52997	33.83593
Norm of CMd_A	0.2976	0.2844	0.3062	0.2940	0.3036	0.2887	0.5043	0.29677	0.301743	0.28446
Norm of CMd_D	2.1447	2.1323	2.1847	2.3639	2.3400	2.3412	2.6664	2.143525	2.339623	2.12712

Table 5.6: (b) Differences of norm of three unknown type faults from known type faults when motors are running under loading condition 1 (1^{st} to 5^{th} level of decomposition)

Unknown type	Known fault types						
	BR	**FB**	**RM**	**RU**	**SF**	**VU**	**HM**
X1	**0.0336**	5.2607	3.4433	2.5945	6.6595	0.1448	19.6883
X2	6.7312	1.4370	3.2544	4.1032	**0.0381**	6.5528	26.3860
X3	5.4359	**0.1417**	1.9591	2.8079	1.2572	5.2575	25.0907

Table 5.7: (a) Composite norms of feature parameters of known type and three unknown type fault under loading condition 2 (1^{st} to 5^{th} level decomposition)

Norm of feature parameters	BR	FB	RM	RU	SF	VU	HM	X1	X2	X3
Norm of CS_A	25.2069	24.8713	25.4462	24.8402	25.4680	24.8295	41.6617	25.2154	25.46603	24.87067
Norm of CS_D	0.5062	0.5800	0.6138	0.5462	0.5839	0.5802	0.8136	0.506291	0.584239	0.579911
Norm of CK_A	6.7221	6.0190	6.1224	6.0153	6.0333	6.0732	5.9370	6.722458	6.033915	6.019044
Norm of CK_D	1.7357	0.6889	0.7652	0.7058	0.7503	0.7606	0.6924	1.735726	0.750391	0.68905
Norm of CR_A	7.4022	2.9274	3.0218	4.1539	2.2740	4.4641	1.6878	7.329981	2.279704	2.958505
Norm of CR_D	82.0372	29.4640	24.1658	30.7249	22.7973	34.6153	16.2217	81.16689	22.76357	29.65494
Norm of CMn_A	19.2255	7.5354	4.7328	7.6250	7.4811	7.6461	10.9035	19.26121	7.476762	7.546559
Norm of CMn_D	34.9419	35.8986	36.6674	35.6299	36.2926	35.7708	59.6168	34.86665	36.20318	35.80774
Norm of CMd_A	0.0575	0.2699	0.2826	0.2694	0.2881	0.2689	0.4520	0.058482	0.28857	0.268865
Norm of CMd_D	1.6617	1.9559	2.0204	1.7711	1.8761	1.9767	2.2400	1.66205	1.874724	1.958642

Table 5.7: (b) Differences of norms of three unknown type faults from known type faults under loading condition 2 (5^{th} level decomposition)

Unknown types	Known fault types						
	BR	**FB**	**RM**	**RU**	**SF**	**VU**	**HM**
X1	**0.7729**	3.7726	4.1437	1.8816	4.0740	4.2943	23.5542
X2	4.0407	2.8940	0.6918	3.4907	**0.0802**	5.9085	24.8189
X3	4.1466	**0.0475**	2.2496	0.5492	2.8613	2.9670	21.8775

Table 5.8: (a) Composite norms of feature parameters of known type and three unknown type faults under loading condition 3(1st to 5th level decomposition)

Norm of feature parameters	BR	FB	RM	RU	SF	VU	HM	X1	X2	X3
Norm of CS_A	30.0926	29.5041	29.9962	29.5228	29.7330	29.8758	43.0912	30.0918	29.7335	29.5025
Norm of CS_D	0.6115	0.6197	0.6568	0.6170	0.6453	0.5936	0.9308	0.611512	0.64586	0.61999
Norm of CK_A	5.9869	5.9945	6.0162	6.1032	5.9904	6.0276	6.2630	5.987372	5.99109	5.99402
Norm of CK_D	0.7213	0.7130	0.7007	0.7909	0.7063	0.6757	0.7473	0.721719	0.706616	0.71282
Norm of CR_A	2.5660	3.9665	3.2453	2.8848	2.9058	1.7226	1.3460	2.531197	2.85292	3.96688
Norm of CR_D	20.5999	29.2010	27.7408	22.7851	26.4396	37.6668	21.1413	20.5305	26.34497	29.1200
Norm of CMn_A	7.9671	7.6755	7.6567	9.3542	8.5706	7.7039	8.3577	7.983213	8.57200	7.66468
Norm of CMn_D	42.7060	42.5388	42.8304	42.6244	42.2241	42.3600	62.7664	42.59888	42.0747	42.4366
Norm of CMd_A	0.2931	0.2856	0.2854	0.2884	0.3046	0.2987	0.4708	0.293469	0.30396	0.284331
Norm of CMd_D	1.9242	2.1706	2.1691	1.9837	2.1227	2.0496	2.6276	1.923377	2.12611	2.17480

Table 5.8: (b) Differences of norms of three unknown type faults from known type faults under loading condition 3 (1st to 5th level decomposition)

Unknown types	Known fault types						
	BR	FB	RM	RU	SF	VU	HM
X1	**0.1048**	3.3776	3.0941	0.8126	2.0407	7.8510	22.7382
X2	1.7850	1.4879	1.2044	1.0772	**0.1510**	5.9613	20.8484
X3	3.1598	**0.1130**	0.1705	2.4520	1.2238	4.5864	19.4736

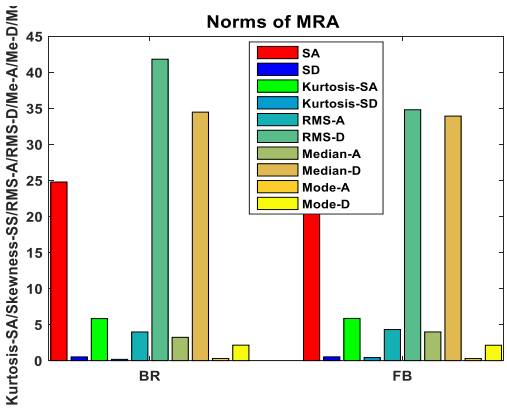

(a)

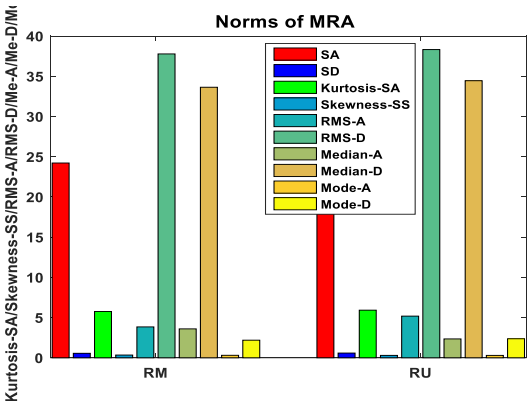

(b)

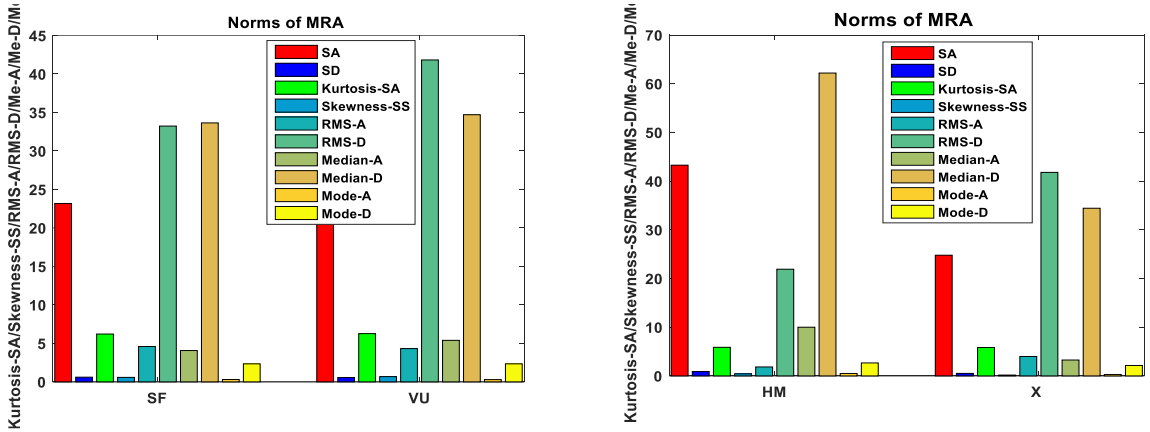

(c) (d)

Figure 5.27*: Composite norms of MRA of different type of faulty motors with unknown type fault 1 under loading condition 1 for 1st to 5th level decomposition,(a) BR and FB, (b) RM and RU, (c) SF and VU, (d) HM and X= unknown type 1*

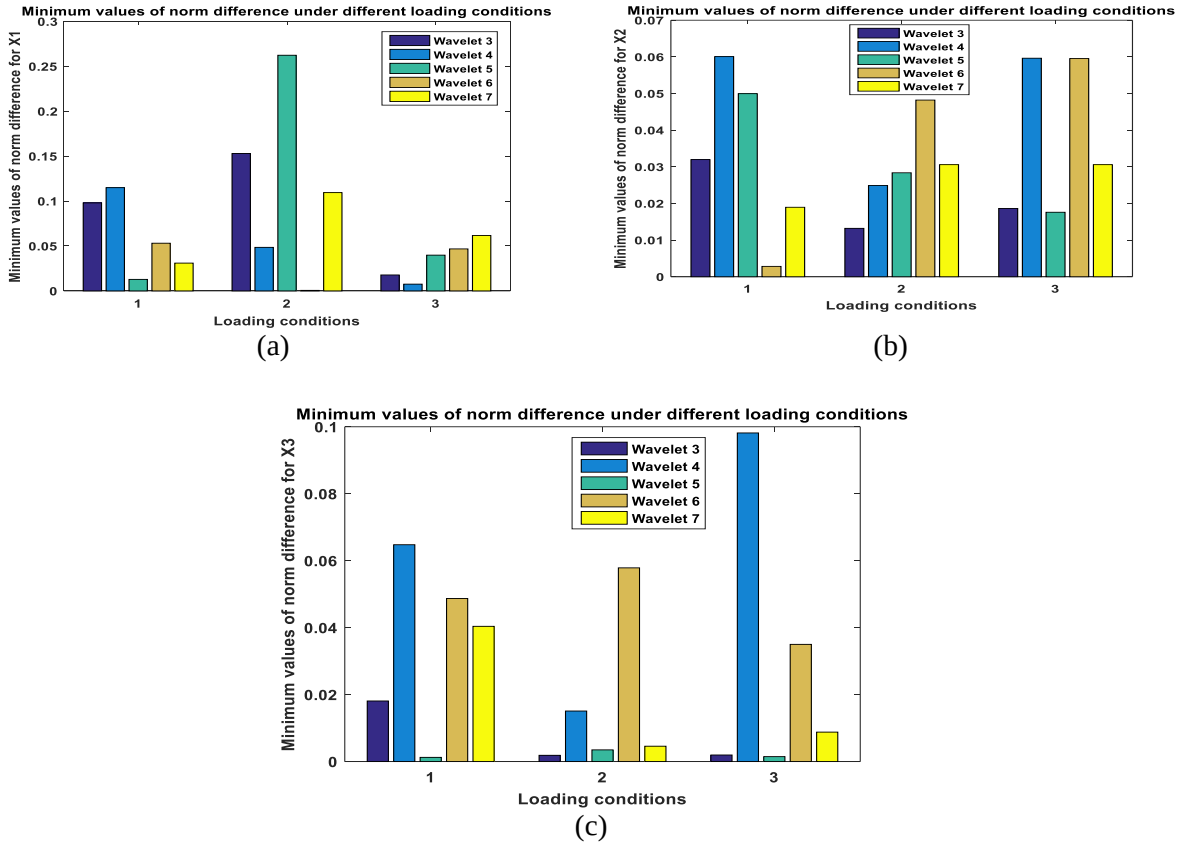

(a) (b)

(c)

Figure 5.28 *: Minimum values of norm differences for three unknown type of faults under three loading conditions at different decomposition levels, Wavelet 3: 1st -3rd level decomposition, Wavelet 4: 1st -4th level decomposition, Wavelet 5: 1st -5th level decomposition, Wavelet 6: 1st -6th level decomposition, Wavelet 7: 1st -7th level decomposition, (a) for X1(unknown type 1),(b) for X2 (unknown type 2) , (c)for X3(unknown type 3)*

The three different loading variations, as described in Section 3.2, are illustrated as follows:

Loading condition 1: The I.M. is running and no mechanical load is connected, Loading condition 2: I.M. has a mechanical load that is a DC generator, Loading condition 3: A 200 watt electrical load coupled to the generator's output (while the full load of the generator is 750 W).

The Fig 5.28 represents the minimum values of norm differences for three unknown type of faults under three loading conditions at different decomposition levels (1^{st} to 3^{rd} level, 1^{st} to 4^{th} level , 1^{st} to 5^{th} level and 1^{st} to 7^{th} level) and the minimum values of norms differences are nor increasing or decreasing with the increase of decomposition levels. It can be said from the result that the sensitivity of norm difference does not depend on the level of decomposition.

Chapter 6

Fault Classification using PNN in different domains

A probabilistic neural network (PNN)-based robust classifier has been developed in this work for the classification and authentication of induction motor faults using the features of three domains. The decomposition level of the wavelet has also been selected to get the highest classification accuracy, and the optimal value of the PNN spread parameter has also been estimated in this work. Induction motors' three phase line currents are measured under three different loading conditions for six classes of defects and one healthy state. Time domain, time-frequency domain, and frequency domain features are analysed here using direct fault current signals, their FFT spectra, and wavelet transforms of the same, respectively; followed by principal component analysis (PCA). PNN is used to develop the final classifier using PCA features. The inclusion of variability in loading ensures robustness. The PNN model is further tuned with varying spread parameters to obtain the optimum level of accuracy, and the results are also recorded. The model presented here is found to detect faults with a mean accuracy exceeding 99%. The classification accuracy estimates, obtained using different schemes, are analysed and compared. Besides, this method incorporates a low-computation PNN architecture. High accuracy of fault classification combined with simplicity of analysis indicates its effectiveness for the diagnosis of various induction motor faults; as well as, its ease of implementation in developing real time condition monitoring and fault diagnosis schemes.

6.1 Introduction

The behaviours of induction motor current and torque are also studied using simulation modelling [177]; although these methods suffer from uncertainties in practical implementation. Artificial intelligence (AI)-based models are widely employed now-a-days for induction motor fault identification with a high success rate [47]. Supervised learning models, combined with other methodologies, have been used often for developing hybrid classifier models. Some of the methods include MLP [178, 179], adaptive neuro-fuzzy inference systems, Mahalanobis-Taguchi systems, deep neural networks [180], artificial neural networks (ANN), and support vector machines (SVM). Other models include modified forms of neural networks, such as the probabilistic neural network (PNN), which uses Bayes' optimal classification to generate accurate predicted target probability scores [181–184] and is faster than a multilayer perceptron network. These methods primarily aim at feature selection by reducing noisy and irrelevant features; as well as the dimension of the fault signals; thereby, providing an exact description of the condition of faults, a diagnosis, and a prognosis . Statistical techniques are also used in abundance for feature extraction from signals [185]. Principal component analysis (PCA) is one such method, used widely in this domain of research. PCA allows for the reduction of dimensions by identifying the main directions of variation in a signal in the order

of importance. A statistical model such as PCA is often combined with supervised learning methods such as PNN to develop hybrid networks. The authors of [186–188] have extracted features through PCA and used the same with PNN to develop a classifier model for rotating machines for detecting a single class of fault; although a multiple fault detection algorithm was not taken care of. The authors of [187] have extracted features from a vibration signal through PCA in one domain to classify one type of fault, and the authors of [188] have also extracted features from the wavelet energy spectrum of a vibration signal through PCA to detect one type of fault. Current signals have not been used earlier to detect multiple types of fault patterns in rotating machines through PCA and PNN. In this work, the features are extracted from current signals in different domains through PCA not only to classify multiple unknown faults among trained classes in the frequency domain, time domain, and time-frequency domain individually using PNN but also to compare the classification performances of the features of these three domains.

The work described here aims at classifying and authenticating unknown types of faults in induction motors; as well as identifying the location of the same. PNN is used in this work for developing the classifier for identifying three independent types of faults. Fast Fourier transform (FFT) and wavelet transform are applied here to transform the current signals into the frequency and time-frequency domains, respectively; followed by the application of PCA to extract final fault features from the signals separately. The time-frequency analysis has been done by decomposing the current signals into an optimum Symlet-5 mother wavelet; as it has been found in an earlier work, the Symlet5 mother wavelet has the lowest values of RMSE and the highest values of correlation coefficient among the Daubechies wavelet family (db3-db10), the Coiflet wavelet family (Coif 1-Coif 5) and other Symlet wavelet families (Sym3-Sym8) for different electrical and mechanical faults of an induction motor [162]. These features, so extracted, are analysed using PCA and trained for six different classes of motor faults: faulted bearing, broken rotor bar, unbalanced rotor, misaligned rotor, stator winding fault, single phase voltage unbalance, and one healthy motor using the proposed PNN. The line currents are recorded from the inverter-fed three phase induction motor. The model has been validated for three unidentified faults under various loading scenarios. The experiments are conducted multiple times, and each unknown fault is carried out with three different loading conditions. The fault classification algorithm is run for each phase, for each unknown class of fault, and for each loading condition. This ensures generalisation of the model since it is observed that the frequency spectra of fault currents change under varying speed conditions [120, 189, 190]. Validation of the work is carried out using only three types of unknown faults. The performance of classification is assessed after calculating the success rate at different loading conditions for induction motors with features in the time domain, frequency domain, and time-frequency domain. Analysis of all three time domain, frequency domain, and time-frequency domain features for the assessment of classifier accuracies ensures the robustness of the model; especially considering load variability on the motor.

The model presented here doesn't possess high computational complexity as is found with other supervised learning models, including complex neural networks, machine learning, and support vector machines, which are found in abundance in similar research. Thus, the present model could be applied to developing a real time fault classifier model.

6.2 Feature extraction from signals in time domain, frequency domain and time-frequency domain

Reduction of features is essential for reducing computation times and memory storage of an algorithm to make the classification process simpler. Simultaneously, it is important to retain the most important features from the data and delete the redundant ones. PCA is an efficient feature extraction and dimension reduction tool that reduces a large and diverse data set into the directions of the most variability, while retaining most of the variations. PCA orthogonalizes the vector components that are uncorrelated with each other, so that the components with the least variation contribute the most variation first. The training and test fault current signals from the induction motor are preprocessed by three major feature extraction methods. The time domain fault current signals are directly analysed using PCA. Further, the same fault current signals are processed using two major analysis techniques, such as the FFT and wavelet transform. These two models convert time domain signals into frequency and time-frequency domain spectra, which are then analysed using PCA to yield spectra features. Here, we have used the Symlet-5 mother wavelet and analysed the signals up to five levels of decomposition independently. In each of the cases, PCA is used to extract the final fault features in the form of PC scores. Two of the most important eigenvectors, denoted the first and second principal components (PC1 and PC2, respectively), for each phase, are computed by the PCA algorithm. The three phase PCs of a faulty induction motor and one healthy motor are fed to the PNN architecture for training. In each run, one unknown fault is tested using the trained PNN model and classified independently for the three phases. The three test fault features are fed sequentially to the PNN model to yield classification results. The major techniques used here are briefed in the subsequent sections.

6.2.1 *Feature extraction from current signals using PCA*

The collected current signals are collected from different types of faulty motors, and these current signals in the time domain have different types of harmonics. It is essential to extract relevant features of each type of fault from each phase of current signals, reducing the irrelevant features. PCA has been used here to extract features from each faulty current signal, reducing the dimensions. Dimensional reduction of retrieved features is also necessary to lighten the workload of processing data and strengthen the classifier [109]. Reduction of the input feature vector's size is crucial for streamlining the network model, which decreases recognition time and boosts recognition effectiveness. Principal component analysis (PCA)-based feature extraction and dimension reduction techniques have been found to be more efficient than all other dimensionality reduction techniques in

terms of classification accuracy. By expressing the variable space with a small number of orthogonal, uncorrelated variables that collectively include the majority of the primary variability, PCA is a method for extracting pertinent features and reducing the dimensionality of the variable space. The mathematical expression of PCA has been discussed in chapter 2. The principal components (PCs), or new variables, are created as a linear combination of starting features so that they are uncorrelated. The PCs are independent of one another and perpendicular to one another in Cartesian space. PCs are computed from each phase's current signals. The PCs are fed into PNN for unsupervised fault classification.

6.2.2 *Feature extraction from FFT spectrums using PCA*

Both the time domain and the frequency domain can be used to represent a periodic or non-periodic signal. By using the Fourier transform, a signal's time domain can be transformed into its frequency domain (spectrum). To simplify the analysis of a complicated signal and break it down into simpler components, a frequency domain analysis is required. The actual signal is converted to a discrete signal for continuous FFT analysis using a sampling technique. The description of the FFT and PCA algorithms in brief has been discussed in Chapter 2. The FFT spectra of each phase current signal from each type of motor are used to compute PCs. The proposed PNN model has been fed PCs of FFT spectra from known and unidentified faulty motors to classify unknown faults in the frequency domain.

6.2.3 *Feature extraction from Wavelet Coefficients using PCA*

The theory of wavelet has been discussed in chapter 2 and chapter 5. The concept of a mother wavelet has been discussed in Chapter 5, and Symlet5 has been selected as the optimal mother wavelet for induction motor fault analysis. Wavelet analysis decomposes the signal into ‘approximate’ and "detail" coefficients; where the low-frequency signal components are the ‘approximate’ coefficients and the high frequency signal components are denoted as the ‘detail’ coefficients. In this work, we have applied wavelet analysis to classify the three different classes of faults in the time-frequency domain. The three phase current waveforms of all faulty induction motors, including the healthy one, are decomposed multiple times using the Symlet-5 mother wavelet up to the 5^{th} level of decomposition. Features are extracted from approximate coefficients from each of the decomposed current signals. Approximate coefficients from the decomposed signals have multiple dimensions, so PCA has been applied to extract exact fault features from the approximate coefficients, reducing multi-dimensional data to two dimensional data. To classify the unknown faults, the PCs from approximate coefficients of current signals of known and unknown faulty motors were fed into a PNN-based classifier.

6.3 Probabilistic Neural Network

PNN is incredibly helpful for tackling many classification problems [191]. PNN can provide fast and precise operation for various fault classifications compared to radial basis function and feed forward neural networks [192]. The probability density function (PDF) is created using the Parzen window estimator, and the class with the highest probability is chosen as the anticipated output class [193]. The input layer, pattern (or hidden) layer, and output layer make up the PNN architecture, as depicted in Fig. 6.1. The input layer receives the *n*-dimensional feature vector, $x=(x_1,x_2,..x_n)$.The neurons receive the feature input vector as input, and the neurons in the following hidden layer receive it as well. Thus, the entire feature vector *x* is input to each hidden layer node. When a test input is provided, the first layer computes the distances between the test input vector and the input vectors for training and also creates an error vector.

A single sample x_k's PDF is written as follows:

$$f_k(x) = \frac{1}{(2\pi)^{\frac{n}{2}}\mu^n} e^{((\|x-x_k\|^2)/(2\mu^2))}, 0 \le k \le C \quad (6.1)$$

where, μ is the smoothing (or spread) parameter for Gaussian function and *n* is the dimension of the input vector *x* and $\|x - x_k\| = \sum_{i=1}^{k}(x - x_k)^2$ is the Euclidean distance between the test vectors x_k. and *x*.

There are *C* output nodes since all of the Gaussians in a class feed their functional values into the same node of the output layer. A probability vector representing the average of the PDFs for C samples was created by adding these multivariate densities at the *k*-th output node as follows:

$$p_k(x) = \frac{1}{(2\pi)^{\frac{D}{2}}\mu^D C} \sum_{k=1}^{C} e^{((\|x-x_k\|^2)/(2\mu^2))}, 0 \le k \le C \quad (6.2)$$

The output is finally set to "1" for the input class with the highest joint PDF and "0" for all other classes. As a result, if $p_k(x) > p_{k'}(x)$ for every $k' \neq k$. then *x* is an unknown feature input that belongs to class *k*. The neuron in the decision layer uses the Bayes decision rule to evaluate if pattern x belongs to a class under the following conditions: $c(x) = \text{argmax}\{p_k(x)\}$, where *k*=1, 2,..., *C*, and *c*(*x*) is the estimated class of the pattern *x*. The maximum value of the sum functions $f_1(x)$, $f_2(x)$, *and* $f_k(x)$ determine which class out of the m classes will be chosen *x*.

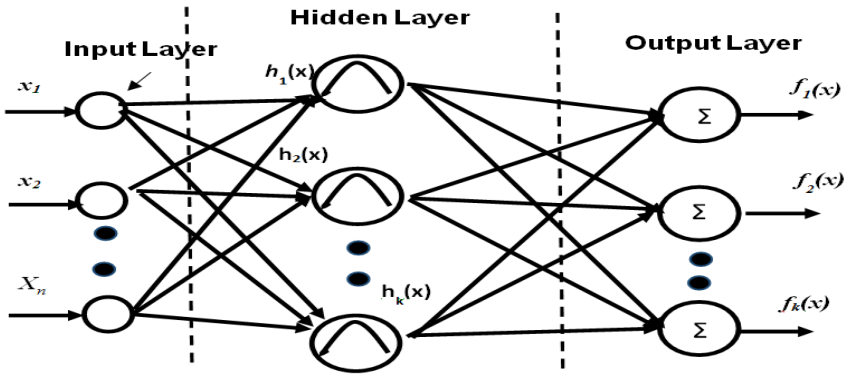

Figure 6.1: *The PNN architecture.*

The PCs of each phase of current signals, PCs of the FFT spectrum, and PCs of approximate coefficients are inputs to PNN to classify three unknown faults in the time domain, frequency domain, and time-frequency domain individually. Multiple PCs of each phase of each known faulty motor under no load condition are the trained known class, and PCs of each phase of each unknown faulty motor under three loading conditions are the test class.

PNN Algorithm for classification:

```
//  The number of examples is M, The number of classes is B, Mk are from class k
//  the smoothing factor is σ and e is the dimensionality of the training examples
// the example to be classified is test_ example[e]
// Examples[M][e] are the examples of training
int PNN(int B, int M, int e, float test_ example[e], float Examples [M][e], float μ)
{
int classify = -1;
float lrgst = 0;
float sumn[B];
// The pdf is computed by output layer for each class B
for ( int k=1; k<=B; k++ )
{
Sumn [ k ] = 0;
// The pdf is accumulated by Summation layer
// for each example from the particular class k
for ( int l=0; l < Mk; l++ )
{
float prdct = 0;
// The  test example is multiplied by  Pattern layer by the weights
for ( int n = 0; n < e ; n ++ )
```

```
prdct += Examples[l][n]* test_ example[n];
prdct = ( product – 1 ) / ( μ*μ );
prdct = exp ( prdct );
sum[ k ] += prdct;
}
sum[ k ] /= Mk;
}
for ( int k = 1; k <= B; k ++ )
if ( sumn [ k ] > lrgst )
{
lrgst = sumn [ k ];
classify = k;
}
return classify;
}
```

6.3.1 *Authentication of unknown faults using PNN*

In this study, we provide a wavelet, PCA, and FFT-based fault characteristics-based PNN-based fault classification model for three-phase induction motors. The current signals of R, Y, and B phases and their FFT spectra are analysed using PCA in order to extract major fault signatures; simultaneously reducing the dimensionality for ease of computation. Two-dimensional feature vectors, extracted using these schemes, for six classes of fault conditions, viz., failed bearing (FB), broken rotor bar (BR), Misalignment rotor(RM), stator fault (SF), unbalanced rotor (RU), and single phase voltage unbalance (VU), along with one healthy condition (HM), corresponding to all three phases, are used to train the designed PNN model. These feature vectors are constructed using the PC scores of current signatures, their FFT spectra, and their wavelet coefficients. Faults, carried out under different levels of loading and unknown fault conditions, are used to test the present classifier as well as validate the trained PNN model. The classification accuracy is computed for multiple experiments using different methodologies and for different levels of decomposition for analysis using the wavelet transform. The steps of designing the motor fault classifier are illustrated with the help of a work flow diagram in Fig. 6.2.

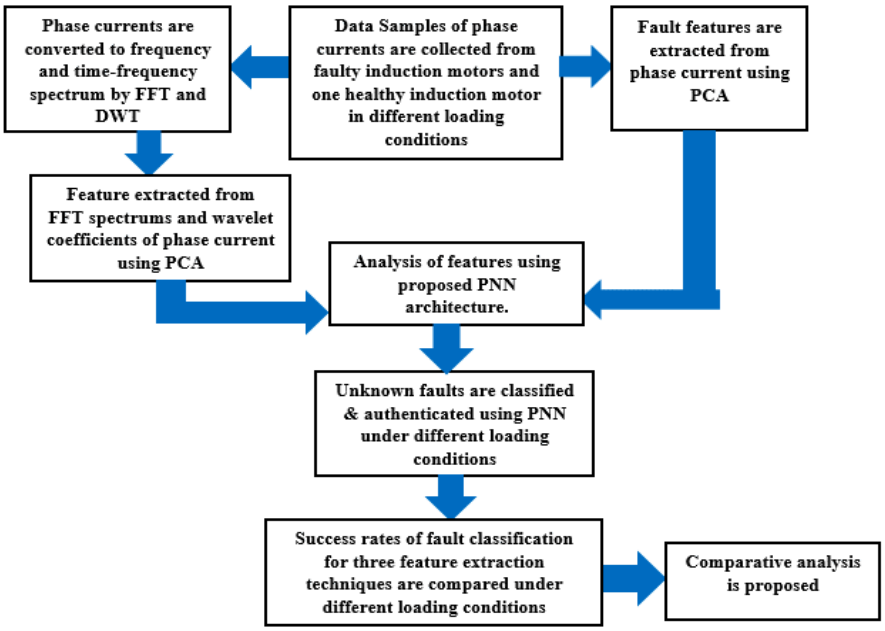

***Figure 6.2**: Work flow diagram of the work*

6.4 Experimentation

The experiment was carried out using the same setup as shown in Chapter 3, and data of three-phase current signals were collected using six different faulty induction motors and one healthy motor. The current signals are captured independently by a three phase power analyzer (Yokogawa WT 500) when the motors are running at no load, or running as a prime mover to a DC generator with a 200-watt electrical load connected to the output. This ensures that variations in loading conditions are accounted for. The data samples from unknown or faulty motors are collected four times at a time interval of 5 to 6 minutes, under different loading conditions. The data samples from six known and three unknown faulty motors are also collected six times at a time interval of 5 to 6 minutes, under three different loading conditions.

6.5 Result and Analysis

6.5.1 *Analysis of fault features*

The experimental results were recorded for each of the six classes of faults and the healthy condition. The three-phase current waveforms at no load and under three major fault conditions are shown in Figs. 6.3–6.5. The 5th-level decomposed three-phase current signals of an induction motor under a broken rotor bar condition have been shown in Fig. 6.6. The two dimensional PC score plot of all the six faulty motors and one healthy motor, obtained by applying the PCA directly over the time domain fault signal is also shown in Fig. 6.7.

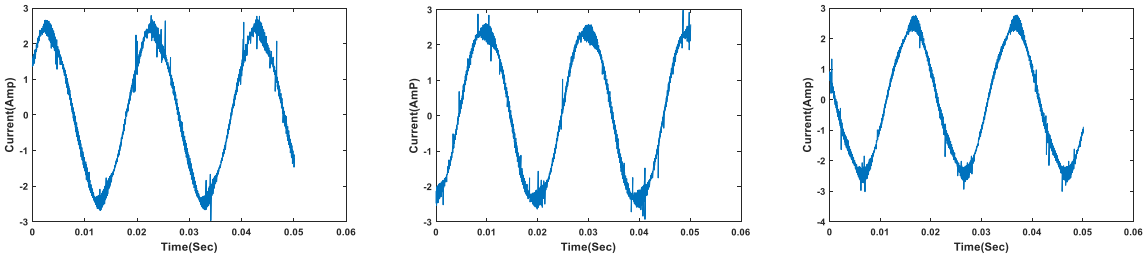

(a) (b) (c)

Figure 6.3: *Three phase current signals of induction motor under broken rotor bar (BR) condition for (a) Phase R, (b) Phase Y and (c) Phase B*

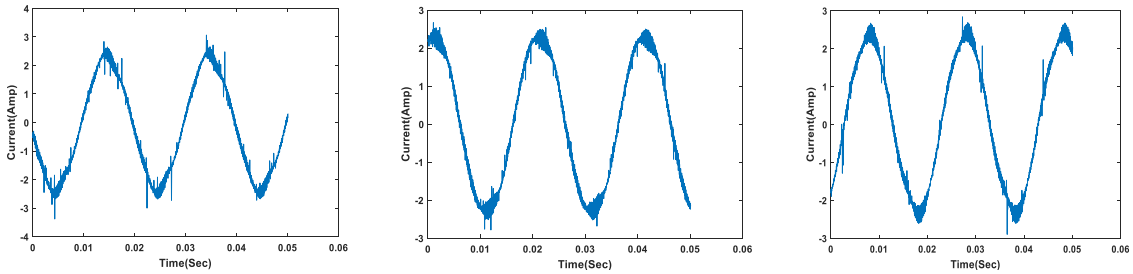

(a) (b) (c)

Figure 6.4: *Three phase current signals of induction motor under Stator winding fault (SF) condition for (a) Phase R, (b) Phase Y and (c) Phase B*

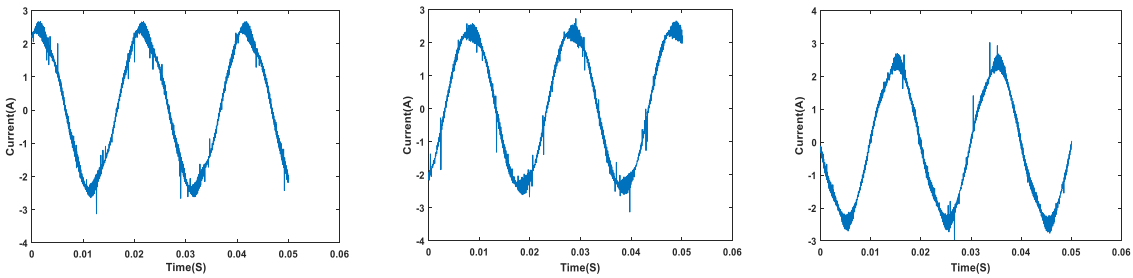

(a) (b) (c)

Figure 6.5: *Three phase current signals of induction motor under Faulted bearing (FB) condition for (a) Phase R, (b) Phase Y and (c) Phase B*

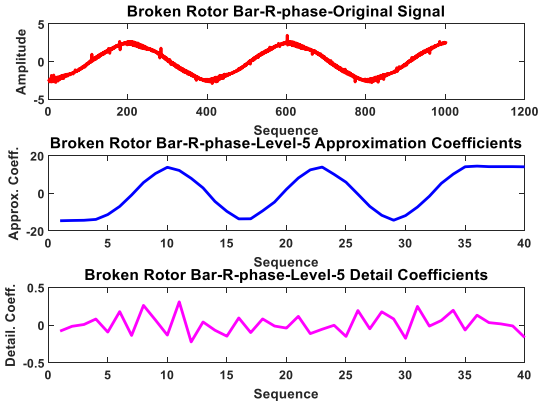

(a)

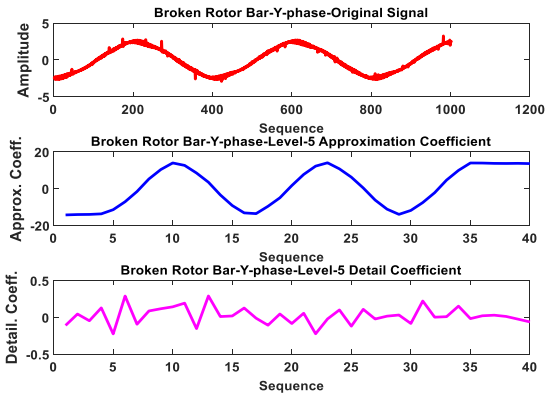

(b)

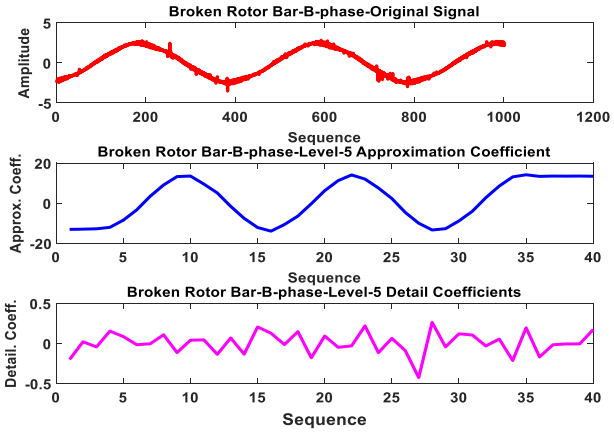

(c)

Figure 6.6: *Three phase 5th level decomposed current signals of induction motor using Symlet5 mother wavelet under Broken Rotor Bar (BR) condition for (a) Phase R, (b) Phase Y and (c) Phase B*

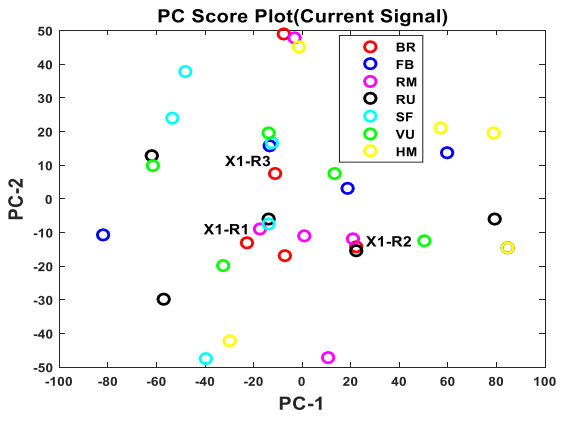

(a)

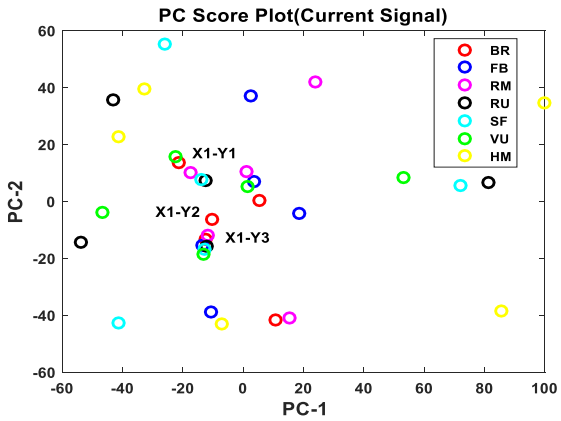

(b)

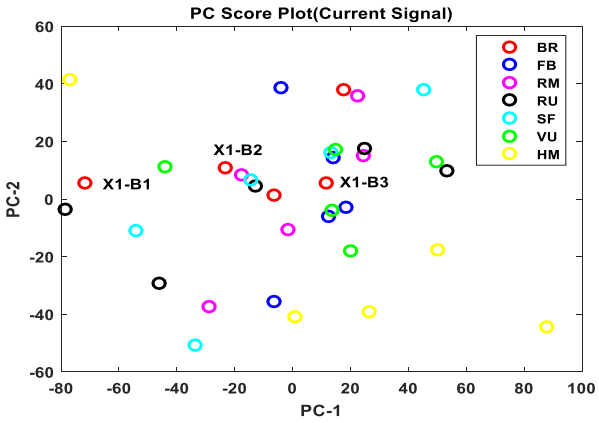

(c)

Figure 6.7: *Three phase PC score plots of (a) Phase R, (b) Phase Y, (c) Phase B current signals of six fault classes and healthy motor at no load (loading 1) condition, as well as unknown fault 1(X1) at three different loading conditions; where, X1 is the unknown fault class in each sub-figure. The six fault classes are indicated by Class A: BR (Broken rotor), Class B: FB (Faulted bearing), Class C: Misaligned rotor), Class D: RU (Unbalanced rotor), Class E: SF (Stator fault), Class F: VU (Single phase voltage unbalance), Class G: HM (Healthy motor)*

Current signals in the time domain are once again converted to signals in the frequency domain and time-frequency domain using the FFT method and wavelet transform, respectively, up to five levels of decomposition. The FFT spectrum data and the wavelet coefficients are fed independently to the PCA algorithm to extract the final fault features in terms of PC scores. The score plots of the PCs obtained from the features of the FFT spectrum and wavelet approximate coefficients are shown in Figs. 6.8 and 6.9, respectively. It should be mentioned here that for all the sub-figures of Fig. 6.7 to Fig. 6.9, R1, Y1, and B1 refer to the three phase PC score plots of unknown fault 1 (X1) under the first loading condition; similarly, R2, Y2, and B2 refer to the plots of the second loading condition, and R3, Y3, and B3 denote the plots obtained under the third loading condition.

The three phase PC scores of time-domain current samples, FFT spectra, and wavelet approximate coefficients corresponding to each class of fault and a healthy condition are considered input vectors to three independent PNN models. The target vectors are assigned to seven classes, including six fault types and one healthy condition. These are numbered A (BR), B (FB), C (RM), D (RU), E (SF), F (VU), and G (HM), respectively. The necessity of fault prediction performance using a classifier should be load independent because finding test data and training data at the same load is not always possible, That's why the training of the model is carried out with faults and the number of fault current signatures recorded at no-load condition (loading 1) only, but the testing of the model is carried out with current signatures of unknown faults at three loading conditions (loading 1, 2, and 3). Five PC scores of each phase of each known faulty motor at no load (total 5 x 7 = 35) are used for designing the classifier, and PC scores of each phase of each unknown faulty motor, under three

loading conditions, are used for testing the same. Three data points of X1 have been classified phase wise among 35 trained data points, and the success rate of classification or classification accuracy for X1 has been calculated depending on the total number of successful classifications of the three phases under each loading condition individually. The same procedure has been applied for unknown fault 2 (X2) and unknown fault 3 (X3) to find the classification accuracy of other two unknown faults under each loading condition individually, the details have been explained below.

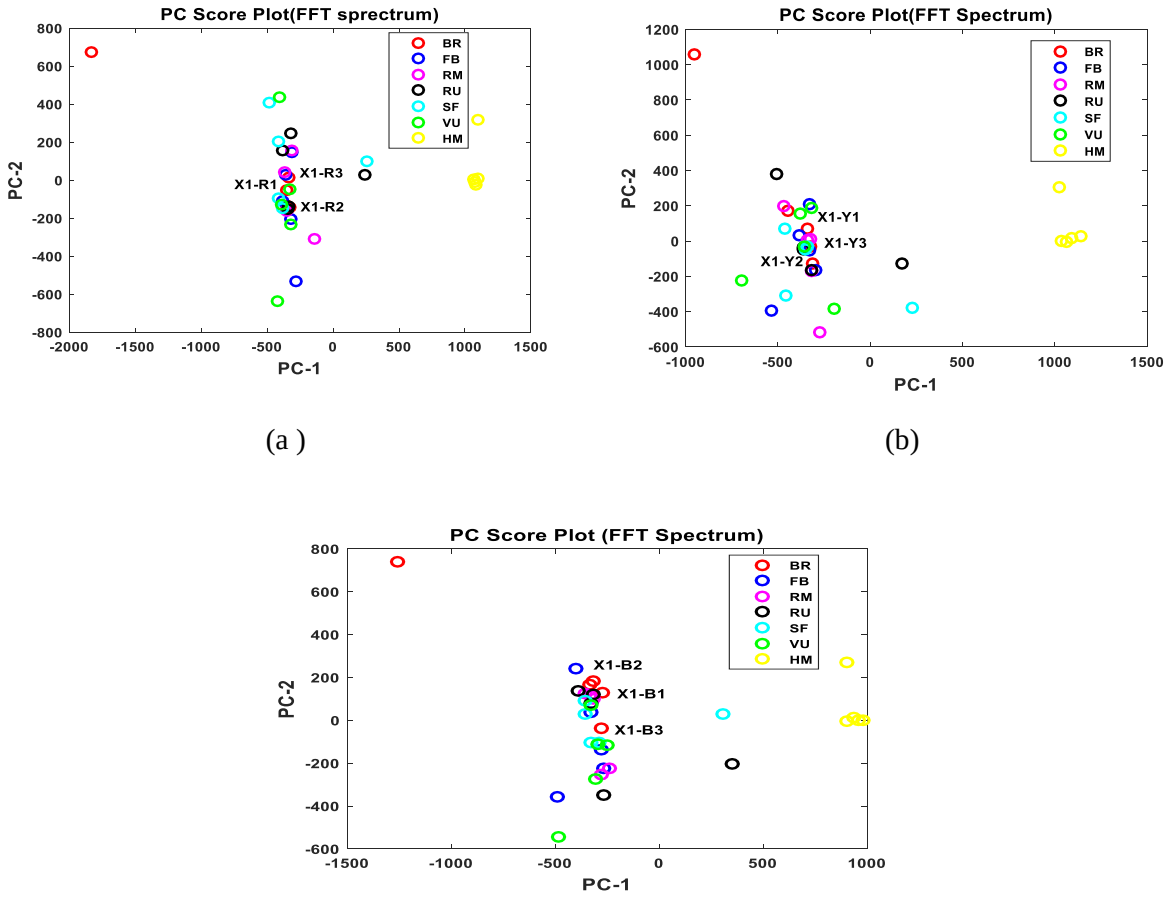

(a) (b)

(c)

Figure 6.8: *Three phase PC plots of FFT spectrums of (a) Phase R, (b) Phase Y and (c) Phase B current signals of six fault classes and healthy motor at loading 1 condition, as well as unknown fault 1 at three different loading conditions; where, X1 is the unknown fault 1 class in each sub-figure. The seven fault classes are indicated by Class A: BR (Broken rotor), Class B: FB (Faulted bearing), Class C: RM (Misaligned rotor), Class D: RU (Unbalanced rotor), Class E: SF (Stator fault), Class F: VU (Single phase voltage unbalance), Class G: HM (Healthy motor)*

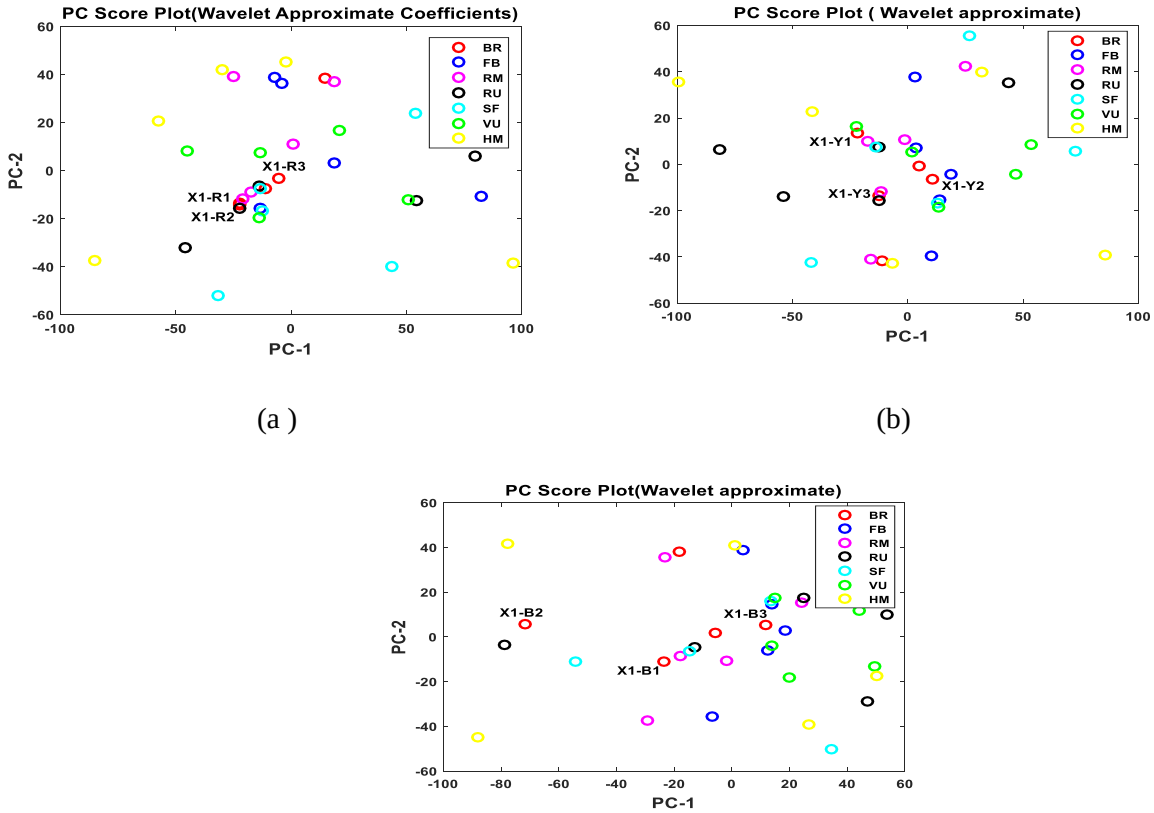

(a) (b)

(c)

Figure 6.9: *Three phase PC plots of wavelet first level approximate coefficients of (a) Phase R, (b) Phase Y and (c) Phase Bing current signals of six fault classes and healthy motor at no load condition(loading 1), as well as unknown fault 1(X1) at three different loading conditions; where, X1 is the unknown fault class in each sub-figure. The six fault classes are indicated by Class A: BR (Broken rotor), Class B: FB (Faulted bearing), Class C: RM (Rotor Misalignment), Class D: RU (Unbalanced rotor), Class E: SF (Stator fault), Class F: VU (Single phase voltage unbalance), Class G: HM (Healthy motor)*

Apparent observation of the PC plots in Figs. 6.7–6.9 reveals that the three test score points are close to one of the seven signature fault score points. In order to establish this fact, these PC features are fed to the designed PNN model; thereby validating the same. Close observation reveals that the three unknown fault classes, viz., classes 1 (X1), 2 (X2), and 3 (X3), are close to the signature fault classes of class A (BR), class E (SF), and class B (FB), respectively, for all the three phases. Validation of the models is carried out with three phase motor fault current signals corresponding to three fault classes only; i.e., for BR (broken rotor), SF (stator fault), and FB (failed bearing) faults, respectively. Most importantly, loading is varied in three steps to develop the fault current signatures, and these signals are analysed using three different feature extraction models: direct time domain analysis followed by PCA, fast Fourier transform followed by PCA, and wavelet approximate coefficients followed by PCA. The motor is run with no mechanical load; next, the motors are run with a D.C. generator as a mechanical load and with a 360-watt electrical load connected to the generator. These data, which

correspond to variable loading conditions, are used to validate the models, whereas training was done using only fault features from the no load condition.

6.5.2 *Classifier outcomes*

We have further varied the spread parameter in the range 0.2, to 0.8, in steps of 0.2 to tune the PNN during training because spread value estimation is also an important task for PNN based classification [194]. This enables the incorporation of robustness into the classifier model. The classifications are performed multiple times in different loading conditions, changing the values of the spread of the PNN architecture to compare the success rates of classification, using the features extracted in the time, frequency, and time-frequency domains. The better technique is selected by comparing the classification accuracy rates.

Data samples are collected 6 times from each unknown faulty induction motor with three different loading conditions. The test fault is classified for each of the 6 cases and for each phase individually. Thus, the total number of test cases for one loading condition of fault classification stands at 6 times 3 phases, i.e., 18. The classification accuracy of the model is determined as follows:

$$Classification\ accuracy\ (\%) = \frac{Number\ of\ correct\ classification}{Total\ number\ of\ tested\ cases} \times 100$$

The classification accuracies are computed using the above expression for the three independent models:

i) Time domain analysis of fault currents using PCA, followed by PNN,

ii) Frequency domain analysis of fault current spectrums using PCA, followed by PNN and

iii) Time-frequency domain analysis of fault currents with wavelet with five levels of decomposition using Symlet-5 mother wavelet, followed by feature extraction using PCA and classification using PNN

The success rates are calculated for each of the three methods independently by changing the spread parameter of the PNN model for three different loading conditions. The overall accuracies of three unknown faults under different loading conditions and obtained with different spread parameters are also represented in Table 6.1.

Table 6.1: Classifier outcomes of three unknown type of faults using seven modes of feature extraction, under variable loading conditions and for variation in spread parameter of the PNN model

Feature extraction method	Loading Type											
	Loading condition 1				Lading condition 2				Loading condition 3			
	Spread parameter											
	0.2	0.4	0.6	0.8	0.2	0.4	0.6	0.8	0.2	0.4	0.6	0.8
PCA of current signals	69.14	81.48	85.18	82.71	71.6	80.24	85.18	80.34	71.6	82.71	85.18	81.48
PCA of FFT spectrums	74.07	88.88	90.12	87.75	76.54	88.88	91.35	88.88	76.54	88.98	90.12	87.65
PCA of L1	76.54	90.12	90.12	88.88	79.01	90.12	91.35	90.12	81.48	91.35	91.35	90.12
PCA of L2	81.48	93.82	96.29	92.59	82.81	93.82	97.53	93.92	82.71	93.82	97.53	93.82
PCA of L3	84.05	96.29	**98.76**	92.59	85.18	98.76	**100**	93.92	83.95	100	**100**	93.82
PCA of L4	81.48	93.82	96.29	92.59	82.81	93.82	97.53	93.92	82.71	93.82	97.53	93.82
PCA of L5	70.37	81.48	85.18	82.71	71.6	80.24	85.18	80.34	71.6	82.71	85.18	81.48
Mean	76.73	89.41	**91.71**	88.55	78.51	89.41	**92.59**	88.78	78.66	90.49	**92.41**	88.88

The three different loading variations, as described in Table 6.1, are illustrated as follows:

Loading condition 1: No mechanical load, Loading condition 2: Induction motor with a D.C. generator as a mechanical load, Loading condition 3: A 200-watt electrical load connected to the output of the generator (while the rated load of the generator is 750 W).

**Note: L1, L2, L3, L4 and L5 are the wavelet decomposition in level 1, 2, 3, 4 and 5 respectively.*

6.5.3 *Analysis of results*

From Table 6.1, as well as the present scheme of work, it can be seen that there are three major parameters involved in this work. These are respectively the type of load, spread parameter, and feature extraction method. In this work, we have used three major modes of fault feature extraction from the induction motor fault current signals, which are direct time domain analysis of fault currents using PCA, frequency domain analysis of fault current spectrums using PCA, and time-frequency domain analysis with wavelet analysis using the Symlet-5 mother wavelet, followed by feature extraction using PCA. We have further experimented with five levels of decomposition for the wavelet transform. In addition, three types of faults are tested with the models to validate them. Thus, the analysis of the results is carried out in three folds, in order to illustrate the effect of these three governing parameters.

We have first plotted the average classifier accuracy values against the spread parameters and analyzed the three loading conditions separately. We have kept the seven fault feature extraction modes, as described here, as the varying parameters of the plot. These are illustrated in Fig. 6.9. It is observed, for all three loading conditions and all seven fault feature extraction modes, that the classifier accuracy reaches the optimum level for the spread parameter of 0.6.

The above observation is emphasised further by plots in Fig. 6.10a, which show the grouped distribution of mean accuracy levels with respect to spread parameters when all seven feature extraction models are considered. Each group has sub-levels with different loading conditions. It is observed from Fig. 6.10a that the accuracy level is higher for a spread of 0.6, for almost all the loading conditions. All these accuracy levels corresponding to different loads are considered together to form a mean accuracy level, which is shown with a magnified accuracy scale in Fig. 6.11c. It is readily observed from here that the mean percentage accuracy of fault classification is highest for a spread value of 0.6. The mean accuracy of classification reduces on both sides of the spread level of 0.6, i.e., as the spread level is either decreased or increased. Thus, it could be confirmed from here that a spread parameter of 0.6 is optimal for the present work. Hence, this analysis yields a vital inference regarding the tuning of the described PNN architecture.

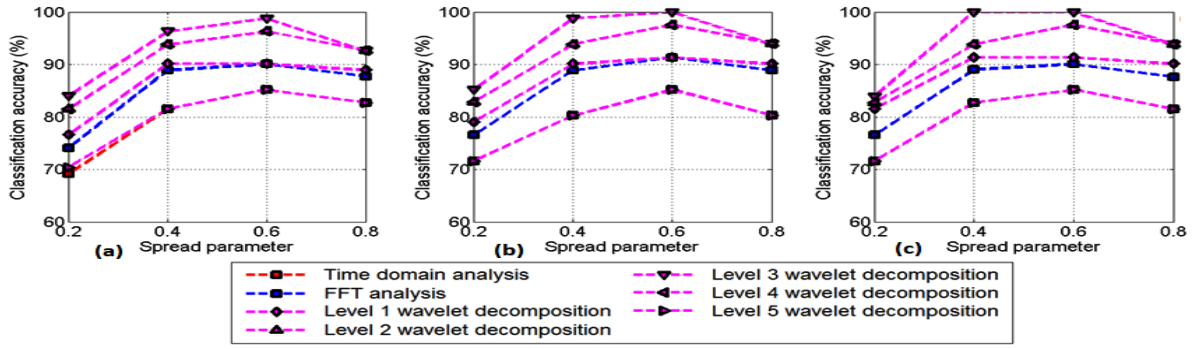

Figure 6.10: *Mean variation of classification accuracy considering all the seven feature extraction models for variation in spread parameter and for variation in loading conditions, (a) Loading condition 1, (b) Loading condition 2, (c) Loading condition 3*

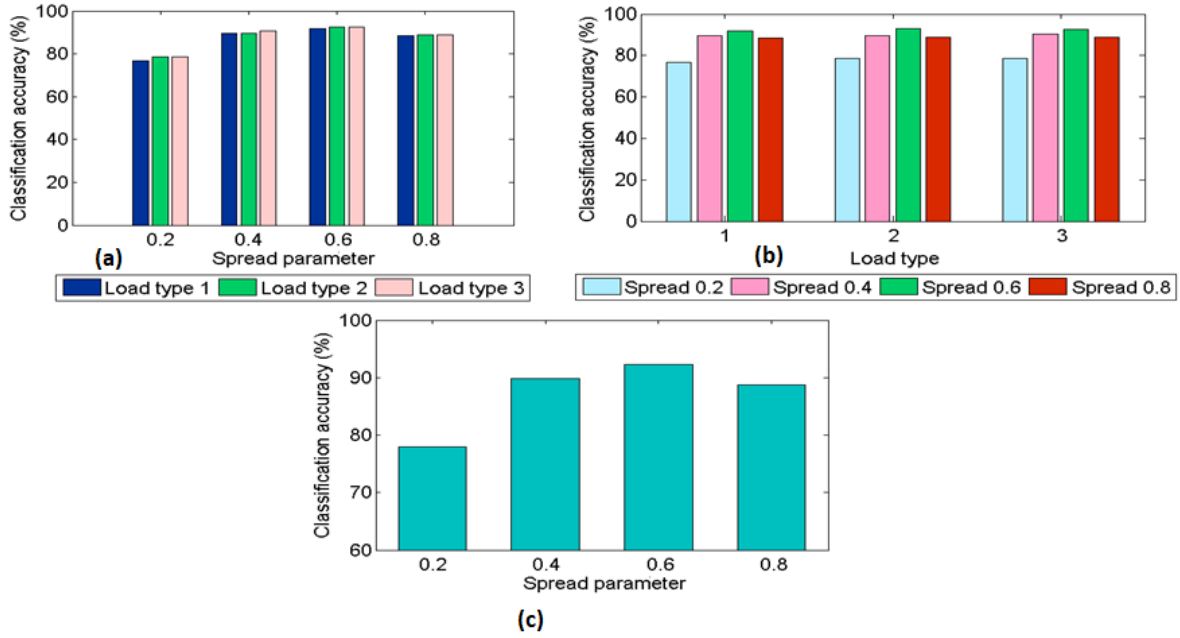

Figure 6.11: *Mean variation of classification accuracy considering all the seven feature extraction models for* ***(a)*** *variation in spread parameter considering independent loading condition,* ***(b)*** *variation in loading conditions considering independent spread parameter,* ***(c)*** *variation in spread parameter considering all the three different loading conditions together*

Another analysis is performed from a different perspective using the same set of results, with the variable parameter being the type of loading. This variation is shown in Fig. 6.10 (b). The three groups of accuracy parameters indicate the three different loading arrangements, and the sub-levels indicate the different spread parameters ranging from 0.2 to 0.8. It is observed from here that the pattern of accuracy levels is almost similar, irrespective of loading on the motor. This indicates a vital inference regarding the robustness of the model. It shows that the model presented here is robust enough to negate the disturbances caused by differences in loading on the motor, thereby, enabling the classifier to cater to diverse loading conditions. This is one of the key outcomes of the work described here. Thus, it is concluded from the above discussion that a spread of 0.6 produces the optimal level of classifier accuracy. Thus, we have considered this level of spread parameter as optimal for this work.

Finally, we have analyzed the outcomes from the seven different feature extraction methods independently and compared the results. For the purpose of comparison, we have considered the classification accuracy values of the seven feature extraction methods obtained with a spread of 0.6 only and discarded the rest. These results are plotted in magnified scale in Fig. 6.12, which shows a comparison of results obtained using seven models, followed by PNN. In this figure, we have also plotted the results obtained for different loading conditions and for three different classes of faults used for testing the same. This figure apparently shows that the results, obtained from the wavelet feature extraction method, especially for the 2nd, 3rd, and 4th levels of decomposition, are superior to the rest for most of the loading conditions. Wavelet level-3 decomposition produces nearly 100% classifier accuracy in almost all tested cases with varying loading and fault conditions. These results are summarized further, and the mean accuracy levels are computed considering all nine individual conditions in Fig. 6.12 (a). These mean accuracy values are plotted again in Fig. 6.12 (b), which clearly displays the superiority of results obtained with the 3rd level of wavelet decomposition compared to the rest of the levels; as well as, the direct time domain PCA or FFT-PCA model of feature extraction. Hence, level 3 wavelet decomposition is considered optimal for the present work.

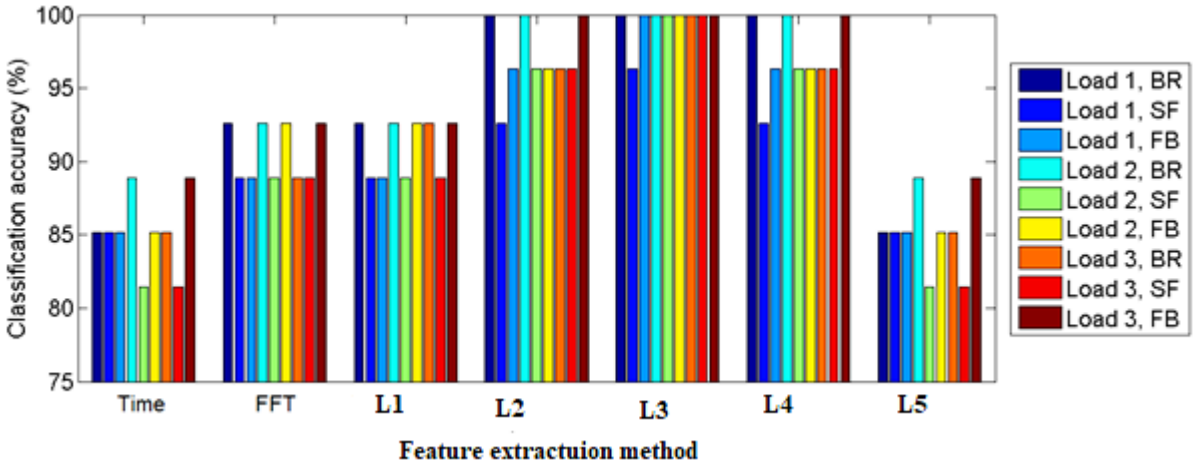

(a)

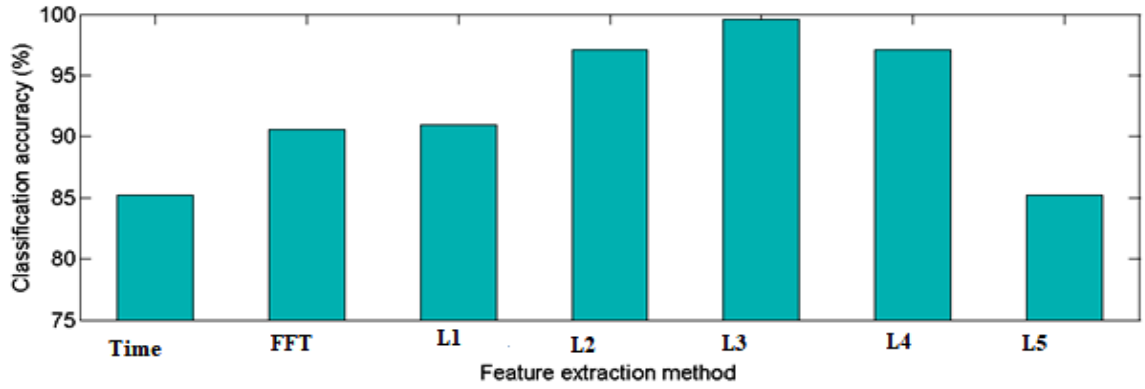

(b)

Figure 6.12: *Magnified view of mean variation of classification accuracy for the seven feature extraction models,* ***(a)*** *considering load type and class of fault independently, and (b) considering all load types and classes of faults together*

**Note: L1, L2, L3, L4 and L5 are the wavelet decomposition in level 1, 2, 3, 4 and 5 respectively.*

Thus, the work described is able to produce the best outcomes in terms of classification accuracy for the detection of three major classes of three phase induction motor faults. The presented PNN architecture is found to work best with a spread value of 0.6. It is observed from Fig. 6.12 (b) that classifier accuracy is increasing monotonically from level 1 to level 3, and decreasing thereafter. Hence, the wavelet's 3rd level of decomposition from the Symlet-5 mother wavelet has been chosen as the optimum feature extraction model for developing the most accurate classifier. Thus, the combined approach of wavelets for feature extraction, and PNN, for classifier design, has been found to be the final and optimum fault-discriminating model of the present work.

The wavelet decomposition of the input signal reduces the noise to get exact time-frequency information about the particular type of fault. But as the level of decomposition increases, the chance of loss of information also increases. This is also evident from the present study. It could be observed from Fig. 6.12b that the classification accuracy of all classes of unknown faults is increasing from 1st level to 3rd level; but thereafter it decreases again under all loading conditions. Thus, level 3 of wavelet decomposition has been found to be the optimal level of decomposition in the present work. This is another key observation obtained from the present study.

Both wavelet and PNN are well used methods in this field of research. Besides, the fault detection accuracy achieved using the optimum combinations of wavelet and PNN, as described before, is able to produce a classification accuracy of 99.6%, as is found from Fig. 6.12(b), which is very high. Besides, the experiments are carried out in real time hardware setups rather than simulation models; which nullifies the presence of errors that may creep in during software simulation of machine faults. As a result, this classifier could be used to develop a real-time fault classifier model for induction motors in the future.

Chapter 7

Comparison of fault classification using different signal processing techniques

Identification of faults in electrical machines is an integral part of their continuous and reliable operation. In this work, we have developed a scheme for the identification of faults in a three phase induction motor under three variable loading conditions. We have used the cross correlation method followed by principal component analysis (PCA) on the motor fault signals and analysed the PCA score features using the nearest neighbourhood criterion for fault authentication. We have also extracted features directly from the fault current signals, in the frequency domain using fast Fourier transform (FFT) and in the time-frequency domain using wavelet transform, followed by analysing the features using PCA. A comparison of results revealed that cross correlation produced the least distance from the true class in most cases, providing the highest authentication of faults. The sensitivities of wavelet decomposition at different levels have also been verified, and it is found that the results are almost insensitive to the level of decomposition. Besides, in several cases, wavelet analysis of the fault signals was also less effective compared to other methods of analysis. Several other faults were used to validate the results.

7.1 Introduction

The research is carried out for multiple fault detection of induction motors by extracting features from different types of signals, and the sensitivities of these signals have been compared after analysing the faults. Previously, time domain analysis, time-frequency analysis, and frequency domain analysis of current or vibration signals were used to detect electrical or mechanical faults in rotating machines. Cross correlation is also another signal processing technique that is used in this work to detect faults in the induction motors, and the sensitivities of cross-correlated signals with other signals have been compared. Experiments have been performed for motor current signature analysis (MCSA) to collect three-phase current data samples from six different faulty induction motors, three unknown faulty motors, and one healthy induction motor under different loading conditions. Cross-correlated signals have been developed to find the degree of correlation between the current signals of healthy motors and the current signals of faulty motors. FFT, DWT have also been applied to find the frequency spectra of current signals and to decompose the current signals at different levels of decomposition for time-frequency analysis. Features are extracted by PCA transformation from the cross-correlated signals, current signals in the time domain, FFT spectra, and approximate coefficients from the decomposed signals. Using four different feature extraction techniques and the low-cost, low-calculation-time neighbourhood classification method, three different types of unknown faults were

identified among the mixture of various types of faults. The classifications have been performed phase-wise for every feature extraction technique under three different loading conditions. Each fault pattern has been identified if the classification results of the three phases are the same. The sensitivity of feature extraction from each type of signal depends on the magnitude of the minimum distances from unknown faults to known faults. The sensitivities of four types of signals have been compared by calculating the mean minimum distances of three phases for each type of unknown fault under three loading conditions. The best feature extraction technique has been selected by comparing the mean minimum distances, and the advantages of the cross-correlation technique have been discussed.

The classification of fault is intended to determine the kind of fault that occurred in the machine and to distinguish the causes of the observed abnormal conditions. Following the determination of the fault condition, the necessary actions will be taken immediately to troubleshoot the problem and reduce economic loss by avoiding an unscheduled machine shutdown. The conventional classification system consists of two steps: first, the features are extracted from the input signals, and the feature vectors are fed to the classifier [195]. In machine learning or pattern recognition applications, feature extraction from the input signal is critical for improving classification performance while reducing data computation time. Time-based and spectrum-based signal analysis from current and vibration signals are the conventional methods for different fault analysis in the motor [12].Time domain analysis [196], FFT-based frequency domain analysis [197], and DWT-based time-frequency analysis [198, 199] have been used for induction motor fault identification and extracting relevant features. Previous references show that current signature analysis in the time domain, time-frequency domain, and frequency domain has been applied individually to detect particular types of faults in induction machines, but these techniques have not been applied simultaneously to detect multiple faults in induction machines. The correlation based feature extraction method is superior to other conventional methods in fault classification systems due to its characteristics of eliminating irrelevant noise content in the signal [200, 201]. The cross-correlation technique assesses the degree of similarity between two input signals through the sequence between them, and the concept of a cross-correlation-based feature extraction technique is novel in the field of pattern recognition [202, 203]. Earlier features from cross-correlated signals have been applied as input to classifiers like SVM, K-NN, and ANN for biomedical applications [204–207]. Cross-correlation-based feature extraction techniques have been applied to the fuzzy means algorithm with wavelet networks and ANN based classifiers to classify the dynamic insulation faults in transformer windings [208, 209]. Cross correlation has been applied for condition monitoring of rotating machines [210], for gearbox fault monitoring [211], for stator fault monitoring [212], and for covering faults and decision-making stages of induction machines [210]. The correlation technique has also not been applied to detect multiple types of fault patterns in induction machines. Three unknown types of faults were classified and authenticated using features of signals from different domains, such as time domain signals, cross-correlated signals, FFT spectra, and time-

frequency domain (DWT) signals in multiple decomposition levels, using the nearest-neighborhood classification method. A comparative study has also been illustrated for the sensitivity analysis of these feature extraction techniques in the fault classification of induction motors. The nearest-neighborhood classification method was used here to classify unknown faults among multiple classes because it has several advantages over other classifiers, including being very simple to implement, being robust to classify if classes are not linearly separable, and being extremely cheap to update online as new instances of known classes are supplied [213].An experiment has been performed to collect current data samples three times from six induction motors with six faulty conditions, viz., broken rotor bars, rotor misalignment, faulted bearing, stator winding fault, rotor unbalance, single phase voltage unbalance, and one healthy motor in three loading conditions. It has been seen that the frequency spectra of motor fault current change under time varying speed conditions [214]. Fault classification has been performed using current signature analysis because both electrical and mechanical faults can be identified using motor current signature analysis [215, 216]. Data samples from three unknown type faulty motors are also collected three times in three different loading conditions. The cross-correlation technique was used to determine the degree of correlation between healthy motor current signals and faulty motor current signals. FFT and DWT are also applied to find the frequency spectrum of current signals and time-frequency information of current signals at different decomposition levels. The time-frequency analysis has been done by decomposing the current signals into an optimum Symlet-5 mother wavelet and comparing the values of the RMSE and correlation coefficient; it has been described in an earlier work. The Symlet5 mother wavelet has the lowest values of RMSE and highest values of correlation coefficient among the Daubechies wavelet family (db3-db10), the Coiflet wavelet family (Coif1-Coif5), and other Symlet wavelet families (Sym3-Sym8) for different electrical and mechanical faults of induction motors [162]. A PCA-based dimensionality reduction technique has been applied to current signals in the time domain, cross correlated signals, frequency spectra, and wavelet coefficients at different decomposition levels because PCA gives higher accuracy for fault classification among various dimensionality techniques [217].

The nearest neighbour (NN) rule is one of the most straightforward classification decision-making processes [218]. A sample is classified based on the classification of its closest neighbor. It can be demonstrated that this rule's probability of mistake, when applied to large samples, is less than twice the optimal error; as a result, it has a lower probability of error than any other decision rule [219]. Cross correlation and k-nearest neighbor were previously used for transmission line fault detection [220].

In the work described here, each unknown sample is classified phase wise following the minimum distance to the nearest neighborhood criterion, and the fault is also authenticated if the results for the three phases are the same. The procedure is applied for four types of feature extraction techniques

individually, not only to classify multiple unknown faults of induction motors in various domains but also to compare the sensitivities of the cross-correlation technique with those of the other three feature extraction techniques. The four techniques are able to authenticate the faults, but the magnitude of the nearest distances is not equal for every feature extraction technique. The sensitivity of fault classification for these feature extraction techniques depends on the magnitudes of the nearest distances; the higher the distance, the lower the chance of misclassification due to the large data boundary. The sensitivities of fault classification for these four feature extraction techniques have been compared, and the best feature extraction technique has been selected among the four depending on the magnitude of the nearest distance. The sensitivities of wavelet decomposition at different levels have also been verified.

7.2 Methods Applied

PCA has been used not only for feature extraction but also for the dimension reduction of input signals. The two principal components (PCs) are considered the exact fault features of each phase, and the PC plots of the three phases of each type of motor are considered one class. The mean of the three phase plots of each type of motor is calculated, and the Euclidean distances are calculated from one centroid to another. The details of all the techniques are explained below.

7.2.1 *Feature extraction from current signals*

Fault detection through time domain signal analysis is implemented to check for abnormal changes in machine features over time. Electrical related faults can be identified using model based fault detection techniques. This technique necessitates the creation of precise mathematical models, which suffer from uncertainties in real-world applications. Current signature analysis allows for fault classification utilising an unsupervised approach without the necessity for system modelling; all that is required is accurate training. The test data sample can be classified among many trained data samples. Unsupervised fault classification in the time domain has been performed here through PCA based feature extraction and dimensionality reduction techniques. The mathematical expression of PCA has been explained in Chapter 2, and it has been used to minimise the dimensions as well as extract features from signals. The PCA has been used to extract features and reduce the dimension of features in current signals from known-faulty motors, which are used for trained classes, while features from unknown-faulty motors are used for test classes. The two PCs are computed from each phase's current signals.

7.2.2 *Feature extraction from FFT spectra*

Additional frequency components emerge in the form of various spectra as a result of vibration or current signals generated by various machine faults. Fast Fourier Transform (FFT) is the simplest way to explore the spectral properties of signals. The theory of the fast fourier transform (FFT) has been

demonstrated in Chapter 2. The amplitude vs. frequency spectra of the current signals of known and unknown faulty motors have been computed using the FFT algorithm. PCA has been used to extract features by reducing the dimensions of the FFT spectra of current signals.

7.2.3 *Feature extraction from wavelet coefficients*

Analysis of non-stationary data can be done using cutting-edge time-frequency domain signal processing techniques. These methods are used to perform an accurate continuous spectral analysis of the dynamic properties of a machine. It offers a limited moving temporal window in which non-stationary signals are treated as constant. The most popular time-frequency analysis method is wavelet transform (WT), which has better time-frequency characteristics and is more flexible than other time frequency analysis methods. The discrete wavelet transform was covered in Chapter 2. The current signals of faulty motors and healthy motors are decomposed multiple times using the Symlet5 mother wavelet function. There will be approximate and detailed coefficients for each level of the decomposed signal, and features are extracted from the approximate coefficients of each decomposed signal by PCA transformation for classification of unknown faults in the time-frequency domain among the trained classes of known faults. Earlier researchers have extracted features from wavelet coefficients and applied PCA for fault classification and location tasks [221].

7.2.4 *Feature extraction from cross-correlated signals*

In Chapter 2, the theoretical explanation and mathematical derivation of cross correlation techniques are detailed. The cross-correlation approach compares two input signals in a way that gauges how similar they are to one another. Cross-correlated signals of each faulty motor have been developed by computing the sequence between the phase current signals of a healthy motor and those of each faulty motor for the purpose of eliminating irrelevant noise content from the phase current signals of each faulty motor. The extracted features from cross correlated signals have multiple dimensions, so it is essential to find exact fault features by reducing the dimensions. PCA has been used to extract features from cross correlated signals, reducing the multiple dimensions to two dimensions because two PCs contain the exact fault features of each faulty signal.

7.2.5 *Classification through nearest distance neighbourhood*

Classifiers based on nearest neighbours classify a test pattern by using some or all of the patterns in the training set. Finding the similarities between each pattern in the training set and the test pattern is essentially what these classifiers do. This is done in the following way:

The nearest neighbor algorithm assigns the class label of a test pattern's nearest neighbor. Let's say there are n training patterns: (X_1, θ_1), (X_2, θ_2), ..., (X_n, θ_n),where X_i is a classifier based on the nearest neighbour, and θ_i is the class label for the i-th pattern.

If *P* is considered as the test pattern, then if [*distance (P, X_k)*] = *min {distance (P, X_i)}* where *i = 1, 2,..., n;* then pattern *P* is assigned to the class θ_k associated with X_k.

Now, assuming a test pattern exists, it is necessary to calculate the separation between *P* and each training pattern. Let the distance between training pattern *X* (X_1, X_2) and *P* (P_1, P_2) be the Euclidean distance, given by:

$$distance\,(X,P) = \sqrt{(X_1 - P_1)^2 + (X_2 - P_2)^2} \tag{7.1}$$

The PC plots of three phases of one fault type are considered a single class, and the Euclidean distances are calculated from the mean of a particular class to the centroid of another class. The mean, considering all the three phases, is computed as shown in Fig. 7.1. The mean is computed by considering the mean of the coordinates of the three vertices of the triangle. Hence, the coordinate of the mean obtained from the results by analysing the three values of *R*-phase only is found as:

R1 = {PC1 (R1), PC2 (R1)};

R2 = {PC1 (R2), PC2 (R2)};

R3= {PC1 (R3), PC2 (R3)};

where, *R1*, *R2*and *R3* are the centroids obtained by analyzing the values of red phase respectively and *PC1(i)*is the coordinate of the principal component obtained from the analysis of the *i*-th number of R-phase; where, *i = R1, R2* and *R3*.

Hence, the mean (*M*) would have coordinates of:

$$M = \left[\frac{PC1(R1)+PC1(R2)+PC1(R3)}{3}, \frac{PC2(R1)+PC2(R2)+PC2(R3)}{3}\right] \tag{7.2}$$

Similarly, the means for three values of Y phase and B phase have been calculated. The test class is identified by computing the least Euclidean distance from mean of any specified class and the test class, as described graphically in Fig.7.1.

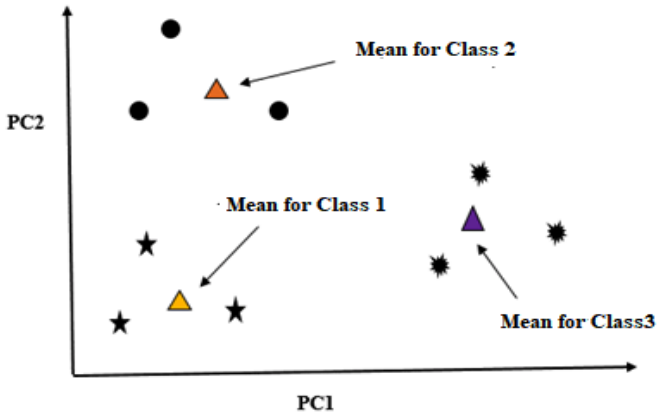

Figure 7.1: *Identification of fault class using the vector distance of the means of all specified classes from the mean of the test class*

7.3 Methodology of algorithm development

The present work is based on the cross correlation analysis of the fault signals, although several other tools have also been used here for extracting the major fault features, and the combined analysis has been used here to finally identify the most suitable technique in this regard. The cross-correlation method is applied directly over the time domain fault signals in order to obtain the degree of correlation between the current signals of healthy motors and those of faulty motors. In addition, the fault signals have been subjected to discrete wavelet transforms (DWT) and fast Fourier transforms (FFT). Following the use of each of these techniques, PCA is used to extract significant features in terms of the principle components (PCs) in descending order of variances. PCA is also applied directly over the fault signals to extract the features directly before applying cross correlation, FFT, or DWT filters. Because PCA considers only the most important directions of variation in the fault signals, it ensures a dimension reduction of the input signals. The two most important principal components (PC1 and PC2), which bear the most significant fault information, are considered fault features of each phase and PC plots of three phases are constructed individually, which is considered the fault signature of each of these fault classes. The mean of the three PC scatter plots of each fault class is calculated, and the Euclidean distances are calculated between the means of each class and that of the test fault. The entire method of analysis has been illustrated graphically in Fig. 7.2.

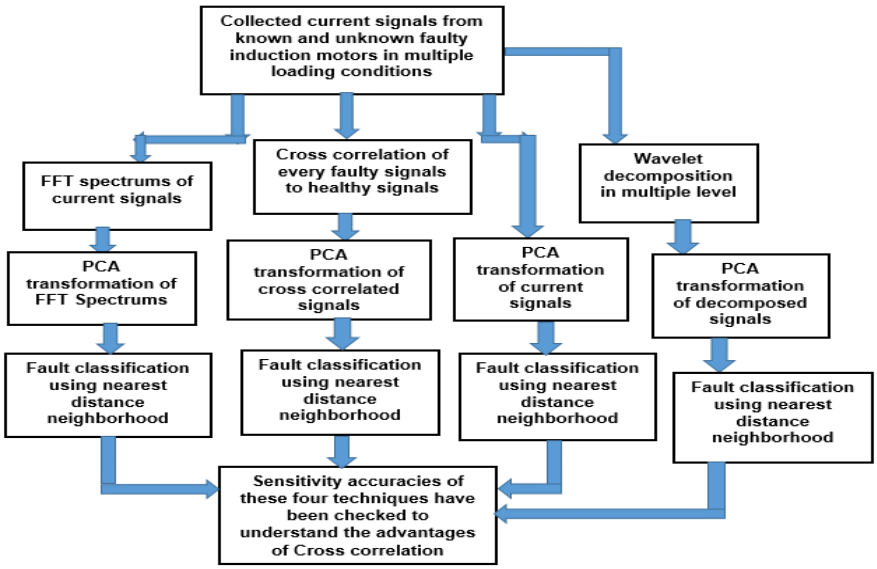

Figure 7.2: *Flow diagram of this present work*

FFT converts time-domain fault current signals into frequency spectrums, and wavelet analysis decomposes the fault waveforms into different decomposition levels to produce a time-frequency spectrum. PCA has been used over these cross correlated signals, current signals in time domain, FFT spectra, and approximate coefficients from decomposed signals to extract time domain, frequency domain, and time-frequency domain features of the different fault signatures, which have been effectively analysed. Wavelet analysis is also applied in the present method in the following way: The current signals of faulty motors and healthy motors are decomposed multiple times using the Symlet5 mother wavelet function, as this has been found optimal in similar research as cited in [162]. Features are extracted from the approximate coefficients of each decomposed signal. Finally, in each of the steps, the PCA-extracted features have been analysed using the nearest-neighbor neighbourhood model to identify the closest fit of the test signal to one of the fault prototypes. This is done in the following way.

Three times, under three different loading conditions, the three-phase current waveforms from six induction motors with known faults (broken rotor bar or BR fault, rotor misalignment or RM fault, faulty bearing or FB fault, faulty stator winding or SW fault; rotor unbalance or RU fault, and single-phase voltage unbalance or VU fault) and one motor with no known faults (HM) were collected. A cross-correlation technique has been performed between each class of faulty current signal and the healthy current signal. This is followed by reducing the dimensions of the cross-correlated signals into their two most significant dimensions using PCA. The first two principal components, PC1 and PC2, are assigned to the eigenvectors corresponding to the largest eigenvalues of each phase current of a motor, which are considered the most indispensable features of each known and unknown class of fault. The FFT spectra of each phase of each faulted motor have been computed thereafter. Time-frequency analysis of current signals has been performed using DWT at five decomposition levels.

Using the PCA transformation, features are extracted from current signals, FFT spectra, and approximate coefficients of decomposed signals at each level. Three PCs, corresponding to each of the red, blue, and yellow phases of each faulty motor, have been considered as one class, and each unknown fault has been classified using the nearest distance neighbourhood classification method, discussed in the next section.

7.4 Experimentation

The experiment has been done on the same set up as illustrated in Chapter 3. The three phase currents are collected from six separate induction motors in a motor fault simulator laboratory running under six different fault conditions, viz., faulty bearing (FB), broken rotor bar (BR), rotor unbalance (RU), rotor misalignment (RM), stator winding fault (SW), single phase voltage unbalance (VU), and one healthy motor (HM). The data were collected for all the faulty induction motors as well as for three induction motors with unknown faults. The experimentation has been carried out with three separate loading conditions for the motors in order to incorporate robustness into the design of the algorithm. The motors are initially run under no mechanical load; next, they are coupled to a DC generator, and this DC generator works as a mechanical load on the motor; and finally, the generator is loaded with an electrical load of 200 watts, which in turn works as an enhanced load on the motor. The suggested approach has been developed and validated for the motor's three different loading scenarios. The data samples from the three unknown faulty motors are also collected three times at a time interval of 5 to 6 minutes, under three different loading conditions.

7.5 Result and Discussion

Classifications are performed for three phases individually for authentication of each unknown fault. Three loading conditions are tested sequentially in this work. The means of three PCs of each known class, including one unknown class for all types of signals, have been displayed in Figs. 7.3 – 7.14 under one loading condition. Euclidean distances from the mean of an unknown class to the means of other known classes are computed phase-wise, initially under one loading condition. This technique is applied subsequently to classify three unknown types of faults (X1, X2, and X3*)* under three different loading conditions using four feature extraction techniques. The Euclidean distances so found are reported phase-wise in Tables 7.1, 7.2, and 7.3 for X1, X2, and X3, respectively. Faults are authenticated if the Euclidean distances so found are the least for all three phases.

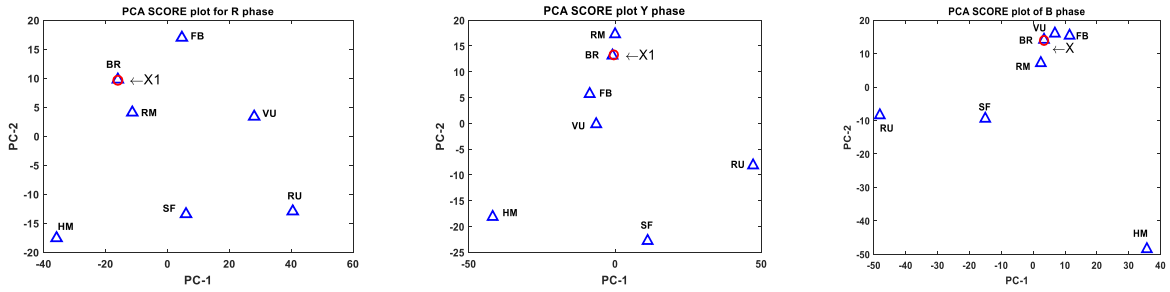

Figure 7.3: *Means of PCA score plots of current signals for known faults and one unknown class under loading 1 condition for (a) R phase, (b) Y phase, (c) B phase respectively; X1: unknown 1*

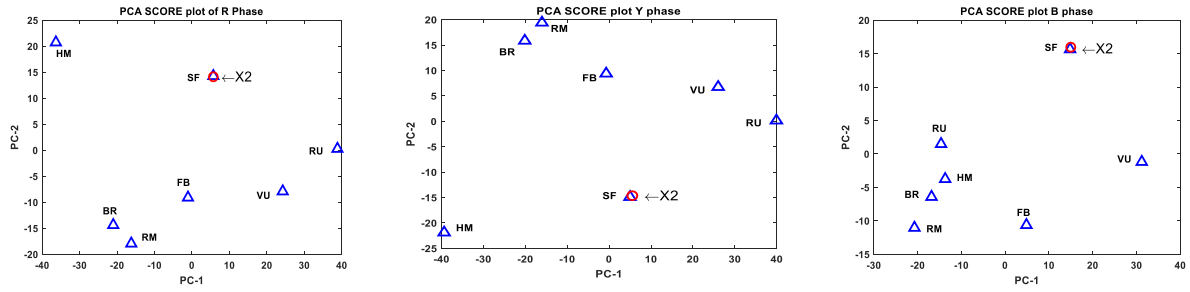

Figure 7.4: *Means of PCA score plots of current signals for known faults and one unknown class under loading 1 condition for (a) R phase, (b) Y phase, (c) B phase respectively; X2: unknown 2*

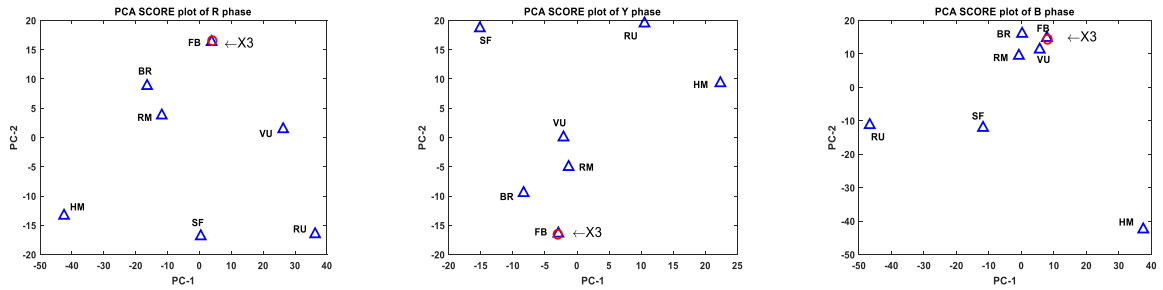

Figure 7.5: *Means of PCA score plots of current signals for known faults and one unknown class under loading 1 condition for (a) R phase, (b) Y phase, (c) B phase respectively; X3: unknown 3*

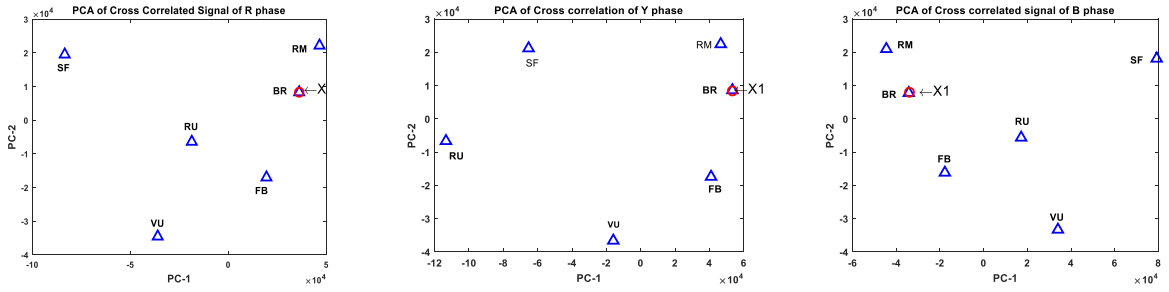

Figure 7.6: *Means of PCA score plots of cross correlated signals for known faults and one unknown class under loading 1 condition for (a) R phase, (b) Y phase, (c) B phase respectively; X1: unknown 1*

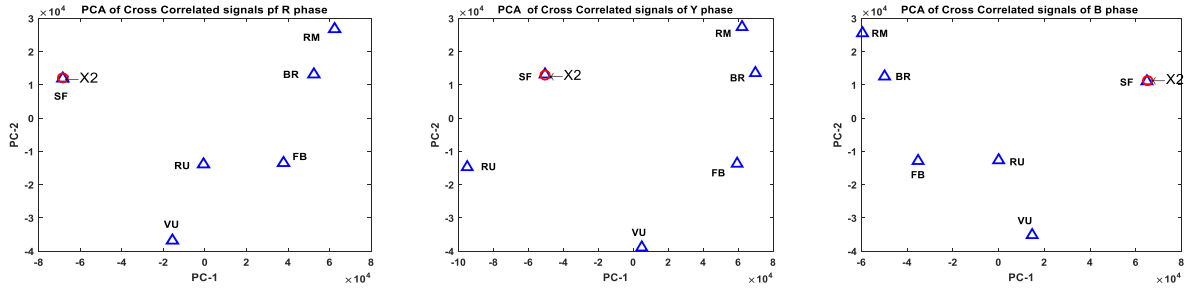

(a) (b) (c)

Figure 7.7: Means of PCA score plots of cross correlated signals for known faults and one unknown class under loading 1 condition for (a) R phase, (b) Y phase, (c) B phase respectively; X2: unknown 2

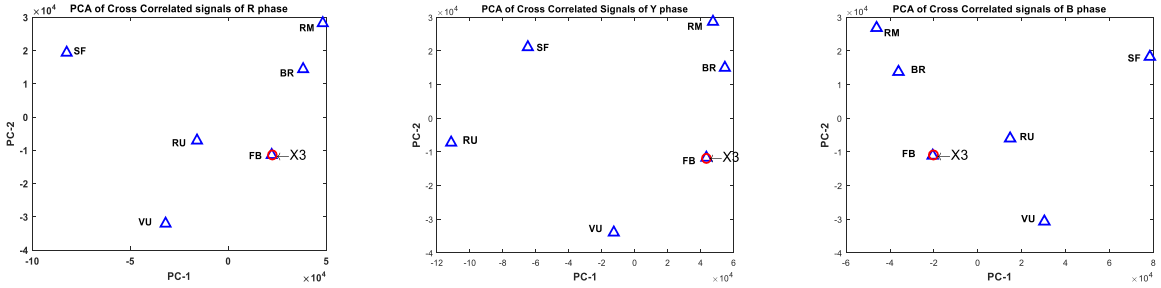

(a) (b) (c)

Figure 7.8: *Means of PCA score plots of cross correlated signals for known faults and one unknown class under loading 1 condition for (a) R phase, (b) Y phase, (c) B phase respectively; X3: unknown 3*

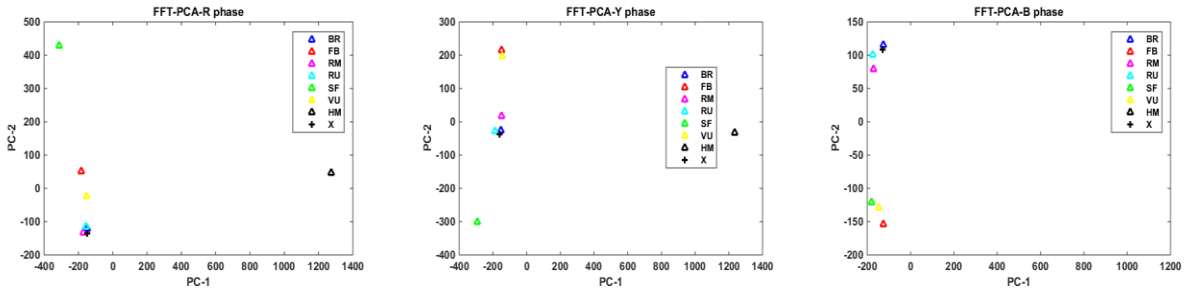

(a) (b) (c)

Figure 7.9: *Means of PCA score plots of FFT spectrums for known faults and one unknown class under loading 1 condition for (a) R phase, (b) Y phase, (c) B phase respectively; X1: Unknown fault type 1*

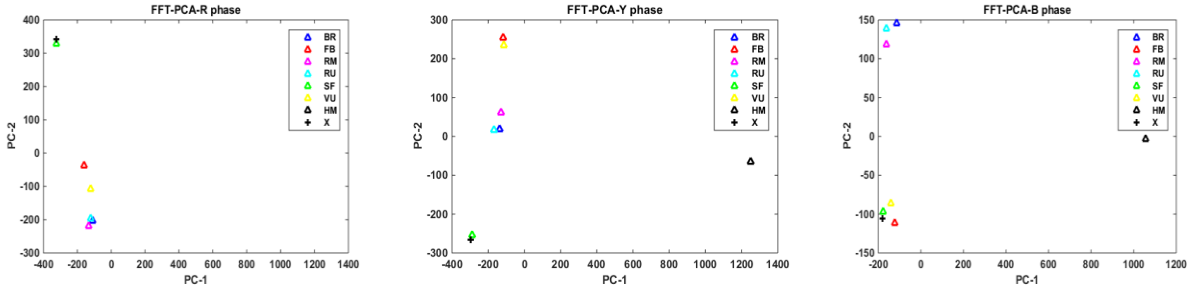

(a) (b) (c)

Figure 7.10: *Means of PCA score plots of FFT spectrums for known faults and one unknown class under loading 1 condition for (a) R phase, (b) Y phase, (c) B phase respectively; X2: Unknown fault type 2*

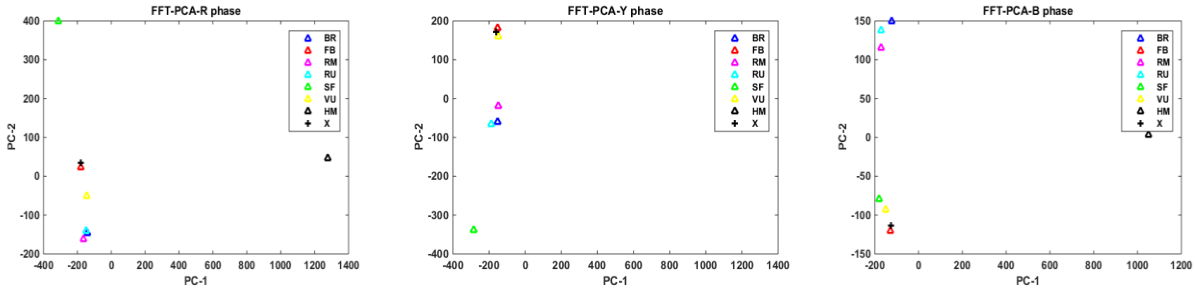

(a) (b) (c)

Figure 7.11: *Means of PCA score plots of FFT spectrums for known faults and one unknown class under loading 1 condition for (a) R phase, (b) Y phase, (c) B phase respectively; X3: Unknown fault type*

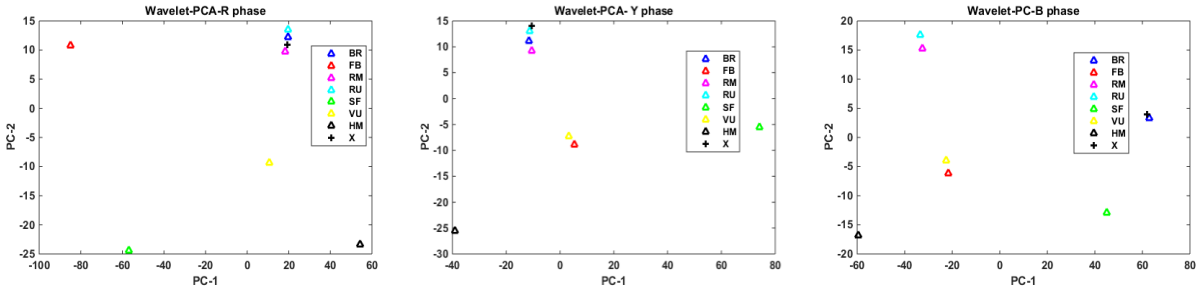

(a) (b) (c)

Figure 7.12: *Means of PCA score plots of wavelet approximate coefficients at first decomposition level for known faults and one unknown class under loading 1 condition for (a) R phase, (b) Y phase, (c) B phase respectively; X1: Unknown fault type 1*

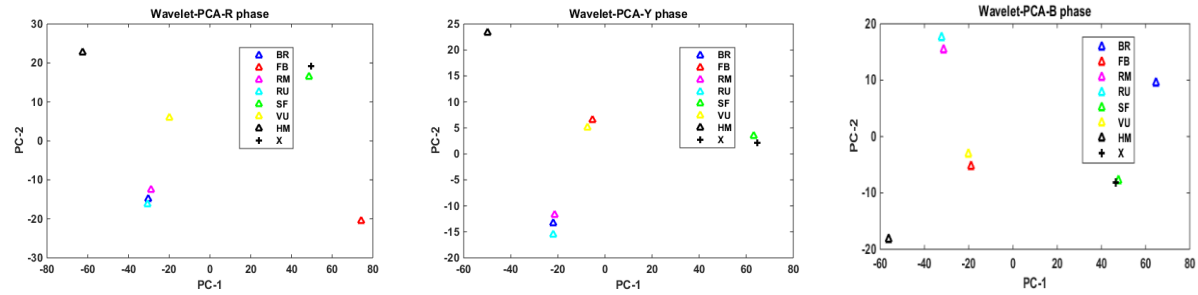

(a) (b) (c)

Figure 7.13: *Means of PCA score plots of wavelet approximate coefficients at first decomposition level for known faults and one unknown class under loading 1 condition for (a) R phase, (b) Y phase, (c) B phase respectively; X: Unknown fault type 2*

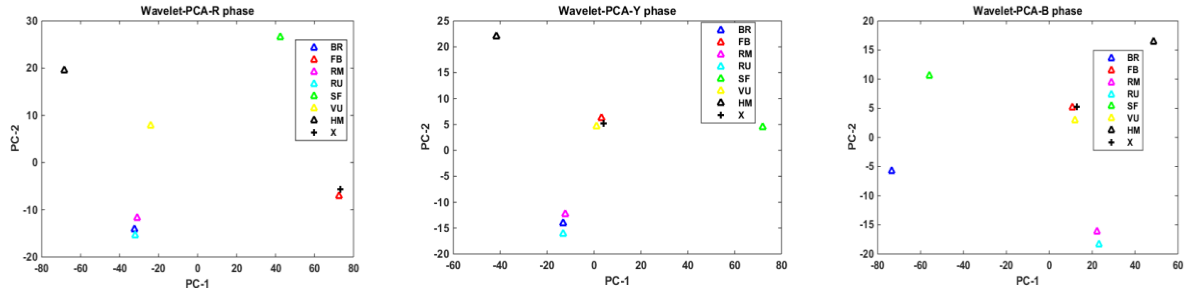

(a) (b) (c)

Figure 7.14: *Means of PCA score plots of wavelet approximate coefficients at first decomposition level for known faults and one unknown class under loading 1 condition for (a) R phase, (b) Y phase, (c) B phase respectively; X: Unknown fault type*

Table 7.1: The Euclidean distances from X1 (unknown fault pattern 1) to other known classes using different feature extraction methods under loading 1 condition

Phase	Method	BR	FB	RM	RU	SF	VU	HM
R Phase	PCA of Cross Correlation	206.939	30136.867	17538.558	56418.324	120774.835	83706.567	-----
	PCA of Current signal	0.112	21.793	8.654	60.527	38.997	5.146	63.253
	PCA of FFT	4.594	137.329	60.036	102.826	190.100	204.587	1429.081
	PCA of W1	1.219	104.555	1.647	2.526	84.279	22.207	48.924
	PCA of W2	1.107	106.502	1.825	2.448	85.295	22.340	49.382
	PCA of W3	1.261	109.859	1.648	2.581	86.796	22.188	50.479
	PCA of W4	1.356	116.646	1.684	2.682	90.146	22.212	52.467
	PCA of W5	1.326	129.309	2.027	2.685	96.656	22.490	56.230
Y Phase	PCA of Cross Correlation	260.460	29207.782	15162.699	167542.530	120077.165	82940.442	-----
	PCA of Current signal	0.517	8.830	6.158	60.970	39.887	6.630	29.950
	PCA of FFT	6.357	33.811	23.824	146.969	112.229	134.691	1399.219
	PCA of W1	0.666	27.354	3.993	2.301	86.859	24.888	48.186
	PCA of W2	1.111	28.418	4.837	3.039	88.624	25.892	48.677
	PCA of W3	1.360	29.047	4.847	3.160	91.252	26.379	48.962
	PCA of W4	1.653	30.536	5.011	3.356	96.737	27.624	49.275
	PCA of W5	2.080	33.494	5.391	3.724	107.158	30.109	49.825
B Phase	PCA of Cross Correlation	201.526	29279.558	16645.178	53146.507	114855.976	79891.231	----
	PCA of Current signal	0.287	8.071	3.506	21.868	38.824	46.404	47.685
	PCA of W1	5.531	206.988	113.886	55.996	109.444	204.151	1239.975
	PCA of W2	1.194	83.984	95.214	96.223	23.832	84.826	123.016
	PCA of W3	1.664	83.571	94.731	95.735	23.958	84.422	122.663
	PCA of W4	1.709	83.568	94.653	95.660	24.497	84.416	122.805
	PCA of W5	1.897	83.882	94.662	95.656	26.157	84.699	123.417
	PCA of W1	1.884	84.386	94.801	95.795	28.753	85.169	124.447

Table 7.2: The Euclidean distances from X2 (unknown fault pattern 2) to other known classes using different feature extraction methods under loading 1 condition

Phase	Method	BR	FB	RM	RU	SF	VU	HM
R Phase	PCA of Cross Correlation	120430.340	109353.830	130156.481	70098.927	185.964	72132.479	---
	PCA of Current signal	32.008	33.618	40.397	36.871	0.159	27.542	78.960
	PCA of FFT	197.919	94.925	157.598	132.449	14.548	67.468	1517.324
	PCA of W1	86.416	46.338	84.138	86.992	2.195	70.298	111.945
	PCA of W2	87.215	46.866	84.899	87.772	2.145	71.122	113.568
	PCA of W3	89.478	48.434	87.080	89.999	3.011	73.255	117.134
	PCA of W4	92.606	51.451	90.081	93.074	3.581	76.200	122.972
	PCA of W5	98.188	56.433	95.440	98.554	4.079	81.585	133.864
Y Phase	PCA of Cross Correlation	119460.708	112964.341	111589.107	54882.577	236.908	75937.489	---
	PCA of Current signal	37.976	37.176	42.305	39.478	0.522	26.661	36.852
	PCA of FFT	120.220	151.486	104.023	226.012	6.923	236.243	1465.008
	PCA of W1	87.935	69.892	86.791	88.237	1.568	71.926	116.177
	PCA of W2	89.901	71.361	88.715	90.195	2.192	73.497	118.056
	PCA of W3	92.593	72.974	91.292	92.876	2.295	75.265	120.527
	PCA of W4	98.568	76.753	97.049	98.848	2.248	79.329	125.866
	PCA of W5	108.771	83.234	106.879	109.031	2.615	86.301	135.516
B Phase	PCA of Cross Correlation	113749.153	102740.929	123522.971	66371.827	216.610	68336.480	-----
	PCA of Current signal	29.819	33.182	38.215	27.796	0.347	33.354	69.377
	PCA of FFT	104.553	127.909	38.212	104.993	4.486	117.140	1296.463
	PCA of W1	25.076	65.838	81.670	83.128	1.121	67.172	103.460
	PCA of W2	25.673	65.392	81.342	82.808	1.531	66.751	103.013
	PCA of W3	26.384	65.241	81.423	82.910	1.698	66.611	102.866
	PCA of W4	26.471	65.602	81.925	83.424	1.525	66.957	103.400
	PCA of W5	29.286	65.462	82.865	84.448	1.586	66.864	103.115

Table 7.3: The Euclidean distances from X3(unknown fault pattern 3) to other known classes using different feature extraction methods under loading 1 condition

Phase	Method	BR	FB	RM	RU	SF	VU	HM
R Phase	PCA of Cross Correlation	30478.712	207.599	47807.025	39191.432	109137.588	57812.401	--
	PCA of Current signal	22.039	0.238	16.545	39.464	24.212	12.844	64.888
	PCA of FFT	146.548	14.529	93.723	54.083	79.274	56.522	1433.617
	PCA of W1	105.621	1.365	104.192	105.634	44.689	98.231	143.850
	PCA of W2	107.241	1.085	105.771	107.240	45.305	99.818	146.183
	PCA of W3	110.759	1.653	109.180	110.728	45.954	103.001	150.833
	PCA of W4	117.423	1.760	115.669	117.334	48.065	109.285	159.985
	PCA of W5	128.981	1.833	126.932	128.797	51.733	120.212	176.217
Y Phase	PCA of Cross Correlation	28539.752	247.096	39555.929	154627.200	113059.767	60292.828	------
	PCA of Current signal	11.273	0.079	19.766	39.970	24.879	13.850	50.363
	PCA of FFT	28.140	6.364	49.604	132.899	140.087	110.071	1388.069
	PCA of W1	25.861	1.222	24.022	27.391	68.029	2.919	48.644
	PCA of W2	26.322	2.132	24.447	27.768	68.266	3.635	49.901
	PCA of W3	27.611	2.021	25.638	29.018	70.000	3.951	50.731
	PCA of W4	28.687	2.066	26.524	30.023	74.204	3.661	51.968
	PCA of W5	32.560	2.045	30.064	33.786	80.681	4.570	55.313
B Phase	PCA of Cross Correlation	29187.488	198.692	45842.409	36554.290	103191.203	54646.073	------
	PCA of Current signal	8.139	0.378	12.355	32.005	28.459	24.695	41.080
	PCA of FFT	193.654	9.958	93.052	218.292	122.263	20.872	1241.166
	PCA of W1	86.215	1.256	23.835	26.163	68.161	2.367	38.103
	PCA of W2	86.799	1.823	23.948	26.282	68.678	2.601	37.603
	PCA of W3	87.013	1.973	23.863	26.210	68.911	2.198	37.747
	PCA of W4	87.147	1.974	24.497	26.866	68.958	1.962	38.182
	PCA of W5	87.508	1.964	26.205	28.615	69.069	2.071	38.758

**Note: Loading condition 1: The motor is initially operated in a no-load condition, meaning that it has no mechanical load attached to its shaft.*

Loading condition 2: Next, the generator runs freely at no-load since it is coupled to the motor simply as a DC generator and not as an electrical load. As a result, only the generator's mechanical load—also known as the generator load—is applied to the motor shaft.

Loading condition 3: Finally, the generator is subjected to a 200 W electrical load. Consequently, the generator's mechanical load and an additional 200 W of electrical load are applied to the motor, while the rated load of the generator is 750 W.

The wavelet decompositions at levels 1, 2, 3, 4, and 5 are denoted by W1, W2, W3, W4, and W5, respectively.

The classification results under one loading condition are the same for four feature extraction techniques as per the data in tables 7.1, 7.2, and 7.3. From the distance tables, it has been seen that X1, X2, and X3 resemble broken rotor bar fault, stator winding fault, and bearing fault, respectively, because the minimum distance is found from one unknown fault pattern to a particular known class among other known classes, and other unknown fault patterns are authenticated following the same process. The classification results are the same for all phases of all types of feature extraction techniques under the other two loading conditions as well.

The mean value of minimum distances for three phases of each unknown type fault has been calculated using the expression as follows:

$$Mean\ of\ mimimum\ distances = \frac{Mininum\ distance(Rphase) + Minimum\ distance(Yphase) + Minimum\ distance(Bphase)}{3}$$

The sensitivities of different feature extraction techniques for fault classification depend on the magnitude of minimum Euclidean distances, if the distance increases, then there is less chance of misclassification. Wavelet signals have been decomposed up to 5 levels and features extracted from the approximate coefficients of the decomposed signals, and each fault has been classified phase wise for each decomposed level. We have further analysed the results obtained from the above experiments and represented the results in graphical form, as shown subsequently. Figs. 7.15, 7.16, and 7.17 represent the PCA score distances between one particular set of test data and the different classes of faults using direct fault current waveforms, cross-correlated signals, and features extracted from FFT spectrums, respectively.

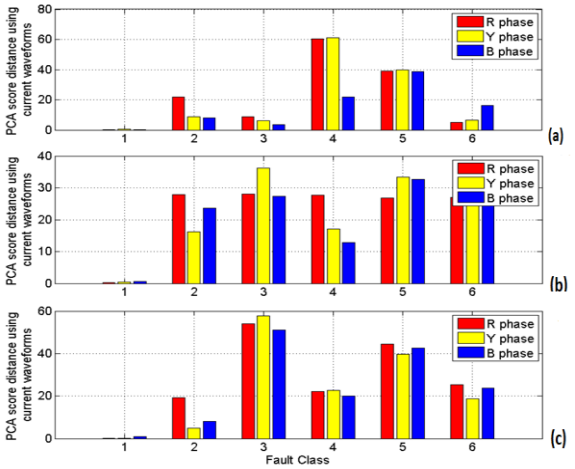

Figure 7.15:*Three phase PCA score distances of unknown fault pattern 1 using fault current signals under three different loading conditions (a) Loading 1, (b) Loading 2 and (c) Loading 3*

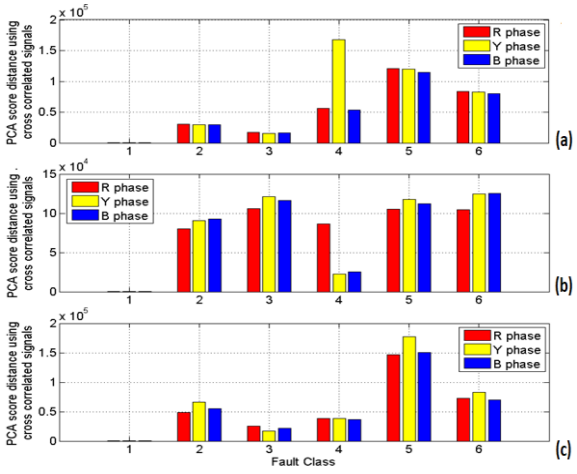

Figure 7.16: *Three phase PCA score distances of unknown fault pattern 1 using features of cross correlation under three different loading conditions (a) Loading 1, (b) Loading 2 and (c) Loading 3*

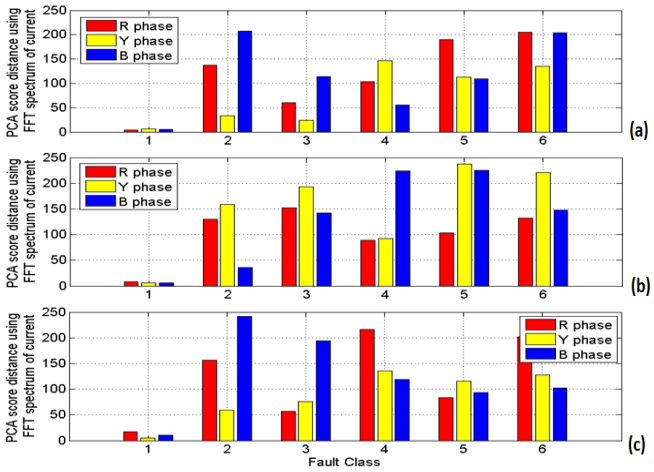

Figure 7.17: *Three phase PCA score distances of unknown fault pattern 1 using features of FFT spectrums under three different loading conditions (a) Loading 1, (b) Loading 2 and (c) Loading 3*

The individual set of columns of each of these sub-figures represents one class of fault, and the distances are also shown for the red, yellow, and blue phases individually. It can be seen from this that the fault test case is the closest to a class 1 fault, which is a BR or broken rotor fault. This particular observation is evident from all three figures, which represent three different loading patterns. It is also observed that this particular inference could be drawn from the features extracted either by analysing the current waveforms directly (Fig. 7.15), the cross-correlated signals (Fig. 7.16), or the FFT spectrum based approach (Fig. 7.17). A closer observation of these three figures reveals that cross correlation produces the maximum difference between the PC distances between the true class and all other classes. This is observable from Fig. 7.16, where we find that the column heights for R, Y, and

B phases corresponding to class 1 (BR fault) are minimum for cross correlation feature analysis (Fig. 7.16), compared to the same column heights for direct current signal analysis (Fig. 7.15) or FFT spectrum analysis (Fig. 7.17). This indicates that the test class resembles the true class the closest, which is BR fault or class 1, compared to all other fault classes using cross correlation features. As a result of the current experiment, it is concluded that the cross-correlation features followed by PC score nearest distance analysis produce the best results for classifying induction motor faults, even when loading patterns vary, yielding the highest sensitivity among all the discussed feature extraction methods.

We further expanded our analysis to the time-frequency domain, where we applied wavelet transformation to extract the fault features from the fault current waveforms, followed by a nearest neighbourhood analysis using the PC scores. These are shown in Fig. 7.18.

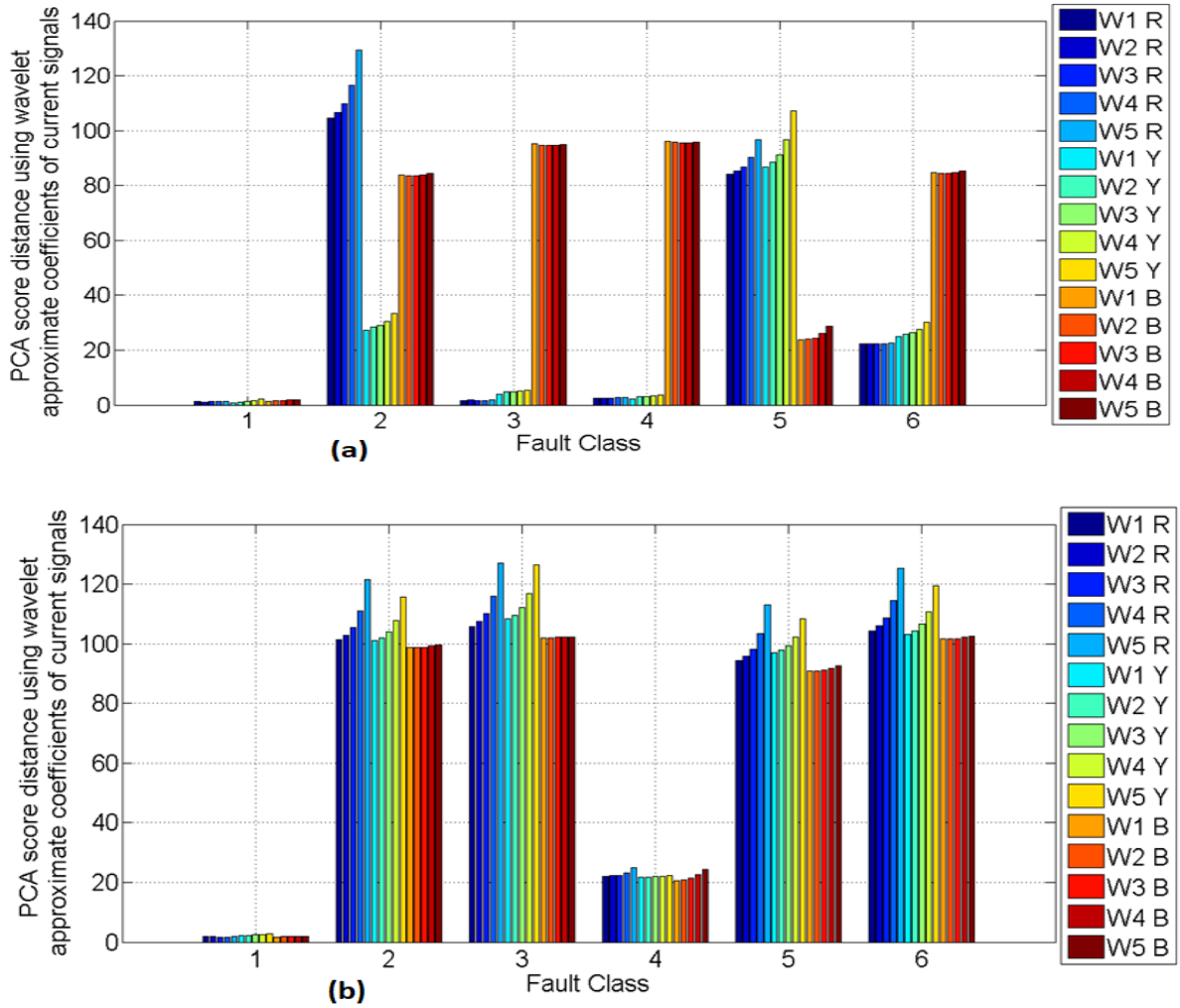

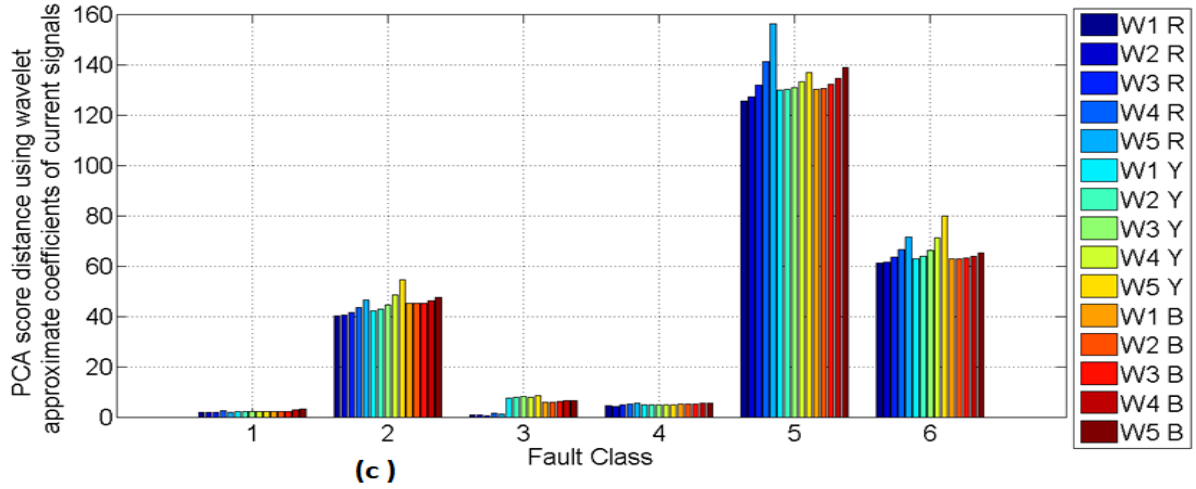

Figure 7.18: *Three phase PCA score distances of unknown fault pattern 1 using features of wavelet approximate coefficients using five levels of decomposition under three different loading conditions, (a) Loading 1, (b) Loading 2 and (c) Loading 3*

We have used five level of decomposition using the wavelength transformation and observed the PC distances between the test fault and each other class of fault. These PC distances are plotted in three sub-figures of Fig. 7.18 for three different loading conditions. It is observed from these Figures that the test class produces least PC distance for the 1st training class, which is BR or Broken rotor fault, compared to the other similar classes; thereby confirming the test fault to be BR. But, more importantly, the difference in column height between the true class and other classes are not as prominent as compared to the previous features incorporating direct current waveform analysis, which is a time domain analysis, cross correlation which is again a time domain analysis or FFT spectrum analysis which is a frequency domain analysis. This is more prominently observed for load 1 and load 3 wavelet features where we find that the test class is also closer to fault class 3 and fault class 4, apart from being closest to the true class which is class 1(BR or broken rotor fault). Thus, the inference of the predicted class is not found as convincing as it was using features of direct current signal, cross correlation or FFT spectrum. Hence, wavelet feature extraction method is least preferred compared to the other methods used in this work.

This observation is found true for all levels of decomposition as well as for all three phases. Further analysis of the graphical representation reveal that there is not much of difference in PC nearest neighborhood distance as the level of decomposition is increased; i.e., sensitivities of wavelet based features are not changing appreciably with the increase in decomposition levels. Thus, it is further concluded that the level of decomposition doesn't possess a major role in extracting fault features in the case of classifying induction motor faults.

Chapter 8

Conclusion

8.1 Conclusion

Three unknown type faults have been authenticated by PCA transformation of stator current data for all phases and FFT spectra of stator currents for all phases. Major feature parameters could be extracted, reducing dimensions, by using the principal component analysis method to improve the accuracy of fault classification. The three unknown faults resemble broken rotor bars, stator winding faults, faulted bearings because the minimum relative distances of unknown fault conditions occur with respect to fault type as broken rotor bars, stator winding faults, and faulted bearings, respectively, in three phases for all loading conditions. According to the results tabulated in Chapter 3, the relative distance metrics between the PCA score of an unknown type and the other known types are much less than those between the PCA score of the stator current spectrum and the other known types. The minimum relative distances of unknown fault conditions occur in all cases with respect to known-type faults, and this technique has detected unknown faults. The sensitivity of fault analysis in both domains (time domain and frequency domain) can be identified from the magnitudes of relative distances. From the tables of relative distances, it has been seen that the relative distances of the PCA spectrum are greater than the relative distances of the raw data PCA value of stator currents.

Table 8.1: Comparison of nearest neighborhood classification with some previous work

Literature	**Features**	**Classifier**	**Fault Classification**
[85]	Extracting the features from current signals in time domain	K-NN	Broken rotor bar
[86]	Current Waveforms	K-NN has been used for decision criteria	Bearing fault, stator fault, and rotor fault
[87]	Spectral analysis of symmetrical current components	K-NN	Stator winding fault
This work	Feature extracted from current signals in time domain and FFT Spectrums using PCA.	Nearest Neighborhood	(a) Broken rotor bar fault, stator winding fault and bearing fault have been classified using the features in both domain. (b) PCA transformation of spectrum is much efficient and sensitive than that by PCA transformation of simple original data.

Thus, it may be concluded that feature extraction by PCA transformation of spectra is much more efficient and sensitive than that by PCA transformation of simple original data. The comparison of nearest neighbourhood based classification with previous works is given below.

Discriminant analysis and multi-class support vector machines have been used in this work to improve classification problems with higher accuracy. In the present work, we also developed a scheme for the performance study of different SVM kernels for fault classification of induction motors. Earlier fault classifications have been performed using one type of kernel and in one domain, but classifications have not been performed in different domains or using different kernels. The aim of this work is to develop a robust classifier that can classify the machine fault pattern among the trained and known classes and authenticate any type of fault if the known classes are more than seven. We have also selected the best SVM kernel for induction motor fault classification in both domains by comparing the classification accuracy of both domains under three different loading conditions. Six different types of faults, including healthy conditions, have been considered for developing a scheme for classifying faults. The fault current signals were analysed using the principal component analysis (PCA) method in both time and frequency domains (using Fast Fourier Transform, i.e., FFT) to extract the two major most directions of variation of the fault signals, in terms of principal components 1 and 2, respectively. The classification results are examined after these features are further analysed using five different SVM kernels, including the linear kernel. This multiclass classification problem was reformulated as a combined binary classification problem using the decision directed acrylic graph (DDAG) algorithm to classify faults. The loading on the motor is also varied in three steps in order to incorporate robustness into the classifier. The classification performances of five different kernels were compared in both the time and frequency domains, and it was discovered that the RBF kernel produces the highest classification accuracies in both domains, taking into account all loading conditions; thus, it is considered optimal in the proposed work. It is further observed that the mean accuracy of classification is higher (in the range of 90%) with frequency domain features, compared to the accuracy obtained with frequency domain features (in the range of 73%), considering all five SVM kernels and three different loadings. Hence, classification using features extracted from the FFT spectrum is found to be better than feature extraction from time domain signals directly. Besides, linear separation is difficult using time domain features due to the scattering of PC values of time domain signals, but it is possible in the space of frequency domain features. Considering the high accuracy of classification achieved using an SVM kernel on the fault current frequency spectrums in the proposed work, the method is well implementable for real life applications.

Table 8.2 : Comparison of SVM based classification with some previous work

Literature	Features	Classifier	Fault classification	Accuracy
[112]	The start-up transient current and DWT with nonlinear feature reduction using kernel ICA and kernel PCA.	SVM OVA	Bowed rotor, broken rotor bars, faulty bearing, eccentricity, phase unbalance.	80.95% using ICA, 78.75% using PCA, 83.33% using kernel ICA, 76.19% using kernel PCA
[113]	Extracted features from Vibration signals using PCA with 6 dimensions.	SVM OVO(polynomial and RBF)	Rolling bearing	97.21%
This work	Extracted features from current signals and FFT spectrums of the current signals using PCA with 2 dimensions.	SVM OVO(Linear, RBF, Polynomial, Quadratic , Sigmoid kernel)	Bearing, Stator winding, Broken Rotor bar	(a) 35.19%(Linear),88.26%,(RBF) 83.34%(polynomial),72.23%(quadratic),85.12%(Sigmoid) (extracting features from signals in time domain) (b) 78.40% (Linear), 99.38%, (RBF) 93.82% (polynomial), 86.42% (quadratic), 95.06% (Sigmoid) (extracting features from signals in frequency domain)

In order to classify faults in three-phase induction motors, an effort has been made to determine the optimal mother wavelet and optimal degree of wavelet decomposition. The work's primary objective is to choose the best mother wavelet from a set of twenty options, including db2 to db10, Symlet3 to Symlet8, and Coif1 to Coif5. The second challenge is finding the optimal level of waveform decomposition for the fault current for categorization of the motor failure is the second challenge. The load has been changed, and the motor has been tested under all three loading conditions: with no load, with the generator acting as the only mechanical load, and with an extra 200 W load on the generator acting as indirect loading on the motor. In previous work, the minimum description length (MDL) criterion [135–138], the correlation coefficient criterion [139, 140], and the energy to Shanon entropy criteria [141–142], were only one type of criteria applied to choose the optimal mother wavelet for compression of a power disturbance signal, de-noising a partial discharge (PD) signal, and bearing fault detection using a vibration signal, respectively. The signal-to-noise ratio (SNR), root mean peak signal to noise ratio (PSNR), square error (RMSE), and correlation coefficient (CC) are four accuracy parameters that we took into consideration in order to find the best solution for reading the optimal mother wavelet and the optimal level of wavelet decomposition. To get the three phase fault current signals, we took into account six possible induction motor faults, including broken rotor bars (BR),

misaligned rotors (RM), faulted bearings (FB), stator winding faults (SF), rotor unbalance (RU), single phase voltage unbalance (VU), and one healthy motor. According to the proposed study, level 4 is found to be optimal, and Symlet5 is the optimal mother wavelet to use, which strikes a balance between computational complexity and getting the efficient wavelet level. In the multi resolution analysis method, the features of the current signatures of a faulty motor are captured over all the phases after decomposing into different wavelet levels. Here, 7 levels are considered during decomposition. DWT is a frequency-based transform that is performed on wavelets. It divides the signal at each level into two sub-bands: the low frequency band and the high frequency band. Also, each sub-band can be decomposed into two sub-bands. In multi resolution analysis, the statistical features of the current signature of a faulty motor at each level of wavelet decomposition are computed, which are skewness, kurtosis, RMS value, mode, and median of approximate and detail wavelet coefficients. The primary objective is to detect the characteristic features of faults of different types in low- and high frequency bands without losing significant information. In multiresolution analysis, the MRA matrix includes the various aforesaid feature parameters based on approximate and detailed wavelet coefficients at different decomposed levels. The dimensions of each data object (item) are the qualities (features) in the data, and they can be thought of as an n-dimensional vector. Thus, utilising common vector-based similarity measures like the Manhattan distance and Euclidean distance, the vector representations enable the computation of the distance between pairs. A norm is a means to gauge a vector's, a matrix's, or a tensor's size. The L2 norm, also known as the Euclidean norm, is the most commonly used norm and is provided by $||x||_2 = \sqrt{\sum_{i=1}^{n} |x_i|^2}$. The shortest distance from the origin is measured by the L^2 norm. If there is less space between two objects, they are said to be similar, and the opposite is true. The norm of the MRA matrix of the data set related to an unknown fault is compared with that of known faults (i.e., BR, FB, RM, RU, SF, VU, and HM) for authentication. If the difference between the norm and the known fault is the least, then the match is found, and it is inferred that the unknown fault is similar to the known fault.

A robust classification model using PNN has been developed for the detection of multiple faults in induction motors, applying features in the time domain, time-frequency domain, and frequency domain. Training of the model has been carried out with faults and the number of fault current signatures recorded at no load condition only, but testing of the model is carried out with current signatures of unknown faults at three loading conditions. The optimal decomposition level to get the highest classification accuracy has also been found in this work, including the optimal value of the spread of PNN. The trained classes were seven in this work, but any unknown type of fault can be identified if the number of trained classes is more than seven. In this work, a fault classification method has been proposed using a probabilistic neural network (PNN)-based model. The model uses principal component score features obtained from three different analysis methods, such as direct

analysis of time-domain fault current signals, frequency-domain analysis using a Fast Fourier Transform (FFT)-based approach; and finally a time-frequency domain method incorporating wavelet transform. Classification has been achieved by analysing each phase independently as well as for three different loading conditions. The spread parameter has been varied experimentally in the initial phase of the work, and the optimal value has been found to be 0.6. Finally, we have compared the classification accuracy obtained from the features of the three modes of feature extraction. The classifier accuracies are also compared for different levels of wavelet decomposition. It is observed from the results that the time-frequency domain analysis incorporating the 3rd level of decomposition of three phase current signals using wavelet analysis is able to produce the highest classification accuracy of 99.6%, which is higher compared to independent time or independent frequency domain analysis. The wavelet decomposition of the input signal reduces the noise to get exact time-frequency information of the particular type of fault, but if the decomposition level increases after a certain level of decomposition, there is a chance of information loss from the current or vibration signal. That's why the classification accuracy of all types of unknown faults is increasing from the 1st level to the 3rd level, but after the 3rd level of decomposition, the classification accuracy is decreasing under all loading conditions, as shown in the figures mentioned above. High accuracy of classification, simplicity in analysis, insensitivity to variability of loading, and ease of implementation all prove the ability of the proposed model as a robust classifier for induction motor faults.

Table 8.3: Comparison of PNN based classification with some previous work

Literature	**Features**	**Classifier**	**Fault classification**	**Accuracy**
[187]	Four dimensional features extracted from vibration signals using PCA.	PNN	Bearing fault	91.25%
[188]	Wavelet energy spectrum of vibration signal process by PCA with three dimensions.	PNN	Bearing fault	97.5%
This work	Two dimensions features are extracted using PCA from time domain signals, FFT spectrums and approximate coefficients of wavelet.	PNN	Broken rotor bar fault, bearing fault and stator winding fault.	Overall accuracy is 99.6% of three faults using the features of third level wavelet decomposition under three loading conditions.

The proposed model also has the potential for application with other three-phase machines. Both wavelet and PNN are well used methods in this field of research. Besides, the fault detection accuracy achieved using the optimum combinations of wavelet and PNN, as described before, is able to produce a classification accuracy of 99.6%, which is very high. Besides, the experiments are carried

out in real-time hardware setups rather than simulation models, which nullifies the presence of errors that may creep in during software simulation of machine faults. Thus, the proposed classifier could be implemented in the future to develop a real-time fault classifier model for induction motors.

A fault protection scheme for three-phase induction motors has been developed. The algorithm is tested under different loading conditions on the motor. Feature extraction has been carried out using time domain, frequency domain, and time-frequency domain analysis at multiple levels, using direct analysis of a time domain signal, the Fast Fourier Transform (FFT), and wavelet transform, respectively, and cross-correlated signals. Cross correlation has also been used for rotating machine condition monitoring for gearbox fault monitoring [210], stator fault monitoring [211], and covering fault and decision-making stages of induction machines [212], but not for detecting multiple types of fault patterns in induction machines. Principal component analysis (PCA) has been applied over the extracted features to identify the key directions of variation of the features for respective faults, followed by a nearest neighbourhood analysis of the PCA distances between the test fault and each fault class to classify the fault. Apart from that, the sensitivities of current signals in different domains have also been considered in the proposed work. The central tendency of the fault dataset has been computed by computing the mean of the given dataset of multiple features for each phase of the faulty motors. It is observed that the mean value of features from cross-correlated signals provides the highest Euclidean distances for all cases compared to feature extraction methods from signals in the time domain, frequency domain, and time-frequency domain; hence, cross-correlation of signals yields the highest sensitivity. It is also found that the sensitivities of wavelet-based features have minimal variation with an increase in decomposition levels.

8.2 Future Scope

The different fault patterns have been identified through an unsupervised classification process that extracts features from current signals from different faulty induction motors. The characteristics of motor voltages and currents can be used to train and test classifiers in the future. Future research can also be done to create a more reliable fault classification system using raw data that contains the vibration spectrum in addition to the stator current spectrum for all phases. Electrical and mechanical faults can both be identified using current signature analysis, but mechanical faults can be identified more accurately using the vibration analysis technique alone. Further fault classifications must be carried out by extracting the features from vibration signals and current signals independently, and comparing the classification results of all the classifiers employed in this work. Additionally, it is proposed that modelling of defective induction motor parameters may result in a different supervised method of fault authentication.

SVM has been used to detect faults, and its RBF kernel is providing greater classification accuracy for fault classification using the features of current signals in the time domain and the frequency domain both. A similar procedure can be used to classify faults using PNN. It will be difficult to distinguish between the two types of faults when electrical and mechanical faults occur simultaneously in a machine. For this reason, classifications must be made utilising features from both current signals and vibration signals separately. Convolutional neural networks (CNN) are another method that can be applied as a classifier. Another alternative for identifying issues with different power system components, such as synchronous generators and transformers, is to use an SVM, PNN, or CNN-based algorithm.

It is necessary to choose the optimal mother wavelet and optimal level of decomposition for the vibration signals coming from various malfunctioning induction motors. The classifiers for fault classification can be trained using the characteristics of the coefficients of decomposed vibration signals. Using different feature characteristics of decomposed vibration signals, the MRA approach can also be used to classify faults.

References

[1] G.K Singh, S. A. S. Al Kazzaz, "Induction machine drive condition monitoring and diagnostic research—a survey", *Electrical Power Systems Research*, 2003, 64 (2), pp :145-158.

[2] P.J. Tavner, "Review of condition monitoring of rotating electrical machines", *IET Electric Power Applications*, 2008, 2(4), pp : 215-147.

[3] M. E. H. Benbouzid, M.Vieira, C. Theys, "Induction motors' fault detection and localization using stator current advanced signal processing techniques", *IEEE Transactions on Power Electronics*,1999, 14(1), pp : 14-22.

[4] M. E. H. Benbouzid, "A review of induction motors signature analysis as a medium for faults detection", *IEEE Transactions on Industrial Electronics*, 2000, 47(5), pp: 983-993.

[5] M. Blodt, M. Chabert, J. Regnier, J. Faucher, "Mechanical load fault detection in induction motors by stator current time-frequency analysis", *IEEE Transactions on Industrial Applications*, 2006,42(6), pp: 1454–1463.

[6] R.C. Bhavsar, R.A. Patel, "Various techniques for condition monitoring of three phase induction motor-a review", *International Journal of Engineering Inventions*, 2013, 3(4), pp: 22–26.

[7] R.K. Patel, V.K. Giri, "ANN based performance evolution of BDI for condition monitoring of induction motor bearings",*Journal of Institution of Engineers (India) Series B*, 2016,98, pp:267–274.

[8] Y. Ying, J. Li, Z. Chen, J. Guo, "Study on rolling bearing on-line reliability analysis based on vibration information processing", *Computers and electrical engineering*, 2018, 69, pp: 842-851.

[9] C. Costa, M.H. Mathias, P.Ramos, P.S. Girao, "A new approach for real time fault diagnosis in induction motor is based on vibration measurement", *Instrumentation and Measurement Technology Conference(I2MTC), IEEE,* May 2010,pp : 1164 - 1168.

[10] A. Nikbakhsh, H. R. Izadfar, M. Jazaeri, "Classification and comparison of rotor temperature estimation methods of squirrel cage induction motors", *Measurement*, 2019, 145, pp : 779-802.

[11] G. Paoletti , A. Golubev, "Partial discharge theory and applications to electrical systems", *IEEE IAS Pulp and Paper Industry Conference in Seattle*,1999, pp : 124 – 138.

[12] P. Gangsar, R. Tiwari, "Signal based condition monitoring techniques for fault detection and diagnosis of induction motors: A state-of-the-art review", *Mechanical systems and signal processing*, 2020,144, pp: 1-37.

[13] S. Altug, M.Y. Chow, H. J. Trussell, "Fuzzy inference systems implemented on neural architectures for motor fault Detection and Diagnosis" , *IEEE Transactions on Industrial Electronics*, 1999, 46(6), pp:1069-1079.

[14] M. A. Awadallah, M. M. Morcos, "Application of AI Tools in Fault Diagnosis of Electrical Machines and Drives—An Overview", *IEEE Transactions on Energy Conversion*, 2003, 18(2), pp: 245-251.

[15] G. Chandrasekhar, F. Sahin, " A survey of feature selection methods", *Computers and electrical engineering*, 2014, 40(1), pp: 16-28.

[16] Ting Yang, Haibo Pen, Zhaoxia Wang, Che Sau Chang, "Feature Knowledge Based Fault Detection of Induction Motors Through the Analysis of Stator Current Data", *IEEE Transactions On Instrumentation and Measurement*, 2016, 65(3), pp: 549-558.

[17] J.F. Martins, V.F. Pires, A.J. Pires, " PCA based on line diagnosis of induction motor stator fault feed by PWM inverter", *IEEE International Symposium on Industrial Electronics,* 2006, 3, pp : 2401-2405.

[18] A. K. Thakur, P. K. Kundu, A. Das, "Comparative study of induction motor fault analysis using feature extraction", *IEEE Calcutta Conference (CALCON),* December 2017, pp: 150-154, doi: 10.1109/CALCON.2017.8280714

[19] E. Alpaydin, "Introduction to machine learning", The MIT Press; 2004.

[20] Y. Han and Y. H. Song, "Condition Monitoring Techniques for Electrical Equipment—A Literature Survey", *IEEE Transactions on Power Delivery*, 2003,18 (1), pp: 4-13.

[21] A. K. Thakur, T. M. Joardar, P. K. Dan, "Modelling a Condition Monitoring Based Control Using Matlab/Simulink for Rotating Electrical Machines", *International Journal of Recent advances in Mechanical Engineering*, 2013, 2(1), pp: 51-61.

[22] A.K. Thakur, A. Das, P.K. Kundu, "Development of Generalized Model of 3-Phase Induction Motor for Performance Study During Different Distorted and Unbalance Voltage*", International Journal of Computer Sciences and Engineering,* 2020, 8(2), pp: 18-25.

[23] L. Navarro, M. Delgado, J. Urresty, J. Cusidó, L. Romeral, **"**Condition monitoring system for characterization of electric motor ball bearings with distributed fault using fuzzy inference tools", *Instrumentation and Measurement Technology Conference (I2MTC), IEEE,* May 2010, pp : 1159-1163.

[24] Vas P, "Parameter estimation, condition monitoring and diagnosis of electrical machines". Clarendon Press, Oxford, 1993.

[25] M'hamed D, Cardoso AJM, "Air gap eccentricity fault diagnosis in three phase induction motor by the complex apparent power signature analysis", 2008, *IEEE Transactions on Industrial Electronics*, 55 (3), pp :1404-1410.

[26] Hwang DH, Lee KC, Lee JH, Kang DS, Lee JH, Choi KH, Kang S et al, "Analysis of a three phase induction motor under eccentricity condition", *In: 31st annual conference of IEEE industrial electronics society, IECON2005*, pp 6–10.

[27] Blodt, M ;Lab. d'Electrotech. de Grenoble, Grenoble Granjon, P. ; Raison, B. ; Rostaing, G. "Models for Bearing damage detection in Induction Motors using stator current monitoring", *IEEE Transactions on Industrial Electronics,* 2008,55(4), pp : 1813 – 1822.

[28] Siddique A, Yadava G. S, Singh B, "A review of stator fault monitoring techniques of induction motors", *IEEE Transactions on Energy Conversion*, 2005, 20(1):106–114.

[29] A. H. Bonnet, "Cause and analysis of stator and rotor failures in three phase squirrel-cage induction motors," *IEEE Transactions on Industry Applications*, 1992,28(4), pp: 921–437.

[30] IEEE recommended practice for the design of reliable industrial and commercial power systems. IEEE Standard 493–1997 [IEEE Gold Book].

[31] Singh GK, Al Kazzaz SAS, "Induction machine drive condition monitoring and diagnostic research—a survey", *Electrical Power System Research,* 2003, 64(2), pp :145–158.

[32] Allbrecht PF, Appiarius JC, McCoy RM, Owen EL, "Assessment of the reliability of motors in utility applications—updated", *IEEE Transactions on Energy Conversion*, 1986, EC-1 (1):39–46.

[33] M. Tsypkin, "Induction Motor Condition Monitoring: Vibration Analysis Technique - a Practical Implementation", *IEEE International Conference on Electrical Machines and Drives*, May 2011, pp : 406-411.

[34] V.P. Raj, K. Natarajan, T.G. Girikumar, "Induction motor fault detection and diagnosis by vibration analysis using MEMS accelerometer", *International Conference on Emerging Trends in Communication, Control, Signal Processing & Computing Applications (C2SPCA)*, October 2013, pp : 1-6.

[35] V V Karanovic , M T Jocanović 1 , J M Wakiru ,M D Orošnjak, "Benefits of lubricant oil analysis for maintenance decision support: a case study", *IOP Conf. Series: Materials Science and Engineering,2018* 393(1) doi:10.1088/1757-899X/393/1/012013.

[36] Yu.T. Chen, J. C. Lai, Yu. M. Jheng, C. C. Kuo, H.C. Chang, "Partial discharge detection for stator winding insulation of motors using artificial neural network", *Advances in Mechanical Engineering*, 2018,10(7), pp: 1–10.

[37] Cardoso AJM, etal. "Inter-turn stator winding fault diagnosis in three-phase induction motors, by Park's vector approach.", *IEEE Transactions on Energy Conversion*, 1999; 14 (3), pp :595–598.

[38] RM. Tallam, TG. Habetler, RG. Harley ,"Transient model for induction machines with stator winding turn faults", *IEEE Transactions on Industry Applications,* 2002, 38 (3), pp :632–637.

[39] Kohler J.L, SottileJ, Trutt F C. "Alternatives for assessing the electrical integrity of induction motors", *IEEE Transactions on Industry Applications*, 1992;28(5), pp:1109–1117.

[40] Bachir S, Tnani S, Trigeassou JC, Champenois G, "Diagnosis by parameter estimation of stator and rotor faults occurring in induction machines", *IEEE Transactions on Industrial Electronics*, 2006;53(3), pp :963–973.

[41] De Angelo CH, Bossio GR, Giaccone SJ, Valla MI, Solsona JA, García GO, "Online model-based stator-fault detection and identification in induction motors", *IEEE Transactions on Industrial Electronics*, 2009;56(11), pp:4671–4680.

[42] Ghanbari T, "Autocorrelation function-based technique for stator turn-fault detection of induction motor", *IET Science, Measurement & Technology*, 2016, 10(2), pp:100–110.

[43] Cruz SMA, Cardoso AJM., "Stator winding fault diagnosis in three-phase synchronous and asynchronous motors, by the extended Park's vector approach", *IEEE Transactions on Industry Applications,* 2001, 37(5), pp:1227–33.

[44] Liu Z, Yin X, Zhang Z, Chen D, Chen W , "Online rotor mixed fault diagnosis way based on spectrum analysis of instantaneous power in squirrel cage induction motors", *IEEE Transactions on Energy Conversion*, 2004;19(3), pp:485–90.

[45] Thomas VV, Vasudevan K, Kumar VJ, "Online cage rotor fault detection using air gap torque spectra", *IEEE Transactions on Energy Conversion*, 2003, 18(2), pp:265–270.

[46] Das S, Purkait P, Dey D, Chakravorti S, "Monitoring of inter-turn insulation failure in induction motor using advanced signal and data processing tools", *IEEE Transactions on Dielectrics and Electrical Insulation,* 2011;18(5), pp:1599-1608.

[47] R. Liu, B. Yang, E. Zio , X. Chen, "Artificial intelligence for fault diagnosis of rotating machinery: A review", *Mechanical Systems and Signal Processing*, 2018, 108, pp:33-47.

[48] P. Baraldi, L. Podofillini, L. Mkrtchyan, E. Zio, V.N. Dang, "Comparing the treatment of uncertainty in bayesian networks and fuzzy expert systems used for a human reliability analysis application", *Reliability Engineering & System Safety*, 2015, 138, pp: 176–193.

[49] D. Wang, "K-nearest neighbors based methods for identification of different gear crack levels under different motor speeds and loads: revisited", *Mechanical Systems and Signal Processin*g, 2016, 70, pp: 201–208.

[50] P. Konar, P. Chattopadhyay, "Bearing fault detection of induction motor using wavelet and support vector machines (SVMs)", 2011, Applied Soft Computing, 11(6), pp: 4203–4211.

[51] Y. Bengio, "Learning deep architectures for ai", Foundations and trends® in Machine Learning, 2009, 2 (1), pp :1–127.

[52] G.E. Hinton, R.R. Salakhutdinov, "Reducing the dimensionality of data with neural networks", *Science 313 (5786),*(2006),pp: 504–507.

[53] Battiti R. "Using mutual information for selecting features in supervised neural net learning", IEEE Transactions Neural Networks, 1994;5(4), pp: 537-550

[54] Formulas, Laboratory statistics (second edition), *Methods in chemistry and health science*, 2018, pp: 1-140.

[55] A. Chattopadhyay, S. Chattopadhyay, S. Sengupta, "Measurement of harmonic distortion and Skewness of stator current of induction motor at crawling in Clarke plane", *IET Science Measurement and Technology*, 2014, 8 (6), pp: 528-536.

[56] R. Bsak, S. Basu, D. K. Ray, S. Chattopadhyay, "Condition Monitoring and Cost Optimization in Solar Roof-Top Generating System**",** *Michael Faraday IET International summit 2020*, 2020, pp: 125-129, doi: 10.1049/icp.2021.1028

[57] D. K. Ray, S. Chattopadhyay, "Fault analysis in solar–wind microgrid using multi-resolution analysis and Stockwell transform-based statistical analysis", *IET Science, Measurement & Technology*, 2019,vol. 14(6), pp:639-650.

[58] Z. Bai, P.R. Krishnaiah, " Encyclopedia of physical science and technology(Third Edition)", 2003, pp: 55-73.

[59] Bryant V., Metric Spaces: Iteration and Application. Cambridge University Press, 1996, New York, USA

[60] Seidl T, "Nearest Neighbor Classification/Liu L., Ozsu MT (eds.)", *Encyclopedia of Database Systems*. 2009, doi : https://doi.org/10.1007/978-0-387-39940-9_561.

[61] Schweizer K, Cattin PC, Brunner R, Müller B, Huber C, Romkes J, "Automatic selection of a representative trial from multiple measurements using Principle Component Analysis", *Journal of Biomechanics*, 2012 ,45 (13), pp: 2306–2309.

[62] I. T. Jolliffe, "Principal component analysis", *NY: Springer-Verlag*(1986).

[63] P. Malhi, P. More, "Enhanced-PCA based dimensionality reduction and feature selection for real-time network threat detection", *Engineering, technology and applied science research* , 2020, 10(5), pp: 6370-6375.

[64] Guyon I, Elisseeff A, "An introduction to variable and feature selection", *Journal of machine learning research*, 2003,3, pp :1157–1182.

[65] V. Vapnik,"The Nature of Statistical Learning Theory", *NY: Springer-Verlag*, 1995.

[66] A. Hur, J.Weston, "A User's Guide to Support Vector Machines", *Data Mining Techniques for the Life Sciences*,2010, pp : 223-239.

[67] X. Yan, M. Jia, "A novel optimized SVM classification algorithm with multi-domain feature and its application to fault diagnosis of rolling bearing",*Neurocomputing*, 2018, 313, pp: 47-64.

[68] A. Agasthian, R. Pamula, L. A. Kumaraswamidhas, "Fault classification and detection in wind turbine using Cuckoo-optimized support vector machine", *Neural Computing and Applications*, 2019, 31(5), pp: 1503–1511.

[69] D. Kancherla, J. D. Bodapati, Veeranjaneyulu N, "Effect of different kernels on the performance of an SVM based classification", *International Journal of Recent Technology and Engineering*, 2019,7(5), pp: 1-6.

[70] T. Menzies, E. Kocagüneli, L. Minku, F. Peters, B. Turhan, "Chapter 24 - Using Goals in Model-Based Reasoning ", *Sharing Data and Models in Software Engineering*, 2015, pp:321-353.

[71] Orr, Mark J L., "Introduction to Radial Basis Function Networks", *Centre for Cognitive Science, University of Edinburgh, Scotland*, April 1996.

[72] F. J. Taylor, " Signal Processing, Digital", *Encyclopedia of Physical Science and Technology (Third Edition)*, 2003, pp: 737-760.

[73] U. Oberst, "The Fast Fourier Transform", *SIAM Journal on Control & Optimixation*, 2007, 46(2), pp:1-45.

[74] Canal, M. R. " Comparison of wavelet and short time Fourier transform methods in the analysis of EMG signals", 2010, *Journal of Medical Systems*, 34(1), pp: 91-94.

[75] E. Schmitt, P. Idowu, A. Morales, "Applications of wavelets in induction machine fault detection" *Ingeniare. Revista chilena de ingeniería*, 2010, 18(2), pp:158-164.

[76] D. Wang, Q. Miao, X. Fan, H.Z. Huang, "Rolling element bearing fault detection using an improved combination of Hilbert and wavelet transform", *Journal of Mechanical Science and Technology*, 2009, 23,pp: 3293-3301.

[77] Chebil, J., Noel, G., Mesbah, M., & Deriche, M., "Wavelet decomposition for the detection and diagnosis of faults in rolling element bearings", 2010, *Jordan Journal of Mechanical & Industrial Engineering*, 4(5), pp: 260-266.

[78] M. Aktas, V. Turkmenoglu, "Wavelet-based switching faults detection in direct torque control induction motor drives", *Science, Measurement and Technology*, 2010, 4(6), pp: 303-310.

[79] A. Dasgupta, S. Debnath, A. Das "Transmission line fault detection and classification using cross-correlation and k-nearest neighbor", *International Journal of Knowledge-based and Intelligent Engineering Systems*, 2015, 19, pp: 183–189.

[80] J. Semmlow, "Chapter 2 - Basic Concepts in Signal Processing", *Signals and Systems for Bioengineers (Second Edition)*, 2012, pp: 35-80.

[81] S. Singh , A. Kumar, N. Kumar, "Motor current signature analysis for bearing fault detection in mechanical systems", 3rd International Conference on Materials Processing and Characterisation (ICMPC 2014), *Procedia Materials Science*, 2014, 6 pp : 171-177.

[82] H. Henao, H. Razik, G-A. Capolino, "Analytical approach of the stator current frequency harmonics computation for detection of induction machine rotor faults", *IEEE Transactions on Industry Applications*, 2005, 41(3),pp: 801-807.

[83] R. R. Obaid, D. J. Gritter, T. G. Habetler, "A simplified technique for detecting mechanical faults using stator current in small induction motors", *Industry Applications Conference, Conference Record of the 2000 IEEE 2000*, 1, pp : 479-483.

[84] T. Wongsuwan, P. Tangamchit, C. Prapanavarat, M. Pusayatanont, "Motor Misalignment Detection Based on Hidden Markov Model", *International Symposium on Communications and Information Technologies, ISCIT '06*, 2006, pp : 422-427.

[85] O. Ondel, E. Boutleux, G. Clerc, "A Method to Detect Broken Bars in Induction Machine Using Pattern Recognition Techniques", *IEEE Transactions on Industry Applications*, 2006, 42(4), pp: 916-923.

[86] A. Bouguerne, A. Lebaroud; A. Medoued; A. Boukadoum, "Classification of induction machine faults by K-nearest neighbor", *7th International Conference on Electrical and Electronics Engineering (ELECO)*, 2011, pp: 1-363.

[87] P. Pietrzak, M. Wolkiewicz, "On-line Detection and Classification of PMSM Stator Winding Faults Based on Stator Current Symmetrical Components Analysis and the KNN Algorithm", *Electronics*,2021,*10*(15), p. 1786, doi: https://doi.org/10.3390/electronics10151786.

[88] N.R. Sakthivel ,Binoy B. Nair , M. Elangovan ,V. Sugumaran, S. Saravanmurugan, "Comparison of dimensionality reduction techniques for the fault diagnosis of mono block centrifugal pump using vibration signals", *Engineering Science and Technology, an International Journal*, 2014, 17(1), pp : 30-38.

[89] A. Malhi, R. X. Gao, "PCA based feature selection scheme for machine defect classification", *IEEE Transactions on Instrumenation and Measurement*, 2004, 53(6), pp : 1517-1525.

[90] J. F. Martins, V. F. Pires, T. Amaral, "Induction motor fault detection and diagnosis using a current state space pattern recognition", *Pattern Recognition Letters*, 2011, 32(2), pp : 321-328.

[91] B.M Ebrahimi, J. Faiz, B.N Araabi, "Pattern identification for eccentricity fault diagnosis in permanent magnet synchronous motors using stator current monitoring", *IET Electric Power Applications*, 2010,4(6), pp: 418-430.

[92] C. I. Christodoulou, C. S. Pattichis, "Unsupervised Pattern Recognition for the Classification of EMG Signals", *IEEE Transactions on Biomedical Engineering*, 1999, 46 (2), pp: 169-178.

[93] M. A. Awadallah, M. M. Morcos,"Applications of AI tools in fault diagnosis of electrical machines and drives- an overview", *IEEE Transactions on Energy Conversion*, 2003, 18(2), pp: 245-251.

[94] D. Ma, Y. Liang, X. Zhao, et al., "Multi-BP expert system for fault diagnosis of power system", *Engineering Applications of Artificial Intelligence*. 2013, 26(3), pp: 937-944.

[95] V. Muralidharan, V. Sugumaran, "Rough set based rule learning and fuzzy classification of wavelet features for fault diagnosis of monoblock centrifugal pump", 2013, *Measurement* 46(9), pp: 3057-3063.

[96] M. Seera, C.P. Lim, D. Ishak, H. Singh, "Fault detection and diagnosis of induction motors using motor current signature analysis and a hybrid FMM–CART Model", *IEEE Transactions on Neural Networks and Learning System*, 2012, 23(1), pp :97-108.

[97] S.S. Tayarani-Bathaie, Z.N.S. Vanini, K. Khorasani, "Dynamic neural network-based fault diagnosis of gas turbine engines", *Neurocomputing*, 2014, 125, pp: 153-165.

[98] T. Boukara, A. Lebaroud, G. Clerc, "Statistical and neural-network Approaches for the classification of induction machine faults using the ambiguity plane representation", *IEEE Transactions on Industrial Electronics*, 2013, 60(9), pp :4034 – 4042.

[99] G. H. Bazan, P.R. Scalassara, W. Endo, A. Goedtel, W.F. Godoy, R. H. C. Palacios, "Stator fault analysis of three-phase induction motors using information measures and artificial neural networks", *Electric Power System Research*, 2017,143, pp : 347-356.

[100] S.G. Kumbhar, P.E. Sudhagar, "An integrated approach of adaptive neuro-fuzzy inference system and dimension theory for diagnosis of rolling element bearing", *Measurement*, 2020, 166, pp : 1-20.

[101] M. Drakaki, Y. L. Karnavas, A.D. Karlis, I.D. Chasiotis, "Study on fault diagnosis of broken rotor bars in squirrel cage induction motors: a multi agent system approach using intelligent classifier", *IET Electric Power Applications*, 2020, 14(2), pp : 245-255.

[102] X. Yan, M.Jia, "A novel optimized SVM classification algorithm with multi-domain feature and its application to fault diagnosis of rolling bearing",*Neurocomputing*, 2018,313, pp :47-64.

[103] W. Zhu, Y. Wei, H. Xiao, "Fault diagnosis of neural network classified signal fractal feature based on SVM", *Cluster Computing*, 2019, 22, pp: 4249-4254.

[104] P. Gangsar , R. Tiwari,"Taxonomy of Induction-Motor Mechanical-Fault Based on Time-Domain Vibration Signals by Multiclass SVM Classifiers", *Intelligent Industrial Systems*, 2016, 2, pp: 269–281.

[105] L.B. Jack, A.K. Nandi, "Support vector machines for detection and characterization of rolling element bearing faults", Proceedings of the Institution of Mechanical Engineers, Part C: Journal of Mechanical Engineering Science, 2001, 215(9), pp: 1065-1074.

[106] J. Milgram, M. Cheriet, and R. Sabourin, "Speeding Up the Decision Making of Support Vector Classifiers", *International Workshop on Frontiers in Handwriting Recognition*, Japan, 2004, pp : 57-62.

[107] H. Xu,X. Bie, H. Feng, Y. Tian,"Multiclass SVM active learning algorithm based on decision directed acyclic graph and one versus one", *Cluster Computing*,2019, 22, pp : 6241–6251.

[108] T. Yang, H. Pen, Z. Wang, C. S. Chang, "Feature knowledge based fault detection of induction motors through the analysis of stator current data", *IEEE Transactions On Instrumentation and Measurement*,2016,65(3), pp : 549-558.

[109] B. M. S. Hasan, A. M. Abdulazeez, "A Review of Principal Component Analysis Algorithm for Dimensionality Reduction ", *Journal of soft computing and data mining*, 2021, 2(1), pp: 20-30.

[110] F.Harrou, J. F. Ramahaleomiarantsoa, M. N. Nounou, H. N. Nounou, "A data-based technique for monitoring of wound rotor induction machines: A simulation study", *Engineering Science and Technology an International Journal*,2016, 19(3) : 1424-1435.

[111] Y.K.Gu, X.Q.Zohu, D.P.YU, Y.J.Shen, "Fault diagnosis method of rolling bearing using principal component analysis and support vector machine", *Journal of Mechanical Science and Technology*, 2018, 32(11), pp : 5079-5088.

[112] J. Urbanek, T. Barszcz, J. Antoni, "Integrated modulation intensity distribution as a practical tool for condition monitoring", *Applied Acoustics*, 2014,77, pp: 184-194.

[113] M. Li, "The application of PCA and SVM in rolling bearing fault diagnosis", *Advanced Materials Research*, 2012, 430, pp : 1163-1166.

[114] L. Saidi, J. Ben Ali, F. Fnaiech, "Application of higher order spectral features and support vector machines for bearing faults classification", *ISA Transactions*, 2015, 54, pp: 193-206.

[115] V.F. Pires, M. Kadivonga, J.F. /martins, A. J. Pires, "Motor current signature analysis for induction motor rotor diagnosis", *Measurement*, 2013, 46(2), pp : 942-948.

[116] J. R. Stack, T. G. Hebetler, R. G. Herley, "Bearing fault detection via autoregressive stator current modeling", *IEEE Transactions on Industry Applications*, 2004, 40(3), pp : 741-747.

[117] M. El H. Benbouzid, "A Review of Induction Motors Signature Analysis as a Medium for Faults Detection",*IEEE Transactions on Industrial Electronics*, 2000, 47(5), pp: 984-993.

[118] Kancherla D, Bodapati JD, Veeranjaneyulu N, "Effect of Different Kernels on the performance of an SVM based classification", *International Journal of Recent Technology and Engineering*, 2019,7(5), pp: 1-6.

[119] P. Gangsar, R. Tiwari, "Comparative investigation of vibration and current monitoring for prediction of mechanical and electrical faults in induction motor based on multiclass-support vector machine algorithms", *Mechanical system and signal processing*, 2017, 94, pp: 464-481.

[120] Chen, X., & Feng, Z, " Induction motor stator current analysis for planetary gearbox fault diagnosis under time-varying speed conditions", *Mechanical Systems and Signal Processing*, 2020, *140*, p: 106691.

[121] S. Abe , "Analysis of multiclass support vector machines", *Thyroid*, *21*(3), p: 3772.

[122] K. Varpa, H. Joustijoki, K. Iltanen, M. Juhola, "Applying One-vs-One and One-vs-All Classifiers in k-Nearest Neighbour Method and Support Vector Machines to an Otoneurological Multi-Class Problem", In *User Centred Networked Health Care*, 2011, pp: 579-583.

[123] J.D. M-Morales, E.R.P-Hernández, D.U. Campos-Delgado, "Multiple-fault diagnosis in induction motorsthrough support vector machine classification at variable operating conditions", *Electrical Engineering*, 2018, 100, pp :59–73.

[124] B. Kijsirikul, N. Ussivakul, S. Meknavin, "Adaptive Directed Acyclic Graphs for Multiclass Classification", *In PRICAI 2002: Trends in Artificial Intelligence: 7th Pacific Rim International Conference on Artificial Intelligence*, 2002, Proceedings 7, pp:158-168.

[125] M. Petrovskiy, "A Game Theory Approach to Pairwise Classification with Support Vector Machines", *International Conference on Machine Learning and Applications, IEEE*, 2004, pp: 115-122.

[126] Wu TF, Lin CJ, Weng R, "Probability Estimates for Multi-class Classification by Pairwise Coupling", NIPS 2003 proceedings, MIT Press, 2004.

[127] B. Kijsirikul, N. Ussivakul, "Multiclass support vector machines using adaptive directed acyclic graph", *IJCNN 2002 proceedings*, 2002, pp. 980-985.

[128] J. Platt, N. Cristianini, J. Shawe-Taylor, "Large margin DAGs for multi-class classification", *Advances in Neural Information, Processing Systems 12*,MIT Press, 2000, pp. 547-553.

[129] H. Xu,X. Bie, H. Feng, Y. Tian,"Multiclass SVM active learning algorithm based on decision directed acyclic graph and one versus one", *Cluster Computing,2019*,22, pp: 6241–6251.

[130] Ponci, F, et al.: "Diagnostic of a Faulty Induction Motor Drive via Wavelet Decomposition," *IEEE Transactions on Instrumentation and Measurement*, 2007, 56(6), pp : 2606-2615.

[131] Burrus TV, Burrus C, Narasimhan K, Guo Y, Li C, "Introduction to Wavelets and Wavelet Transforms. A Primer," Brrus CS, 1998.

[132] Daviu, J Antonino, et al: "Validation of a new method for the diagnosis of rotor bar failures via wavelet transformation in industrial induction machines," *IEEE Transactions on Industry Applications*,2006,42(4), pp. 990-996.

[133] S. Y. Wang, X. G. Liu, J. Yianni, T. Z. Aziz, and J. F. Stein, "Extracting burst and tonic components from surface electromyograms in dystonia using adaptive wavelet shrinkage", *Journal of Neuroscience Methods*, 2004, 139(2), pp: 177-184.

[134] M. Flanders, "Choosing a wavelet for single-trial EMG", *Journal of Neuroscience Methods*, 2002, 116, pp: 165-177.

[135] M. F. Faizal, A. Mohamed, "Comparing the performance of various mother wavelet functions in detecting actual 3-phase voltage sags",*2nd IEEE International Conference on Power and Energy*, 2008, pp: 657-661.

[136] E. Y. Hamid, R. Mardiana, Z. I. Kawasaki, "Wavelet-based compression of power disturbances using the minimum description length criterion",2001, *IEEE Power Engineering Society Summer Meeting*, 3, pp: 1772-1777.

[137] M. A. S. K. Khan , T. S. Radwan, M. A. Rahman, Wavelet Packet Transform Based Protection of Three-Phase IPM Motor, *IEEE International Symposium on Industrial Electronics*, 2006, pp : 2122 – 2127.

[138] M. A. S. K. Khan , M. A. Rahman, "A novel neuro-wavelet-based self-tuned wavelet controller for IPM motor drives", *IEEE Transactions on Industry Applications*", 2010, 46(3), pp: 1194-1203.

[139] L. Yang, M. D. Judd,C. J. Bennoch, "Denoising UHF signal for PD detection in transformers based on wavelet technique", *Annual Report Conference on Electrical Insulation and Dielectric Phenomena*, 2004, pp: 166 – 169.

[140] W. Li, "Research on extraction of partial discharge signals based on wavelet analysis", *International Conference on Electronic Computer Technology*, 2009, pp: 545-548.

[141] P. K. Kankar, Satish C. Sharma, S. P. Harsha, "Fault diagnosis of ball bearings using continuous wavelet transform", *Applied Soft Computing*,2011, 11, pp: 2300-2312.

[142] S. Prabhakar, A. R. Mohanty, and A. S. Sekhar, "Application of discrete wavelet transform for detection of ball bearing race faults," *Tribology International*, 2002, 35, pp. 793-800.

[143] V. Purushotham, S. Narayanan, and S. A. N. Prasad, "Multi fault diagnosis of rolling bearing elements using wavelet analysis and hidden Markov model based fault recognition", *NDT&E International*, 2005, 38, pp : 654-664.

[144] J. Rafiee, P.W. Tse, A. Harif, M.H. Sadeghi: "A novel technique for selecting mother wavelet function using an intelligent fault diagnosis system", *Expert Systems with Applications*,2009,36(3), pp : 4862-4875.

[145] K. Chinmaya , A. R. Mohanty, "Monitoring gear vibrations through motor current signature analysis and wavelet transform," *Mechanical Systems and Signal Processing*, 2006, 20(1), pp : 158-187.

[146] R. Yan, R. X. Gao, X. Chen.: "Wavelets for fault diagnosis of rotary machines: A review with applications", *Signal Processing*, 2014,96, pp: 1-15.

[147] Ye, Z, Wu, B , Sadeghian, A, "Current signature analysis of induction motor mechanical faults by wavelet packet decomposition," *IEEE Trans on Industrial Electronics*, 2003, 50(6), pp : 1217-1227.

[148] J. Poshtan, J. Zarei.:"Bearing fault detection using wavelet packet transform of induction motor stator current", *Tribology International*, 2007, 40(5), pp: 763-769.

[149] V. Matz, M. Kreidl, R. Šmíd, "Signal-to-Noise Ratio Improvement based on the Discrete Wavelet Transform in Ultrasonic Defectoscopy", Acta Polytechnica, 44(4), pp :61—66.

[150] Ponci, F, et al.:"Diagnostic of a Faulty Induction Motor Drive via Wavelet Decomposition," *IEEE Transactions on Instrumentation and Measurement*,2007,56(6), pp : 2606-2615.

[151] Kim H, Melhem H, "Damage detection of structures by wavelet analysis", *Engineering structure*, 2004,26(3):347-62.

[152] M. P. Fargues, R.J. Barsanti, R. Hippenstiel: "Wavelet-based denoising: comparisons between orthogonal and non-orthogonal decompositions", *Proceedings of 40th Midwest Symposium on Circuits and Systems. Dedicated to the Memory of Professor Mac Van Valkenburg*, 1997, pp : 929-932.

[153] Rieder, P., &Nossek, J. A, "Implementation of orthogonal wavelet transforms and their applications", *In Proceedings IEEE International Conference on Application-Specific Systems, Architectures and Processors*, pp. 489-498.

[154] Wang W.J., McFadden P.D. ,"Application of orthogonal wavelets to early gear damage detection", Mechanical Systems and Signal Processing, 1995,9(5), pp : 497-507.

[155] C. Pothisarn , J. Klomjit , A. Ngaopitakkul , C. Jettanasen , D. A. Asfani, I M. Y. Negara, "Comparison of Various Mother Wavelets for Fault Classification in Electrical Systems", *Applied sciences*, 2020, 10(4), p. 1203, doi:10.3390/app10041203.

[156] Alrumaih RM, Al-Fawzan MA. Time series forecasting using wavelet denoising an application to saudi stock index. *Journal of King Saud University-Engineering Sciences*. 2002,14(2), pp :221-33.

[157] R. M. Potdar, M. R. Meshram, R. Kumar, "Optimal Parameter Selection for DWT based PCG Denoising",Turkish Journal of Computer and Mathematics Education, 2021, 12(10), pp: 7521-7532.

[158] Z. Qin , H. Chen, J. Chang, "Signal-to-Noise Ratio Enhancement Based on Empirical Mode Decomposition in Phase-Sensitive Optical Time Domain Reflectometry Systems", *Sensors*, 2017,17(8) , p. 1870.

[159] H. Yuan, S.Kwong, "A Virtual View PSNR Estimation Method for 3-D Videos",*IEEE Transactions on Broadcasting*, 2016, 62(1), pp: 134-140.

[160] Mukherjee, A., Kundu, P. K., & Das, A. "A Correlation-Based Classification of Power System Faults in a Long Transmission Line. In Emerging Technologies in Data Mining and Information Security", *Proceedings of IEMIS* , 2021, 2, pp. 113-121, doi: https://doi.org/10.1007/978-981-33-4367-2_12.

[161] N. K. Al-Qazzaz , S. H. B. M. Ali, S. A. Ahmad, M. S. Islam, J. Escudero: "Selection of mother wavelet function for multi channel EEG signal analysis during a working memory task", *Sensors*,2007,15 (11), pp : 497-507.

[162] A.K. Thakur, P.K. Kundu, A.Das, "Selection of Optimal Mother Wavelet for Fault Analysis in Induction Motor Using Stator Current Waveform", *Advances in Data Science and Computing Technology*, 2022, pp: 197-217, doi:10.1201/9781003277071-20.

[163] Z. A. Jaffery, K. Ahmad ,P. Sharma, "Selection of Optimal Decomposition Level Based on Entropy for Speech Denoising Using Wavelet Packet", *Journal of Bioinformatics and Intelligent Control*, 2013, 1(2), pp: 196–202.

[164] Chen. Yu, "Research and Design of Intelligent Electric Power Quality Detection System Based on VI", Journal of Computers,2010, 5(1) , pp : 158-165.

[165] Kar Ray. D, Deb. S, Kumar. T, Sengupta. S, "Diagnosis of Sub-synchronous Inter-harmonics in Power System Signals using Multi-Resolution Analysis of Discrete Wavelet Transform", *IEM International Journal of Management and Technology*, IEMIJMT, 2012, 2(2), pp: 11-16.

[166] Andrei, H., Cepisca, C., Grigorescu, S. and Eberhard, A, "Power quality and electrical arc furnaces", In *Power Quality* , 2011, (No. June 2014, pp. 77-100).

[56] R. Bsak, S. Basu, D. K. Ray, S. Chattopadhyay, "Condition Monitoring and Cost Optimization in Solar Roof-Top Generating System**",** *Michael Faraday IET International summit 2020*, 2020, pp: 125-129, doi: 10.1049/icp.2021.1028.

[167] Kar Ray D, Chattopadhyay S, DasSharma K, Sengupta S., "Inter-turn short circuit assessment of DC motor used in railway locomotive with a case study", *IET Electrical. Power Applications*, 2018, 12 (9), pp : 1272–1282.

[57] D. K. Ray, S. Chattopadhyay, "Fault analysis in solar–wind microgrid using multi-resolution analysis and Stockwell transform-based statistical analysis", *IET Science, Measurement & Technology*, 2019,14(6), pp:639-650.

[168] D. K. Ray, S. Chattopadhyay, S. Sengupta, "Multi-Resolution-Analysis-based Line-to-Ground Fault Detection in a VSC-Based HVDC System", *IETE Journal of Research*, 2020, 66(4), pp: 491-504.

[169] D. K. Ray, S. Sengupta, "Diagnosis of Unbalance in 3 Phase Induction Motor using Multi-Resolution Analysis of Discrete Wavelet Transform", *JECT*, 2013, 4 (Spl – 1), pp:176-179.

[170] D. K. Ray, S. Deb, S. Sengupta, "Diagnosis of Sub-Synchronous Inter-Harmonics in Arc Furnace Transformer using Multi-Resolution Analysis of Discrete Wavelet Transform", *International Journal of Electrical, Electronics and Computer Engineering*, 2012, 1(2), pp : 66-70.

[171] Y.-Yi Hong, M. T. A. M. Cabatac, "Fault Detection, Classification, and Location by Static Switch in Microgrids Using Wavelet Transform and Taguchi-Based Artificial Neural Network", IEEE Systems Journal, 2020, 14(2), pp: 2735-2735.

[172] S. Baloch, S. S. Samsani, M. S. Muhammad, "Fault Protection in Microgrid Using Wavelet Multi resolution Analysis and Data Mining", *IEEE Access*, 2021, 9, pp : 86382 – 86391

[173] M. Arehpanahi,S. H. H Sadeghi,J. Milimonfared, H. R. Akbari Roknabadi, "Broken Rotor Bar Detection in Induction Motor via Stator Current Derivative", *International Conference on Electrical Machines and Systems*, September 2005,pp: 2202-2206.

[174] R. Meka, P. Jain, and I. S. Dhillon, "Guaranteed rank minimization via singular value projection", *In Advances in Neural Information Processing Systems*, 2010, 23, pp:1-9.

[175] D. Zhang, Y. Hu, J. Ye, X. Li, and X. He, "Matrix completion by truncated nuclear norm regularization," *IEEE Conference on Computer Vision and Pattern Recognition*, June 2012, pp: 2192-2199.

[176] Y. Wu, D. Inkpen, A. El-Roby, "Maximum Batch Frobenius Norm for Multi-Domain Text Classification", ICASSP 2022, May 2022, pp: 3763-3767, doi: https://doi.org/10.48550/arXiv.2202.00537.

[177] L. Schreier, J. Bendl, M. Chomat, "Analysis of stator and rotor currents and torque of induction machine with rotor-bar faults", *Electrical Engineering*, 2021, 103, pp: 519-528.

[47] R. Liu , B. Yang, E. Zio , X. Chen, "Artificial intelligence for fault diagnosis of rotating machinery: A review", 2018, *Mechanical Systems and Signal Processing*, 108, pp:33-47.

[178] P. P. R. Philo, N. M. M. Nascimento, I. R. Sousa, C. M.S. Medeiros, V. H. C. de Albuquerque, "A reliable approach for detection of incipient faults of short-circuits in induction generators using machine learning", *Computers and electrical engineering* ,2018, 71,pp: 440-451.

[179] T. Senguler, E. Karatoprak, S. Seker, "A New MLP Approach for the Detection of the Incipient Bearing Damage", *Advances in Electrical and Computer Engineering*, 2010, 10(3),pp: 34-39.

[180] W. Sun, S. Shao, R. Zhao, R. Yan1, X. Zhang, X. Chen, "A sparse auto-encoder-based deep neural network approach for induction motor faults classification", *Measurement*,2016, 89,pp: 171-178.

[181] X. Yang, W. Chen, A. Li, C. Yang, Z. Xie, H. Dong. (2019) " BA- PNN-based methods for power transformer fault diagnosis", *Advanced engineering informatics*, 39,pp : 178-185.

[182] J. Shi, Y. Deng, Z. Wang. "Analog circuit fault diagnosis based on density peaks clustering and dynamic weight probabilistic neural network", *Neurocomputing*, 2020, 407, pp: 354-365.

[183] A. Ngaopitakkul, M. Leelajindakrairerk, "Application of probabilistic neural network with transmission and distribution protection schemes for classification of fault types onradial, loop, and underground structures", *Electrical Engineering*, 2018, 100, pp: 469- 479.

[184] L. Zhao, Y. Zhang, J. Li, "Rolling Element Bearing Fault Diagnosis for Complex Equipment Based on FIFD and PNN", *Journal of failure analysis and prevention*, 2021, 21(1), pp: 303-309.

[185] M. R. Mehrjou, N. Mariun, N. Misron, M. A M. Radzi,"Analysis of statistical features based on start-up current envelope for broken rotor bar fault detection in line start permanent magnet synchronous motor", *Electrical Engineering*, 2017, 99, pp: 187-201.

[186] G. Vinodhini, R.M. Chandrasekaran, "A comparative performance evaluation of neural network based approach for sentiment classification of online reviews", *Journal of King Saud University - Computer and Information Sciences*, 2016, 28(1), pp : 2-12.

[187] D. Dou, J. Yang, J. Liu, Y. Zaho, "A rule-based intelligent method for fault diagnosis of rotating machinery", Knowledge-Based Systems, 2012, 36, pp: 1-8.

[188] K. Shao, M. Cai, G. Zhao,"Rolling Bearing Fault Diagnosis Based on Wavelet Energy Spectrum, PCA and PNN", *Chinese Control and Decision Conference(CCDC)*, 2014, pp: 800-804.

[162] A.K. Thakur, P.K. Kundu, A.Das, "Selection of Optimal Mother Wavelet for Fault Analysis in Induction Motor Using Stator Current Waveform", *Advances in Data Science and Computing Technology*, 2022, pp: 197-217, doi:10.1201/9781003277071-20.

[120] Chen, X., & Feng, Z, " Induction motor stator current analysis for planetary gearbox fault diagnosis under time-varying speed conditions", *Mechanical Systems and Signal Processing*, 2020, *140*, p. 106691.

[189] T. Gökta, MüslümArkan, Ö. F. Özgüven, "Detection of rotor fault in three-phase induction motor in case of low-frequency load oscillation", *Electrical Engineering*, 2015,97, pp: 337-345.

[190] M'hamed D, Cardoso AJM, "Air gap eccentricity fault diagnosis in three phase induction motor by the complex apparent power signature analysis", *IEEE transactions on industrial electronics*, 2008, 55(3), pp:1404-1410.

[109] B. M. S. Hasan, A. M. Abdulazeez, "A Review of Principal Component Analysis Algorithm for Dimensionality Reduction ", *Journal of soft computing and data mining*, 2021, 2(1), pp: 20-30.

[191] M. Mirzaei, M. Z. A. AB. KADIR, H. Hizam, E. Moazami, "Comparative Analysis of Probabilistic Neural Network, Radial Basis Function, and Feed-forward Neural Network for Fault Classification in Power Distribution Systems", *Electric Power Components and Systems*, 2011, 39, pp:1858–1871.

[192] H. Malik, S. Mishra, "Application of Probabilistic Neural Network in Fault Diagnosis of Wind Turbine Using FAST, TurbSim and Simulink", *Procedia Computer Science*, 2015, 58, pp:186 – 193.

[193] D. F. Specht, "Applications of Probabilistic Neural Networks", *SPIE*, 1990, 1294, pp : 344-353.

[194] M. Farrokhrooz, M. Karimi, A. Rafiei, "A new method for spread value estimation in multi spread PNN and its application in ship noise classification", 9th International symposium on signal processing and its applications,2007doi:10.1109/ISSPA.2007.4555402.

[195] H. Yang, J. Mathew, L. Ma, "Fault diagnosis of rolling element bearings using basis pursuit", *Mech. Syst. Sign. Process*, 2005, 19 (2), pp: 341–356.

[12] P. Gangsar, R. Tiwari, "Signal based condition monitoring techniques for fault detection and diagnosis of induction motors: A state-of-the-art review", *Mechanical systems and signal processing*, 2020,144, pp: 1-37.

[196] T. Ghanbari, "Autocorrelation function-based technique for stator turn-fault detection of induction motor", IET Science Measurement and Technology, 2016, 10(2), pp: 100-110.

[197] M. El H. Benbouzid, "A Review of Induction Motors Signature Analysis as a Medium for Faults Detection", 2000, *IEEE Transactions on Industrial Electronics*, 47(5), pp: 984-993.

[198] Rama Devi N, Siva Sarma DV, Ramana Rao PV. "Detection of stator incipient faults and identification of faulty phase in three-phase induction motor-simulation and experimental verification", IET Electric Power Applications,2015,;9(8), pp:540-548.

[199] B. EHE, C. V, B. MEH. "Current frequency spectral subtraction andits contribution to induction machines 'bearings condition monitoring",*IEEE Transactions on Energy Conversion* ,2013;28(1), pp :135–44.

[200] L. G. Kabari, M. B. Chigoziri, "Speech recognition using MATLAB and CrossCorrelation Technique", *European Journal of Engineering Research and Science*, 2019, 4(8), pp: 1-5.

[201] Zhang Y, Zhu D, Zhao L. Fault diagnosis of rolling element bearing using ACYCBD based cross correlation spectrum. *Journal of the Brazilian Society of Mechanical Sciences and Engineering*, 2021, 43, pp :1-8.

[202] G. Farahani, "Feature Selection Based on Cross-Correlation for the Intrusion Detection System", *Security and Communication Networks*, 2020, pp: 1-17, doi: https://doi.org/10.1155/2020/8875404.

[203] D.H. Krishna, I.A. Pasha, T.S.Savithri, "Classification of EEG Motor imagery multi class signals based on Cross Correlation", *Procedia Computer Science*, 2016, 85, pp: 490 – 495.

[204] S. Chandaka, A. Chatterjee , S. Munshi "Support vector machines employing cross-correlation for emotional speech recognition", Measurement, 2009, 42(4), pp : 611–618.

[205] R. Bose, K. Samanta, S. Chatterjee, "Cross-Correlation Based Feature Extraction from EMG Signals for Classification of Neuro-muscular Diseases", *International Conference on Intelligent Control Power and Instrumentation* (ICICPI), 2016, pp: 241-245.

[206] Z. Zang, T. R. Henry, K. H. Parhi, "Seizure Prediction using Cross-Correlation and Classification",*Asilomar Conference on Signals, Systems & Computers*, 2015, pp: 775-779.

[207] B. Chatterjee, S. Debnath, "Cross correlation aided fuzzy based relaying scheme for fault classification in transmission lines", Engineering Science and Technology, an International Journal, 2020, 23, pp: 534-543.

[208] S.Chandaka, A. Chatterjee, S. Munshi, "Cross-correlation aided support vector machine classifier for classification of EEG signals", Expert Systems with Applications,2009, 36, pp: 1329–1336.

[209] P. Rajmani, D. Dey, S. Chakraborty, "Cross-correlation-aided Fuzzy c-Means for Classification of Dynamic Faults in Transformer Winding During Impulse Testing",*Electric Power Components and Systems*, 2010, 38(2), 2010, pp: 1513-1530.

[210] P. Rajamani, D. Dey, S. Chakravorti, "Cross-correlation Aided Wavelet Network for Classification of Dynamic Insulation Failures in Transformer Winding during Impulse Test", *IEEE Transactions on Dielectrics and Electrical Insulation*, 2011,18(2), pp : 521-532.

[211] J. McBain, M. Timusk, "Cross Correlation for Condition Monitoring of Variable Load and Speed Gearboxes",*Journal of Industrial Mathematics*, 2014, Article ID 543056, pp: 1-10.

[212] S. Ray, D. Dey, "Characterization of Stator Turn to Turn Faults of Induction Motor using Cross – Correlation Analysis Based Features", *International Conference on Intelligent Control Power and Instrumentation (ICICPI)* , 2016, pp: 297-301.

[213] S. Choi, B. Akin, M. M. Rahimian, H. A. Toliyat, "Implementation of a Fault-Diagnosis Algorithm for Induction Machines Based on Advanced Digital-Signal-Processing Techniques", *IEEE Transactions on Industrial Electronics*,2011, 58(3), pp: 937-948.

[214] X. Chen, Z. Feng, "Induction motor stator current analysis for planetary gearbox fault diagnosis under time varying speed conditions", *Mechanical System and Signal Processing*, 2020, 140, pp: 106691-106714.

[215] V. F. Pires, M. Kadivonga,J. F. Martins, A. J. Pires, "Motor Square Current Signature Analysis for Induction Motor Rotor Diagnosis", *Measurement*, 2013, 46(2), pp: 942-948.

[216] N. Bhatia, V. SSCS, "Survey of Nearest Neighbor Techniques", *International Journal of Computer Science and Information Security*, 2010, 8(2), pp: 302-305.

[162] A.K. Thakur, P.K. Kundu, A. Das, "Selection of Optimal Mother Wavelet for Fault Analysis in Induction Motor Using Stator Current Waveform", *Advances in Data Science and Computing Technology*, 2022, pp: 197-217, doi:10.1201/9781003277071-20.

[217] N.R. Sakthivel, Binoy B. Nair, M. Elangovan, V. Sugumaran, S. Saravanmurugan, "Comparison of dimensionality reduction techniques for the fault diagnosis of mono block centrifugal pump using vibration signals", *Engineering Science and Technology, an International Journal*, 2014, vol. 17(1), pp: 30-38.

[218] I. Bandyopadhyay, P. Purkait, C. Koley, "A combined image processing and Nearest Neighbor Algorithm tool for classification of incipient faults in induction motor drives", 2016, *Computers and Electrical Engineering*,54(3), pp: 296-312.

[219] V. B. S.Prasath, H. A. Abu Alfeilat, A. B. A. Hassanate, O. Lasassmeh, A. S. Tarawneh, M. B. Alhasanat, H. S. E. Salman, "Effects of Distance Measure Choice on KNN Classifier Performance - A Review", *Big Data*, 7(4), pp ; 1-39.

[220] A. Dasgupta, S. Debnath, A. Das,"Transmission line fault detection and classification using cross-correlation and k-nearest neighbor", *International Journal of Knowledge-based and Intelligent Engineering Systems*, 2015, 19, pp: 183–189.

[221] Jiang JA, Chuang CL, Wang YC, Hung CH, Wang JY, Lee CH, Hsiao YT,"A hybrid framework for fault detection, classification, and location-part I: concept, structure, and methodology", *IEEE Transactions on Power Delivery*, 2011, 26(3), pp. 1988–1998.

Arunava Kabiraj Thakur
27/02/2023

Alok Mukherjee
27/02/2023
Alok Mukherjee
Assistant Professor
Govt. College of Engg. & Ceramic Technology
Kolkata-700010

Anabinda Das
27/02/2023
Professor
Electrical Engineering Department
JADAVPUR UNIVERSITY
Kolkata - 700 032

Pabach Kundu
27/2/23
Professor
Electrical Engineering Department
JADAVPUR UNIVERSITY
Kolkata - 700 032